Measurement of Ventilation and Drying of Vinyl Siding and Brick Clad Wall Assemblies

by

Randy Van Straaten

A thesis
presented to the University of Waterloo
in fulfillment of the
thesis requirement for the degree of
Master of Applied Science
in
Civil Engineering

Waterloo, Ontario, Canada, 2003

I hereby declare that I am the sole author of this thesis. This is a true copy of the thesis, including any required final revisions, as accepted by my examiners.

I understand that my thesis may be made electronically available to the public.

Abstract

The Ventilation of Building Enclosure Assemblies

Control of moisture and heat flow through building enclosure assemblies is a critical component of overall building performance. This thesis shows that significant drying of moisture in wall assemblies is possible and that ventilation of cladding significantly increases the rate of drying in some assemblies without having detrimental impact on the enclosures thermal performance.

A review found that thermal and moisture buoyancy, wind pressure gradients and mechanical equipment drive ventilation airflow. This ventilation flow can theoretically increase the effective water vapour permeance and thermal conductivity. Ventilation has the potential to increase outward drying through relatively impermeable claddings at the low flows expected to occur in service. The impact on thermal conductance is much less.

A methodology for assessing the complicated airflow resistance characteristics of lap sidings was developed and applied to a representative vinyl siding. Field drying studies showed that the sample tested is well ventilated.

Field brick veneer clad wall samples were also tested for system airflow resistance over a range of driving pressures. Theoretical predictions under-estimated the measured flow rate for given steady driving air pressures. Measurements of naturally driven cavity air speeds and smoke pencil testing showed that flow rates were commonly occurring that would in theory significantly affect the hygrothermal performance of the walls. This was confirmed with field drying studies.

A field drying study of east-facing test wall with vinyl siding and brick veneer cladding was conducted in Waterloo, Ontario, Canada. Significant amounts of drying and inward moisture redistribution were measured. Wall sheathing dried quickly in hot summer conditions but in some cases significant inward driven moisture flow occurred. In cool and cold weather the wall dried more slowly and much less moisture moved inward. Increased cladding ventilation significantly increased drying rates and reduced internal wall assembly moisture levels. It was concluded that cladding ventilation acts to increase the effective vapour permeance of cladding and to reduce solar driven inward vapour drives. The use of spun bonded polyolefin sheathing membrane in lieu of #15 asphalt impregnated felt was found to improved hygrothermal performance in the test walls. The difference observed was concluded to be due to the higher vapour permeance of the spun bonded polyolefin and may not hold for wall assemblies with lower permeance sheathings (e.g. oriented strand board and foam plastic). Walls clad with vinyl siding dried faster than those clad with brick veneer. It was concluded that the vinyl siding is a well ventilated cladding system.

This page intentionally left blank

Acknowledgements

I wish to thank Dr. Straube for his patient and commitment to the quality of the graduate student experience and research. His dedication to his work and more important his belief that through engineering research and consulting that we can benefit the world around us was very inspiring.

Dr. Burnett, Chris Schumacher, and Joseph Pinon provided straight foreword advice on my research and were a pleasure to work with. Dr. John Wright provided a thorough review of this thesis and was very patient throughout the process.

My friend and fellow researcher Achilles Karagozis at ORNL always had humorous and insightful advice on graduate studies and the working world.

I would like to acknowledge ASHRAE for supporting our research and organizing their conferences. They are an admirable collection of experts who are fulfilling their mission of advancing the arts and science of their technical field for the good of the public.

Finally, the love of my life Cara Brown, my friends Pat Roppel and Bruce Davison, and my family for emotional support and encouraging me to keep my ideas and research on a practical level.

Table of Contents

List of Tables

List of Figures

1. INTRODUCTION

1.1. Background

Control of moisture and heat flow through building enclosure assemblies is a critical component of overall building performance. Heat flow, moisture flow, and the mechanics of airflow in typical enclosure wall assemblies incorporating ventilation of inter layer airspaces to the outdoor environment is not fully understood.

This thesis explores such systems. The work described in this thesis was part of a project funded by the American Society of Heating, Refrigeration, and Air-conditioning Engineers (ASHRAE) investigating the role of sheathing membranes and cladding ventilation in wood framed wall systems. The project was roughly divided into three parts; field measurements, laboratory testing, and computational modeling. The three tasks were divided amongst three research institutes:

- University of Waterloo Building Engineering Group (UW)
- Pennsylvania State University (PSU)
- Oak Ridge National Laboratory (ORNL)

This thesis focuses on the experimental work at UW.

1.2. Objective

The main objective of this thesis is to investigate the extent and effects of ventilation on the hygrothermal performance of walls clad with vinyl siding and brick veneer cladding.

A further objective of the thesis is to present and interpret the findings of laboratory and field studies. The results are applicable to analysis of a broad range of building enclosures.

1.3. Scope

The analysis portion of the study includes a review of models of heat, moisture, and ventilation airflow in ventilated spaces within a range of building enclosure wall systems. Roofs and crawlspaces, two other enclosure assemblies often ventilated, are explicitly not included. The experimental work presented is limited to wood framed wall systems with vinyl siding and brick veneer cladding systems. A comparison of modeling results and experimental measurements is not within the scope of this thesis.

1.4. Approach

The thesis reviews the fluid mechanics theory needed to predict the amount of airflow ventilating enclosure systems. Analytical methods to predict the effects of this ventilation on heat and moisture flow in these systems are developed. Experimental work exploring the nature and attempting to predict airflow in brick veneer and vinyl systems is then presented. Field studies of full scale wall assemblies intermittently wetted were conducted to investigate the effect of cladding ventilation and sheathing membrane

selection and theses field studies are described. An outline of the thesis is shown in Figure 1-1.

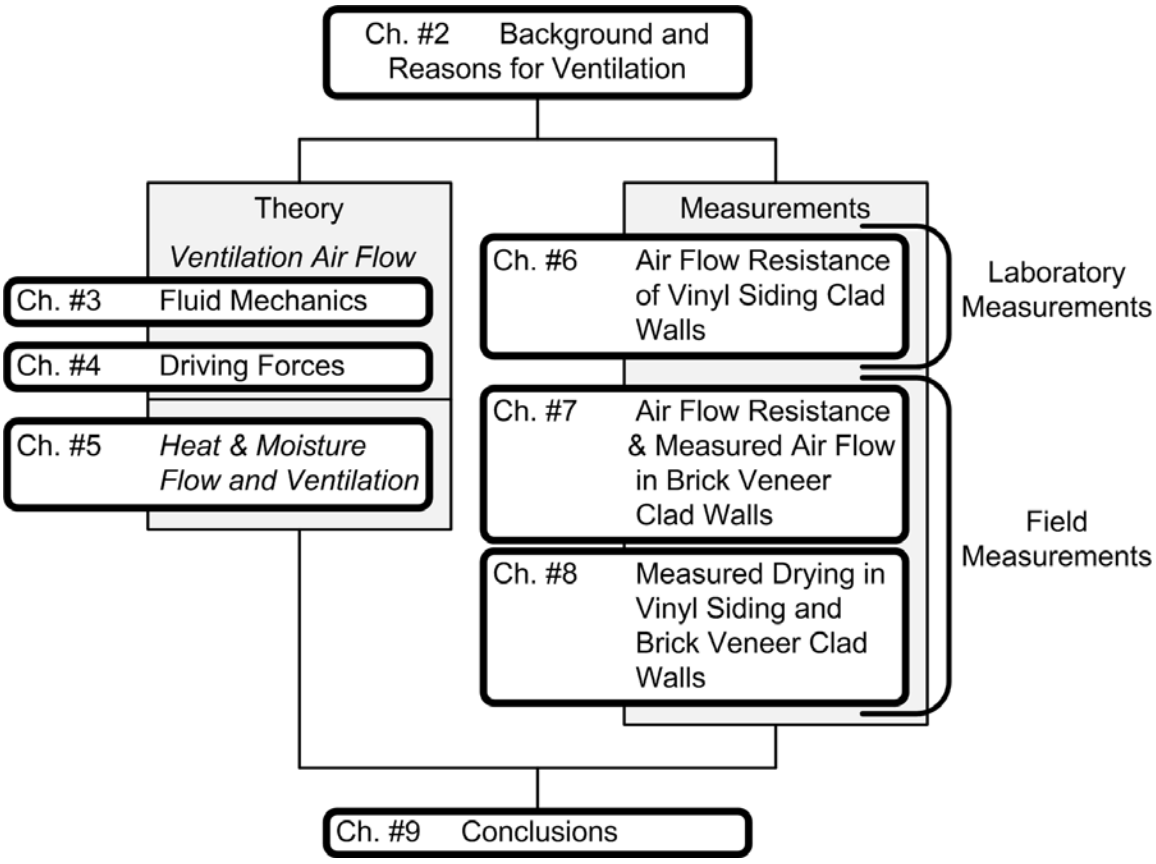

Figure 1-1: Thesis Outline

Chapter 2 includes a general discussion of ventilation and building enclosures, reasons why ventilation is utilized, and a literature review of other studies investigating the mechanics and effectiveness of such systems

A theoretical review of the mechanics of ventilation enclosure wall systems is presented in Chapters 3 to 5. Chapter 3 applies fluid mechanics to airflow systems existing in such systems. Chapter 4 describes the forces driving air through these systems. Chapter 5 develops methods of predicting the effects of ventilation on the heat and moisture flow through and within the building enclosure.

The experimental work is presented in Chapters 6 to 8. Chapter 6 consists of laboratory testing of airflow characteristics of vinyl siding. Chapter 7 describes a field study of airflow resistance, air cavity velocities, and naturally driven airflows through brick veneer clad test walls. Field drying experiments on vinyl siding and brick veneer test walls are described in Chapter 8. The experimental setup is documented in each of these chapters. Conclusions drawn from the interpretation of the results and recommendations for further testing are drawn at the end of each chapter.

General conclusions and recommendations for practice are given in the final chapter.

2. THE BUILDING ENCLOSURE AND VENTILATION

2.1. The Building Enclosure

The building enclosure is that element of a building that separates the indoor from the outdoor environment. The major functional classifications of the enclosure are control, support, and finish as shown in the generalized illustration in Figure 2-1. The loads from the outdoor and indoors are "controlled" by the enclosure. This thesis will focus on the control aspects. These may also be divided into functional sub-classifications included but not limited to heat, air, moisture, fire, sound and vibration, access, and radiation. This thesis focuses on one strategy applied to building enclosures specifically for the control of moisture and heat flow through the enclosure. A further function gathering greater focus today is maintaining the moisture and temperature conditions of the enclosure itself to limit degradation of the materials composing the enclosure.

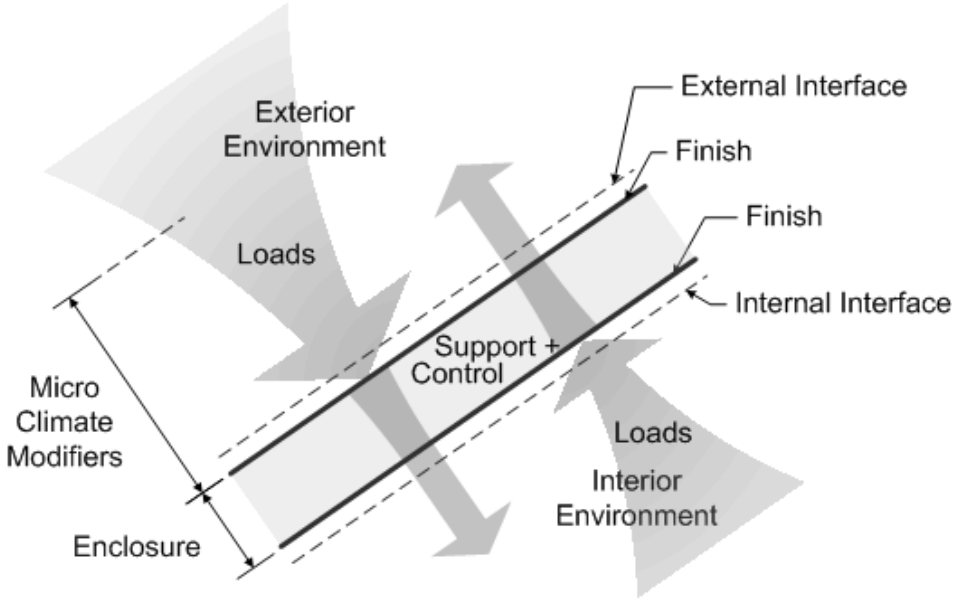

Figure 2-1: The Enclosure and its Functions (Straube and Burnett 2003)

Edward Allen (Allen 1980) describes the original and underlining functional intent of the building (more specifically the building enclosure) as shelter. He provides an excellent review elaborating on the widening of this function for the building to provide a range of distribution services as well. The sheltering effects specifically relate to control aspects through the enclosure. The definition can be viewed in a broad context as sheltering the users from physical (water, radiation, cold, heat, etc.) and social elements (interaction with strangers, enemies, violence). Being inside a building can bring mental comfort to an occupant who fears interaction with strangers. Building on the broad context of control, the conditions inside may not always be preferred by the occupant. An iron smelting plant can maintain uncomfortable conditions for the worker occupant. A prison inhibits a prisoner's need for freedom and social interaction. The term control is more

suitable than shelter as it does not assume a benefit for the user but merely an element that does not allow free flow of mass and energy.

The enclosure surrounds the indoor space in three dimensions. The illustration below (Figure 2-2) shows various enclosure elements separating the indoor and outdoor environments.

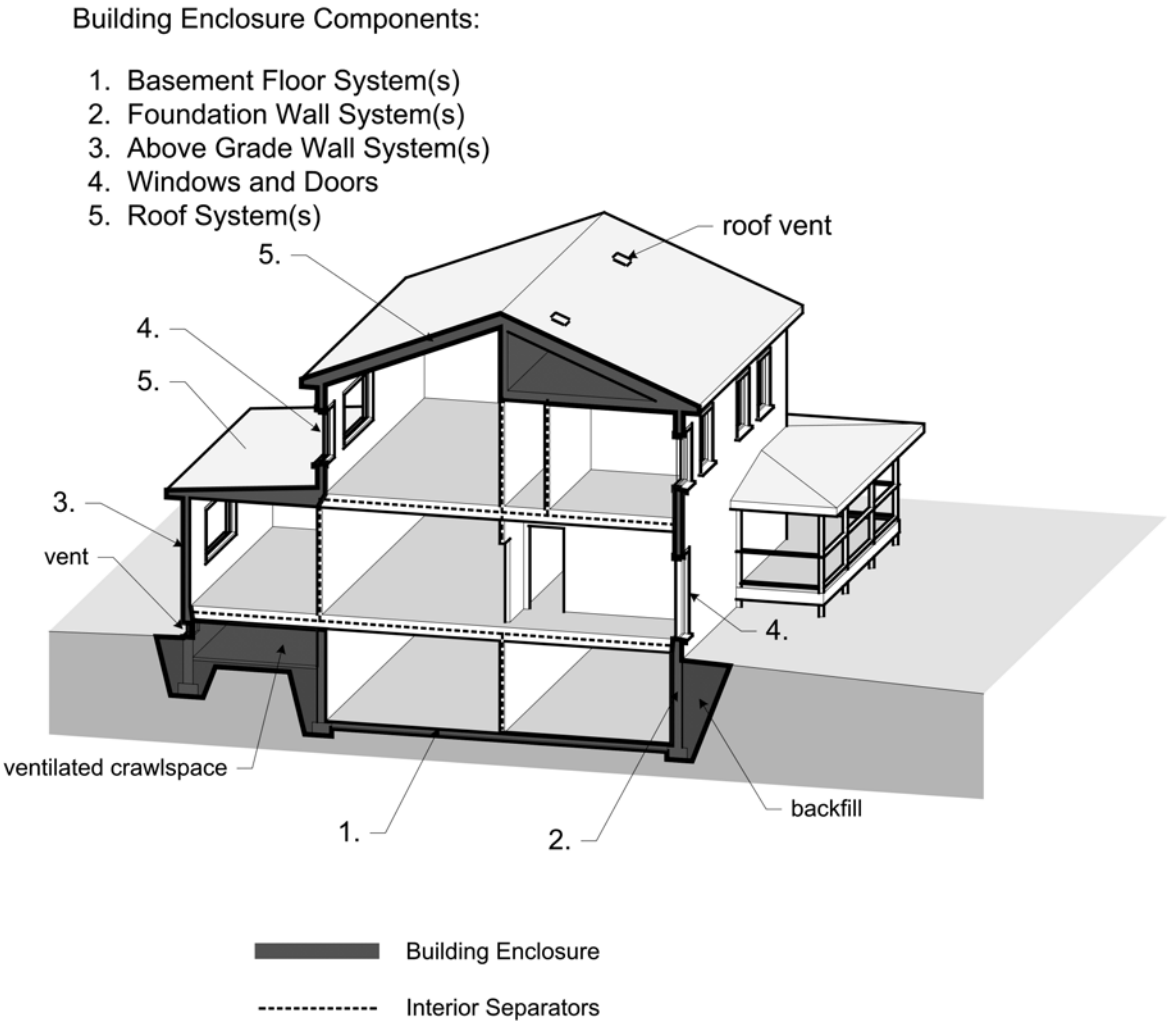

Figure 2-2: Various Enclosure Types in a Building (Straube and Burnett 2003)

The enclosure must control the exchange of mass and energy across it while exposed to a variety of boundary conditions (e.g. above grade/below grade) and while maintaining a variety of other functions related to support, finish, and sometimes distribution of services. To accommodate these functions and because of variance in available construction technology expertise, a wide array of systems and strategies are utilized for the control of heat and moisture flow in enclosure systems (Oliver 2003). This thesis explores systems utilizing ventilation of inter layer air spaces within the building enclosure.

Moisture is one of the most important factors affecting building enclosure durability and performance, especially in cold climates. The design of moisture-tolerant enclosures should involve the simultaneous consideration and balancing of the potentials for wetting, storage, and drying. Design guidelines may stress the avoidance of wetting, but increased safe moisture storage capacity or drying potential can also improve the moisture tolerance of an assembly.

Drainage is usually regarded as the most important drying mechanism, and internal drainage has recently received much attention with regard to walls clad with EIFS (Exterior Insulated Finish System - a popular cladding comprised of foam insulation covered with a stucco-like coating, often polymer based), wood siding, stucco, etc. It has become an axiom of modern enclosure design that wetting will occur at some time during the life of a building in at least some locations. Drainage is often used as the first and fastest means of removing water that penetrates. However, a significant amount of water deposited by condensation or rain penetration will remain in an enclosure, absorbed by the materials, adhered to the surfaces: other drying mechanisms must be provided. One drying mechanism that has not received the attention it is due is ventilation.

2.2. Ventilation

Common positive perceptions of ventilation influence its use in building enclosure design. These positive perceptions are reflected in the several definitions of ventilation. Some available definitions from a dictionary (Merrian-Webster 2003) are given below for "ventilation" and "ventilating".

- "to expose to air and especially to a current of fresh air for purifying, curing, or refreshing.
    - i.e. "*ventilate* stored grain"
    - i.e. "ventilate blood in the lungs"
- to pass or circulate air through so as to freshen or to cause fresh air to circulate through (as in a room or mine).
- to provide an opening in (a burning structure) to permit escape of smoke and heat.
- a system or means of providing fresh air."

The term "fresh" is often used to describe the ventilation air. The following definitions for "fresh" were found (Merrian-Webster 2003).

- " not previously known or used; new or different.
- eager, ardent; brisk, vigorous; not salty; new, novel, recent; having the signs of newness, not tainted, sullied, or worn.
- newly picked, crisp, unwilted; raw, natural, unprocessed."

Intuitively, ventilation is good because it takes away bad air and replaces it with improved "fresh" air. Hence, ventilation is commonly perceived as a positive attribute of any system. Ventilation is applied to a variety of enclosure systems without analysis of whether or not the strategy is effective or beneficial. There persists an assumption that outdoor air has low levels of contaminants. This applies to practical moisture control as

water molecules in the air are in some cases considered an unwanted contaminant. The removal of heat can also be considered in this context. Ventilation to the outdoor air has long been applied as a moisture and heat removal method with varying success depending on climate and application. Ventilation has been added to enclosure spaces with, in some cases, negative impacts on other enclosure functions (including but not limited to):

- Control - Access – Vent openings may provide a path for insect and small animals to enter enclosure
- Finish - Vents visible on outside of building can be aesthetically undesirable
- Control – Moisture – Vent openings may provide a path for rainwater entry into enclosure assembly
- Control – Moisture – Ventilation can allow humid outdoor air into assemblies possibly causing condensation and/or inhibiting drying.

Some examples of intentional encouragement of enclosure ventilation are included in Figure 2-3 , Figure 2-4, and Figure 2-5.

Figure 2-3: Vents for Crawl Spaces

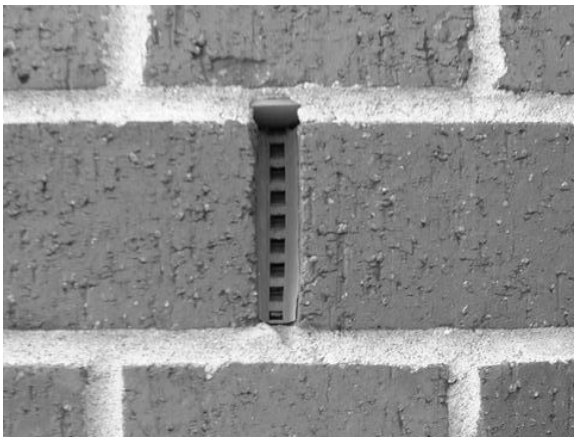

Figure 2-4: Vent for Airspace behind Cladding

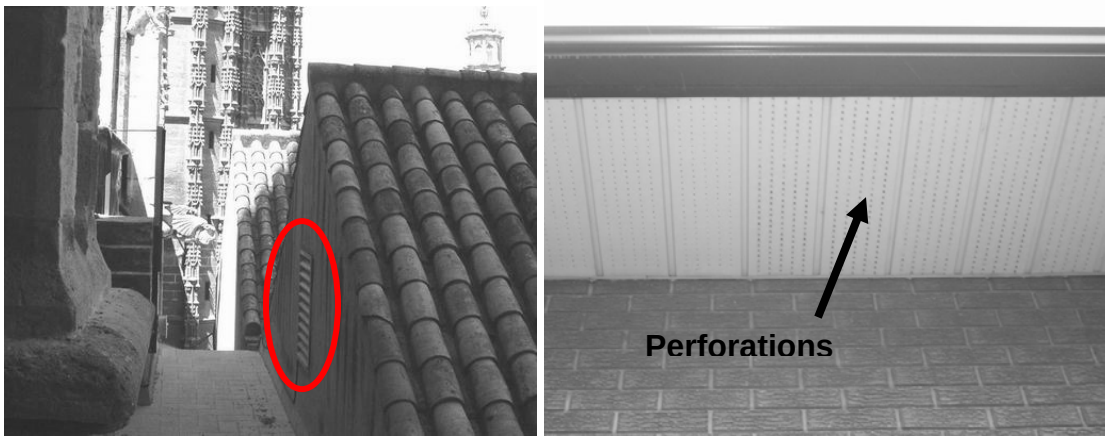

Figure 2-5: Attic Vents

Most enclosures inevitably have some degree of ventilation because of outside air passing through unintentional holes in the cladding. Since enclosures tend to consist of layers, the unintentional holes may connect to airspaces between enclosure assembly layers. Hence, when exposed to driving forces ventilation of the enclosure occurs. This ventilation may significantly affect the enclosure performance and is sometimes intentionally encouraged or discouraged.

Ventilation is typically discouraged to avoid the following:

- Heat loss, uncomfortable drafts, and condensation due to uncontrolled air leakage,
- Potential rain water entry points, and
- Spread of smoke and fire.

Discouraging ventilation also has some challenges for designs:

- It is difficult to build airtight layers,
- There are needs for holes in the cladding for other purposes (drainage, assembly, etc.).

An example of a design where ventilation is discouraged is shown below in Figure 2-6. The main reasoning for avoiding ventilation in this design was to avoid rain water entry past the cladding into the wall assembly.

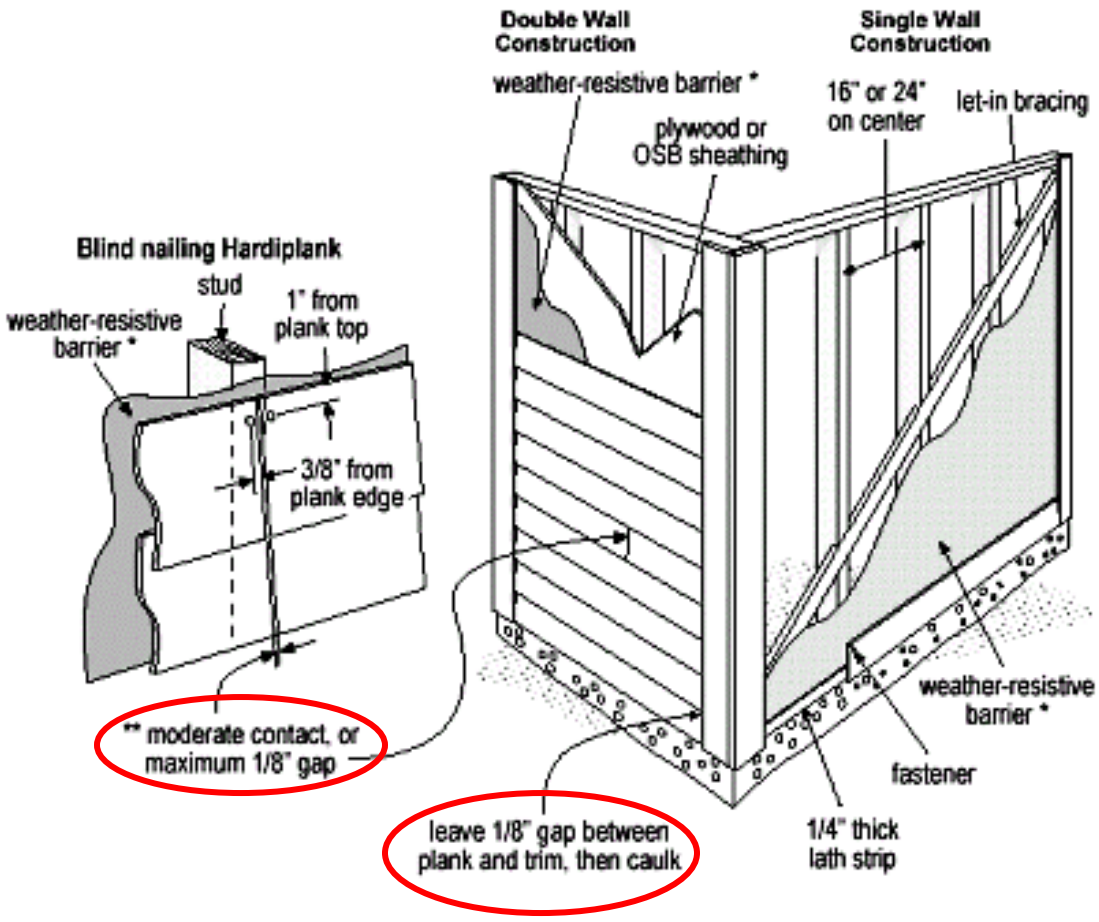

Figure 2-6: Details to Minimize Enclosure Ventilation (www.jameshardie.com)

Despite the wide use and potential importance of enclosure ventilation little is understood about the quantities of ventilation occurring and the effects. Furthermore, laymen's use of the term "ventilation" is poorly defined and measures of ventilation are complicated between occupied and unoccupied space applications.

Walls assemblies get wet primarily from rainwater entry and air leakage. Minimizing water leakage is currently being pursued through improved drainage and flashing design while minimizing air leakage is being pursued through greater building enclosure air tightness. Considering that these problems will persist, the removal of moisture through diffusion and ventilation drying has gained interest (Ojanen and Tuomo 1998 & Salovarna et al. 1998).

In this thesis the term ventilation refers to the exchange of air in a defined space with air not originating within the defined space. The origin of the newly introduced air will be assumed to be the outdoor air unless stated otherwise.

There are several measures for ventilation. The simplest measure is air exchange (I) rate as given below:

$$I = \frac{Q}{V} \qquad (2\text{-}1)$$

where,

Q is the volumetric airflow rate and

V is the volume of the space being ventilated.

When the time unit is hours, the air exchange rate is often called air changes per hour (ACH). Applying ACH to an enclosed space to define the ventilation of the space assumes the air entering the space is instantaneously well-mixed with the air already in the space.

It should be noted that the division of airflow types as infiltration/exfiltration and ventilation is relevant for enclosure ventilation discussions. Ventilation can be defined as the intentional inclusion in design for airflow while infiltration or exfiltration is unintentional. The difference is important. For example, consistent cracks in cladding (i.e., normal joints in vinyl siding) can be designed as ventilation features while non-consistent cracks (i.e., large open joints in vinyl siding due to poor installation) are not designed as ventilation features, but do allow uncontrolled airflow.

2.3. Previous Studies

A consensus in the design community as to the effectiveness of cladding ventilation for the drying and cooling of wall systems has not yet formed.

Straube and Burnett (1995) completed a study of field measurements of wind pressures at the face of a test building. They applied this data to a simple theoretical model to estimate cavity ventilation and to further suggest that moisture transfer by ventilation can effectively bypass low permeance cladding systems and aid the drying of wet wall systems. Straube (1998) expanded these conclusions with field studies showing reduced cavity and batt space air moisture contents in ventilated versus non-ventilated brick veneer wall systems. He also predicted ventilation flows could remove from 10 to 1000 g/m^2/day of moisture from saturated materials behind cladding systems depending on the outdoor environment and ventilation flow rate.

A recent series of climate chamber studies called the Envelope Drying Rate Analysis program (EDRA) were completed in Vancouver in 2001 and summarized by Hazleden and Morris (2002). They acknowledged that little research has to date been directed at determining the effect of wall design on drying rates. In the research program walls were wetted by submersion in water prior to being assembled into test walls. Two phases of tests were completed. In Phase 1 steady outdoor conditions of 5^{o}C and 70% relative humidity were simulated. In Phase 2 the panels were exposed to simulated daily radiation peaking at 120 W/m^2 and a simulated wind pressure difference of 1-5 Pa between the top and bottom to the assemblies. The walls tested are shown below in .

Table 2-1 and the resulting effective permeance values are given in Table 2-2.

Table 2-1: Walls Tested by Hazleden and Morris

Venting Location						
Insulation ***1***	No Vent	No Vent	Bottom Only	Bottom Only	Top & Bottom	Top & Bottom
Venting % ***2***	0%	0%	0.8%	0.8%	0.8% and 0.8%	0.8% and 0.8%
Cavity Size, mm	Bldg. Paper	SBPO	Bldg. Paper		Bldg. Paper	SBPO
0	#1. Stucco on OSB	#2. Stucco on OSB				
10					#7. Stucco on OSB	
19			#3. Stucco on OSB	#4. Stucco on OSB	#5. Stucco on OSB	#6. Stucco on OSB
0	#8. Wood on OSB					
19			#9. Wood on OSB			
0	#10. Stucco on Plywood					
10					#12. Stucco on Plywood	
19			#11. Stucco on Plywood			

1 All panels had RSI 2.45 (R-14) friction fit glass-fiber batt insulation.
2 Venting % = the face of the vent / the area of the panel x 100

Table 2-2: Hazleden and Morris Results

Panel #	Total Calculated Permeance (no ventilation)	Total Measured Effective Permeance Over 1500 hrs	Total Measured Effective Permeance over 2000 hrs
	Phases 1 and 2	Phase 1, no solar	Phase 2, with solar
1	296	259	396
2	389	486	472
3	265	326	389
4	337	199	408
5	265	787	504
6	337	389	537
7	266	359	233
8	249	331	252
9	246	364	557
10	398	768	1014
11	344	1175	1444
12	346	1030	990

The findings of importance for the first phase of the study were the following:

- Panels with cavities dried faster than comparable panels without cavities.
- Panels with wider cavities dried faster than panels with narrow cavities.
- Panels with top and bottom vented cavities dried faster than comparable panels with bottom-only vented cavities.

A second series of tests that simulated low levels of solar radiation resulted in the observation that:

- Solar radiation had little or no effect on panels without cavities.

- Solar radiation caused an increase in the difference between panels' effective permeance (including ventilation) and calculated permeance (of material only).
- Panels with bottom venting performed similarly to panels with top and bottom venting.

Unfortunately, the EDRA study was limited to steady state winter conditions (low temperature of 5^{o}C and low solar radiation of 120 W/m^{2}) and did not assess the effects of summer time conditions, fluctuating wind pressures, and typical solar radiation. The quantity of ventilation in the wall cavities was never measured.

Lawton, Brown, and Lang (2002) also presented a paper based on climate chamber work at the same conference at which the EDRA study paper was presented. Their study consisted of investigating the drying capacity of five stucco-clad wall systems with various drainage and ventilation systems. Water was injected into the walls using a custom technique. The moisture content increase in the plywood sheathing was uneven (0% to 25% change) and water wicked into some of the wood studs and/or out the bottom of the assemblies. Within the climate chamber cool outdoor temperatures (10 ^{o}C) and high relative humidity conditions were imposed. The relative humidity in the assemblies began at 50% to 60%, rose quickly to 85% to 90% then settled to 70% to 75%. The wall assemblies were left for 5 ½ months. Little movement of moisture was observed in test walls. Their conclusions contradicted the conclusions from the EDRA study:

- The drying process was slow and took months to achieve any significant effect.
- The rainscreen design (inclusion of a cavity behind cladding systems) does not enhance drying of water that penetrates into the stud cavity, nor is the drying rate affected by cladding design or by drainage cavity design.
- Moisture movement within the specimens was very limited. From a practical point of view where water initially accumulated it stayed.

There are several characteristics of the Lawton, Brown, and Lang experiment that may have caused the walls in these two studies to perform differently than in the field:

- Since wind and solar affects were not simulated there was nothing forcing air through the ventilation cavity and hence the low vapour permeance cladding inhibited outward drying,
- Under the conditions tested the water vapour would be expected to flow inward, but the inclusion of a vapour barrier in all the test walls limited inward drying, and
- The small temperature difference applied (less than 10^{o}C) drives minimal moisture redistribution within the assemblies.

Hansen, Nicolajsen, and Stang (2002) performed a field study investigating the effects of ventilating cavities on timber wall assemblies. After initial modeling work they stated "However, ventilating with dry air will remove moisture from the construction whereas ventilating with humid air might add moisture to the construction." and "the simulations indicated that a ventilated cavity behind the cladding might increase the moisture content behind the wind barrier." They conducted a field exposure test hut experiment with 12

different full-scale wall assemblies with various types of cladding and wind barriers and ventilated/non ventilated cavities and cavity/no cavity combinations. Replicates were constructed and exposed to southern and northern Danish conditions over a two-year period. The walls were exposed to normal weather conditions without a simulated wetting event. All walls remained below critical wood moisture content levels (below 20% MC) and seasonal variations were observed. It was concluded that ventilation had no significant effect on timber framed wall systems. The authors concluded, "the behaviour of wood frame walls with non-ventilated cavities, in terms of the moisture content behind the wind barrier, was not found to be inferior to the behaviour of wood frame walls with a ventilated cavity". This study was limited in that it did not include an imposed wetting simulation and hence only studied best case scenarios for the wall performance. These walls were not tested at high wall moisture conditions where drying is required. They did show that ventilation wetting was not a concern for their climate.

A recent climate chamber study by Pressnail et al (2003) included the testing of wood frame wall assemblies with soaked wood cladding under conditions conducive to inward vapour flow. Ventilation of the cladding systems cavity was varied from no ventilation, controlled mechanical ventilation, and natural ventilation due to thermal and moisture buoyancy. The moisture movement inward was measured as a percent of the moisture that left the cladding to condense on the indoor-side polyethylene vapour barrier. Ventilation was found to significantly reduce or eliminate condensation due to inward vapour drives.

Straube and Joensig (2003) recently presented an analysis of the potential for ventilation conditioning in crawlspaces in various climates. It was found that ventilation on average brought moisture into crawlspaces under warm humid outdoor conditions. Since warm humid conditions are conducive to mold growth and material deterioration they concluded that climates with significant lengths of time with warm humid outdoor conditions should avoid crawlspace ventilation.

2.4. Closure

While some techniques and guidance are available for estimating the effects ventilation of specific systems (ASHRAE 2001, Straube and Burnett 1995) there has been limited scientific validation of the particular systems studied and a range of other systems have not been studied.

The field and laboratory studies included in this thesis aim to bring about some agreement and improved predictions regarding the effects of enclosure ventilation.

2.5. References

Allen, E., *How Buildings Work,* 2nd Ed. Oxford Press 1980.

ASHRAE, *Handbook of Fundamentals* Atlanta, Ga, 2001.

Hansen, M., Nicolajsen, A., Stang, B., "On the influence of ventilation on moisture content in timber framed walls", *Building Physics 2002 – 6th Nordic Symposium,* Trondheim Norway 2002

Hazleden, D., Morris, P., "The Influence of Design on Drying of Wood-Frame Walls Under Controlled Conditions" *Thermal Performance of Building Envelopes VIII 2002* Clearwater Florida 2002.

Lawton, B., Brown, W., and Lang, A., "Stucco Clad Wall Drying Experiment" *Thermal Performance of Building Envelopes VIII 2002* Clearwater Florida 2002.

Merrian Webster Dictionary – www.m-w.com, 2003.

Oliver, P., *Dwellings,* Phaidon Press Inc. NewYork 2003.

Pressnail K., Timusk J., Kan L., Dong B., Kan V., University of Toronto "In Search of a Wall for All Season: Controlling Sun Driven Moisture", *9th Canadian Conference on Building Science and Technology,* Vancouver 2003.

Straube, J., and Burnett, E., Vents*, Ventilation, and Pressure Moderation*, Canadian Mortgage and Housing Corporation Report, Ottawa 1995.

Straube, J., *Moisture Control and Enclosure Wall Systems* PhD dissertation, University of Waterloo 1998.

Straube, J. Joeng, J. "Analytical Means of Assessing the Influence of Ventilation on Crawlspace Performance" *9th Canadian Conference on Building Science and Technology* Vancouver Canada 2003.

Straube J., Burnett E., *Building Science for Building Enclosures*, in progress, 2004.

www.jameshardie.com July 2003.

3. FLUID MECHANICS OF AIRFLOW SYSTEMS

3.1. Introduction

Many enclosure systems are constructed in such a way that intentional and unintentional ventilation of inter layer air spaces can occur. The ventilation types related specifically to enclosure systems can be classified into three separate categories based on the source and sink of the ventilation air:

- Outdoor air to outdoor air,
- Conditioned and/or indoor air to indoor air, and
- From the indoor to the outdoor or outdoor to indoor.

Each strategy can be beneficial in some situations. Ventilating with indoor air may be used to collect solar heat gains for conditioning the inside space (e.g. Trombe walls). Operable windows that allow control of airflow between the indoors and outdoors are used to naturally ventilate many North American houses. Ventilating to the outdoors with outdoor air can be employed to remove moisture and heat from the enclosure system and several examples will be described in this chapter.

Fluid flow analysis can be used to understand, predict, and aid the design of ventilated enclosure systems. Fluid flow analysis is widely applied in several engineering disciplines for common flow applications (e.g. HVAC air duct and piping design). This chapter briefly reviews fluid mechanics concepts and focuses on its application to cladding ventilation.

3.2. Fluid Flow Analysis

Fluid mechanics analysis for streamline flows is based on two principles: conservation of mass and conservation of energy. Conservation of mass is applied to flow streams by the continuity equation (ASHRAE 2001 F2.2):

$$\int \rho \cdot V_{normal} \cdot dA = \text{constant} \qquad (3\text{-}1)$$

where,

ρ is density,

V_{normal} is the velocity of the fluid normal to the area, and

A is the area.

By assuming the flow is incompressible, one can derive:

$$Q = \bar{V}_{normal} \cdot A = \text{constant} \qquad (3\text{-}2)$$

where,

Q is the flowrate.

The mass flow rate must therefore be the same along an enclosed flow system except where branching occurs.

Conservation of energy is applied to enclosed systems by Bernoulli's equation:

$$\left(P + \frac{\rho V^2}{2} + \rho g h\right)_1 = \left(P + \frac{\rho V^2}{2} + \rho g h\right)_2 + E_L \cdot \rho \qquad (3\text{-}3)$$

where,

P is the static pressure,

g is the gravitational constant,

h is the height or head, and

E_L is the energy dissipated between the two points.

The energy losses in airflow systems can be described as pressure losses allowing the energy balance to be written in terms of static pressure, i.e.:

$$P_1 = P_2 + \Delta P_{losses} \qquad (3\text{-}4)$$

A basic simplification can be applied to systems with segments of approximately constant properties. Flow can be modeled as two nodes at different pressures separated by a resistance to flow as in Figure 3-1. The resultant fluid flow rate will depend on the boundary conditions at the nodes (P_1 and P_2) and the characteristics of the flow system (ΔP_1 and ΔP_2), which often varies with flow rate. The boundary conditions will be described in the next chapter and the flow system characteristics relevant to this analysis will be covered in this chapter.

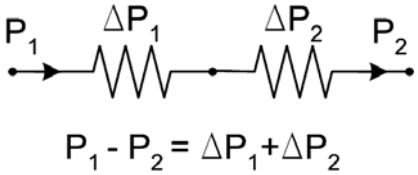

Figure 3-1: Simple Series Circuit

Flow systems in ventilation systems generally consist of a cavity separated into segments by a series of geometric anomalies resisting fluid movement. The effects of the cavity and the anomalies will be described separately and the basic method for combining the effects will be described later.

Analysis of these systems could be undertaken with the aid of Computational Fluid Dynamics (CFD) simulations. The ASHRAE Handbook of Fundamentals (2001 F33) includes a short section on research applications for CFD simulations for room air motion, external flow fields, and internal flows with non-standard components. The basis for CFD analysis is usually the incompressible Navier-Stokes equation, which describes the motion of a viscous Newtonian fluid. Determining an exact solution for typical ventilation applications is beyond the realm of available computational ability and has only been accomplished for a few very simple flow conditions. Simplified iterative methods are applied in available CFD software allowing updating of a condition

converging to a mass, momentum, and energy balance. The value of these methods is in determining pressure drop, aero/hydrodynamic loads, and convective heat transfer coefficients. Saelens (2002) observed in his literature review of CFD simulations of naturally driven flow in double facades that the results have mainly been illustrative, no validations are typically available, and that wind effects are either not taken into account or only with limited ability. Validation of ventilation simulations is difficult due to current limitations and expense of airflow velocity measurement techniques (Loomans 1998). Further CFD analysis of the systems in this study could generate a greater understanding of the airflow in ventilated wall cladding systems.

3.3. Conduit Flow

In enclosed fluid flow systems, fluid flow analysis is used to correlate pressure differentials with flow rates using the characteristics of the conduit and fluid as input variables. This study will begin with a study of fluid flow in a pipe as shown in Figure 3-2.

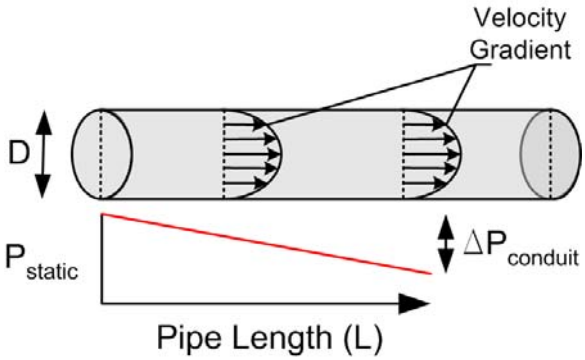

Figure 3-2: Flow Through a Pipe

Viscous shears occur near the pipe walls producing a lateral velocity profile. The flow stream overcomes the shear stresses with the conversion of potential energy to heat. This energy loss is observed in the decline of static pressure along the pipe and can be predicted by the Darcy-Weisbach equation (ASHRAE 2001 F2.8):

$$\Delta P_{conduit} = f \cdot (\frac{L}{D}) \cdot (0.5 \rho \cdot V^2) \qquad (3\text{-}5)$$

where,

f is the friction factor,

L is the pipe length, and

D is the pipe diameter.

The Reynolds number is the ratio of inertial to viscous forces. The magnitude of the Reynolds number indicates if the fully developed flow is laminar (less than about 2300), turbulent (greater than 15000), or transitional (in between depending on surface

roughness). Laminar, transition, and turbulent flow were originally defined from Osborne Reynolds's (1842-1912) experiment illustrated below.

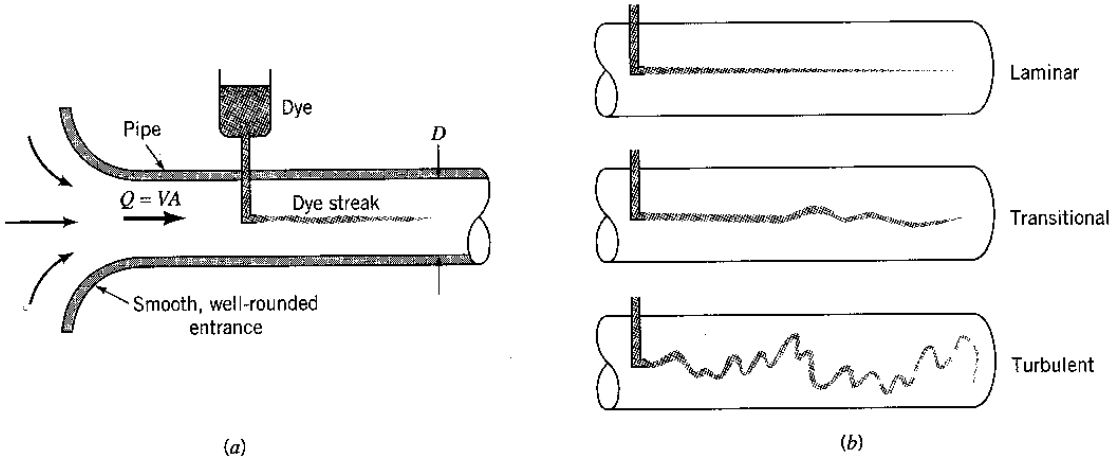

Figure 3-3: Experiment to Illustrate Type of Flow (a). Typical Dye Streaks (b) (Munson et al 1998)

The definitions are based on the behaviour of dye within the fluid flow from this experiment. A more theoretical definition is that during laminar flow there is only in-plane element to the fluid velocity while during turbulent flow there is an out of plane fluctuating component to the fluid velocity. This is illustrated below in

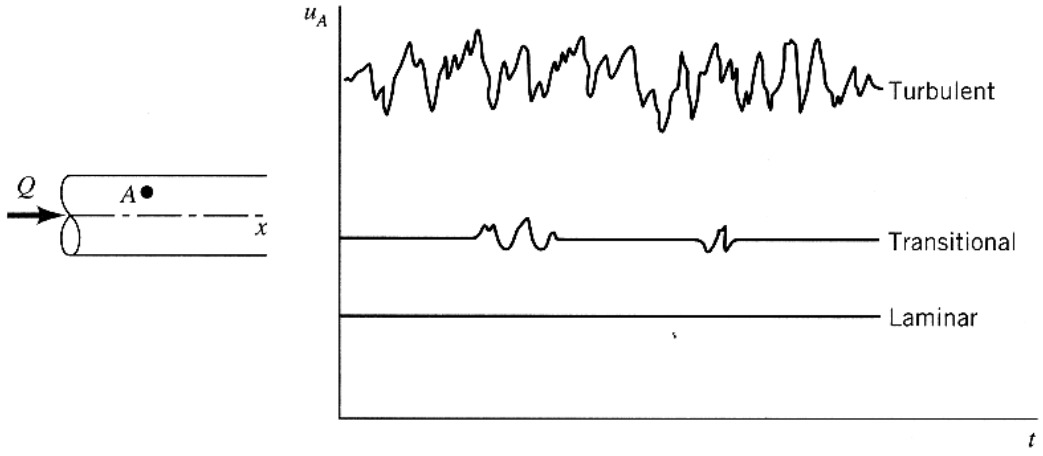

Figure 3-4: In-Plane Instantaneous Velocity Measurements (Munson et al 1998)

Flow resistance relations generally depend on the type of flow if not Reynolds number specifically.

$$\mathrm{Re} = \frac{D \cdot V \cdot \rho}{\mu} \tag{3-6}$$

where,

μ is the dynamic viscosity.

The airflows in cladding ventilation circuits tend to be laminar but can also achieve transitional and turbulent flows in some cases (Figure 3-5). The sample velocities were taken from measured velocity data from this study and from the literature.

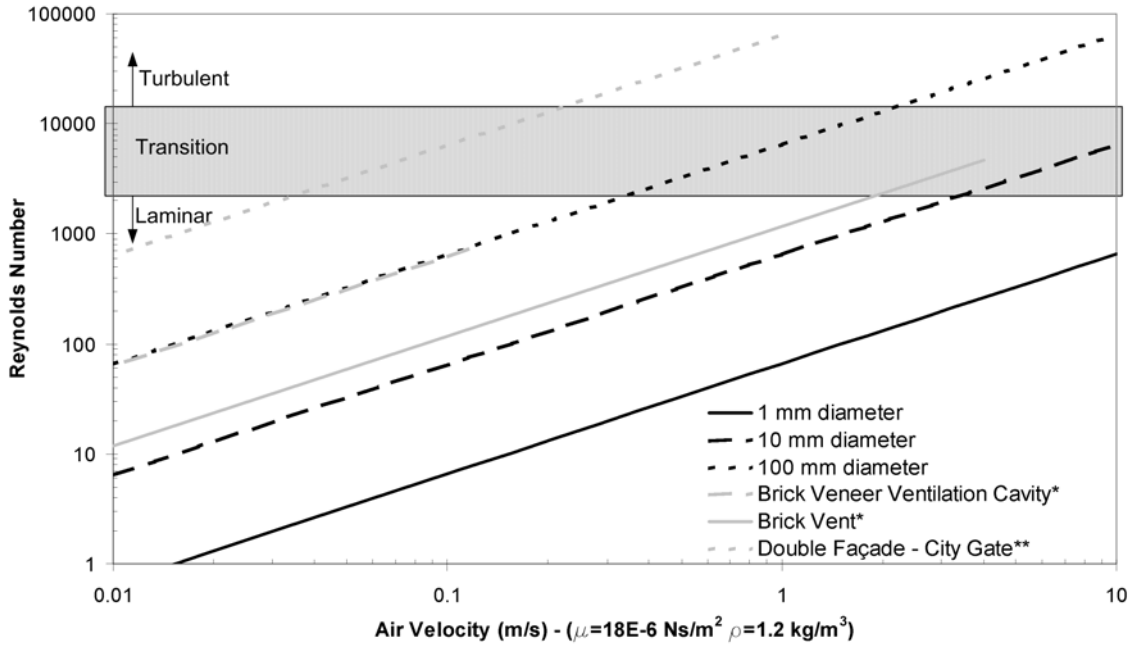

Figure 3-5: Reynolds Number and Air Velocity for various conduit diameters

*Derived from data collected in this study

** (Oesterile et al 2001)

The type of flow of concern for systems with small hydraulic diameters tends to be laminar as shown in Figure 3-5. The case of double facades with large ventilation cavities and relative small flow resistances at vents will be discussed separately in section 3.7.1 of this chapter. Since most components of building enclosure ventilation systems tend to consist of components with small hydraulic diameters, this chapter will focus on laminar flow.

Due to the overriding effects of the viscosity forces in laminar flow, even flow past rough surfaces appears smooth (i.e. no vortices form). Therefore the roughness of the walls, unless it is very significant, does not affect the flow resistance. Since the friction factor in Equation 2-5 is independent of surface roughness, the Hagen-Poiseuille law gives the relationship for laminar flow in a circular tube (Idelchik 1993).

$$f_{circular} = \frac{64}{\mathrm{Re}} \tag{3-7}$$

For laminar flow between parallel plates

$$f_{parallel\_plates} = \frac{96}{\mathrm{Re}} \tag{3-8}$$

For turbulent flow, the functional dependence of the friction factor on the Reynolds number and the relative surface roughness is rather complex and has not, as yet, been obtained from a theoretical analysis. The friction factor can be found on the Moody chart (Munson et al. 1998).

The relationship between average and maximum velocity across the cross section of flow for fully developed laminar flow between two fixed plates can be found in most fluid dynamics texts (Munson et al. 1998). The maximum velocity (V_{max}) is along the centerline of the cavity depth.

$$\bar{V} = \frac{2}{3} V_{\max} \tag{3-9}$$

In the case of rectangular cavities the Darcy-Weisbach equation is still valid when used with a modified friction factor and the hydraulic diameter (ASHRAE 2001 F2.10) in place of diameter. The hydraulic diameter is an effective diameter used to allow application of relations derived for circular conduit to non-circular conduits.

In non-circular conduits, the boundary layer shear stresses vary around the perimeter (White 1991). Idelchik (1993) recommends the hydraulic diameter be used only where the boundary layer thickness is very small relative to the diameter of the conduit. While this requirement will generally hold for turbulent flow, laminar flow models require corrections for various cross-sectional profiles. Laminar flow corrections are based on the turbulent flow relation for hydraulic diameter:

$$D_h = \frac{4 \cdot \text{Area}}{\text{Wetted Perimeter}} \tag{3-10}$$

For a rectangular conduit:

$$D_h = \frac{4 \cdot w \cdot d}{w + d + w + d} \tag{3-11}$$

where,

w is the conduit width and

d is the conduit depth.

The hydraulic diameter can be used without a friction factor modifier to determine the equivalent diameter of rectangular ducts (Straube and Burnett 1995) but some inconsistencies have been found in measurements (ASHRAE 2001 F34.8).

Table 3-1: Correction Factor (k_f) for Rectangular Conduit (Idelchik 1995)

d/w =	0	.01	0.2	0.4	0.6	0.8	1.0
Laminar regime (Re < 2000)							
k_f =	1.50	1.34	1.20	1.02	0.94	0.90	0.89
Turbulent regime (Re > 2000)							
k_f =	1.10	1.08	1.06	1.04	1.02	1.01	1.0

Employing Idelchik's corrections for friction factor as in Equation 3-9 allows for the prediction of frictional pressure loss in a rectangular conduit of any surface roughness with laminar flow:

$$f = k_f \cdot f_{circular} = k_f \cdot \frac{64}{\mathrm{Re}} \tag{3-12}$$

Another complication with real wall assemblies is the inconsistency of the flow path area. Possible causes are the blockage of the cavity by construction materials (e.g. mortar dams, billowing house wraps) and sloping vertical profiles (e.g. lapped siding). In order to apply the Darcy-Weisbach equation Straube and Burnett (1995) recommend the use of a blockage factor. A value of γ =1 is recommended for clear cavities and a value of γ=0.8 for brick veneer with good workmanship.

$$\Delta P_{conduit} = f \cdot (\frac{L}{\gamma \cdot D_h}) \cdot (0.5 \rho \cdot V^2) \tag{3-13}$$

Simplifying the equation:

$$\Delta P_{conduit} = \frac{64 k_f}{D_h \cdot V \cdot \rho / \mu} \cdot (\frac{L}{\gamma \cdot D_h}) \cdot (0.5 \rho \cdot V^2) = \frac{32 k_f \cdot V \cdot \mu \cdot L}{\gamma \cdot {D_h}^2} \tag{3-14}$$

For cavities with varying cross-sectional areas along the flow length, the selection of a velocity in the Darcy-Weisbach equation would be arbitrary based on an average or specific cross-sectional area. In such cases with a wide cavity an equivalent conduit depth is recommended. In the case of a wide rectangular cavity the hydraulic diameter can be simplified:

$$D_h = \frac{4A}{P} = \frac{4wd}{2w + 2d} = \frac{4d}{2 + 2 d / w} \tag{3-15}$$

$$d / w \approx 0 \text{ (very wide cross-section)} \tag{3-16}$$

$$D_h \approx 2 d_{eq} \tag{3-17}$$

$$\therefore \Delta P_{conduit} \propto {d_{eq}}^2 \tag{3-18}$$

Assuming the average conduit depth is the equivalent depth will be inaccurate because the relationship to pressure drop is non-linear. The averaging would be inaccurate because some flow profiles will cause eddies or dead spaces. The effect of eddy formation would be to further restrict the flow. The equivalent depth (d_{eq}) could be determined analytically with the use of CFD simulation or empirically by the measurement of flow resistance. The advantage of the adoption of equivalent conduit depth is that it allows a simple and physically understandable comparison between different system conduits. The Darcy-Weisbach equation (3-14) modified for a very wide and narrow rectangular duct with the use of equivalent diameter is, for fully developed laminar flow:

$$\Delta P_{conduit} = \frac{32 k_f \cdot V \cdot \mu \cdot L}{4 d_{eq}^{\ 2}} \tag{3-19}$$

For turbulent flow the equation becomes:

$$\Delta P_{conduit} = \frac{f(\mathrm{Re}, \varepsilon / D_h) \rho \cdot V^2 \cdot L}{4 d_{eq}} \tag{3-20}$$

3.4. Local System Resistances

Local losses of total pressure (ΔP_{local}) are caused by the following phenomenon (Idelchik 1993):

- Local disturbances of the flow,
- Separation of flow from surfaces, and
- Formation of vortices and strong turbulent agitation of the flow.

Loss coefficients are a standard method of accounting for fluid flow pressure losses at these anomalies in the flow stream path. Many empirical coefficients for a variety of possible flow systems are included in ASHRAE (2001 F34) and Idelchik (1993). The loss coefficient (C) is defined as:

$$C = \frac{\Delta P_{local}}{0.5 \rho \cdot V^2} \tag{3-21}$$

There are limitations to the use of empirical loss coefficients. Most of the published coefficients were measured at high Reynolds's number and only a limited number of potential flow system components have been characterized. However, loss coefficients are the best simple and available method of modeling these systems.

3.4.1. Exit and Entrance Resistances

At entrances and exits the flow stream contracts or expands causing local resistances to the fluid flow. Entrance and exit coefficients used by Straube and Burnett (1995) were 0.5 and 0.88 respectively. These exit coefficients were derived from HVAC literature and are valid for turbulent flow. Idelchik provides a method for determining the entrance and exit coefficients at transitional and laminar flow rate. The coefficients are determined from the following equations for $30 < \mathrm{Re} < 10^5$:

$$C = \frac{\Delta P_{local}}{0.5 \rho \cdot V^2} = \frac{C'}{\bar{A}^2} + C'' C_t \tag{3-22}$$

where,

C_t is the constant value of the coefficient under turbulent flow, and

C' and C" are coefficients dependant on Reynolds number and are included by Idelchik in tabular format.

A power law equation was developed for C' from Idelchik data and is shown in Figure 3-6.

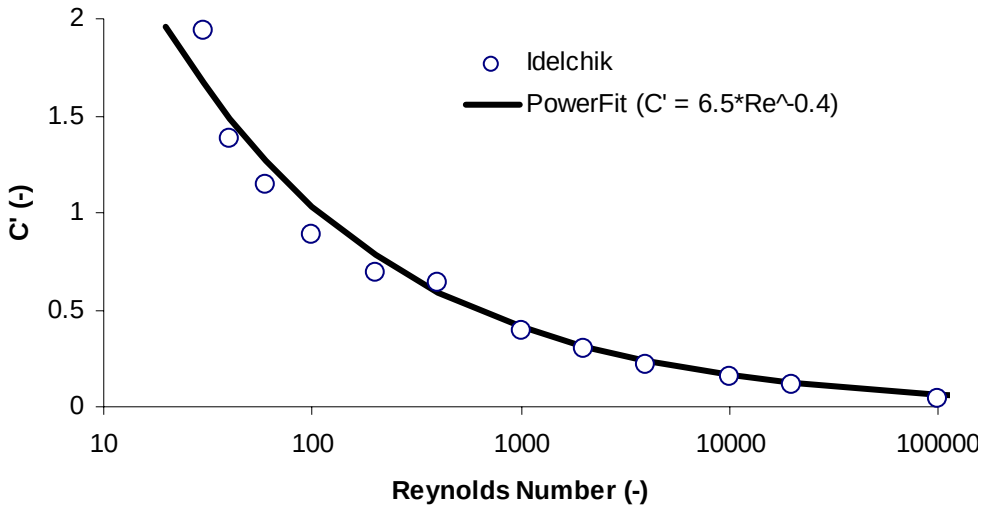

Figure 3-6: Curve Fit to C'

A log relation was found for C" and is shown in Figure 3-7.

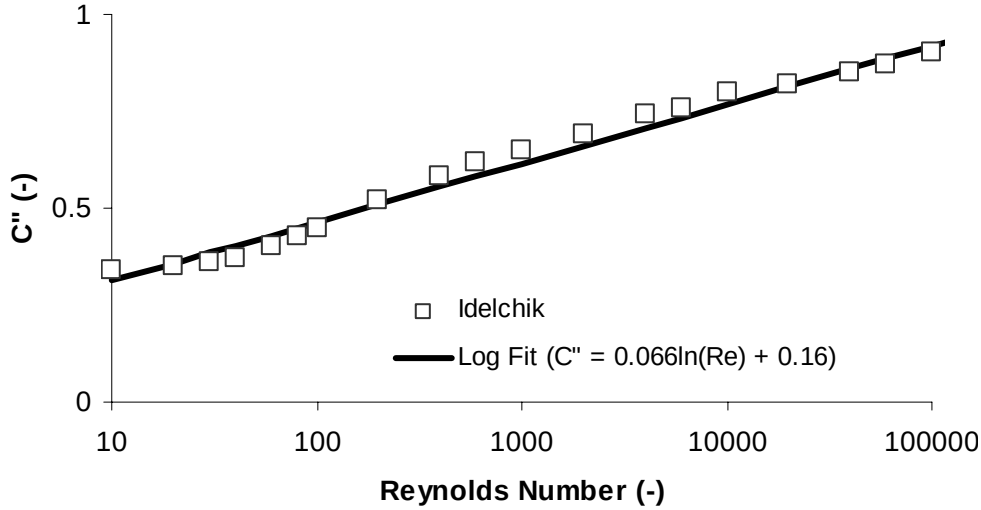

Figure 3-7: Curve Fit to C"

Combining the curve fits found for C' and C" and Equation 3-20 gives:

$$C = \frac{\Delta P_{local}}{0.5\rho \cdot V^2} = \frac{6.5\,\mathrm{Re}^{-0.4}}{\bar{A}^2} + (0.066\ln(\mathrm{Re}) + 0.16) \cdot C_t \qquad (3\text{-}23)$$

Solving with $\bar{A}$ equal to unity and the entrance and exit coefficients is shown in Figure 3-8 and Figure 3-9 are calculated.

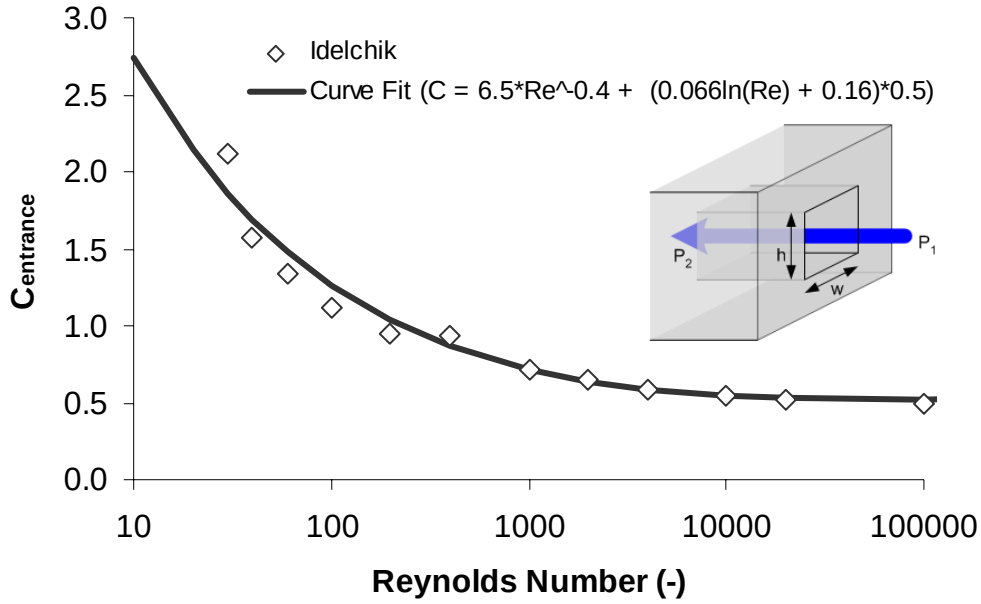

Figure 3-8: Loss Coefficient for a Wall Entrance at 30 <Re < 100000

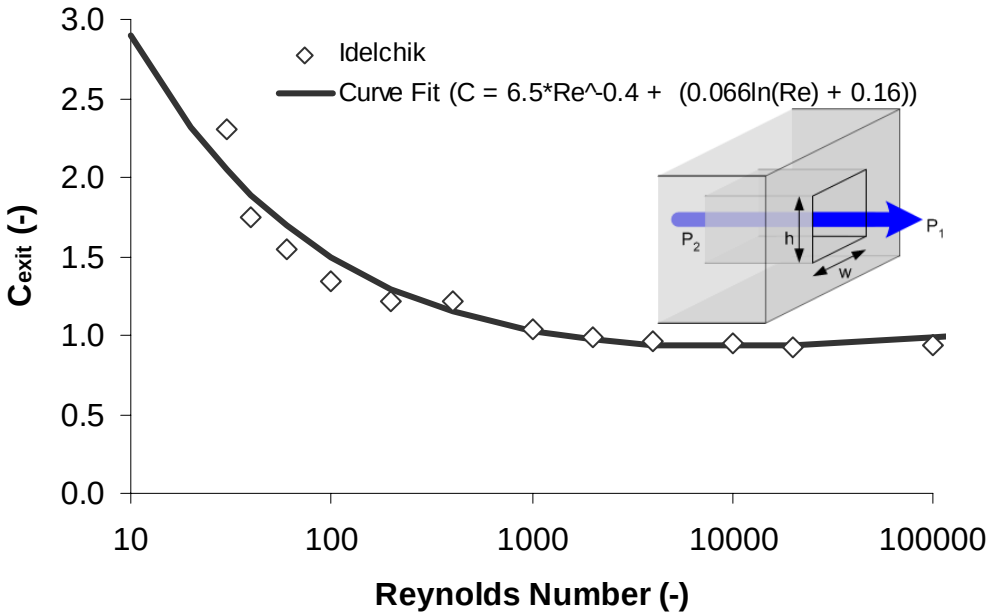

Figure 3-9: Loss Coefficient for a Wall Exit at 30 <Re < 100000

The ASHRAE Handbook of Fundamentals provides an entrance coefficient of 0.5 (turbulent flow) and an exit coefficient of 1.0 for turbulent flow and 1.55 for laminar flow. These coefficients are within the range of the relationships reported by Idelchik. At low Reynolds (e.g. 100) the entrance and exit loss coefficients predicted by Idelchik are 1.25 and 1.45 respectively.

3.4.2. Elbow

For sharp elbows Straube and Burnett (1995) recommend the following relationship:

$$C = 0.885 \cdot (\frac{d_1}{d_2})^{-0.86} \quad (3\text{-}24)$$

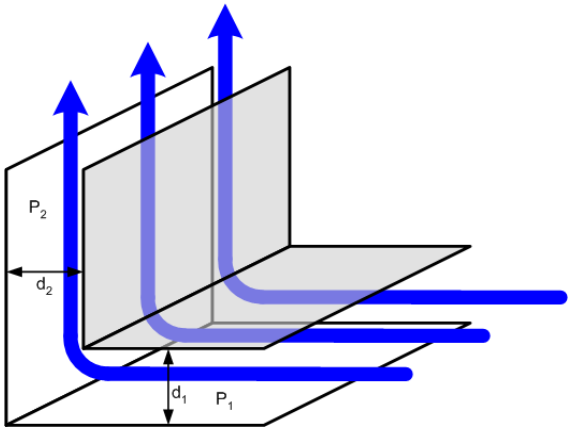

Figure 3-10: Simple Elbow

Although the validity of this relationship within the laminar flow regime could not been determined it will be assumed sufficient for this study. No other applicable references could be found.

3.4.3. Thin and thick walled orifice

A stream of fluid must contract to pass through an orifice. For a well-rounded entrance, the contraction will result in little energy loss and the discharge coefficient (C_d) will range from 0.96 to 0.98 (Handegord and Hutcheon 1995). For a sharp-edged orifice or square-edged orifice the effective jet cross-section is reduce by contraction to about 0.62 of the orifice area and the discharge coefficient is commonly taken as 0.60.

$$Q = C_d A \sqrt{\frac{2\Delta P}{\rho}} \quad (3\text{-}25)$$

$$\left(\frac{Q}{A}\right)^2 = \frac{2\Delta P \cdot C_d^2}{\rho} \quad (3\text{-}26)$$

$$V^2 = \frac{\Delta P}{(1/C_d^2)0.5\rho} \quad (3\text{-}27)$$

From Equation 3-19 the discharge coefficient can be defined as

$$C = 1/C_d^2 \quad (3\text{-}28)$$

An illustration of orifice flow is shown below in Figure 3-11.

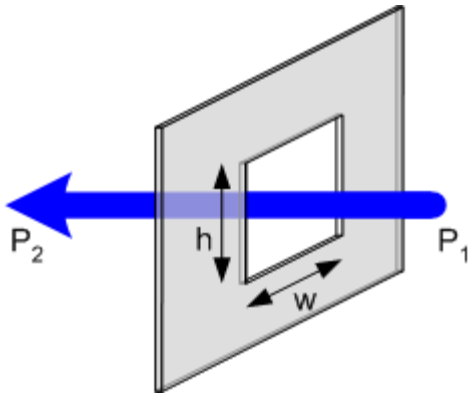

Figure 3-11: Thin Walled Orifice

This relationship was derived from experiments where a thin walled orifice was included in a pipe. In practice measuring the pressure drop across an orifice determined an unknown flow rate with the standard orifice relationship. As the ratio of the pipe diameter to the orifice diameter becomes large the discharge coefficient for low Reynolds number values approaches 0.60 as shown in Figure 3-12. For this plot pressure taps are located one diameter upstream and one-half diameter downstream. The values are applicable for pipe diameters between 32 and 76 mm.

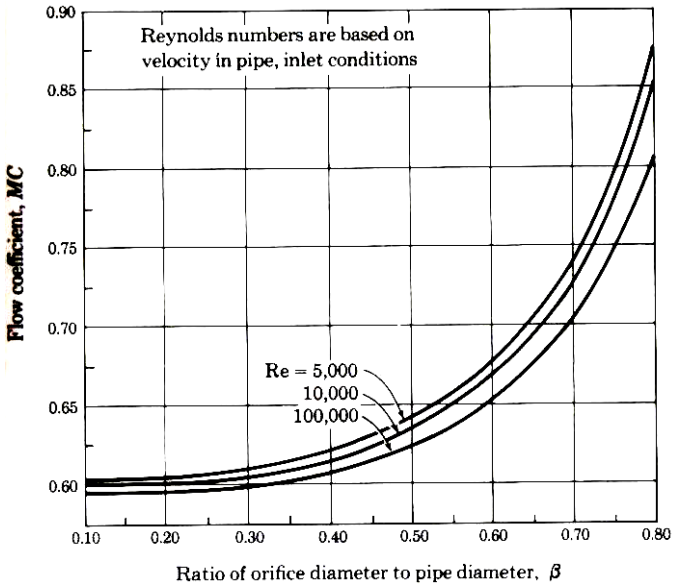

Figure 3-12: Discharge Coefficients for Concentric Orifices in Pipes (Holman 1994)

The plot in Figure 3-12 also suggests an increase in loss coefficient (shown as MC on plot) with lower Reynolds numbers. This is also shown in Figure 3-13 where the loss coefficient at the lowest A_0/A_1 of 0.05 rise at the lowest Reynolds Numbers less than 7000. Laminar flow may therefore have effective discharge coefficients greater than 0.60.

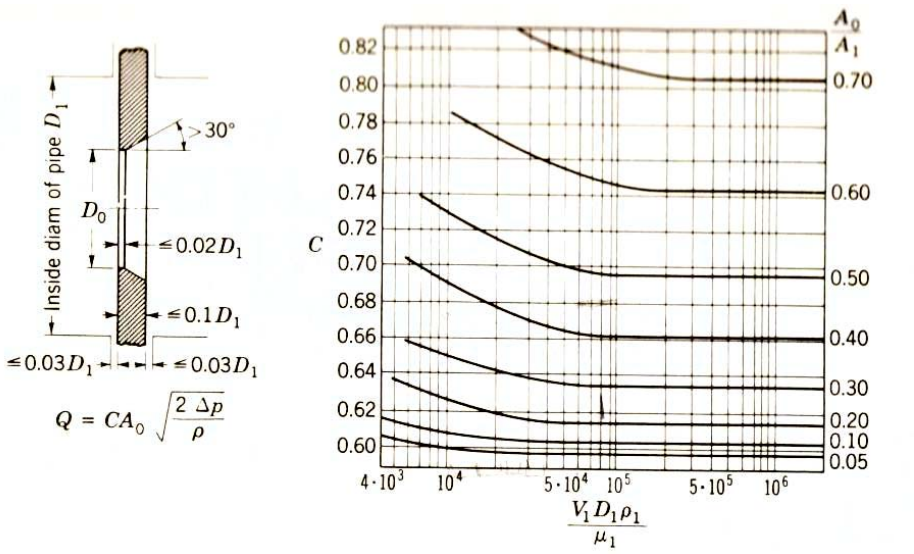

Figure 3-13: Sharp Edged Orifice and Discharge Coefficients (Streeter and Wylie 1995)

Another potential limitation with the use of the sharp edged orifice model occurs when the orifice walls are thick. This could be significant with the use of certain vent inserts in brickwork as shown in Figure 3-17. The ratio of length (l) to hydraulic diameter (D_h) is the main variable in this relation.

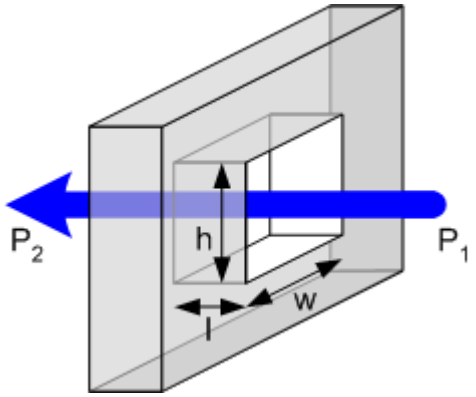

Figure 3-14: Thick Walled Orifice

If the length, l, shown in Figure 3-14 is long, the system could be modeled as an entrance and exit (assuming friction losses along the vent length are negligible). The loss coefficient for turbulent flow would be 1.5. This results in 37% less airflow than predicted using the thin walled orifice equation. For a greater vent length, the friction losses along the length become significant. At this point determining the flow resistance along the vent requires treatment as a conduit with entrance, conduit friction, and exit losses.

A reference for the approximate length at which the orifice equation applies is the entrance length along the vents required for fully developed flow. In the case of laminar flow (Re < 2300) Incropera and Dewitt (1996) recommend

$$\frac{l_{entrance}}{D_h} \approx 0.05\,\mathrm{Re}_{D_h} \tag{3-29}$$

For turbulent flow they recommend

$$10 \le \frac{l_{entrance}}{D_h} \le 60 \tag{3-30}$$

Figure 3-15 shows these relationships graphically,

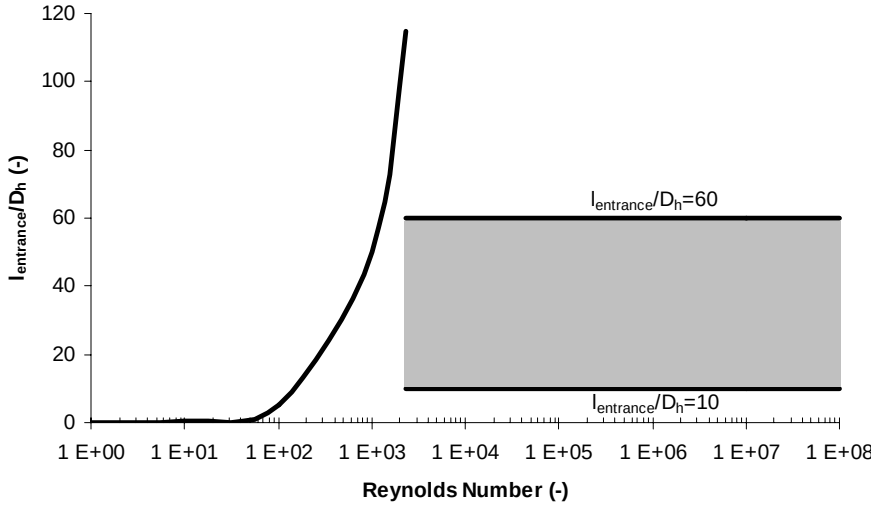

Figure 3-15: Entrance Length – recommended by Incropera and Dewitt

Figure 3-15 shows an irregularity with the equations suggested by Incropera and Dewitt in that the entrance length gets very long when Reynolds are greater than 1000. In this thesis it will be assumed that entrance length at Reynolds numbers greater than 1000 is equal to 50 hydraulic diameters. If the length of the vent is in the order of the entrance length determine by the relationships in Equations 3-29 and 3-30 then the application of entrance and exit coefficients is recommended. This finding will be applied later to specific cases.

3.5. Network Flow

In a complete flow network the local pressure drops and friction pressure drop in the conduit are added to determine the total pressure drop. This is illustrated in Figure 3-1.

$$\Delta P_{Total} = \Delta P_{conduit} + \Delta P_{local} \tag{3-31}$$

The cross-sectional area of the flow stream changes along the many complex flow networks. Due to continuity, the velocity will not be constant. Flow rate and specific cross-sectional areas are substituted for velocity in the pressure loss equations. The flow rate is constant in a single path network and can be readily solved. In multi-path flow networks, the various flow rates will be determined with the pressure drop being equal along parallel paths.

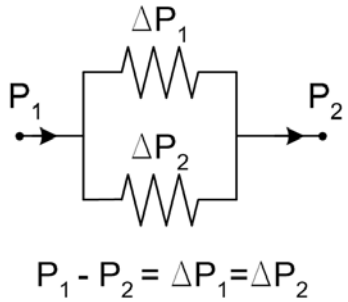

Figure 3-16: Parallel Circuit

Single entrance and exit flow networks are analyzed with these networks. Flow systems with multiple entrances and/or exits can also be solved with some iteration. However, complex multiple flow paths will not be explored in this study.

3.6. Effect of Transient Air Flows

The equations in this chapter have dealt only with steady-state flow to this point. The dynamic nature of the driving pressures also needs to be considered.

With a diurnal change in driving pressure due to solar effects the equations described in this chapter can be applied over hourly time-steps. The solar radiation source is relatively constant on an hourly basis and the effects of clouds and other anomalies are dampened by the thermal mass of the claddings.

Within highly fluctuating driving pressures and other anomalies an average pressure differential is typically applied. This method assumes incompressibility when volumetric flow rate is applied to the continuity equation. This assumption can be validation by examining the ideal gas law.

$$P_1V_1 = P_2V_2 \text{ (assuming constant temperature)} \quad (3\text{-}32)$$

where,

V is volume.

Assuming standard atmospheric pressure of 101300 Pa and considering that the dynamic pressure differences will tend to be below 10 Pa, the potential error due to the assumption of compressibility is in the order of 0.01%, which is insignificant for this analysis.

Another consideration is that system flow components can have a nonlinear pressure vs. flow rate relationship. Straube and Burnett's (1995) study of vents found that under dynamic (1 to 6s periods) applied pressures, the coefficient of discharge (for the orifice equation) increased for the vents tested. For a simple open vent slot the C_d value ranged from 0.89 to 1.37 for n value of 0.5. The C_d value depended on the applied pressure, application period, and the amplitude of applied pressure. These values are much greater than the theoretical C_d of 0.611 for n value or 0.5.

Another relevant concern is the well-mixed air assumption applied when analyzing the heat and mass transfer in these systems. This will be explored in the following chapters.

3.7. Airflow Circuits in Cladding Systems

The review of fluid flow analysis included in this chapter has been directed at the application to air flow networks within cladding systems. This section will describe some of the common ventilation systems behind wall claddings.

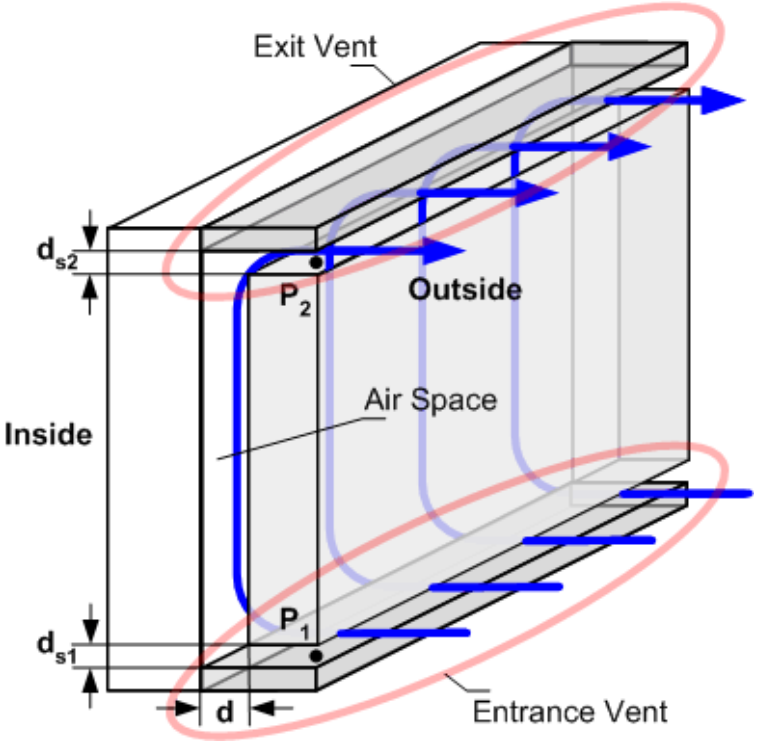

Figure 3-17: Wall with Top and Bottom Slots

A basic configuration for ventilating a cladding system is shown in Figure 3-17. Generally flow systems are simplified to

- an entrance vent,
- an air cavity, and
- an exit vent.

The system shown in Figure 3-17 consists of the following;

- an entrance vent consisting of
  - an abrupt entrance,
  - a short length of undeveloped flow, and
  - an elbow.
- an air cavity consisting of
  - a short length of undeveloped flow,
  - a wide and shallow rectangular conduit of developed flow, and
  - a short length of undeveloped flow.
- an exit vent consisting of
  - an elbow,
  - a short slot with undeveloped flow, and
  - an exit.

Assuming the slot length is relatively short, the undeveloped flow resistance can be assumed to be negligible.

The resistance through the cavity can be determined using the Darcy-Weisbach equation for a wide rectangular slot and assuming the flow immediately fully develops. The relationship between applied pressure and flow is:

$$\Delta P_{Total} = \Delta P_{entrance} + \Delta P_{cavity} + \Delta P_{exit} \tag{3-33}$$

$$= C_{entrance} \cdot 0.5\rho V^2 + \frac{32 k_f \cdot V \cdot \mu \cdot L}{4 d_{eq}^{\ 2}} + C_{exit} \cdot 0.5\rho V^2 \tag{3-34}$$

The loss coefficients are found for laminar flow by applying Equations (3-33) and (3-34):

$$C_{entrance} = \frac{6.5\,\mathrm{Re}^{-0.4}}{\bar{A}^2} + (0.066\ln(\mathrm{Re}) + 0.16)\cdot 0.5 + 0.885\cdot\left(\frac{d_{s1}}{d}\right)^{-0.86} \tag{3-35}$$

$$C_{exit} = \frac{6.5\,\mathrm{Re}^{-0.4}}{\bar{A}^2} + (0.066\ln(\mathrm{Re}) + 0.16) + 0.885\cdot\left(\frac{d}{d_{s2}}\right)^{-0.86} \tag{3-36}$$

3.7.1. Double Facades

Ventilated double facades are similar in configuration to a wall with top and bottom slots as shown in Figure 3-17 but with glazing as the cladding. The space behind the glazing is ventilated to reduce solar gains and to reduce condensation occurrence (Oesterle et. al 2001). These walls typically have a high ratio of clear glazing and contain shading devices. The solar radiation passes through the outer glazing and is absorbed by the shading elements. In order to avoid the flow of this heat inward, the space containing the shading is typically ventilated to the outdoors at each floor or over the entire wall height. For example consider the Helicon Building shown in Figure 3-18. Ventilation of the space is intended to reduce condensation on the outer glazing from the air passing outward through leaks in the inner curtain wall by diluting the air moisture content with drier outdoor air.

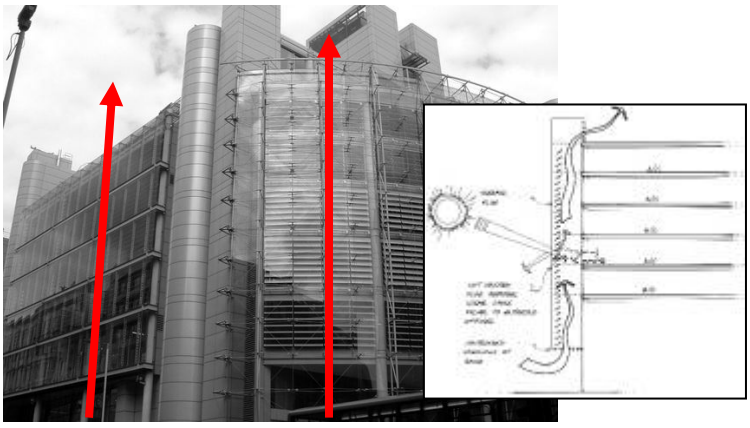

Figure 3-18: Airflow in Double Façade (Helicon, London)

Double facades vary from designs as simple as the schematic shown in Figure 3-17 to the elaborate design shown in Figure 3-21. Many contain shading that separates the vertical

cavity into two independent cavities as in the test assembly used by Saelens 2002 shown in Figure 3-19 and shown in the test flow results in Figure 3-20. More advanced designs (Figure 3-21) also incorporate optimized entrance and exit vents with vanes to reduce flow resistance. Air leakage from the inside to the cavity is significant with the use of typically leaky curtain systems. Many double facades also incorporate natural ventilation with controlled opening to the indoors. This investigation is limited to ventilation to the outdoors.

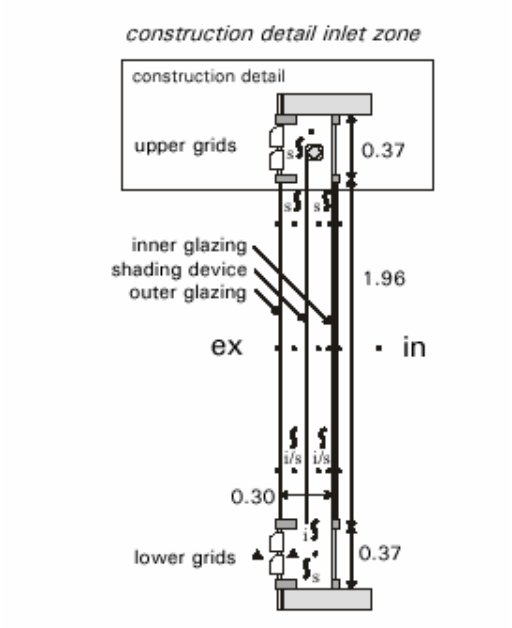

Figure 3-19: Test Double Façade Configuration with Divided Cavity (Saelens 2002)

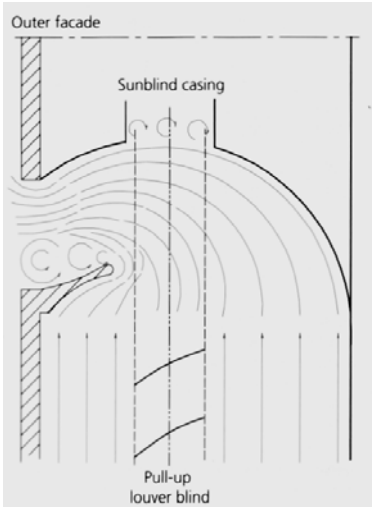

Figure 3-20: Advanced Double Façade Design (Oesterile et al 2001)

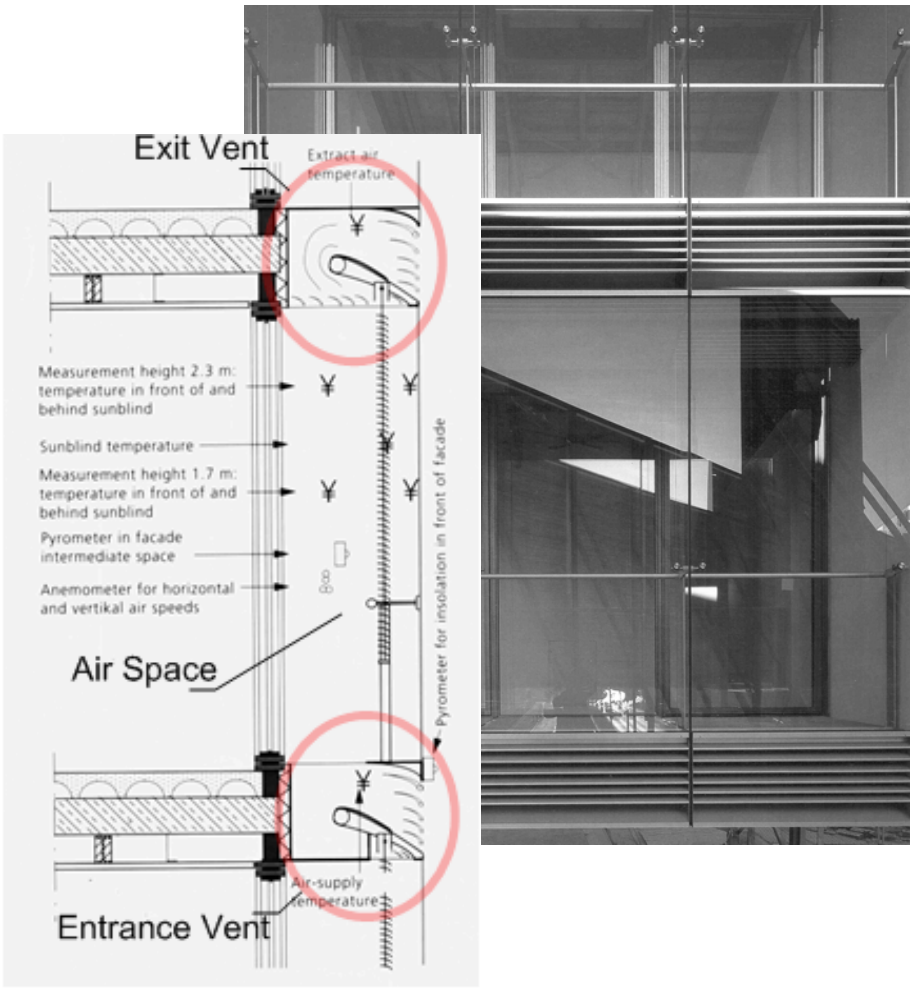

Figure 3-21: Advanced Double Façade Design (Oesterile et al 2001)

The loss coefficients of entrance and exit grids, turning vanes and other obstructions in double facades may not be found in the literature and may also interact with each other. Hence, determining the loss coefficient from theory may be difficult or impossible. However, in the practical design of these systems the vent components resistances would be determined and optimized with CFD analysis or flow resistance measurements at steady-state pressures. This optimization effort is applied to reduce the resistance in these systems and thereby encourage maximum ventilation.

A further difficulty with the airflow design in double façade cavities is the effects of shading elements dividing and directing the cavity airflow. These effects are most prevalent in continuous division of the separate spaces by pull down blinds as shown in Figure 3-19 and in Figure 3-20 for a tilted blind design. It is generally recommended to keep the shades positioned toward the outside layer of glass and hence not interfering with ventilation at the surface of the middle layer of glass. Since the shades are employed to reduce solar gains, removing heat from the inner portions of the glazing unit

is important. The shades can be lifted or opened allowing airflow during condensation period to remove moisture.

Equations similar to those used for slotted wall systems can be applied to these systems.

$$\Delta P_{Total} = \Delta P_{entrance} + \Delta P_{conduit} + \Delta P_{exit} \tag{3-37}$$

In this case the pressure drop across the conduit can be calculated for turbulent flow using Equation 3-38. There are two choices for analyzing the air cavity. One choice would be to ignore the division of the cavity by the sun shading device and use one large equivalent diameter.

$$\Delta P_{Total} = C_{entrance} \cdot 0.5\rho V^2 + \frac{k_f \cdot f(\mathrm{Re}, \varepsilon / D_h)\rho \cdot V^2 \cdot L}{4d_{eq}} + C_{exit} \cdot 0.5\rho V^2 \tag{3-38}$$

A more comprehensive approach would be to divide the cavity into two separate air streams. This approach allows more accurate prediction of temperatures and heat transfer coefficients adjacent to the inner and outer surface, but it is assumed that the shading device will act as a reasonable airflow separator.

$$\Delta P_{Total} = C_{entrance} \cdot 0.5\rho V^2 + \frac{k_f \cdot f(\mathrm{Re}_1, \varepsilon_1 / D_{h1})\rho \cdot V_1^2 \cdot L}{4d_{eq1}} + \frac{k_f \cdot f(\mathrm{Re}_2, \varepsilon_2 / D_{h2})\rho \cdot V_2^2 \cdot L}{4d_{eq2}} + C_{exit} \cdot 0.5\rho V^2 \tag{3-39}$$

Determining loss coefficients and the division of the flow between the potentially separate cavity airstreams would need to be determined by laboratory testing or predicted by CFD modeling.

3.7.2. Brick Veneer

Brick veneers are typically backed by an air space. The airspaces behind brickwork range from completely clear depths of over 50 mm to spaces completely filled with fibrous insulation or mortar. A repaired brick wall is shown in Figure 3-22. In this case the previous brick wall with only weep holes (bottom vents) was replace with multi-vented approach to encourage ventilation and thereby increase the wall's drying rate.

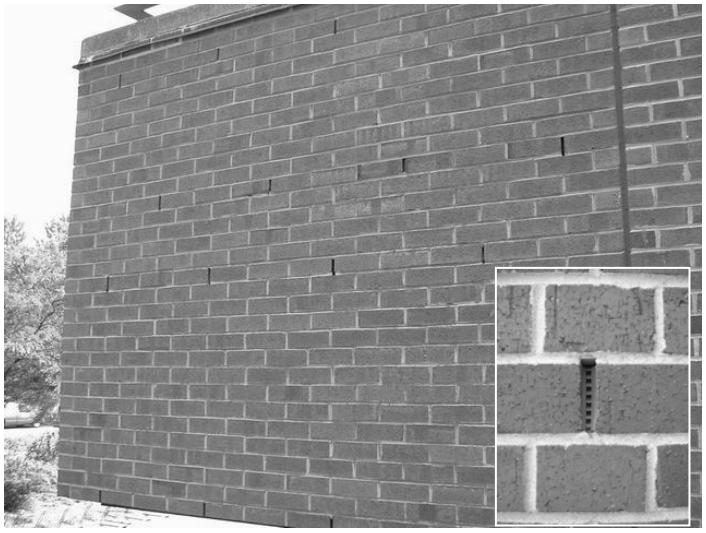

Figure 3-22: Repaired Ventilated Brick Veneer (Hagey Hall – Waterloo)

Straube and Burnett simplified such a system to two orifices separated by a cavity. As stated "Ventilation flow can be seen to be analogous to flow through an orifice into a rectangular duct and out again through an orifice"

Flow through the cavity is analyzed similar to the method presented in this section. The flow through the orifice is characterized by the sharp-edged orifice equation

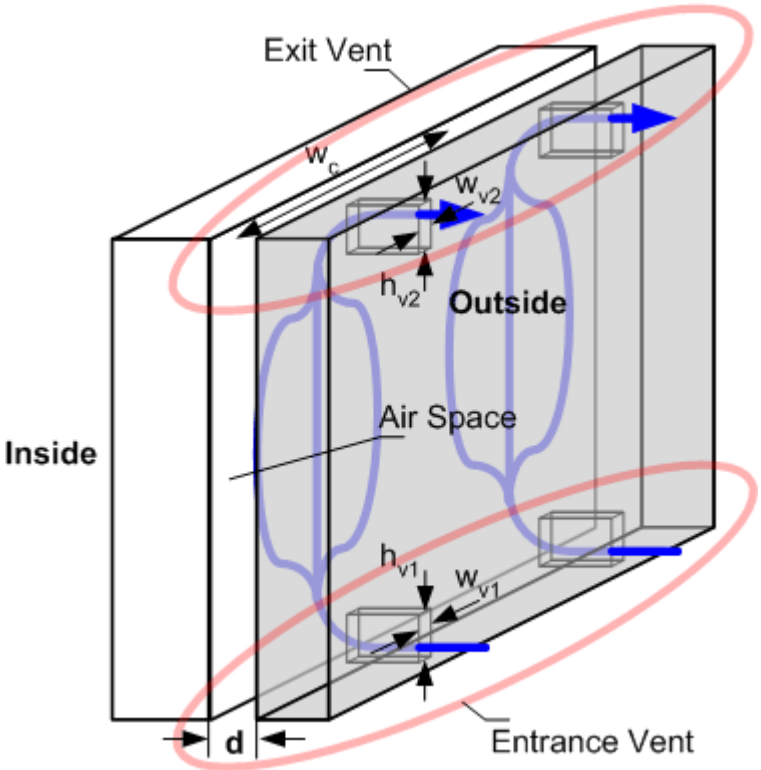

Figure 3-23: Wall with Top and Bottom Vent Holes.

In Straube and Burnett's analysis the airflow network is simplified to an entrance orifice, a cavity, and an exit orifice. The orifices are modeled as standard sharp edged orifices (ASHRAE 2001 F26.12).

$$\Delta P_v = \left(\frac{Q_v}{0.6 \cdot h_v \cdot w_v} \right)^2 \tag{3-40}$$

where,

Q_v is the airflow through the vent,

h_v is the vent height, and

w_v is the vent width.

Combining the entrance, cavity, and exit results in the following flow system equation

$$\Delta P_{Total} = \Delta P_{entrance} + \Delta P_{cavity} + \Delta P_{exit} \tag{3-41}$$

$$\Delta P_{Total} = \left(\frac{Q_{v1}}{0.6 \cdot h_{v1} \cdot w_{v1}} \right)^2 + \frac{32 k_f \cdot V \cdot \mu \cdot L}{4 d^2} + \left(\frac{Q_{v2}}{0.6 \cdot h_{v2} \cdot w_{v2}} \right)^2 \tag{3-42}$$

Assuming that the air flows in through the vent holes, immediately spreads evenly across the cavity and then travels vertically and exits results in the following equation:

$$\Delta P_{Total} = \left(\frac{Q}{0.6 \cdot h_{v1} \cdot w_{v1}} \right)^2 + \frac{32 k_f \cdot Q \cdot \mu \cdot L}{4 d^3 \cdot w_c} + \left(\frac{Q}{0.6 \cdot h_{v2} \cdot w_{v2}} \right)^2 \tag{3-43}$$

The value for k_f in the above equation would be 1.5 for wide wall sections. For narrow wall sections Table 3-1 should be consulted for an appropriate value.

The use of the orifice equation is justified based on the laboratory testing by Straube and Burnett (1995). This testing included steady state and dynamic flow resistance measurements for several brick inserts. However, dynamic flows did not result in predictable pressures using orifice theory.

Several assumptions and simplifications remain in the application of this equation:

- The change in flow direction between the vent and cavity adds negligible resistance,
- The air stream spreads across the indicated cavity width and fully develops immediately upon entrance, and
- The air stream follows a single path between vertical vents.
    - Vents in brickwork are often situated at the bottom of an enclosed cavity space to perform the dual function of a drainage outlet for water in the cavity. The placement of the vents at the top and bottom of closed sections of the cavity justifies the simplification of a single entrance and a single exit along the vertical plane. Upper vent holes are typically situated under some break in the air cavity space (i.e. a window sill, a sill plate, a parapet, etc.).

The assumption that a majority of the airflow is in a vertical path instead of crossing over to other horizontally displaced vents depends on the characteristics of the driving pressure characteristics and will be discussed in the next chapter.

In many residential installations brick veneers are applied with bottom vents and the cavity is left open at the top to ventilate into the attic. This is the likely configuration of the brick veneer wall shown in Figure 3-24.

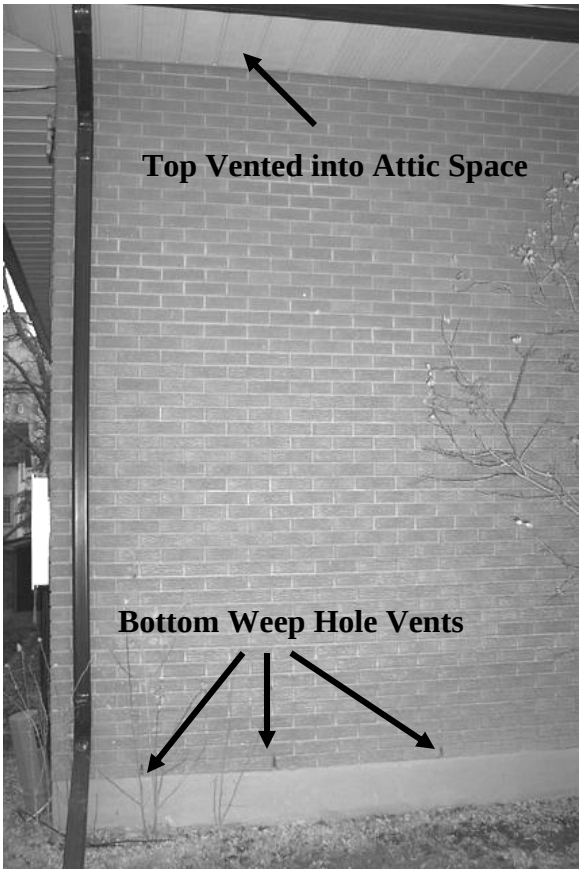

Figure 3-24: Brick Veneer with Bottom Vents and Open Slot at Top

This system would be modeled as an orifice, a cavity, and an exit

$$\Delta P_{Total} = \left(\frac{Q}{0.6 \cdot h_{v1} \cdot w_{v1}} \right)^2 + \frac{32 k_f \cdot Q \cdot \mu \cdot L}{4 d^3 \cdot w_c} + C_{exit} \cdot 0.5 \cdot \rho \left(\frac{Q}{d \cdot w_c} \right)^2 \qquad (3\text{-}44)$$

In multistory applications of brick veneer, the top of the cavity is typically blocked by a shelf angle or capped at parapets. In brick veneer systems with bottom weep holes, ventilation would only still occur due to the pressure gradient between the horizontally spaced weep holes and moisture and thermally induced circulation within the cavity. While it would be difficult to predict these flows, the effects of ventilation were observed in laboratory testing by Hazleden and Morris (2001). The air travels between vertically displaced vents, enters and exits through different portions of the vent area, or the density of the air in the airspace is changing causing billowing. In field wall systems there will likely be some crack openings at the joints at the top of wall allowing limited vertical

flow. The ventilation in such wall systems is difficult to predict but will be further investigated in this thesis.

3.7.3. Ventilated Stucco and EIFS

The airflow through a ventilated stucco or EIFS typically enters through a vent or slot inlet, through a narrow cavity with a consistent complex cross section, and exits through a vent or slot outlet. The models from the previously described systems apply to this case with the additional consideration of hydraulic diameter. These systems will tend to have complex cavities that are inserted mainly for the purpose of drainage and are very narrow.

Three examples of ventilated stucco systems are included in Figure 3-25, Figure 3-26 and Figure 3-27.

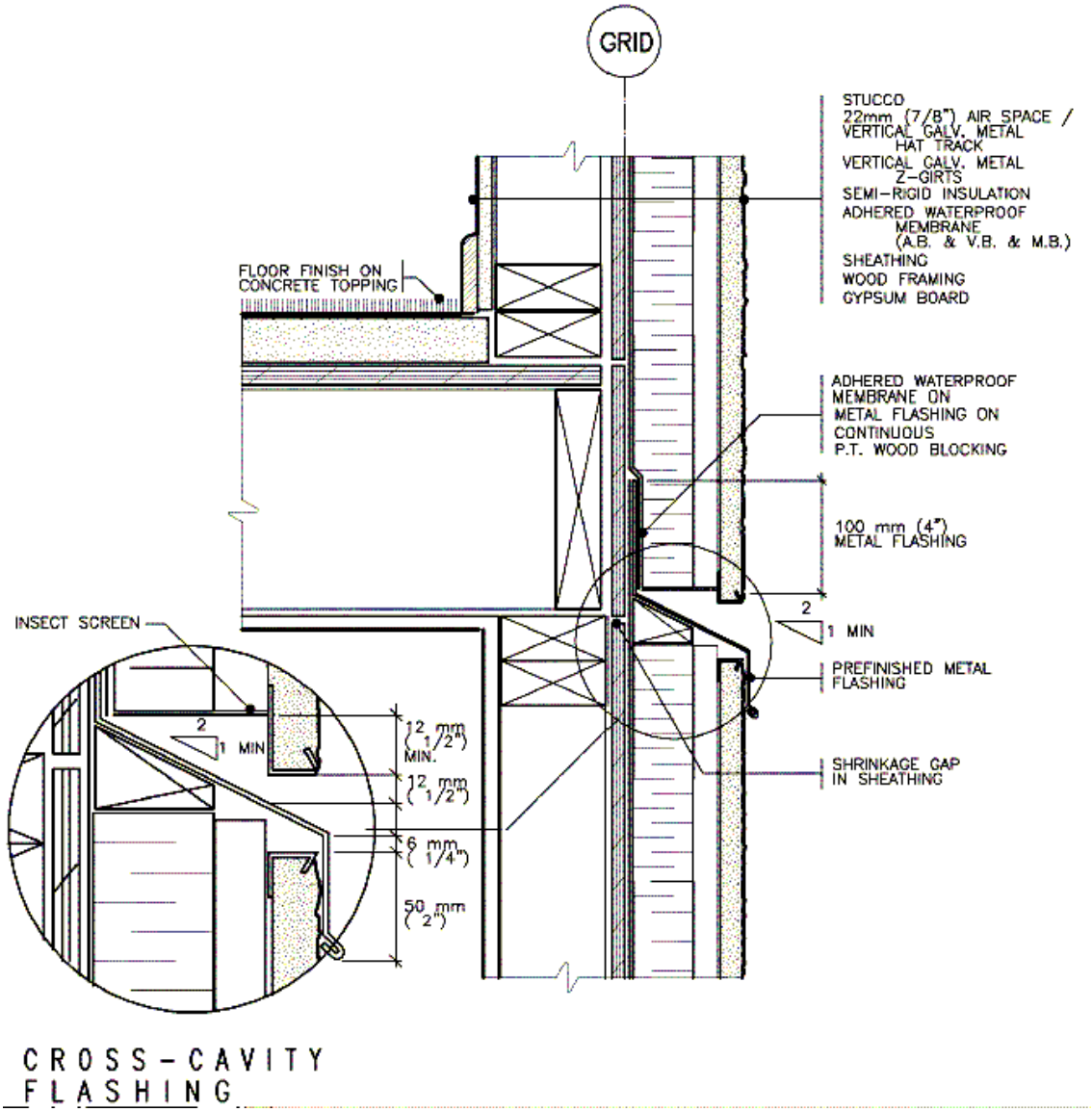

Figure 3-25: Rim Joist Detail for Ventilated Stucco (CMHC 1999)

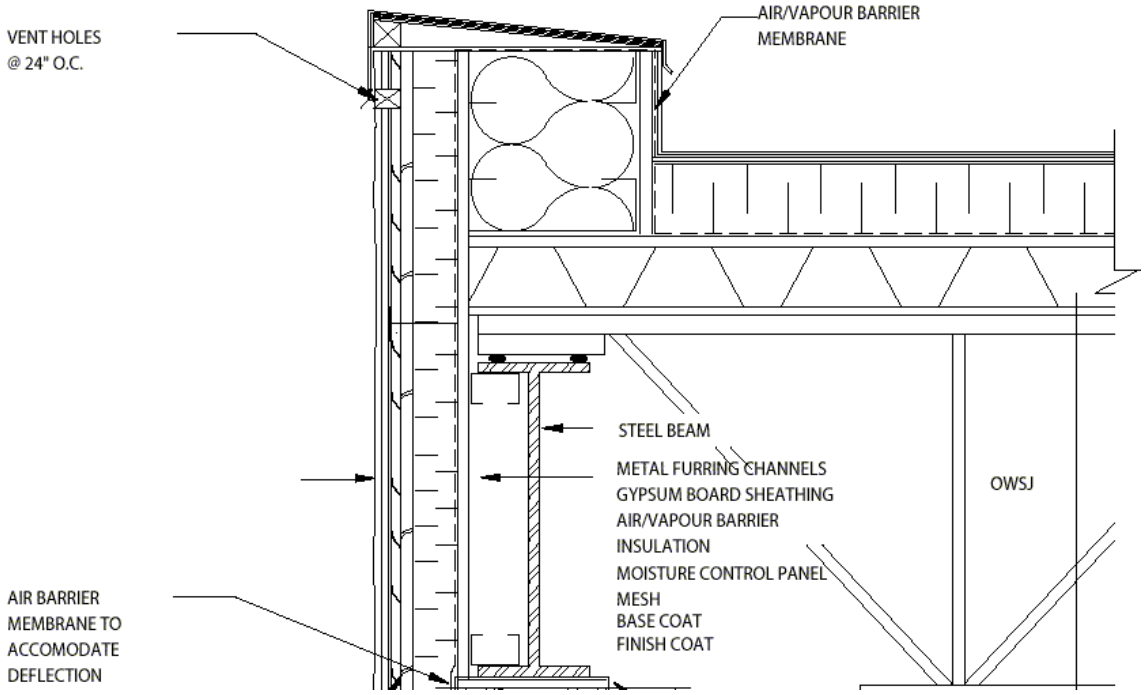

Figure 3-26: Parapet Detail of Ventilated Stucco System (www.Koraxtech.com)

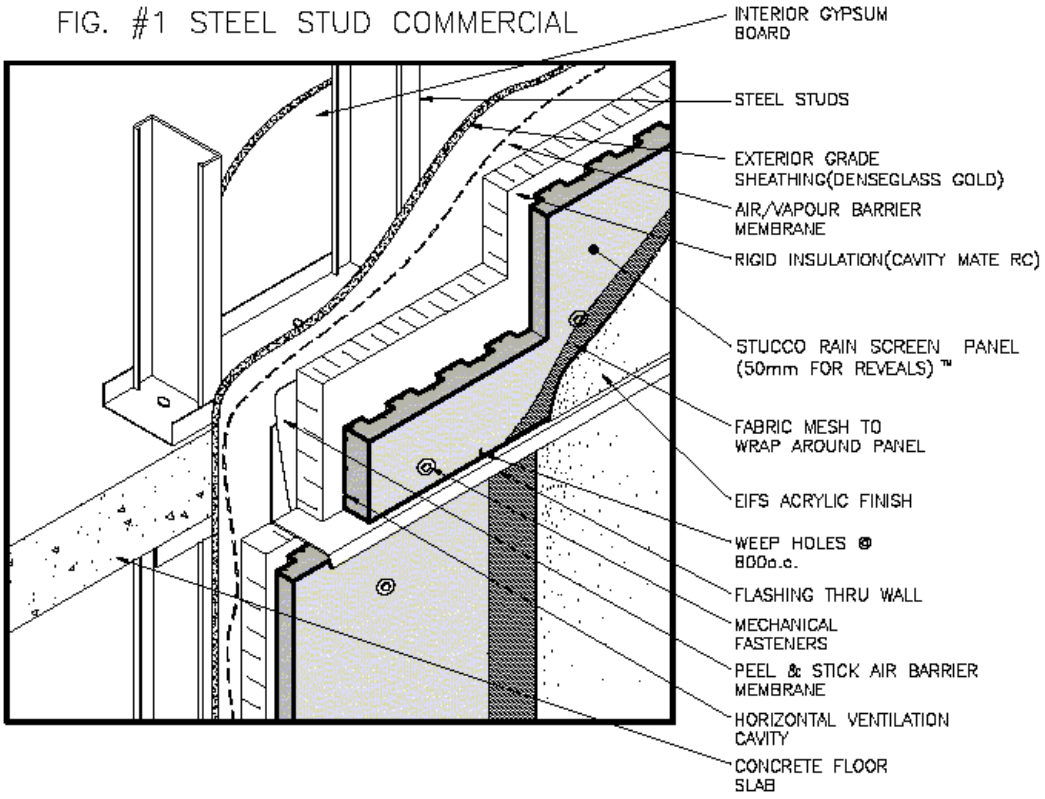

Figure 3-27: Mid-Floor Detail of Rainscreen Stucco System (www.Koraxtech.com)

A simplified schematic of a ventilated stucco or EIFS system is shown in Figure 3-28.

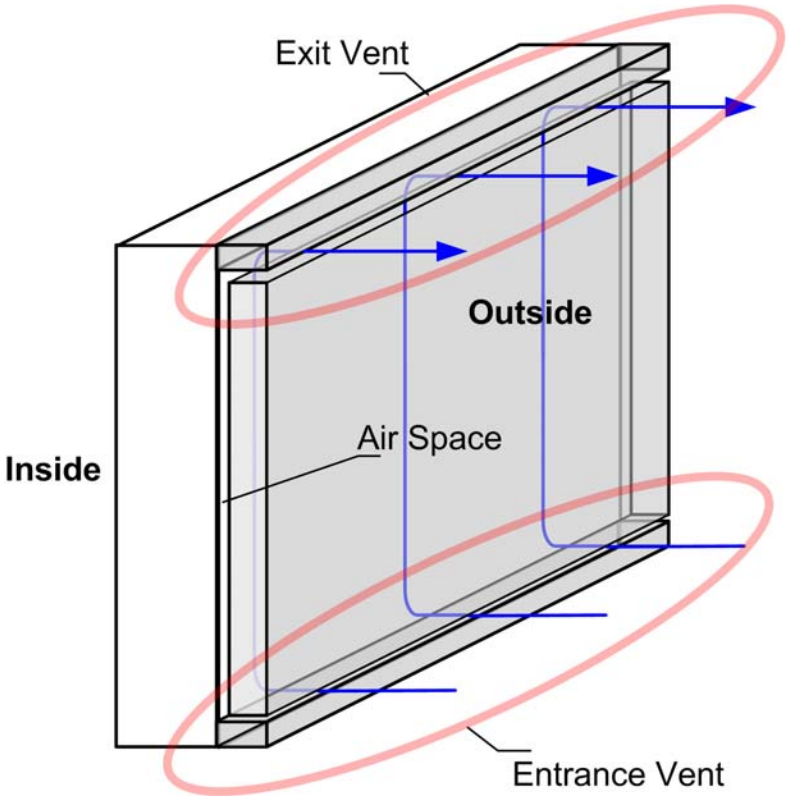

Figure 3-28: Ventilated EIFS or Stucco Wall System

If a system contains complex cross sections blockage factors and loss coefficients at entrances and exits need to be found empirically. After a body of results for these parameters has been built, estimations for airflow resistance characteristics of such systems that have not been laboratory tested could be made. The airflow resistance of these systems would be in the following form:

$$\Delta P_{Total} = \Delta P_{entrance} + \Delta P_{cavity} + \Delta P_{exit} \tag{3-45}$$

$$\Delta P_{Total} = C_{entrance} \cdot 0.5\rho V^2 + \frac{32 k_f \cdot V \cdot \mu \cdot L}{\gamma \cdot D_h{}^2} + C_{exit} \cdot 0.5\rho V^2 \tag{3-46}$$

Since these systems typically contain small tortuous air cavities, systems with only drainage holes will have minimal airflow and ventilation.

3.7.4. Siding Systems

Horizontal lap wood siding and its cement fibreboard, polyvinyl chloride, and aluminum replicas are examples of cladding systems with cavities ventilated through distributed vent holes. To this point in the chapter, flow direction has been largely assumed to be vertical. In the case of contact applied siding, the majority of the flow may run horizontally, entering and exiting through loosely assembled joints and edges.

Pressnail el al (2003) studied the effect of ventilation on wood clad walls in a series of studies of the drying rates of walls placed in a climate chamber and exposed to simulate solar heating. In the study, long slots of different thicknesses were left at the bottom of the 1.2 m wide by 2.4 m high cladding sections. This was done to control the ventilation rate of stack driven flow. As the wood siding dried, 2 mm gaps were observed to form between the 200 mm wide wood cladding elements. This was found to allow significant ventilation and was assumed to affect the performance the wall specimen. To confirm this, the joints were taped in one wall test and the drying rate was significantly affected. An illustration of potential airflows behind a siding is shown in Figure 3-29 and Figure 3-30.

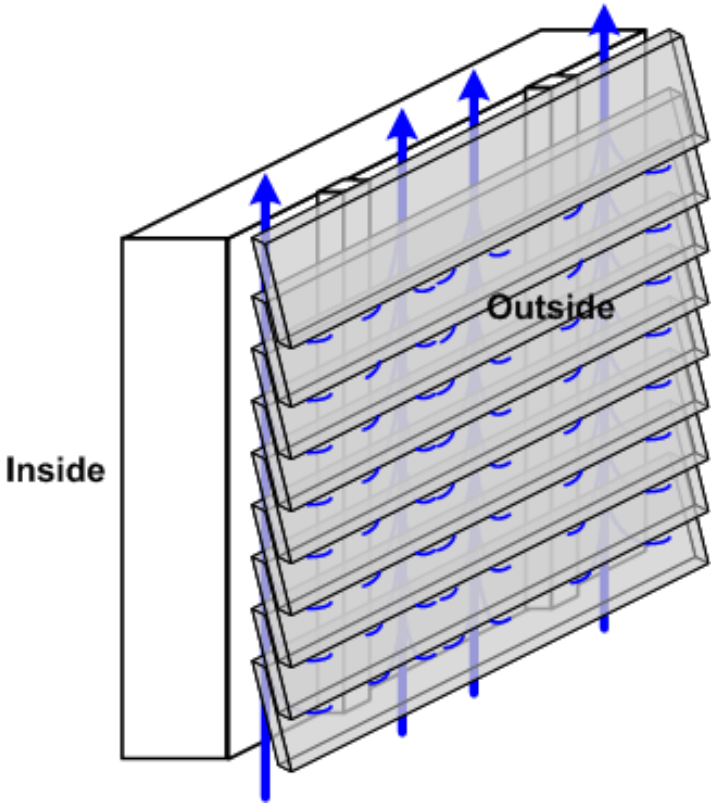

Figure 3-29: Ventilation of Siding on Strapping

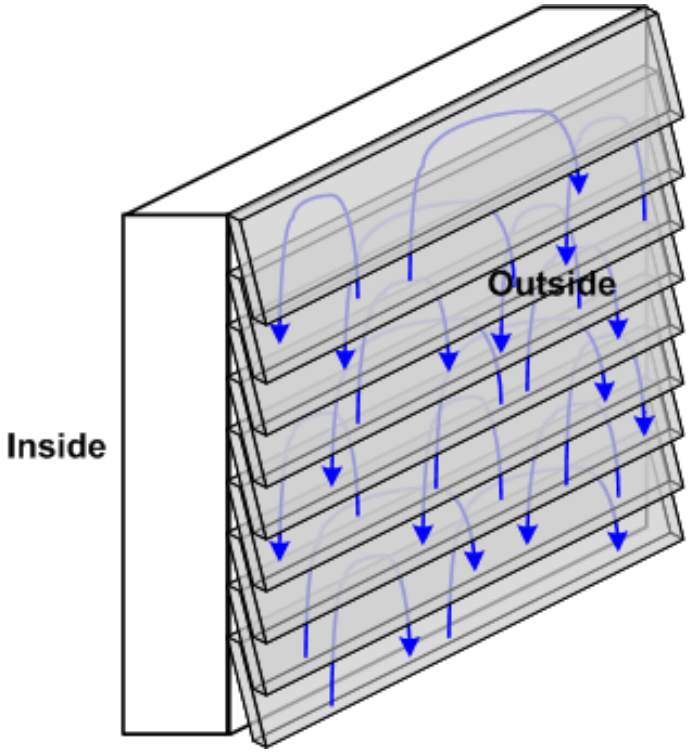

Figure 3-30: Ventilation of Contact Applied Siding

Figure 3-29 and Figure 3-30 show simplified airflow networks in typical wood and cement fibreboard siding application and are probably similar to the actual flows occurring in Pressnail's experiments. Modeling the airflow networks within field installations is complicated since flow is dominated by openings at edges and joints in these systems. Such geometries in installations of aluminum and vinyl siding are shown in Figure 3-31 and Figure 3-32. A multitude of possible flow paths exist in these installations. Modeling the many airflow paths directly and choosing reasonable applied pressures is difficult and will not be attempted in this study.

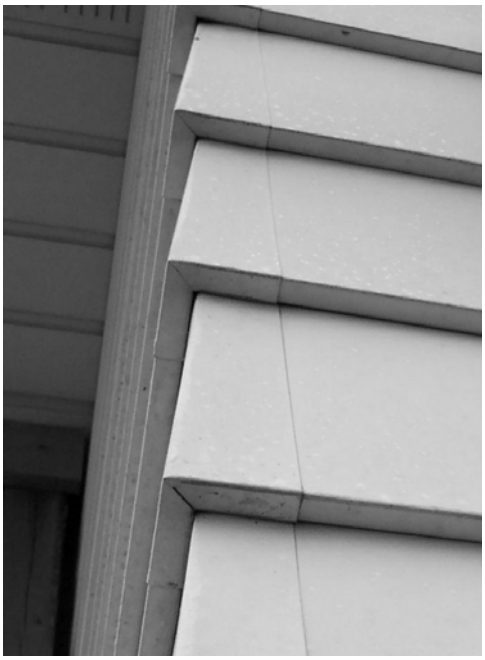

Figure 3-31: Typical Installation of Aluminum Siding (Waterloo, Canada)

Figure 3-32: Typical Installation of Vinyl Siding (Waterloo, Canada)

Most of the available work is speculative but reasonably derived from calculations of drying rates (Straube and Burnett 1995). Laboratory exploration of the airflow characteristics of one type of vinyl siding is documented in the next section of this thesis.

3.8. Closure

The ventilation airflow systems of several common wall systems can be modeled employing available airflow resistance correlations. The systems investigated included

naturally ventilated double facades, ventilated brick veneers, and ventilated EIF systems. An exception that was also discussed was horizontal lap siding systems. Further investigation of an example of such a system will be described Chapter 6.

3.9. References.

ASHRAE, *Handbook of Fundamentals* Atlanta, Ga, 2001.

CMHC Best Practise Guide Wood-Frame Envelopes in the Coastal Climate of British Columbia, Canadian Mortgage and Housing Corporation, Ottawa 1999.

Handegord G., Hutcheon, N. Building *Science for a Cold Climate,* Canadian Institute for Research in Construction, Ottawa 1995, pg 133.

Hazleden, D., Morris, P., "The Influence of Design on Drying of Wood-Framed Walls Under Controlled Conditions", *Proc of Thermal Performance of Building Envelopes VIII* Florida, 2001.

Holman, J., *Experimental Methods For Engineers* 6th Ed. McGraw-Hill 1994, pg 273.

Idelchik *Handbook of Hydraulic Resistance* Hemisphere Publishing 1993, pg 77, pg 75, pg 118, pg 36.

Incropera, F., DeWitt, D., *Fundamentals of Mass and Heat Transfer* 4th Ed. Wiley 1996, pg 421.

Loomans, M., *The Measurement and Simulation of Indoor Airflow,* Techniche Universiteit Eindhoven 1998.

Munson, B., Young, D., Okiishi, T., *Fundamentals of Fluid Mechanics,* 3rd edition Wiley 1998, pg 461, pg 493, pg 364.

Oesterle, E., Lieb, R., Lutz, M., Heusler, W. *Double-Skin Facades.* Prestel, Munich, 2001.

Pressnail K., Timusk J., Kan L., Dong B., Kan V., University of Toronto "In Search of a Wall for All Season: Controlling Sun Driven Moisture", *9th Canadian Conference on Building Science and Technology,* Vancouver 2003.

Saelens, D., *Energy Performance Assessment of Multiple-Skin Facades*, PhD dissertation, Leuven: KU Leuven, Laboratory of Building Physics, 2002.

Straube, J., Burnett E., *Vents, Ventilation Drying, and Pressure Moderation,* Report for CMHC 1995, pg 4.4, pg 2.13, section 2.

Streeter, V., Wylie, B., *Fluid Mechanics,* McGraw-Hill 1985.

White, F., *Viscous Fluid Flow,* McGraw-Hill 1991, pg 122.

4. MECHANISMS DRIVING ENCLOSURE VENTILATION

4.1. Introduction

The concept of ventilating building enclosures and the fluid mechanics of typical airflow systems involved have been presented in the previous two chapters. This chapter will describe the forces driving the airflow through these systems. Airflow as a function of steadily applied pressures has been investigated. In this chapter the applied pressures will be determined from mechanical system parameters and/or weather induced effects and non-steady pressure effects will be investigated.

These driving forces will be discussed in terms of pressure differentials forcing airflow through an airflow system circuit. This static pressure differential can be described as driving flow from two different standpoints (Munson et al 1998); in terms of force balance, the pressure force is needed to overcome the viscous forces generated; and in terms of energy balance, the work done by the pressure force is needed to overcome the viscous dissipation of energy throughout the fluid. The difference of P_1 and P_2 in Equation 4-1 is the driving force.

$$\Delta P_{1-2} = \Delta P_{losses} \tag{4-1}$$

P_1 and P_2 represent the nodes in the simple circuit diagram shown below in Figure 4-1.

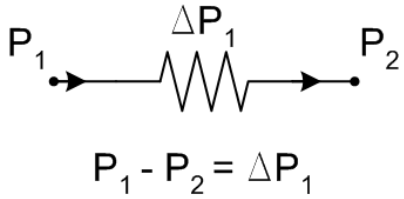

Figure 4-1: Simple Circuit

The forces that drive air movement in building systems are typically categorized as mechanical, stack, and wind forces. These forces will be discussed separately in the following sections of this chapter.

The primary categorization of ventilation systems due to driving forces are mechanical, natural, or hybrid ventilation systems. Mechanical systems involve the generation of driving forces by means of energy applied through the operation of an appliance. This definition includes all appliances except those that generate the driving pressure through diverting wind forces or creating buoyancy driven flow. Hence, in natural ventilation systems the driving force is generated by means of wind forces or by buoyancy driven flow. For natural ventilation the generation also must be direct. An example of indirect generation would be the use of a wind turbine to generate electricity or turn a crank that runs a fan: this system would be a mechanical ventilation system. Changing air density (i.e. by heat production) in a space to driving buoyancy forces would be a natural

ventilation system. Hybrid systems employ a combination of mechanical and natural forces to drive airflow.

4.2. Mechanical

Mechanical ventilation typically employs a fan through which lift and drag forces create a pressure differential across the fan blades. Mechanical ventilation tends to be a steady applied force that is controlled. Dynamic effects typically need not to be considered as the controls are typically activated over long (> 1 hour) periods.

The pressure differential for enclosure ventilation can change with varying airflow system resistances. Hence, mechanical systems have a performance curve or a fan curve that is used to estimate the resultant flowrate. Fan curves are plots of system static pressure drop versus airflow rate generated by the fan. For a direct drive fan a single curve for the fan performance is plotted. A difficulty with such plots is that the system static pressure curve will change with time as filters fill and dampers are opened and closed. Typically the fans are oversized to compensate but variable speed drive fans can be employed to compensate for such changes. The characteristic of mechanically applied driving pressure is mathematically described below.

$$\Delta P_M = f(\Delta P_{System}, \text{fan performance}) \tag{4-2}$$

$$\Delta P_{System} \ \& \ \text{fan performance} \approx \text{constant} \tag{4-3}$$

$$\therefore \Delta P_M \approx \text{constant} \tag{4-4}$$

Mechanical systems are rarely employed for maintaining enclosure conditions or enhancing enclosure performance due to maintenance and cost issues.

The Telus building in Vancouver, Canada was renovated in the late 1990's by adding a mechanically ventilated air space behind a glass façade and a schematic is shown in Figure 4-2. The space is semi-conditioned by outdoor air driven by a combination of buoyancy and photovoltaic-powered fans. A simplified illustration of this approach with only one set of bottom vents is show in Figure 4-3.

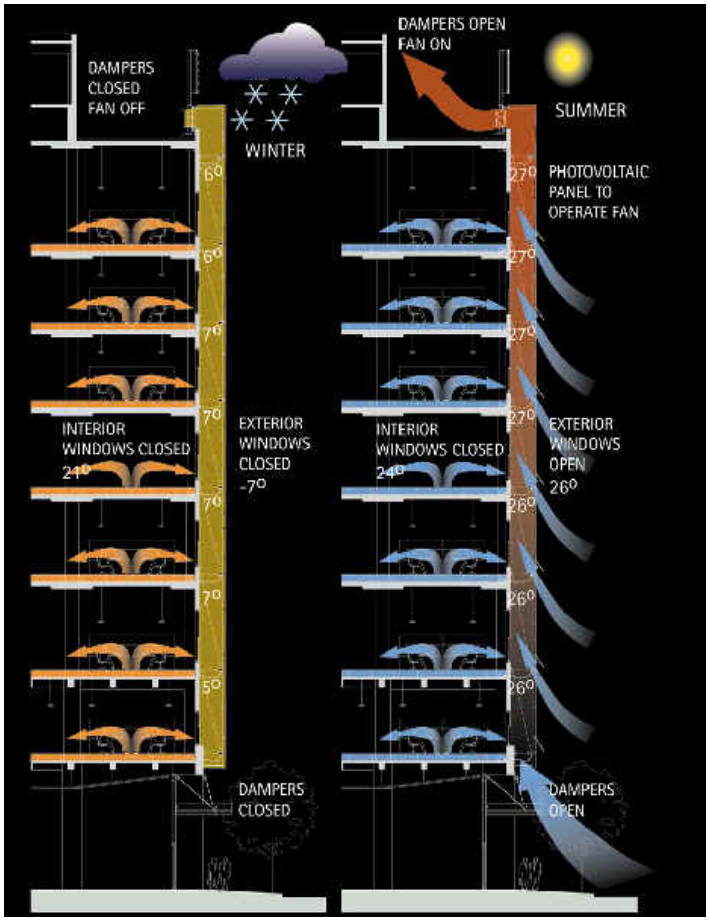

Figure 4-2: Mechanical Ventilation of Double Façade (Telus Building Vancouver).

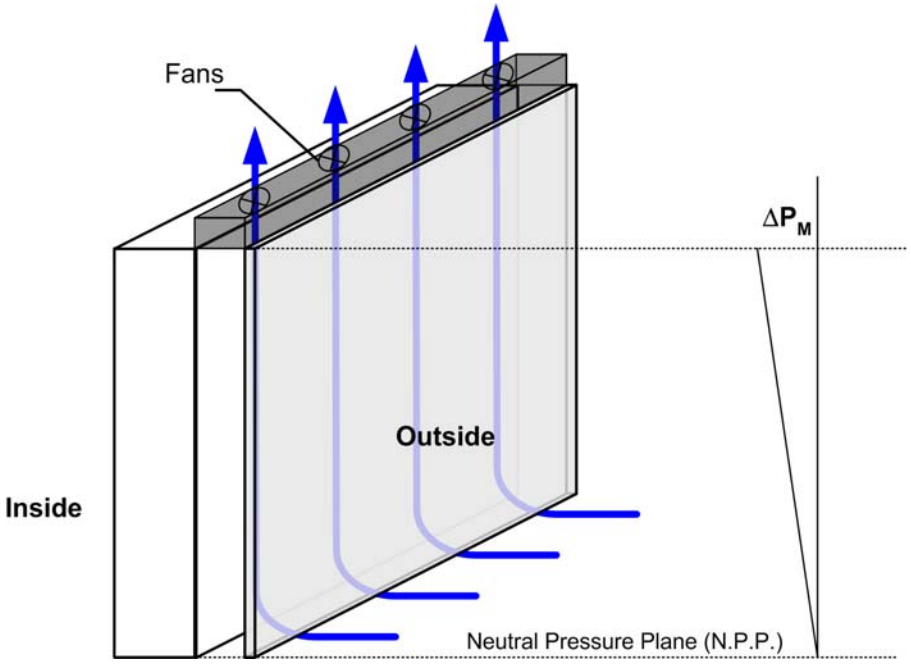

Figure 4-3: Simplified Mechanically Ventilated Double Façade

4.3. Buoyancy

Within the category of natural ventilation systems the airflow can be forced through the system by buoyancy, wind pressures, and to a lesser extent by natural pumping effects. Buoyancy forces result from a density differential over a vertical gradient. The pressure generated is independent of the system flow resistance. Buoyancy forces are generated internally within the airflow system. Bernoulli's equation describes the quantity of these forces.

$$\Delta P_B = \Delta \rho g h \tag{4-5}$$

where,

$\Delta\rho$ is the difference in density,

g is the gravitational constant, and

h is the height over which the density gradient exists.

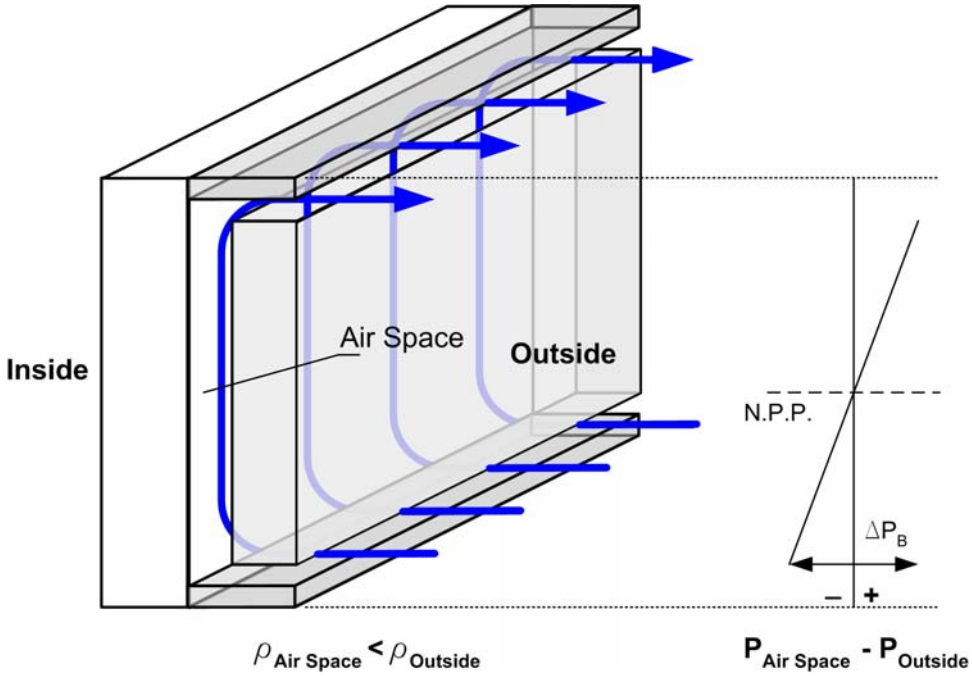

Figure 4-4: Buoyancy Forces

Density differentials due to thermal and moisture buoyancy drive enclosure ventilation. Air and water vapour can be treated as ideal gases. Through the ideal gas law, density changes directly with pressure and inversely with temperature.

$$\rho_a = \frac{P_a}{R_a T} \tag{4-6}$$

where,

ρ_a is the air density,

P_a is the absolute static pressure of the air,

R_a is the gas constant for air, and

T is the temperature.

$$\rho_v = \frac{P_v}{R_v T} \tag{4-7}$$

where,

ρ_v is the density of water vapour,

P_v is the absolute vapour pressure (or partial vapour pressure), and

R_v is the gas constant for water vapour.

The partial vapour pressure can be found from relative humidity and temperature conditions (ASHRAE 2001 F6). Assuming a total pressure at standard conditions of about 101325 Pa, Dalton's Law of partial pressures (Handegord and Hutcheon 1995) can be applied to determine the resultant dry air portion of the pressure.

$$P_T = P_a + P_v \approx 101325 \text{ Pa} \tag{4-8}$$

where,

P_T is the atmospheric pressure.

The total air densities of the cavity and outdoor air need to be determined. If the cavity density is lower than the outdoor air density then the air will tend to flow upward within the cavity and vice-versa. The densities of the cavity and outdoor air can be found by employing the ideal gas relations.

$$\rho_{exterior} = \rho_{a,exterior} + \rho_{v,exterior} = \frac{P_{a,exterior}}{R_a T_{exterior}} + \frac{P_{v,exterior}}{R_v T_{exterior}} \tag{4-9}$$

$$\rho_{cavity} = \rho_{a,cavity} + \rho_{v,cavity} = \frac{P_{a,cavity}}{R_a T_{cavity}} + \frac{P_{v,cavity}}{R_v T_{cavity}} \tag{4-10}$$

Combining Equations 4-5, 4-8, 4-9, and 4-10 results in the following equation for buoyancy pressure as a function of cavity and outdoor temperature and humidity conditions.

$$\Delta P_B = \left[\rho_{exterior} - \rho_{cavity} \right] gh \tag{4-11}$$

$$\Delta P_B = \left[\left(\frac{P_{a,exterior}}{R_a T_{exterior}} + \frac{P_{v,exterior}}{R_v T_{exterior}} \right) - \left(\frac{P_{a,cavity}}{R_a T_{cavity}} + \frac{P_{v,cavity}}{R_v T_{cavity}} \right) \right] gh \tag{4-12}$$

Figure 4-5 and Figure 4-6 show Equation 4-12 applied to very damp (100% relative humidity) cavity conditions and Figure 4-7 and Figure 4-8 are for a less damp condition (85% relative humidity). Results from calculations for buoyancy pressures considering only thermally induced buoyancy are also plotted using short dashed lines. The outside temperature and relative humidity are indicated in the legend as Te and Rhe, respectively.

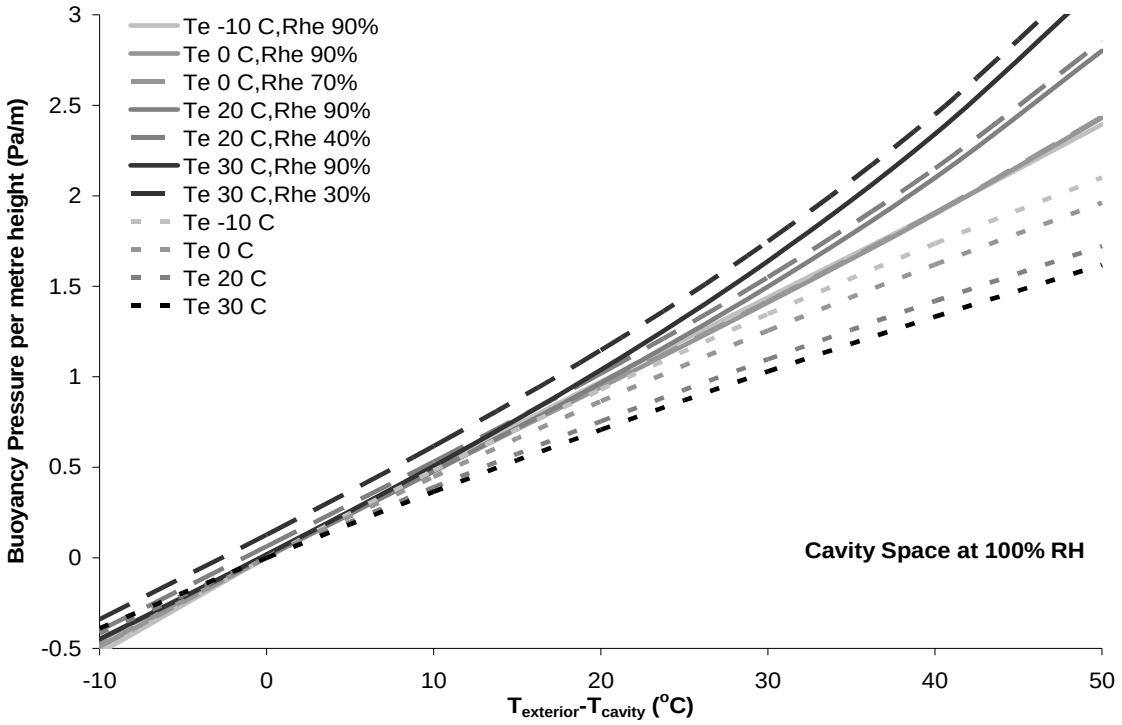

Figure 4-5: Buoyancy Pressures Generated within a Very Damp Cavity

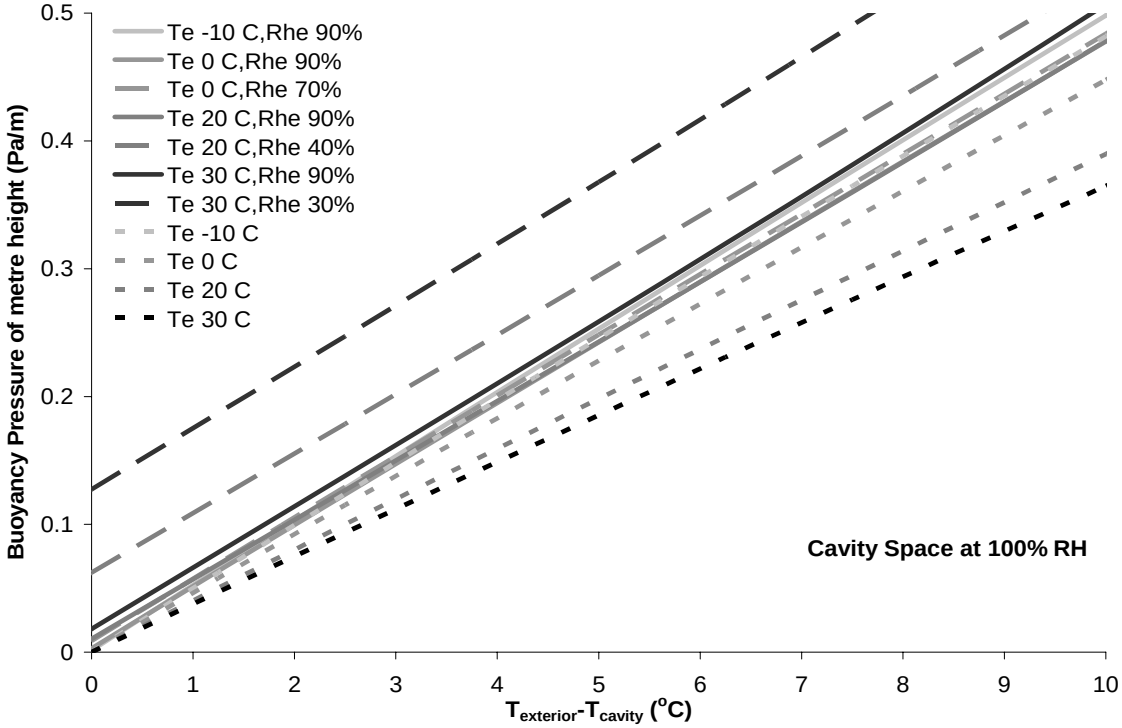

Figure 4-6: Buoyancy Pressures Generated within a Very Damp Cavity (detail)

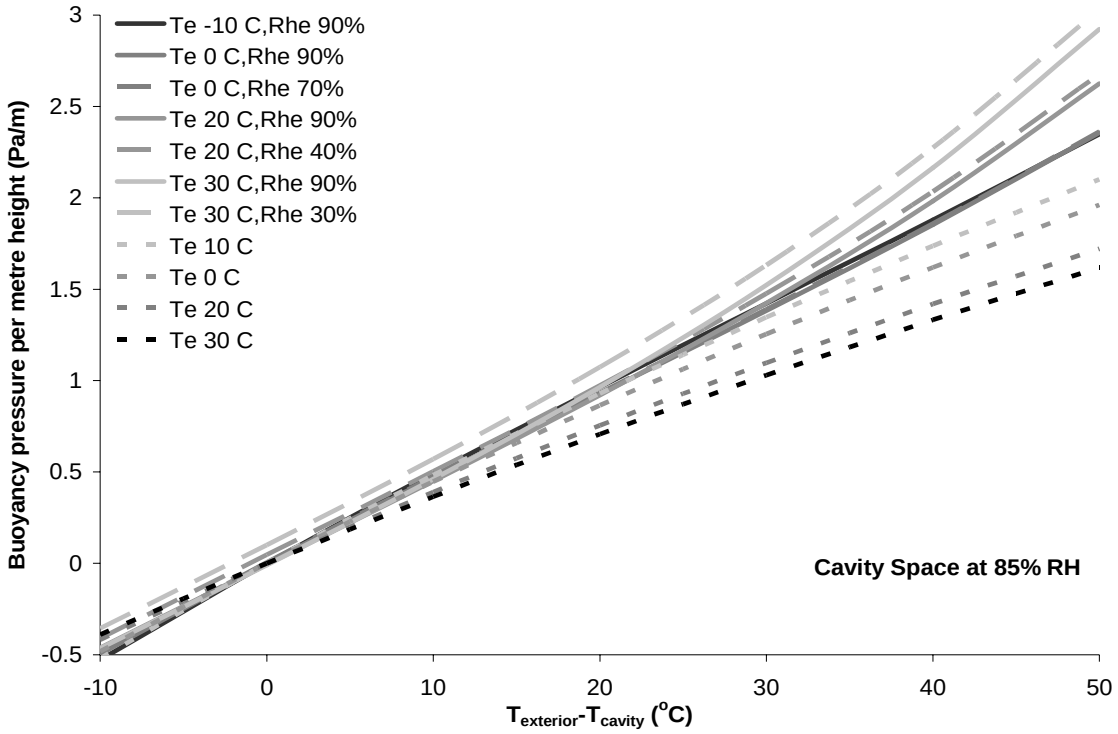

Figure 4-7: Buoyancy Pressures Generated within a Damp Cavity

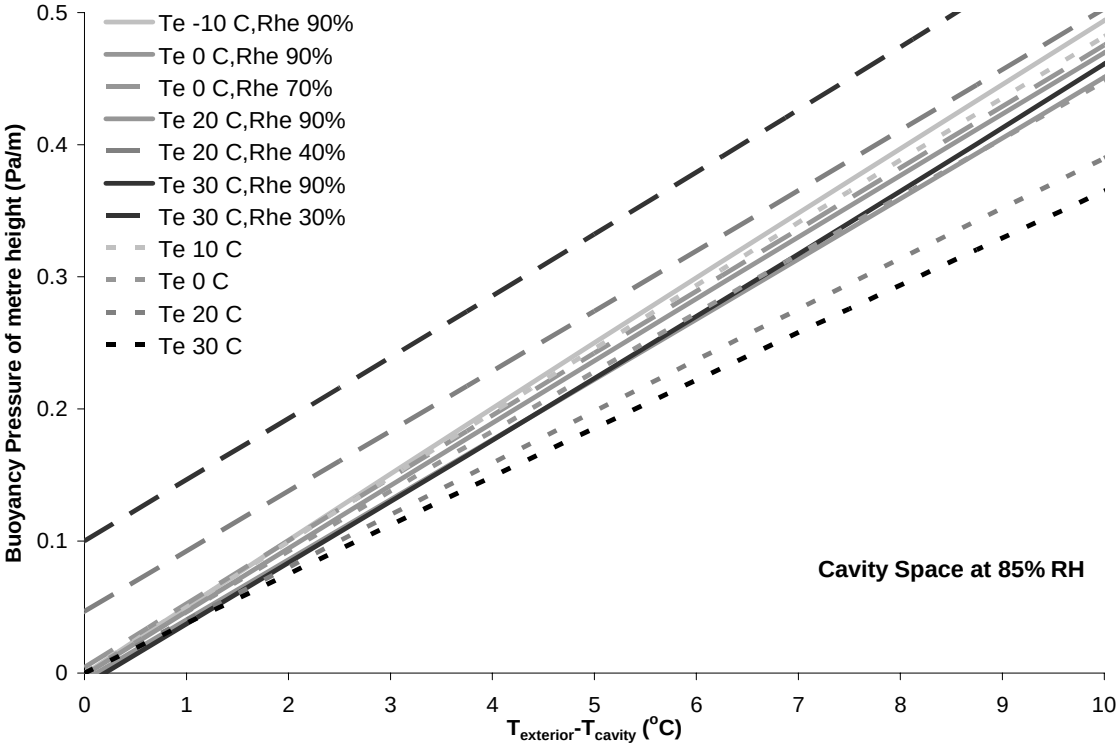

Figure 4-8: Buoyancy Pressures Generated within a Damp Cavity (detail)

Buoyancy pressures are commonly calculated only considering thermal effects. The addition of water vapour to air lowers it density because water vapour is less dense than dry air. Pressnail et. al. (2003) demonstrated the relevance of moisture induced buoyancy during laboratory testing of solar driven inward vapour flow. At high temperatures (30^{o}C) the driving buoyancy pressure could be 30% to 50% greater for wet cavities than predictions considering only thermal effects. Hence, moisture buoyancy can have a significant effect on cavity ventilation in enclosure wall systems when the ventilation cavity is surrounding by wet materials.

Thermally induced buoyancy pressures tend to vary due to the diurnal cycling of temperature and solar input. Solar radiation heats the cladding and in turn elevates the cavity air temperature above the outdoor air temperature. Although the solar input can fluctuate due to scattered cloud, the thermal mass of the cladding has a dampening effect and allows the buoyancy pressures to be determined on an hourly basis for accurate calculations.

Moisture induced buoyancy will tend to vary on either a diurnal cycle (inward vapour drives and exfiltration air leakage condensation) or from sporadic moisture loads (rain water leaks). The diurnal cycling is similar to thermal effect and can be handled with transient modeling incorporating the hygric capacity of building materials. Sporadic moisture loads may require varying lengths of time to dry. However, moisture loads that dry out within an hour are not of concern in typical building enclosure systems.

4.4. Wind

Wind induced pressures also drive airflow in naturally ventilated systems. Wind imposes horizontal and vertical pressure gradients on building surfaces. The entrances and exits of enclosure airflow networks may be situated across these gradients. Hence a driving pressure is formed across the airflow network as illustrated in Figure 4-9. The pressure differentials generated are independent of the system flow resistance.

$$\Delta P_W = P_{1,surface} - P_{2,surface} \tag{4-13}$$

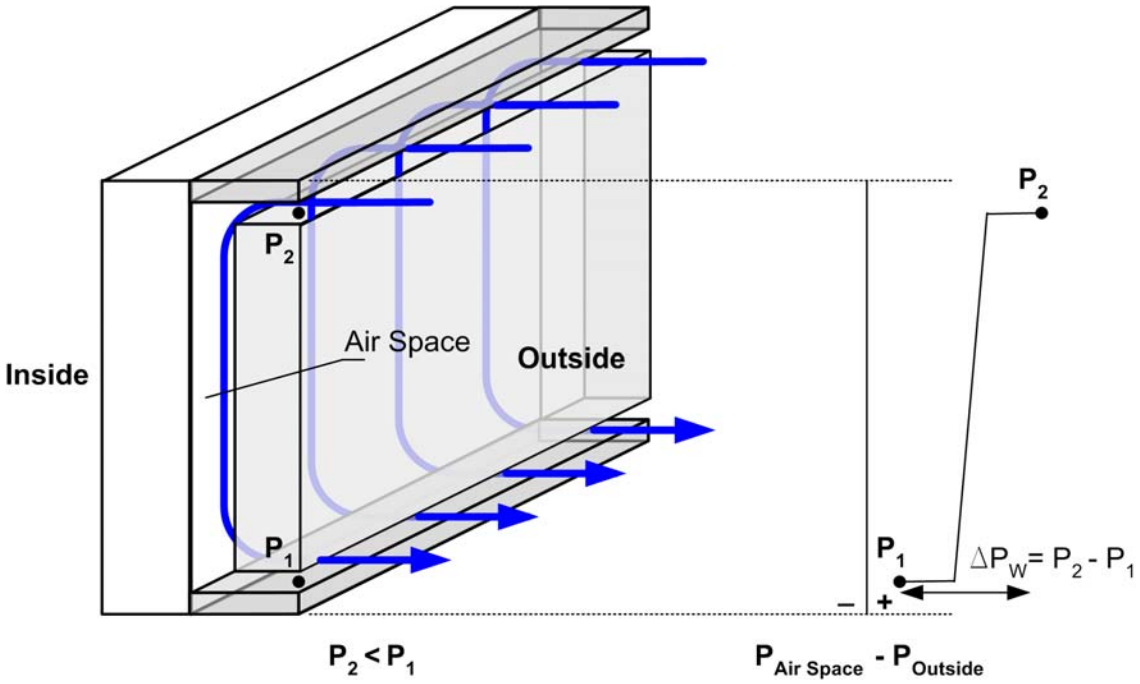

Figure 4-9: Wind Forces

The interruption of wind flow by buildings causes the kinetic energy of the wind to convert to a potential energy as the air maneuvers around the disturbance. The resulting stagnation pressure can be determined by Bernoulli's equation.

$$P_{stagnation} = \frac{\rho V^2}{2} \tag{4-14}$$

where,

V is the air speed.

Most of the streamlines of airflow do not actually stop at the face of the building but redirect along easier paths. The stagnation pressure is a maximum potential pressure. Little of a building's surface will be exposed to the full forces of the wind. Furthermore, much of the sides and backside of the building will see pressure below the atmospheric pressure as the wind rushes past and pulls away from the building creating lift forces. A dimensionless wind surface pressure coefficient C_p is employed to describe pressure gradient at the building surfaces. The pressure coefficient is the ratio of pressure impinging an area of the wall to the stagnation pressure. Surface wind pressures are given in the Bernoulli equation as follows.

$$P_{surface} = C_p \frac{\rho V^2}{2} \tag{4-15}$$

The pressure coefficient is derived from surface pressures

$$C_p = \frac{P_{surface}}{P_{stag}} \tag{4-16}$$

Since the surface pressures vary over time, a mean hourly pressure is commonly used:

$$\overline{C}_p = \frac{\overline{P}}{\overline{P}_{stag}} \tag{4-17}$$

The stagnation pressure (P_{stag}) is typically measured at either at 10 m (at weather stations), the height of the roof eave, or the height of the building (for tall buildings). Both stagnation and mean pressure are relative to the "base pressure" at ground level unexposed to the wind. Plots of C_p for basic building geometries can be found in the literature (ASHRAE 2001 F14) or can be derived from wind tunnel testing or direct measurement.

The plot in Figure 4-10 below shows a one minute long sample measurement of wind speed. In this case the wind is coming from the east and its mean speed over the hour was about 5 m/s.

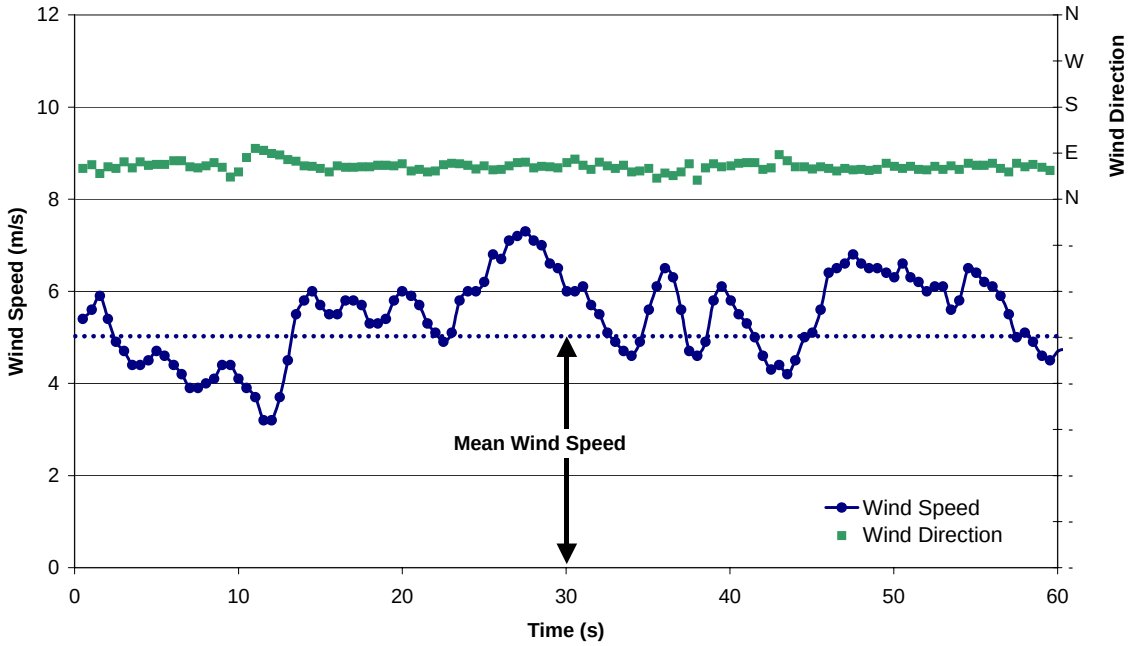

Figure 4-10: Wind Data

Burnett and Straube (1995) introduce a mean spatial pressure coefficient ($C_{p,v@1\text{-}2}$) specifically for cavity venting calculations $C_{p,v}$.

$$C_{p,v@1-2} = C_{p1} - C_{p2} \tag{4-18}$$

$$C_{p,v@1-2} = \frac{\Delta P_{1-2}}{P_{stag}} \tag{4-19}$$

The resultant driving pressure between two locations due to wind using Burnett and Straube's method becomes

$$\Delta P_W = C_{p,v} \frac{\rho V^2}{2} \qquad (4\text{-}20)$$

The velocity is measured similarly as for the stagnation pressure. An illustration of how driving wind pressures are determined from Cp values is shown in Figure 4-11.

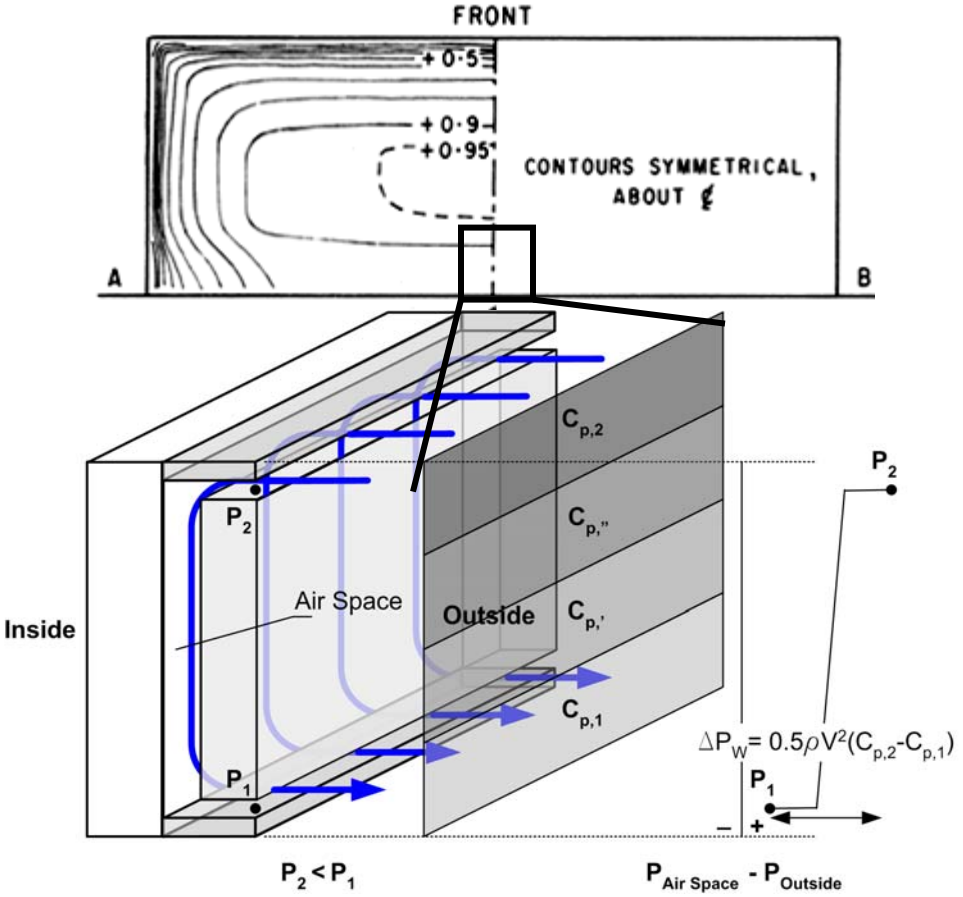

Figure 4-11: Wind Forces on building with Cp values (Dangleish and Schiever)

The plot in Figure 4-12 shows a hypothetical building with ventilation cavity entrance and exit slots with pressure coefficients of 0.8 and 0.7, respectively for the given wind directions. Coherence is defined as the state at which two signals maintain a fixed phase relationship. In simpler terms coherence is a measure of how closely two signals "wiggle" up and down together. An example set of stagnation and surface pressure signals is plotted in Figure 4-12.

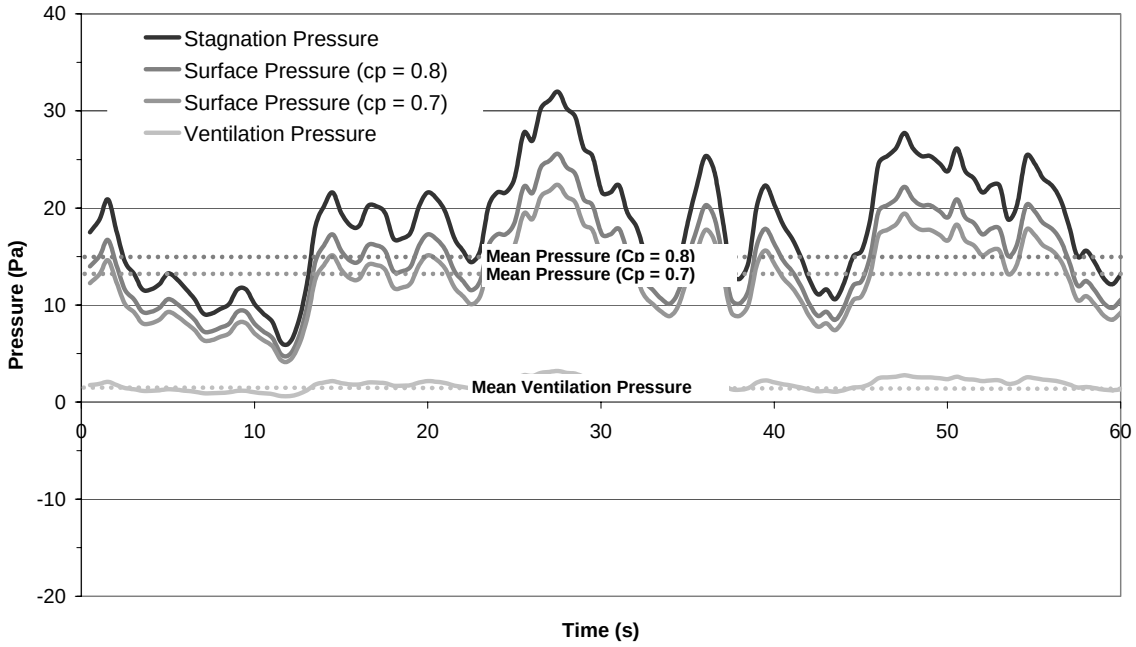

Figure 4-12: Hypothetical Surface Pressure for Figure 4-9 (with Perfect Coherence)

As shown in Figure 4-12 the derived ventilation pressures range between 1 and 3 Pa. Straube and Burnett (1995) further applied Equation 4-20 to weather data collected at their field test hut to make the following predictions.

> Wind pressure is probably the most important force driving ventilation flow. For most locations, the wind speed exceeds 1 m/s 80 to 90% of the time, but the average wind velocity is generally quite low (3 m/s to 4 m/s at 10 m above grade). Although low-rise houses are often protected from wind effects (both by neighbouring buildings and their location close to the ground), mid- and high-rise buildings are usually fully exposed to the wind. Measurements on low-rise buildings (Straube and Burnett 1995) show that average wind pressures driving ventilation can be expected to be in the order of 1 Pa. The average pressure will fall in a wide range between 0.1 Pa and 10 Pa, depending on the geometry and size of the building, the vent positions, and wind speed and wind direction.

Unfortunately, the techniques described in this thesis may not be adequate for predicting ventilation rates. The effects of gusts require more detailed investigation. This limitation was acknowledged by Straube and Burnett (1995).

> Short duration (i.e. less than about 3-5 seconds) gusts can occur over small regions of a building creating temporary but large pressure gradients. We have yet to attempt to quantify the influence of these variations on ventilation…

The potential for error in this technique was also explored by Potter (1979) who measured typical errors of 25% between measurement and mean pressure coefficient method calculations of net airflow between windows at similar C_p levels. However, the windows used in his studies were on opposite sides of a square building with wind

travelling parallel to the wall. Obviously in this case the coherence would be much less than the coherence between two openings on the same building face.

The cause of these complications is that winds typically contain gusts. Gusts are sudden rushes of wind caused by turbulent effects in free flowing wind caused by flow disturbances. In some situations air can flow at high mean speeds with relatively few gusts while in other cases at very low mean speeds with large gusts. In Figure 4-10 the 5 m/s wind fluctuates 2-3 m/s. In one sample of Straube and Burnett's (1995) field measurement data, the average measured ventilation pressure was only –0.27 Pa but the standard deviation over the period was 1.82 Pa.

The plots of pressures shown in Figure 4-11 show a good coherence in the surface pressure at the two vents. Since gusts have a limited physical size, the assumption of good coherence may not be valid for points relatively far apart as shown below in Figure 4-13.

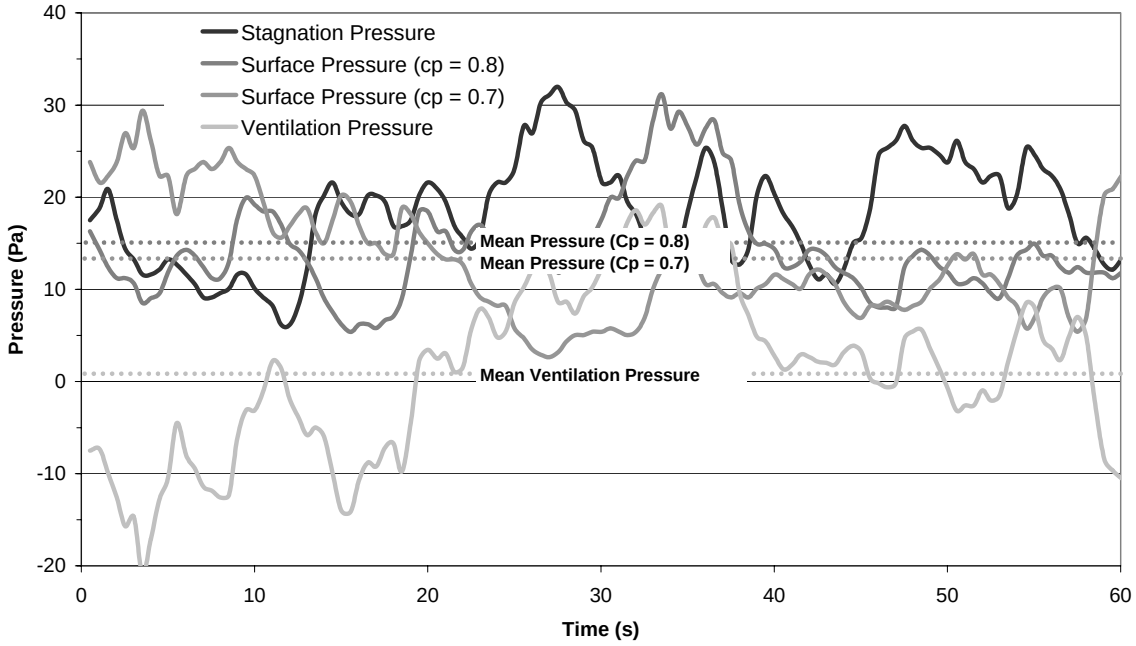

Figure 4-13: Hypothetical surface pressures for Figure 4-9 with No Coherence

The mean ventilation pressure calculated from the data plotted in Figure 4-13 with poor coherence is 1 Pa. However, employing the absolute pressure difference to the data shown in Figure 4-13 would result in a mean ventilation pressure of 9 Pa.

Two potential concerns related to gusts affecting cavity ventilation predictions are

1. For ventilation cavity vents with poor coherence the mean ventilation pressures may be much larger than predicted because the flow reversals are being cancelled out, and
2. The changing speeds and directions of the applied pressure may cause eddies within some cavities which may restrict flow. This may even be of concern for ventilation cavities with vents with good coherence.

4.5. Closure

The pressure differences due to wind pressures stack pressures, and mechanical systems are considered in combination by simple addition.

$$\Delta P_{1-2} = \Delta P_M + \Delta P_B + \Delta P_W \tag{4-21}$$

These driving pressures can be applied to the various airflow systems described in Chapter 3 to estimate airflow rate through such systems.

Buoyancy induced pressures and the complicated effects of gusting on wind driven pressures will be further examined with field measurement described in Chapter 7.

4.6. References

ASHRAE, *Handbook of Fundamentals* Atlanta, Ga, 2001.

Dangleish, W., Schiever, W., "Wind Pressures on Buildings", *Canadian Building Digest* 34.

Munson, Young, Okiishi *Fundamentals of Fluid Mechanics,* 3rd edition Wiley, 1998.

Potter, I. "Effects of fluctuating wind pressure on natural ventilation rates" *ASHRAE Transactions* 1979, Vol. 85(2), pp. 445-457.

Pressnail K., Timusk J., Kan L., Dong B., Kan V., "In Search of a Wall for All Season: Controlling Sun Driven Moisture", *Proc. 9th Canadian Conference on Building Science and Technology,* Vancouver Canada 2003.

Straube, J., and Burnett, E., *Vents, Ventilation, and Pressure Moderation*, Building Engineering Group, Report for Canada Mortgage and Housing Corp, Ottawa 1995.

5. HEAT AND MOISTURE FLOW AND VENTILATION

5.1. Introduction

This chapter presents available models and correlations for determining the effect of ventilation on heat and moisture transfer within ventilated enclosures. The physical nature of moisture and heat transfer in multilayer assemblies is introduced. Specifically, the modelling of interlayer airspaces and ventilating these air spaces will be discussed. For a more thorough background on basic heat, air, and moisture flow see Incropera and DeWitt (1996) and Handegord and Hutcheon (1995). This background can also be found in a more concise format specifically for building enclosures in the ASHRAE Handbook of Fundamentals (2001 F23 and F24). This chapter provides a brief review followed by a specific description of the analysis of interlayer airspace ventilation effects.

5.2. Heat and Moisture Flow through Materials

Enclosures consist of porous and nonporous materials. Many building materials such as wood, concrete, gypsum, and masonry contain pores in the range of 10 nm to 100 μm. Non-porous materials, such as glass, steel, and glazed ceramics are also widely used. Condensation may be absorbed into porous materials until excessive quantities can no longer be absorbed and immediately creates surface droplets or a film. Condensation on nonporous materials is not absorbed and creates surface droplets or a film. The difference is significant as liquid water diffuses through porous material and such materials may have significant moisture storage capacity as shown in Figure 5-1.

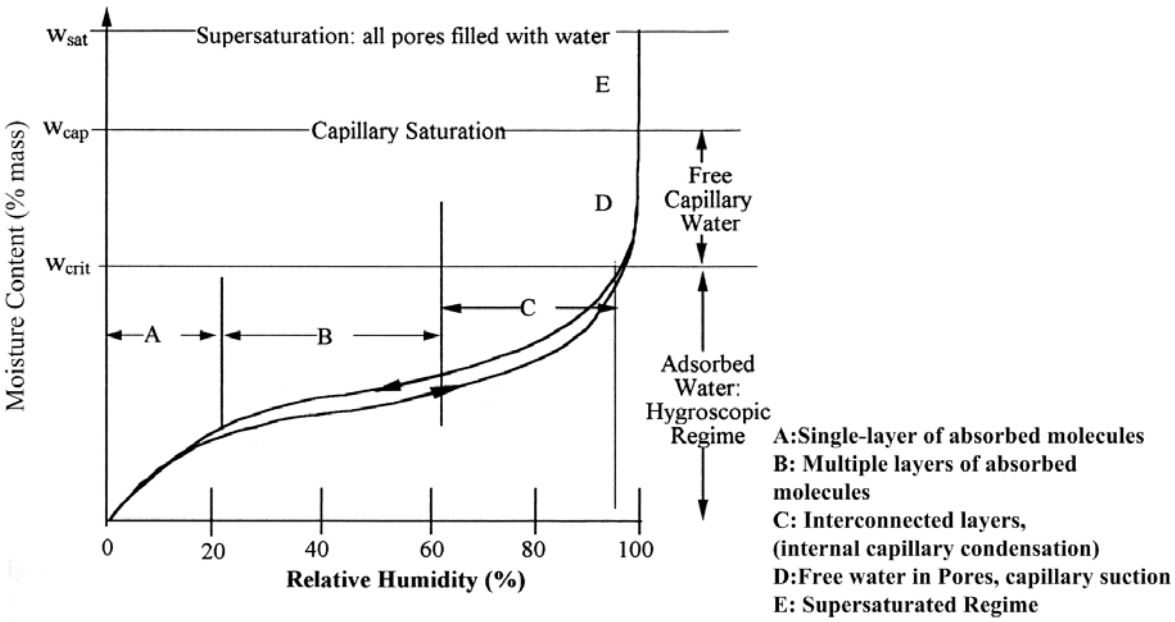

Figure 5-1: Regimes of Moisture Storage in a Hygroscopic Porous Material (Straube 1998)

Moisture flow in nonporous material is very slow relative to porous materials because the lack of void spaces does not allow easy flow. Adsorbed water molecules can travel along pore surfaces and vapour can diffuse across the gas filled pores. Within a porous material, liquid transport is the dominating moisture transport mechanism at high moisture contents and vapour transport dominates at low moisture contents. A generalized plot of flow function under different degree of saturation/relative humidity of porous materials is given in Figure 5-2.

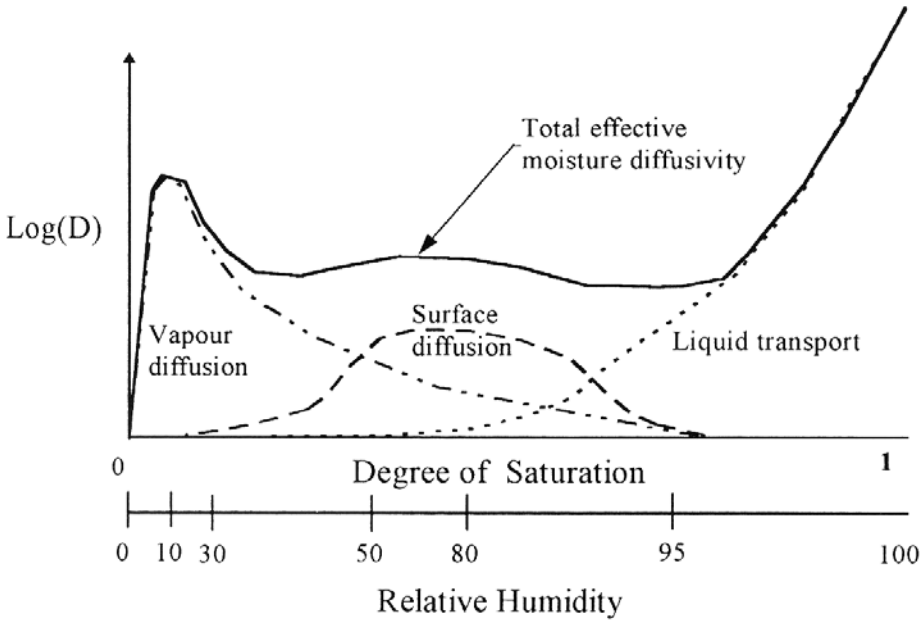

Figure 5-2: Hypothetical Total Isothermal Moisture Transport Function – D is δ (Straube 1998)

Most models of heat and moisture flow though materials are based on a diffusion paradigm. This means that the rate of mass and energy flow is linearly related to differences in concentration.

For example, water vapour diffusion is often analyzed using Fick's Law:

$$\dot{m}_v = -\delta A \frac{dP_v}{dx} \tag{5-1}$$

where,

$\dot{m}_v$ is the mass flowrate of water vapour,

δ is the water vapour permeability of the material,

A is the area across which the vapour is flowing, and

dP_v/dx is the vapour pressures gradient normal to A.

Similarly, diffusion is applied to analyze heat conduction as follows:

$$\dot{q} = -kA \frac{dT}{dx} \tag{5-2}$$

where,

$\dot{q}$ is the heat flow,

k is the conductivity of the material, and

dT/dx is the temperature gradient of the thickness.

A typical profile of temperature and vapour pressure through a material is illustrated in Figure 5-3.

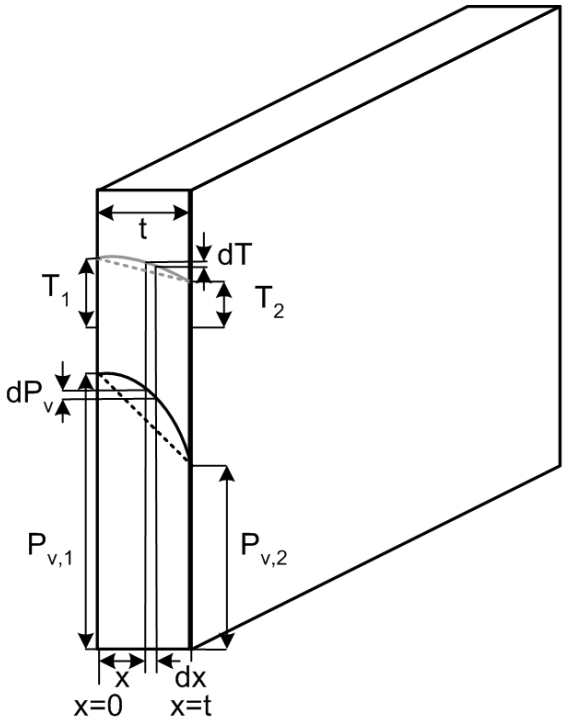

Figure 5-3: Heat and Moisture Flow Through Single Layer

The rate of vapour and heat ransport across the layer can be solved for steady state conditions by integrating from x=0 to x=t and from the inner and outer layer conditions and using an averaged permeability and conduction and rearranging.

$$\dot{m}_v = \frac{\bar{\delta} A(P_{v,1} - P_{v,2})}{t} \tag{5-3}$$

$$\dot{q} = \frac{\bar{k} A(T_1 - T_2)}{t} \tag{5-4}$$

where,

t is the thickness of the material.

It is often convenient to combine vapour permeability δ and thermal conductivity k with thickness t to generate a permeance (M):

$$M = \frac{\bar{\delta}}{t} \tag{5-5}$$

and conductance (C):

$$C = \frac{\bar{k}}{t} \tag{5-6}$$

for materials that are commonly used in particular thicknesses or when particular thicknesses have unique properties.

Permeance and conductance values for many common building materials and some assemblies (i.e., painted materials) have been previously measured and can be found in Hutcheon and Handegord (1995) and in the ASHRAE Handbook of Fundamentals (2001) or determined experimentally. Vapour permeance and heat conductance, as discussed earlier, can vary significantly with temperature and moisture content. Hence, the test conditions for the derived properties should always be considered when applying them to practical building science analysis.

5.3. Heat and Moisture Flow Through Multi-Layer Systems

Many contemporary enclosure systems consist of multiple and composite layers of materials. Often the purpose of performing a hygrothermal analysis through an enclosure is to determine the moisture content and temperature of the various layers.

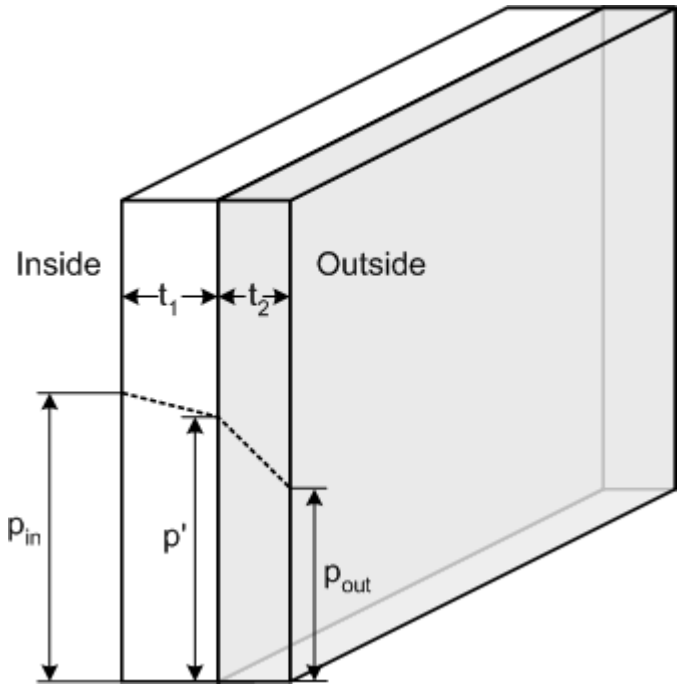

Figure 5-4: Simplified Multi Layer Vapour Pressure Profile

Equations 5-1 and 5-2 can be applied to each layer. For any layer (j):

$$\dot{m}_v = M_j \cdot A(\Delta P_{v,j}) \tag{5-7}$$

and

$$\dot{q} = C_j \cdot A(\Delta T_j) \tag{5-8}$$

For an assembly of n layers:

$$\dot{m}_v = A \cdot \frac{P_{v,interior} - P_{v,exterior}}{\sum_{j=0}^{n} R_{v,j}} \quad (5\text{-}9)$$

and

$$\dot{q} = A \cdot \frac{T_{interior} - T_{exterior}}{\sum_{j=0}^{n} R_j} \quad (5\text{-}10)$$

where,

R_v is the vapour diffusion resistance or the inverse of the permeance and

R is the thermal resistance or the inverse of the conductance.

These equations can be combined to solve for $\Delta P_{v,j}$ and ΔT_j:

$$\Delta P_{v,j} = \frac{P_{v,interior} - P_{v,exterior}}{M_{v,j} \cdot \sum_{j=0}^{n} R_{v,j}} \quad (5\text{-}11)$$

and

$$\Delta T_j = \frac{T_{interior} - T_{exterior}}{C_j \cdot \sum_{j=0}^{n} R_j} \quad (5\text{-}12)$$

To assess the influence of different environmental conditions, only the outdoor and indoor vapor pressure and temperature need to be modified.

5.3.1. Surface and Mass Transfer Coefficients

The inside and outside surface conditions may not be the same as those for the surrounding environment and further surface heat and mass transfer coefficients are necessary. The heat transfer from a material surface to the surrounding environment will vary with the air temperature, the surface temperature, the orientation or inclination of the surface, the direction of the heat transfer, exposure to radiation, and the dimensions of the heated or cooled surface (Hutcheon and Handegord 1995). The effect is illustrated in Figure 5-5.

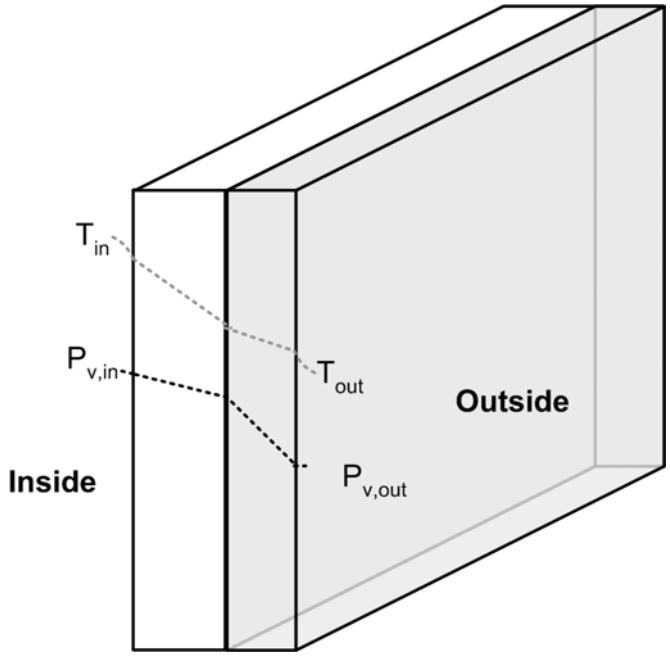

Figure 5-5: Multilayer Wall with Surface Films

The heat transfer will further change with the velocity at which air moves past the surface as shown in Figure 5-6. The moisture transfer resistance at the outside and inside surfaces of building components is so low relative to the vapour resistance of the building materials, that it is typically ignored in models. However, it may be significant with dynamic drying from a wet surface.

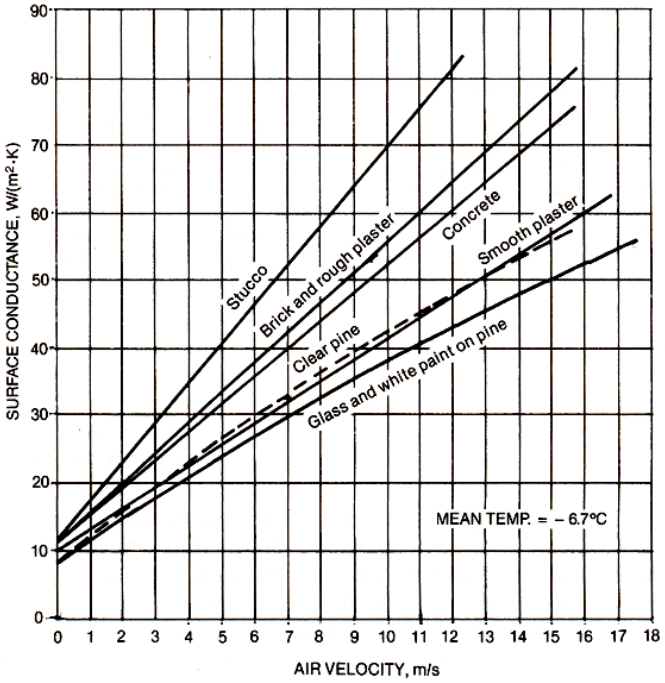

Figure 5-6: Surface Conductance as Affected by Air Movement (ASHRAE 2001 F25.1)

Heat transfer coefficients can be converted from heat to mass using the Lewis correlation (ASHRAE 2001 F).

$$h_w = 6100 \cdot h_c \tag{5-13}$$

where,

h_w is the mass transfer coefficient for water vapour in unit ng/(Pa·s·m^2) and

h_c is the heat transfer coefficient in units of W/m^2·K.

5.3.2. Airspaces

Still air can be treated similar to other solid layers in the analysis of a wall assembly. The vapour permeability of still air is can be found using correlation provided in ASHRAE 2001 (F25.4 Table 3) or derived from hot box testing using ASTM C236 or C976.

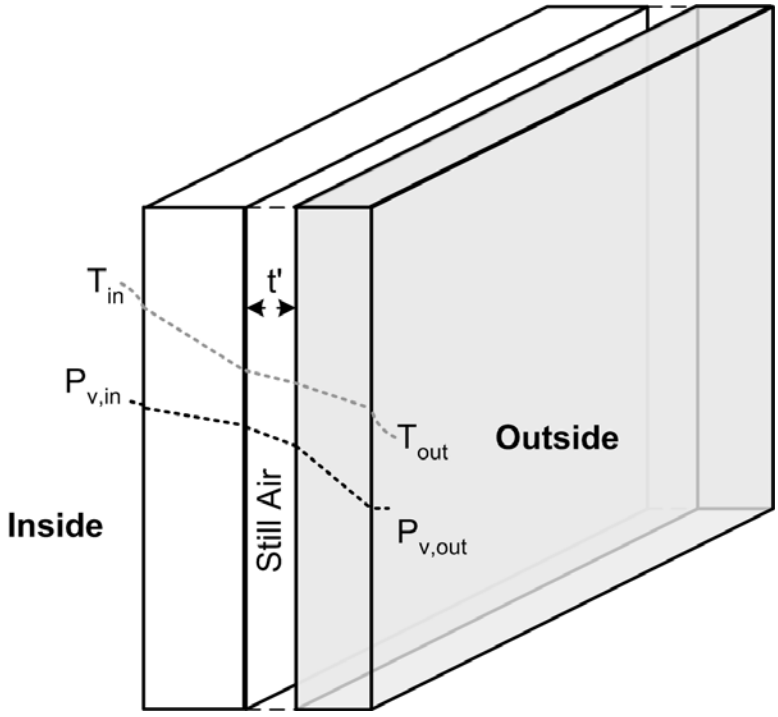

Figure 5-7: Air Space within Enclosure

Density gradients due to differences in temperature and moisture content may occur across the air space and cause circulation cells to form. Much work has been undertaken and correlations determined for the heat transfer coefficients of a variety of enclosed rectangular cavities (Incropera and DeWitt 1996). ASHRAE (2001 F23 and F25) provide the tabulated values in Table 5-1.

Table 5-1: Equivalent conductances for plane airspaces (W / m^2·K)

Thickness of Airspace		13 mm		20 mm		40 mm		90 mm	
Position of Surface	Direction of Flow	Emmittance Factor							
		0.05	0.90	0.05	0.90	0.05	0.90	0.05	0.90
Mean Temp. 32 ^{o}C									
Horizontal	Up	2.78	7.69	2.56	7.69	2.38	5.26	2.13	7.14
	Down	2.44	7.14	1.72	6.67	1.06	5.88	1.45	5.56
Vertical	Horizontal	2.44	7.14	1.75	6.67	1.56	6.67	1.67	6.67
Mean Temp. -18 ^{o}C									
Horizontal	Up	2.78	4.55	2.63	5.56	2.44	5.26	2.17	5.00
	Down	2.00	5.00	1.41	4.35	1.18	3.70	1.82	3.45
Vertical	Horizontal	2.00	5.00	1.59	4.55	1.69	4.55	1.69	4.55

5.3.3. Condensation and Evaporation

Condensation occurs on surfaces when the surrounding water vapour pressure exceeds the saturation vapour pressure for the surface temperature. The phase change releases heat that is mostly transferred to the surface.

The energy transfer flux for this change of phase is

$$\dot{q}_l = \dot{m}_w \cdot h_{fg} \tag{5-14}$$

where,

$\dot{q}_l$ is the flux rate of latent heat transfer, and

h_{fg} is the difference in enthalpy between the water at vapour and liquid state and is equal to 2490 kJ/kg at room temperature.

The heat flow will be negative for evaporation and positive for condensation.

5.4. Heat and Moisture Flow and Ventilation

Water vapour moves through the building enclosure in two primary modes; diffusion and advection. Advection is the transfer of energy or mass by the bulk movement of fluid. Water vapour can be easily transported by the bulk transport of the air itself, and this advection transport mechanism, analogous to heat advection, is very significant for the performance of typical building enclosure systems. The combined transport of mass by diffusion and advection is termed convection

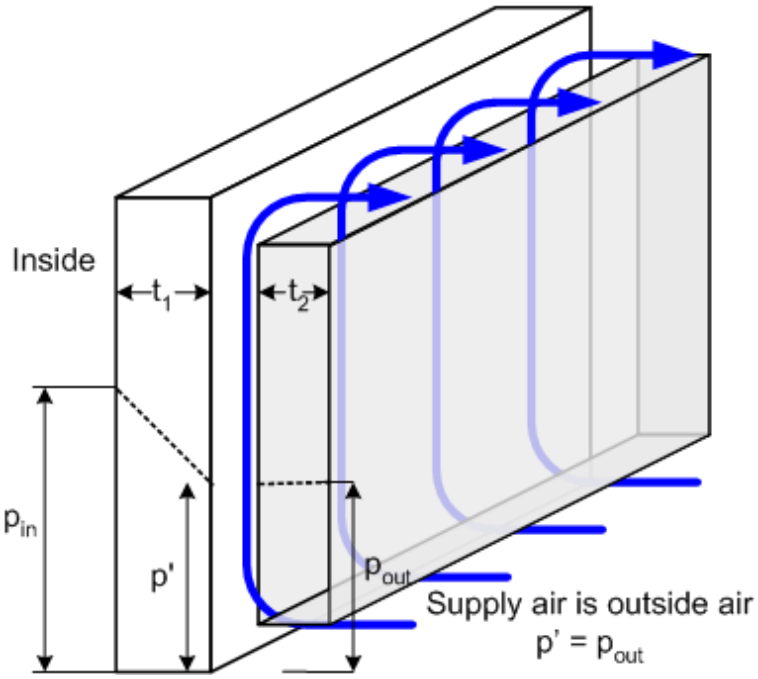

Figure 5-8: Ventilation of Inter Layer Airspace

The simplest analysis of such a system is to only consider the extreme conditions that the cavity acts as either highly ventilated or non-ventilated still air. Analysis of these conditions provides a maximum and minimum ventilation effect.

For maximum ventilation effect the following is assumed.

$$I_{cavity} = \infty \tag{5-15}$$

$$T_{cavity} = T_{\text{ventilation source}} \tag{5-16}$$

$$P_{v,cavity} = P_{\text{v,ventilation source}} \tag{5-17}$$

where,

I_{cavity} is the ventilation rate inside the cavity airspace.

For minimum ventilation affect the following is assumed.

$$I_{cavity} = 0 \tag{5-18}$$

$$R_{Cavity} = R_{\text{Still Air}} \tag{5-19}$$

$$M_{Cavity} = M_{\text{Still Air}} \tag{5-20}$$

The following example shows a practical application of this analysis. It is noted that this method overestimates condensation rate. For condensation due to diffusion the major source of error in these calculations is from not accounting for the condensation surface temperature rise as latent energy from the condensate is transferred to the material. However, the condensation rate does provide a maximum and will indicate high humidity at the identified surface.

Example: Adobe Addition, Ourem Portugal (2002)

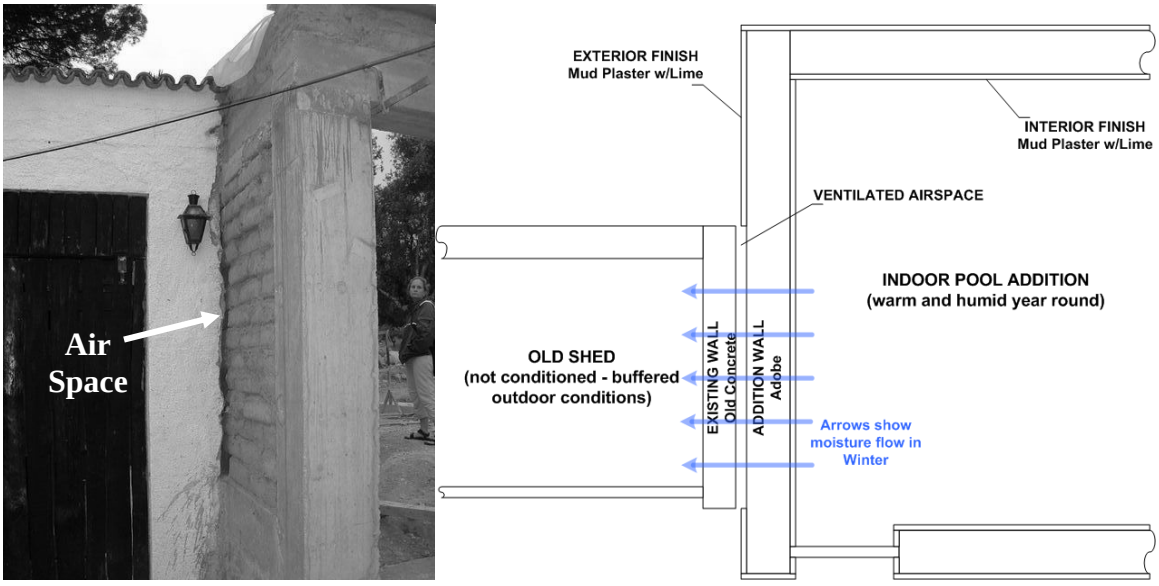

The picture above is of an interface between a new adobe enclosed swimming pool enclosure and an old lime-plastered concrete shed. The architect was concerned about water condensing at this interface and decided to leave a gap to allow water to be ventilated away. He had heard that the adobe breaths (has a high vapour permeability).

Is this sufficient? Should he have left the gap at all? His decision was based on a conversation we had had a few months early on the ability of low flow ventilation to remove moisture. His decision making would have greatly benefited with the moisture physics already covered in this chapter.

The results shown below are for the assembly above. In this case his design choice should have been based on the construct complexities, aestitic issues, and results from the simple steady state analysis results below. Mid Portugal has a mild climate where little condensation (1.5 g/m^2 per day) would occur. Practically, he should be worried most about the potential rain leaking into the gap and turning the adobe back into mud.

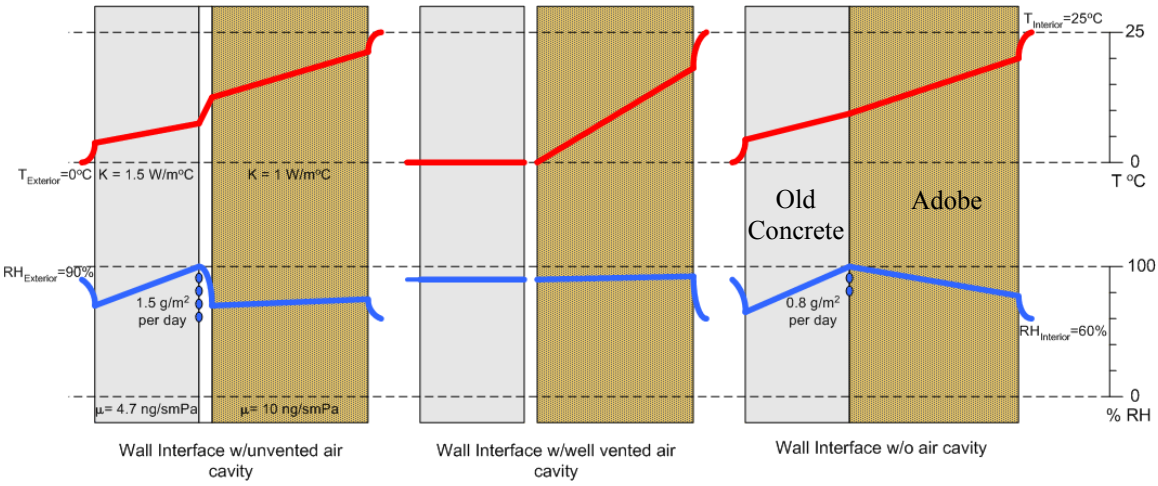

The analysis of multi-layer wall assemblies with inter-layer ventilation can be expanded as required for more precise inter-layer conditions and dynamic analysis. An equivalent vapour permeance can be calculated for the ventilated airspace and outward layers. This equivalent permeance combines the effects of both diffusion and advection and is written by Straube and Burnett (2003) in the form

$$M_{v,equivalent} = \frac{1}{R_{v,equivalent}} = \frac{1}{R_{v,bulk}} + \frac{1}{R_{v,outer\_layers}} = M_{v,bulk} + M_{v,outer\_layers} \tag{5-21}$$

An equivalent thermal resistance can also be determined similarly

$$\frac{1}{R_{equivalent}} = \frac{1}{R_{bulk}} + \frac{1}{R_{outer\_layers}} \tag{5-22}$$

TenWolde (ASHRAE F23.17 2001) solved for the ventilation components as in equations 5-22 and 5-23. The parallel resistance accounts for the heat and vapor bypassing the outer material layers with "bulk" outside ventilation air. The magnitude of the parallel resistances may be determined from the following equations:

$$R_{bulk} = \frac{A}{Q\rho c_p} \tag{5-23}$$

$$R_{v,bulk} = \frac{A}{Q\rho c} \tag{5-24}$$

where,

A is the area,

Q is the volumetric flowrate of the ventilation air,

ρ is the air density,

c_p is the heat capacity of the air, and

c is the ratio of humidity ratio and vapor pressure (approx 6.13 g/kg·kPa).

The concept of a parallel resistance to account for ventilation is illustrated in Figure 5-9.

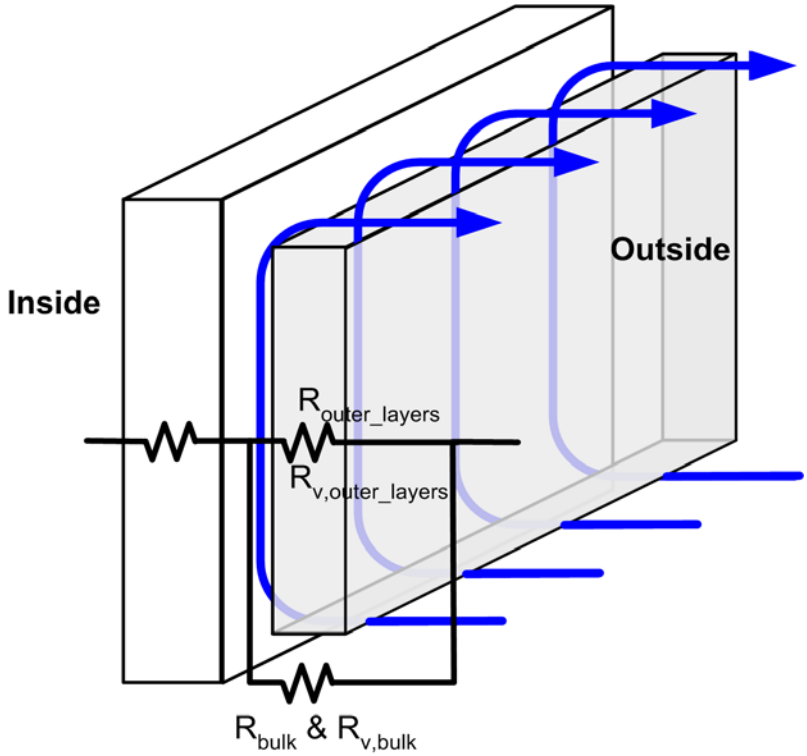

Figure 5-9: Illustration of Parallel Resistance Concept

The effects of ventilation determined using parallel resistances can be applied to cladding systems to determine equivalent permeance as shown in Figure 5-10.

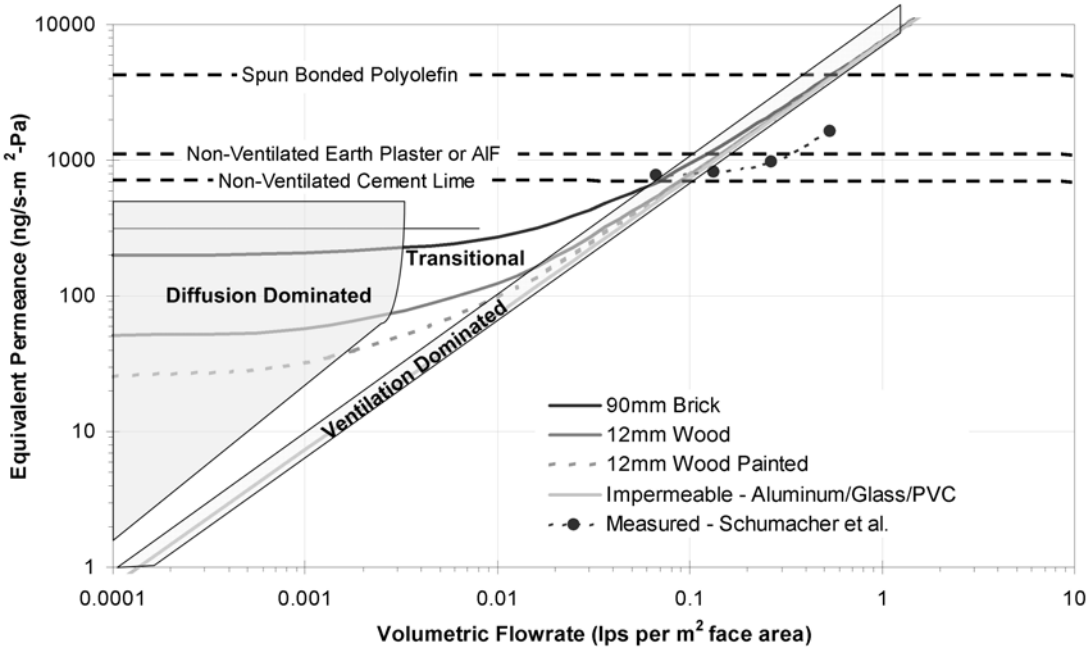

Figure 5-10: Equivalent Vapour Permeance of Typical Claddings

As seen in Figure 5-10 impermeable claddings can be greatly affected by ventilation. Small levels of ventilation significantly affect impermeable claddings (Aluminum/Glass/PVC). Moderate levels of ventilation are capable of effectively allowing low permeance claddings (Wood/Brick) to perform similar to highly permeable claddings and materials. Any cladding system can reach the level of permeance of permeable sheathing membranes and plasters. Highly permeable claddings would only benefit from very high ventilation levels. Schumacher et al (2003) measured a similar trend for metal cladding as shown by the data points in Figure 5-10.

A similar plot for thermal resistance is included in Figure 5-11. Equations 5-22 to 5-24 are applied for a number of materials commonly on the outside of wall ventilation cavities.

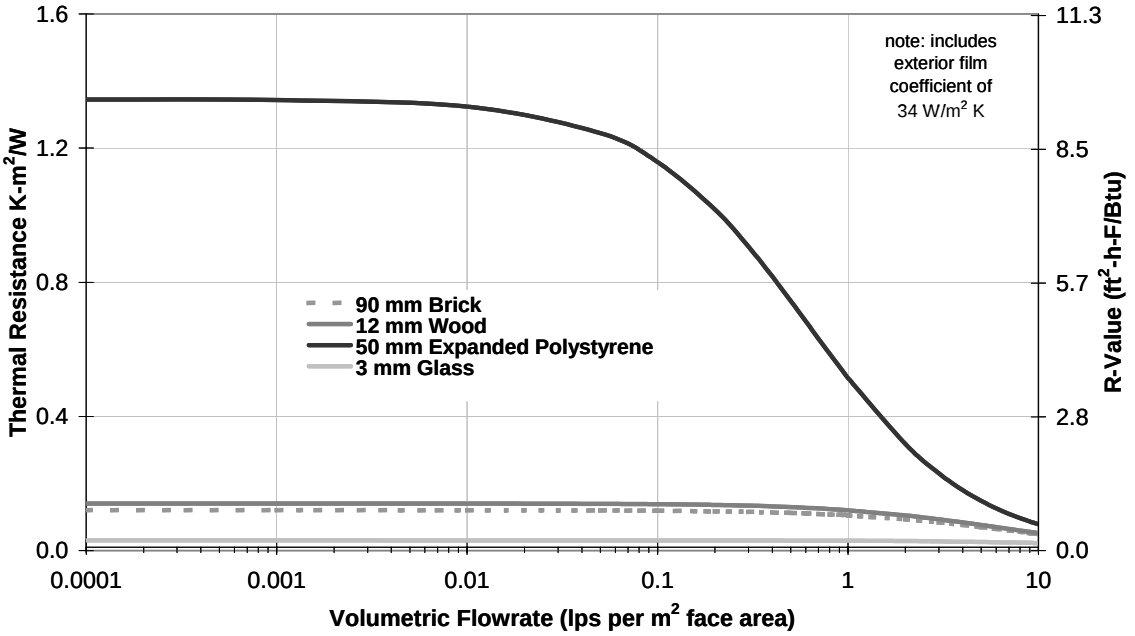

Figure 5-11: Equivalent Thermal Resistance of Typical Claddings

The equivalent thermal resistance of typical cladding systems, are significantly reduced at ventilation rates beyond 0.05 to 2 lps/m^2 as shown in Figure 5-12. The greater the thermal resistance, the less flow required to impact the thermal resistance. For practical insulated cladding systems (such as EIFS), flows of 0.05 lps/m^2 can be tolerated. Since these systems tend have very low vapour permeance strategies to increase equivalent permeance without significantly reducing thermal resistance are possible. This design strategy could be applied to ventilated EIFS as described earlier in Section 3.7.3.

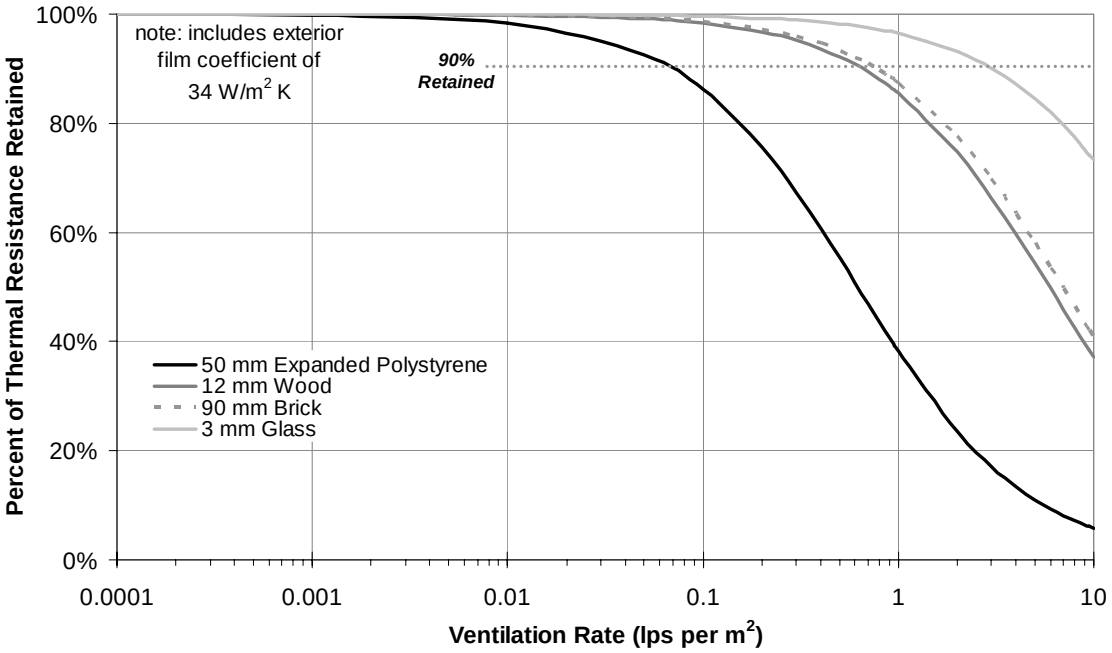

Figure 5-12: Loss in Thermal Resistance in Various Claddings

Figure 5-13 shows the predicted relationship for volumetric flowrate and ventilation rate and air velocity for various wide rectangular cavities. This plot shows the relative flows required to achieve the equivalent permeance and resistance values in Figure 5-10 and Figure 5-11.

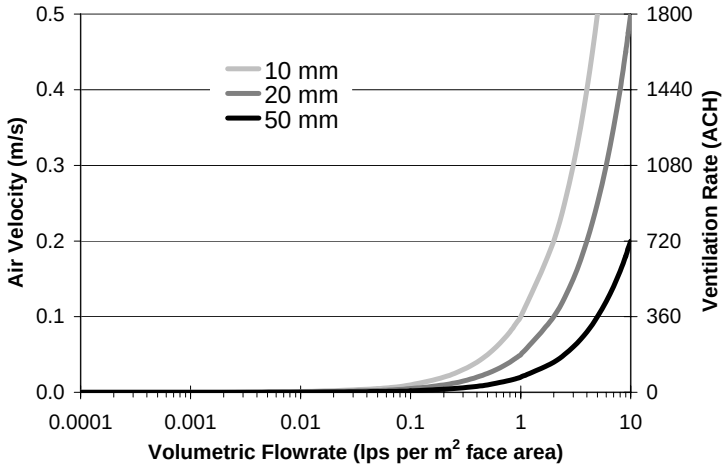

Figure 5-13: Airflow Rates for Wide Rectangular Cavities

5.5. Limitations of Steady State Hygrothermal Analysis

There are two major limitations to the steady analysis used in hygrothermal analysis. One is thermal and hygric mass effect. The second limitation is that damage mechanisms/performance thresholds depend on unsteady hygrothermal conditions and length of exposure.

Thermal mass effects are generally determined using the "lumped capacitance method" (Incropera and DeWitt 1996) as a linear storage function in the energy balance equation.

$$q_{storage} = c_p \cdot m \cdot \frac{dT}{dt} \tag{5-25}$$

where,

$q_{storage}$ is rate of change of energy stored in the mass,

c_p is the heat capacity,

m is the mass,

dT is the change in the average mass temperature, and

dt is the increment of time over which the temperature change is occurring.

Hygric mass effects in building enclosure lend much complication as the water is general changing between liquid and vapour phases and interacts with pores in many building materials. A generalized moisture storage function term "sorption isotherm" is given in Figure 5-14. Hysterisis is not ignored in the relationships shown on the plot.

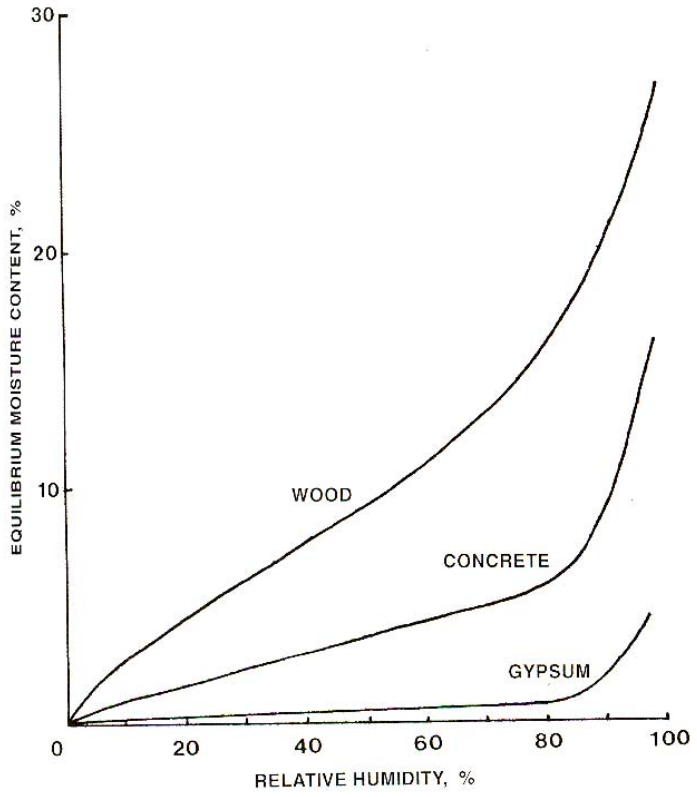

Figure 5-14: Typical Sorption Isotherms for Wood, Concrete, and Gypsum (ASHRAE 2001 F23.13)

Various materials have hygric capacity to storage moisture. This capacity allows wetting events to be managed by storing the moisture to be later dried thereby avoiding excess humidity in various materials and airspaces. This storage can also have negative consequences as moisture that would otherwise have drained can cause further detrimental effects to the enclosure system.

Materials with large hygric capacities (such as wood studs) rarely attain the steady state conditions determined from a Glaser analysis. Other materials, such as brick (similar sorption isotherm as concrete) may pick up moisture from repeated rain events and attain saturation levels. In order to address these significant effects further transient analysis is required.

Due to the unsteady boundary conditions of hygrothermal models of enclosures the ability to perform transient analysis greatly enhances the capability to predicted performance of enclosure systems.

5.5.1. Transient Hygrothermal Analysis

Transient hygrothermal analysis requires the inclusion of thermal and moisture storage effects in energy and mass balance equations. These effects and the repetitive nature of the analysis typically require computation modeling due to the complexity of the simulations. An optimal model would have parallel circuits for moisture and heat flow representing ventilation. The rate of transfer alond this parallel circuit would be a function the natural driving forces affecting the ventilation rate. Unfortunately this feature does not exist in available hygrothermal simulation packages. However, there are some limited techniques that can be applied to simulate the effects of ventilation.

One technique is to simply apply an equivalent vapour permeance for the outward layers of the composite system. Unfortunately, this method causes error with the transient effects of water storage in the outward layers. In reality the ventilated water vapour completely circumvents the outward layers. Since this technique will be the most readily available for engineering practitioners in the near future the capabilities of one-dimensional modeling incorporating equivalent vapour permeance values should be further explored and compared to field data.

Another technique would be to create a two dimensional model with hygrothermal short circuit to the outward layers. This would reduce the water storage issues but add a high level of complexity to the model. Currently available software packages do not allow material properties to change with outdoor conditions. Hence the model would have limited applicability and rigour.

The addition of a source/sink term for moisture and heat at air space layers within composite assemblies would be the best method of modeling the dynamic affects of these walls. The function of the source/sink would need to be tied to outdoor conditions. The addition of such a feature to a hygrothermal modeling package would be a great asset to analysis of ventilated composite systems.

5.6. Closure

Steady state analysis of the hygrothermal effects of enclosure ventilation has been presented. The coupling of this analysis with methods presented in Chapters 3 and 4 for predicting the amount ventilation allow thermal and moisture analysis of such system.

The limitations of steady state analysis have been discussed. Potential strategies for transient models have been presented. Field measurement of heat and moisture flows in ventilation wall assemblies will be presented in Chapter 8.

5.7. References

ASHRAE *Handbook of Fundamentals* Atlanta, Ga, 2001.

Burnett, E., Straube, J., *Building Science for the Building Enclosure*, to be published 2004.

Handegord G., Hutcheon, N. *Building Science for a Cold Climate* IRC 1995 pg. 177.

Incropera, F., DeWitt, D., *Fundamentals of Mass and Heat Transfer* 4th Ed. Wiley 1996 pp. 509-511, pp. 556-569, pp. 212-218.

Schumacher C., Shi X., Davidovic D., Burnett E., Straube J., "Ventilation Drying of Walls" *Building Physics Conference*, Leuven, Belgium 2003.

Straube, J. *Moisture Control and Enclosure Wall Systems,* PhD dissertation, University of Waterloo 1998, pg. 58.

6. VINYL SIDING AIRFLOW CHARACTERISTICS

This chapter reports on a laboratory study of vinyl siding airflow characteristics performed to investigate measurable flow resistances effecting the ventilation of vinyl siding. Characterizing, in this sense, is to define and measure the features of an installed cladding system affecting the quantity of ventilation (with outdoor air) that is likely to occur with exposure in the field. The chapter

Vinyl siding is a common cladding for low-rise residential buildings. It has long been hypothesized that ventilation must play a major role in the hygrothermal behaviour of vinyl siding since the basic material (about 1.2 mm of polyvinyl chloride) allows essentially zero vapour diffusion. Hence, the significant outward drying behaviour observed in the field studies (McCuaig 1988, Burnett and Reynolds 1991) must be due to some other mechanism. Similar conclusions will also be drawn from the field wall drying studies also performed as part of this research (see Chapter 8).

Figure 6-1 and Figure 6-2 are illustrations of possible airflow path ventilating the siding and show the two installation configurations examined in this laboratory study and in the field studies in chapter 8.

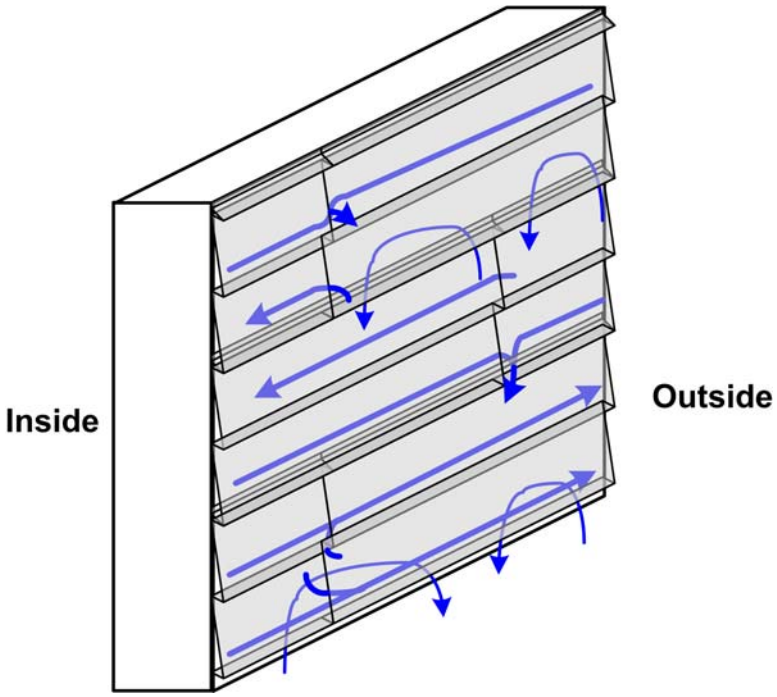

Figure 6-1: Airflow Around Contact Applied Vinyl Siding

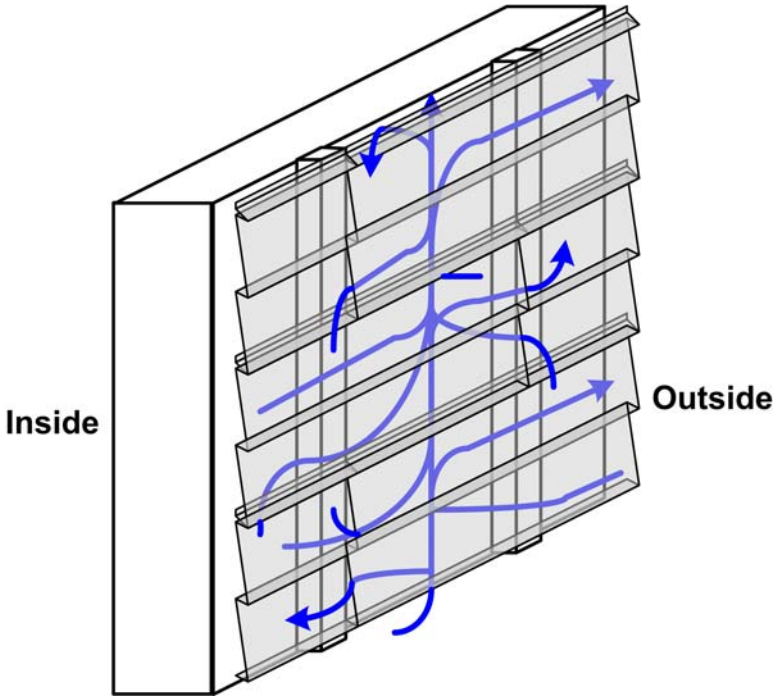

Figure 6-2: Airflow around Vinyl Siding Installed on Furring

Quantitative knowledge of airflow behind and through vinyl siding is limited. The quantity of ventilation airflow is the result of a balance of two factors: the forces generating the pressure differences that drive airflow and the resistance to airflow through and within the cladding system.

6.1. Objective

The objective of the testing and investigation was to physically assess the nature and extent of ventilation airflow behind vinyl siding to assist in the study of the role of convective drying in vinyl siding clad enclosure wall systems.

6.2. Scope

The work reported in this report investigates the airflow resistance of one type of vinyl siding cladding system. This report details a laboratory study of vinyl siding airflow characteristics performed to investigate measurable flow resistances affecting the system. Characterizing, in this sense, is to define and measure the features of an installed cladding system affecting the quantity of ventilation (with outdoor air) that is likely to occur in the field.

6.3. Approach

The approach taken was to characterize the airflow resistance through and behind vinyl cladding in three directions:

- airflow through the face of the cladding,
- airflow along vertical paths behind the vinyl siding, and

- airflow along horizontal paths behind the vinyl siding.

These flow directions are illustrated in Figure 6-3.

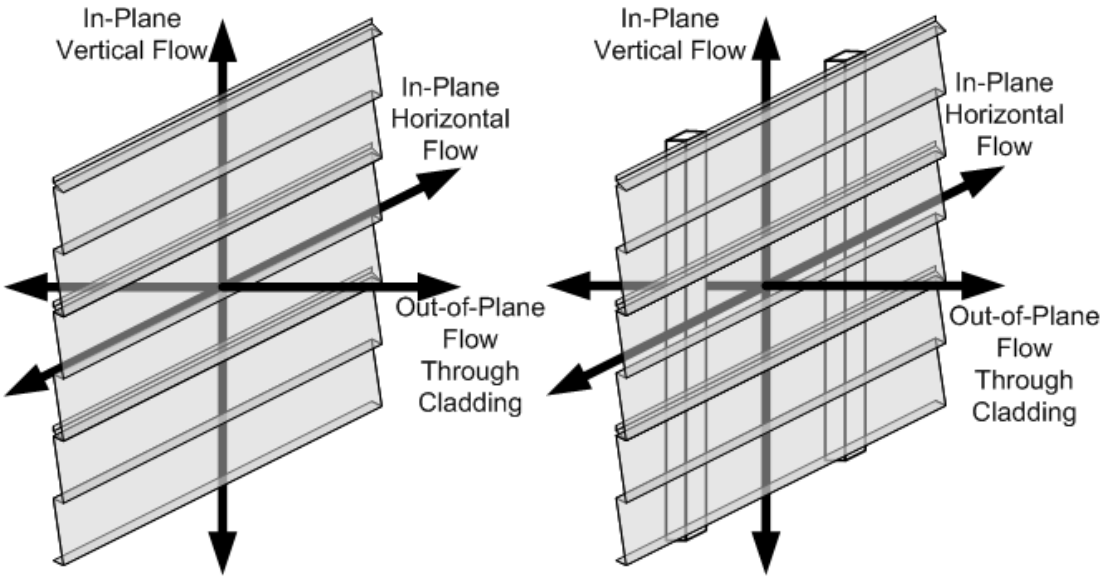

Figure 6-3: Adopted Flow Systems for Vinyl Siding

A multitude of possible flow paths exist due to the distribution of vent holes and joints over inter-connected cavities. Airflow along a set of contributing networks through large face areas and cross sectional lengths of installed vinyl siding were characterized. Airflow and resistance were measured for each of the three flow directions. The airflow resistances along the vertical and horizontal paths behind the siding were tested at varying applied pressure differences across the face of the siding. The pressures differences tested included 100 Pa, 50 Pa, 0 Pa, -50 Pa, and -100 Pa.

This approach does not investigate individual network series of single entrance, cavity, and single exit as outlined in Chapter 3. It is assumed that the generated data will create a baseline for siding airflow characteristics. The field drying study detailed in Chapter 8 indicates the influence of cladding ventilation occurring within the installed vinyl siding exposed to outdoor conditions. In the future, sidings of various configurations can be similarly tested and compared to this baseline for predicting the amount of ventilation.

6.4. Experimental Program

This section describes the design or the test rig, instrumentation, and validation testing as well as the experimental procedure employed.

The test rig consists of a blower that drives air through a manifold at the test base inlet/outlet. The manifold acts as a plenum equalizing the pressure across the panel width. The cladding is attached on top of the test length. The test length consists of 6mm thick acrylic sheet with attachment and access points. The other end of the test length was an identical inlet/outlet manifold. Photos of the test rig and the attachment and access points underneath the test bed are included in Figure 6-4.

Figure 6-4: Test Rig During Setup for In-Plane Horizontal Flow (left - view from top, right - view from bottom)

The access points are plugged with rubber stoppers and set to maintain a flush surface along the bottom of the test cavity. The rubber stoppers were modified to allow for static pressure taps and can be removed to facilitate cladding attachment.

Significant deflections of the vinyl siding were observed during initial airflow tests and the effect on the cavity's airflow resistance was apparent. A lid was designed to surround the cladding and was either positively or negatively pressurized by a separate blower system to control the air pressure difference between the cavity and the air surrounging the outside of the cladding.

Airflow resistance of a slender air space is very sensitive to small differences in the cavity thickness. This sensitivity is to be expected since the Darcy-Weisbach equation shows that $\Delta P_{conduit} \propto 1/d^3$. For the 15 mm air space, the pressure drop will change 20% for a 1 mm decrease in cavity height. Maintaining and measuring the cavity air space to a fraction of a millimeter was challenging. The flexibility of the test bed (6 mm acrylic) compounded the problem. In future studies, a much stiffer test bed is recommended.

Airflow measurements were taken with inline rotometers with an accuracy of +/- 0.01 lps. Pressure differences were measured with 0 to 12 Pa and 0 to 100 Pa differential pressure transducers with accuracies of +/- 0.1 Pa and +/- 1 Pa, respectively.

6.4.1. Test Setup Validation

An initial validation test was performed. The test length consisted of a 15 mm thick, 400 mm wide, 1.2 m long rectangular air cavity. The pressure drop along the test length can be predicted by the Darcy-Weisbach equation (as presented in Chapter 3).

$$\Delta P_{conduit} = f \cdot (\frac{L}{D_h}) \cdot (0.5 \rho \cdot V^2) \qquad (6\text{-}1)$$

For a wide cavity with fully developed laminar flow the friction factor correction (k_f) is 1.5 and the friction factor (f) can be solved from Equation 3-12.

$$f = k_f \cdot f_{circular} = 1.5 \cdot \frac{64}{\mathrm{Re}} = \frac{96}{\mathrm{Re}} \tag{6-2}$$

The Reynolds number (Re) for standard conditions (approximate ρ = 1.2 kg/m^3 and μ = 18 E-6 N s/m^2) is determined using:

$$\mathrm{Re} = 66400 \cdot D_h \cdot V \tag{6-3}$$

Spacers were added at 0.4 m intervals within the cavity to maintain the 14.8 mm depth. Employing a channel width (w) of 0.4 m and a depth (d) of 14.8 mm the hydraulic diameter can be determined from Equation 3-12. The resultant hydraulic diameter (D_h) is 28.5 mm.

The average velocity (V) is the volumetric flowrate over the cross-section of the flow path.

$$V = \frac{Q}{A} = \frac{Q}{w \cdot d} \tag{6-4}$$

Combining Equations 6-2, 6-3, and 6-4 into 6-1 results in the following pressure drop relationship.

$$\Delta P = \frac{L \cdot Q}{1153 \cdot w \cdot d \cdot D_h^2} \tag{6-5}$$

Maintaining cavity thickness tolerances to within 1 mm was difficult. Weights were set on top the test apparatus as shown in Figure 6-5 to maintain the cavity thickness tolerances during testing.

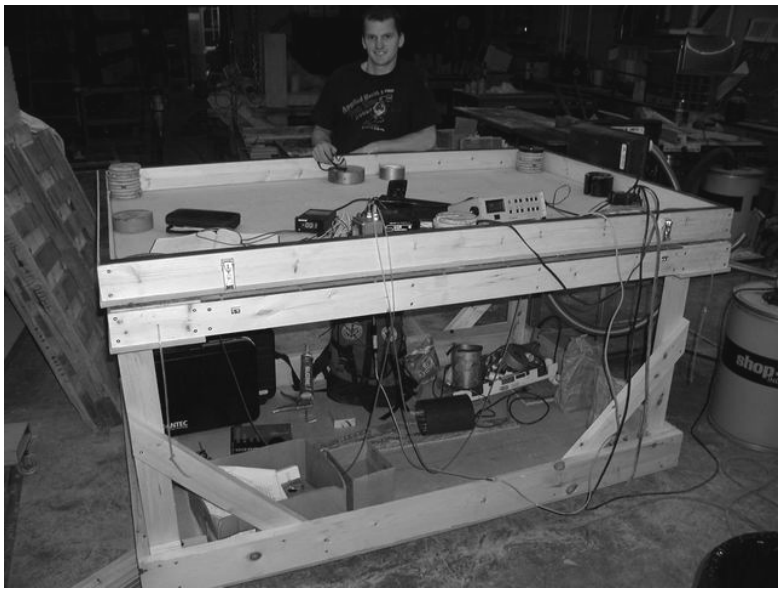

Figure 6-5: Test Rig Setup for Validation

Figure 6-6 is a plot of the test results compared to Equation 6-5. The agreement is within 5%. Hence, the precision and accuracy of the experimental setup was considered adequate for this study.

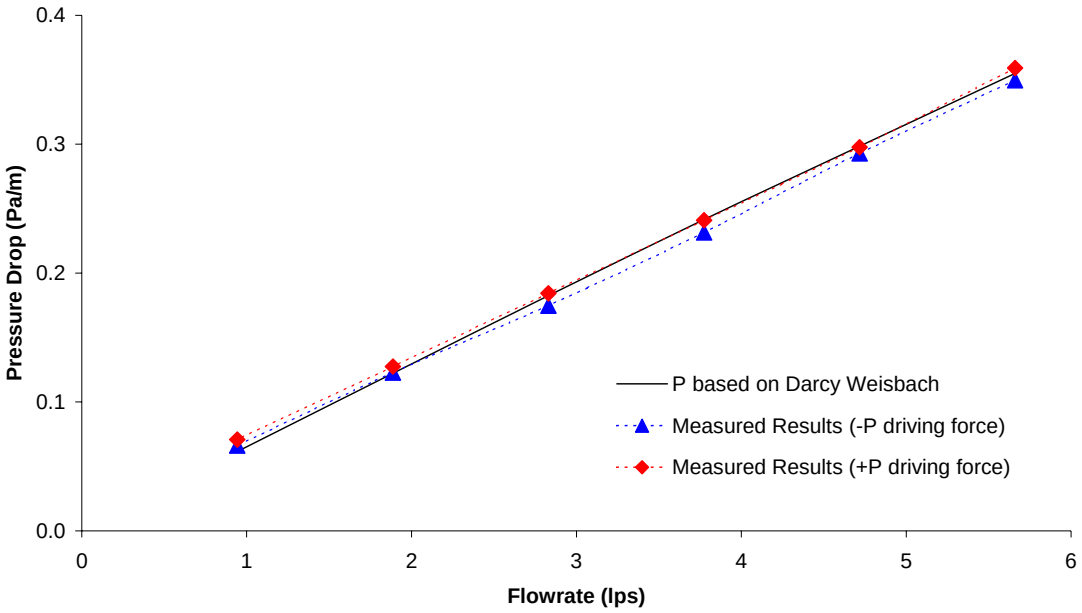

Figure 6-6: Theoretical vs. Actual Pressure Drops for Rectangular Cavity.

6.4.2. Vinyl Siding Installation

A representative type of vinyl siding ("double 4") was installed on the test rig. A typical installation is shown in Figure 6-7 of vinyl siding shows the general layout and a sample of the variability in joint geometries.

Figure 6-7: Typical Installation of Vinyl Siding (Waterloo, Canada)

The dimensions of the vinyl siding are shown below. The siding is either contact applied or installed over 19mm wood spacers (furring). J-trim and other edge connections were not tested.

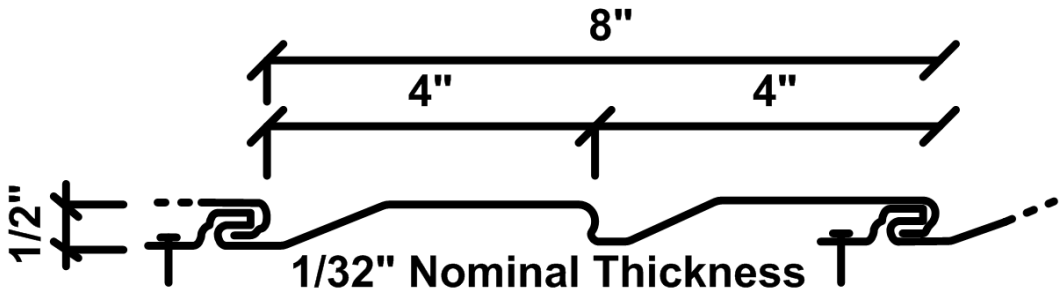

Figure 6-8: Vinyl Siding Dimensions

The test rig was designed to allow airflow through a large area (about 2.5 m^2) of the face of the cladding by forcing air through slots situated at opposite ends of the test length as shown in Figure 6-9. For these measurements the vinyl was installed on 19 mm furring strips to allow a pressure equalized space to form under the entire area of the cladding.

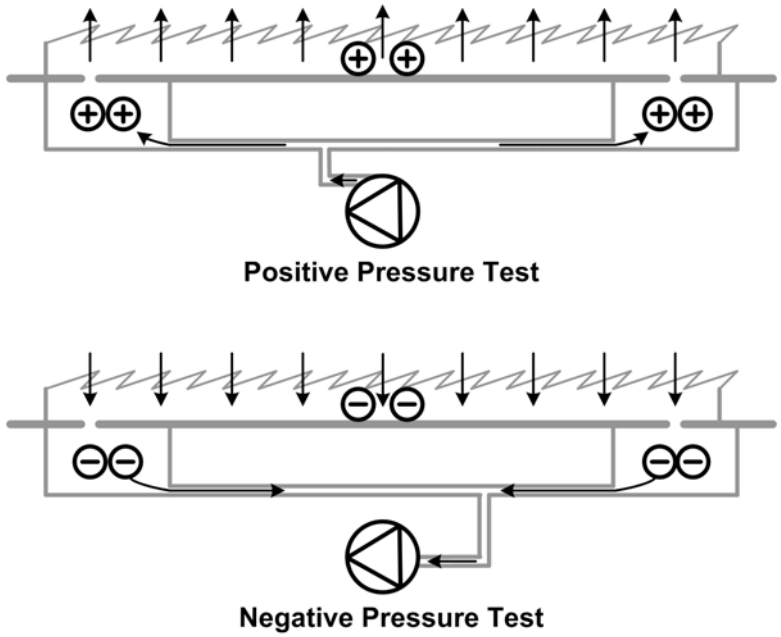

Figure 6-9: Out-of-Plane Flow through Cladding Setup Schematic

A series of positive and negative pressures were applied behind the siding and the resultant airflow rate was measured. The vents in the face of the vinyl siding, including gaps at vertical siding joints, gaps at the horizontal joints, and drainage holes immediately above the horizontal interfaces, were sealed and test setup air leakage was determined.

The vertical and horizontal joints were investigated. In the results, the drainage holes are included as part of the horizontal joints. Vertical joints could be measured independently by sealing the horizontal joints (using duct tape) only and vice versa.

As per the discussion in Section 6.4, a lid was designed to surround the cladding and was either positively or negatively pressurized by a separate blower system to control the air pressure difference between the cavity and the outside of the cladding. Within this lid the siding was attached to test the in-plane vertical flow characteristics. The resulting test deflections and test setup are illustrated in Figure 6-10.

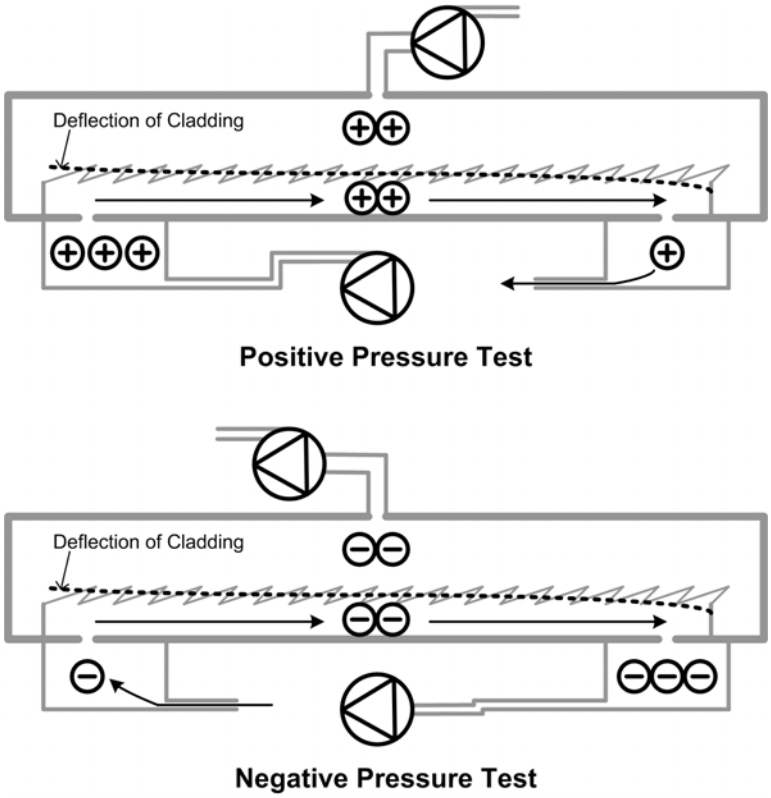

Figure 6-10: In-Plane Vertical Flow Setup Schematic

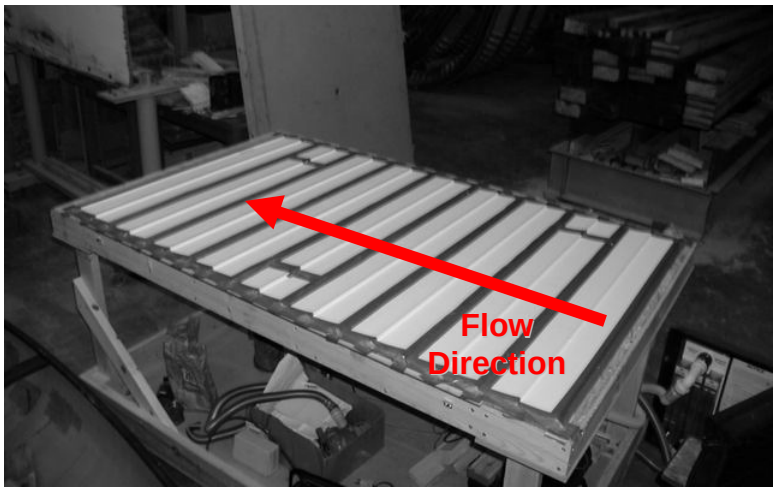

Figure 6-11: In-Plane Vertical Flow Setup

The test rig was also set-up to apply a pressure gradient along a wide cross section (1.2 m) across the backside of the vinyl siding for in-plane horizontal flows (Figure 6-13). For these flows significant deflections of the vinyl siding were also observed during initial airflow tests and the effect on the cavity's airflow resistance was also apparent. The lid was again used to surround the cladding and was either positively or negatively pressurized by a separate blower system to control the air pressure difference between the cavity and the outside of the cladding. The observed deflections and test setup are illustrated in Figure 6-12.

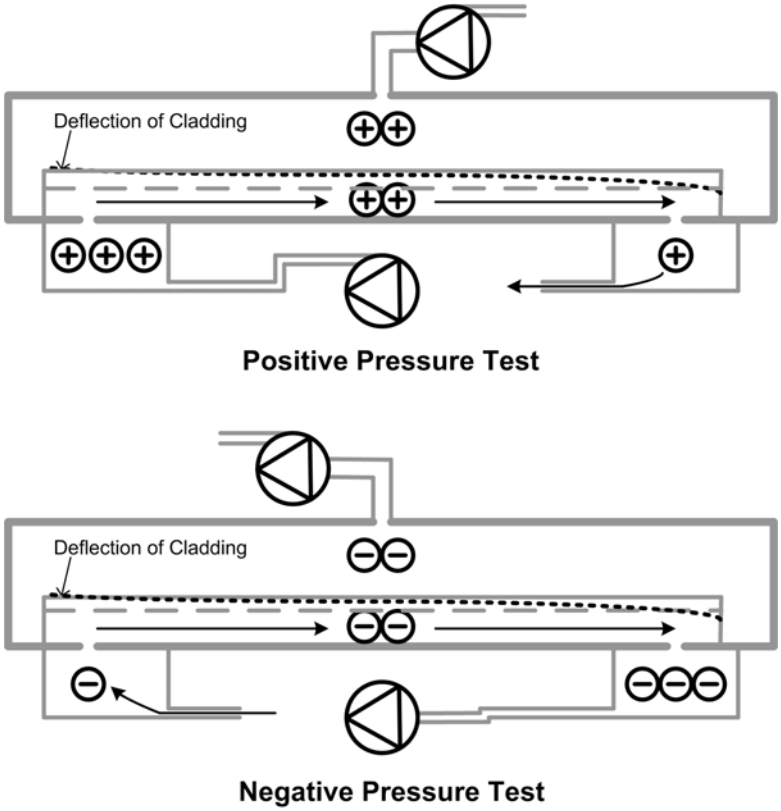

Figure 6-12: In-Plane Horizontal Flow Setup Schematic

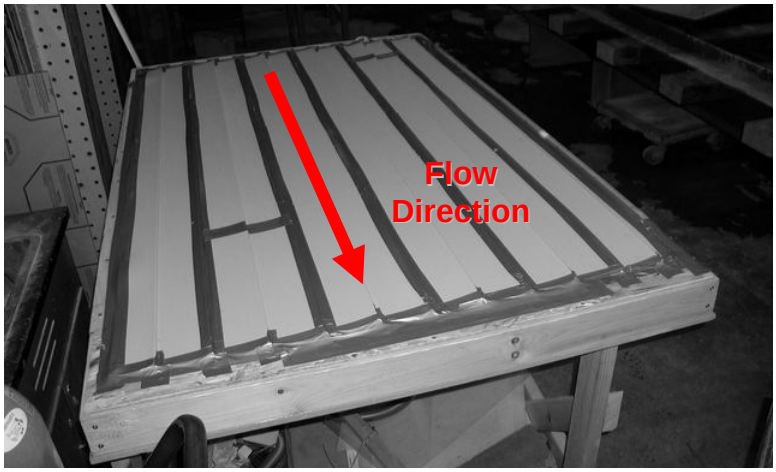

Figure 6-13: In-Plane Horizontal Flow Setup

6.5. Results and Discussion

The results of the experiments are presented in terms of pressure drop measurements as a function of flowrate normalized per unit area or length. For out-of-plane flow the pressure is across the siding and the flowrate is per m^2 of siding face. For the in-plane flows the pressure is per metre length of the siding and the flowrate is across a 1 m wide cross section.

6.5.1. Out-of-Plane Airflow through Cladding– Air Permeability of Vinyl Siding

Two separate equation sets were applied to characterize the resistance of out-of-plane airflow through the cladding. The first equation is the power law equation (ASHRAE 2001 F26.12 Equation 32) that is commonly used for building air leakage measurements (typically conducted using blower door):

$$Q = c(\Delta P)^n \tag{6-6}$$

where,

c and n are constants.

The second equation used is a simplified extension employing Effective Air Leakage Area (EALA) (ASHRAE 2001 F26.12 Equation 33) where n is equal to 0.5 (i.e. valid for leakage through sharp edged orifices)

$$Q = A_L C_d \sqrt{\frac{2\Delta P}{\rho}} \tag{6-7}$$

where,

A_L is the leakage area – labeled AL on graphs, and

C_d is the discharge coefficient – labeled CD on graphs.

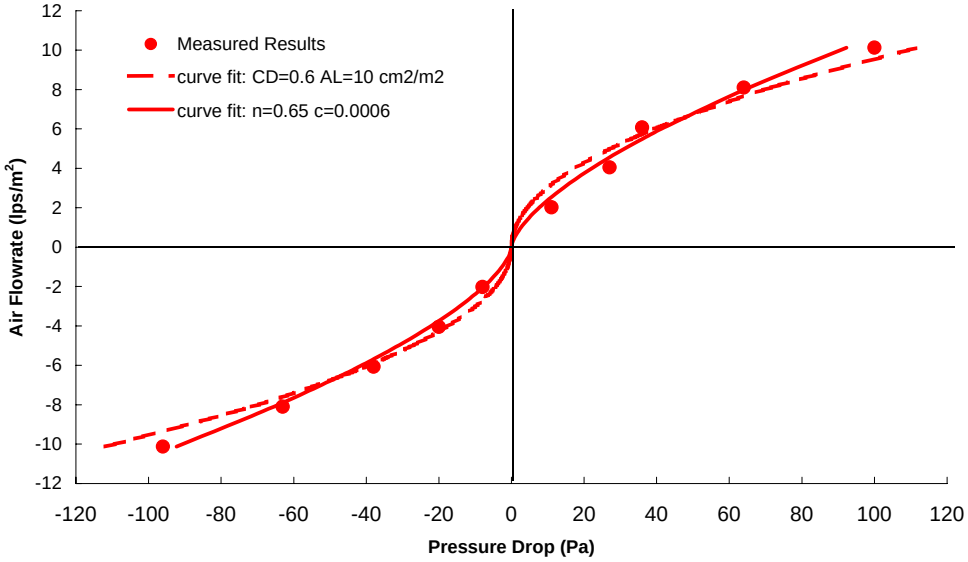

Figure 6-14: Air Flow Resistance through Vinyl Siding

An airflow permeance value (for use in an equation of the form Q = K ΔP) was not determined, because it would not be appropriate for the non-linear flow vs. pressure drop relationship observed. However, over small pressure ranges, such a permeance would be acceptable for some uses, and the appropriate permeance value can be determined from the equations presented. Good correlation is shown for both equations in Figure 6-14. The power law coefficients determined from the experiment are n = 0.65 and c = 0.00060 $m^3/(s\ Pa^n)$. Applied pressures of 1 to 10 Pa would drive airflows of 0.6 to 2.7 lps/m^2. The power law is a superior correlation since the relationship matches the data better at lower (more common in service) driving pressures than the EALA. The superiority of the power law is due to the greater flexibility in the equation to adjust the power n. More data points at low driving pressures would be an improvement upon the study.

EALA is a useful measure due to its simplicity and practicality. The effective air leakage area was found to be 10 cm^2/m^2. This air leakage area is equivalent to a 1 mm vertical joint per metre width and 0.07 mm wide horizontal joints at 200 mm intervals. Joint widths were further investigated by blocking portions of the joint length. The results are shown in Figure 6-15 along with predictions using the estimated joint air leakage characteristics.

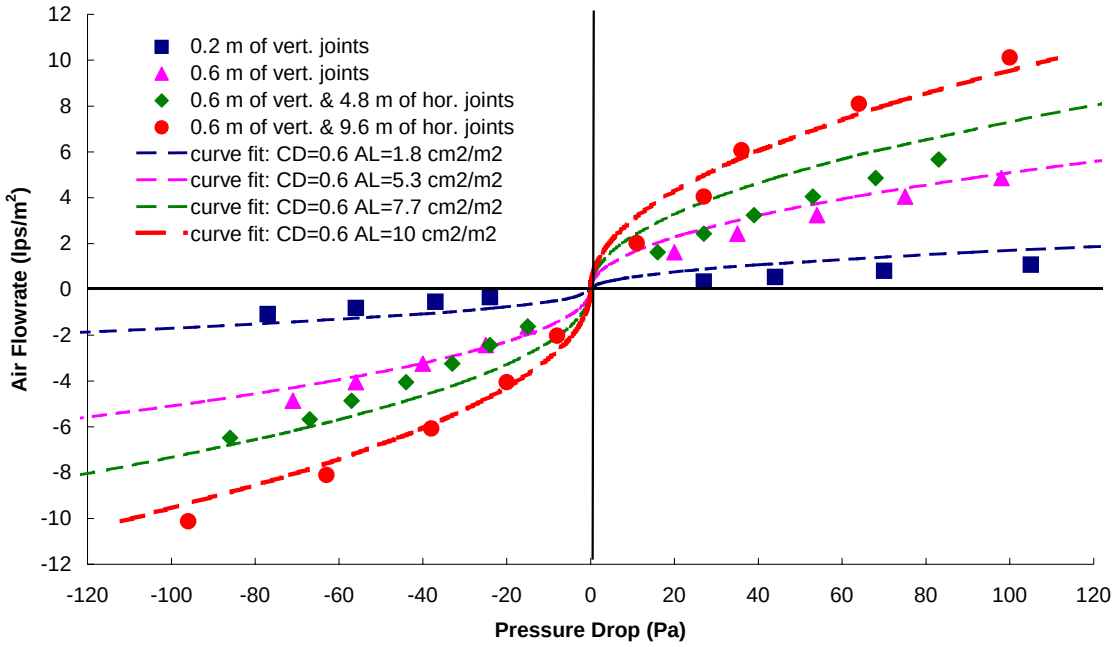

Figure 6-15: Air Flow Resistance for Various Joint Lengths

The EALA correlations have limited accuracy because the actual flow paths are not all sharp edged orifices. Figure 6-15 shows the inaccuracy of the effective air leakage area correlation. Another challenge to assigning coefficients for either equation is that the vinyl siding is flexible and hence joint widths and shapes will change as the openings bend with varying applied pressure. The joints will open up at high positive pressures and close at high negative pressures.

It is interesting to note that the flow behavior in the outward direction is different than the flow inward in some situations (Figure 6-15). However, the difference is not drastic and will have a negligible effect on in-service ventilation flow.

6.5.2. In-Plane Vertical Airflow Behind Cladding

Airflow resistance for flow behind the installed siding in the in-plane vertical flow direction (see Figure 6-3) was investigated. Figure 6-16 shows the results for upward and downward flow.

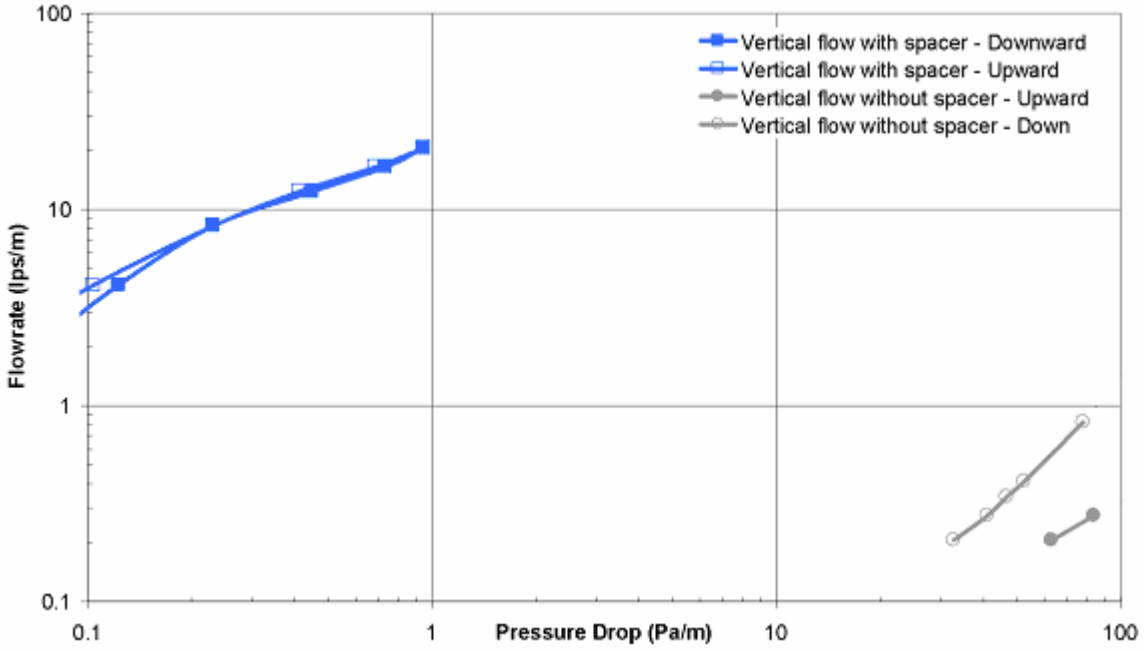

Figure 6-16: Air Flow Resistance Measurement of In-Plane Vertical Flow (Different Flow Directions)

In the vertical direction little airflow occured at large applied pressures without the inclusion of furring. The results derived for the low flowrate measurements have poor accuracy considering the similar magnitude of the measured flowrates and the system air leakage through the duct-taped surface seal. This airflow is low enough to be insignificant in subsequent modeling and hence, efforts to improve the accuracy were not undertaken.

Air easily flowed vertically with the inclusion of the spacer. This was expected because the flow cavity was greatly enlarged.

Changing the direction of the vertical in-plane flow (between upward and downward) had a significant effect only when the siding was contact applied. The dependence of flow resistance on direction in this case is assumed to be due to the development of eddies in the downward flow case. For upward flow the tapering of the profile avoids the formation of such eddies. This is shown below in Figure 6-17. These flows have not yet been confirmed with flow visualization.

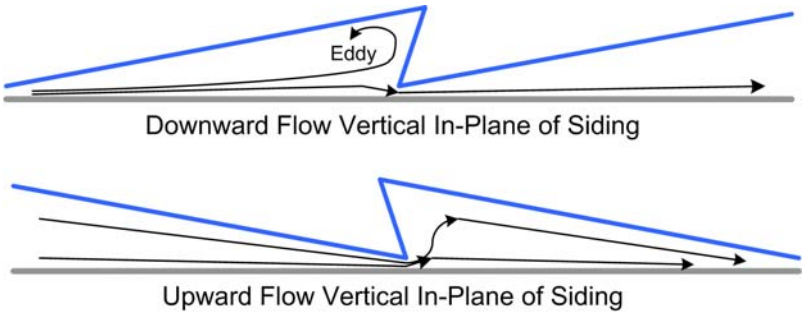

Figure 6-17: Speculated Contact Applied Vertical In-Plane Air Flow

It was observed that varying the static cavity pressure relative to the air pressure outside the siding had a significant effect on the vertical airflow. The effect was most prevalent for the contact applied installation. These results are shown in Figure 6-18.

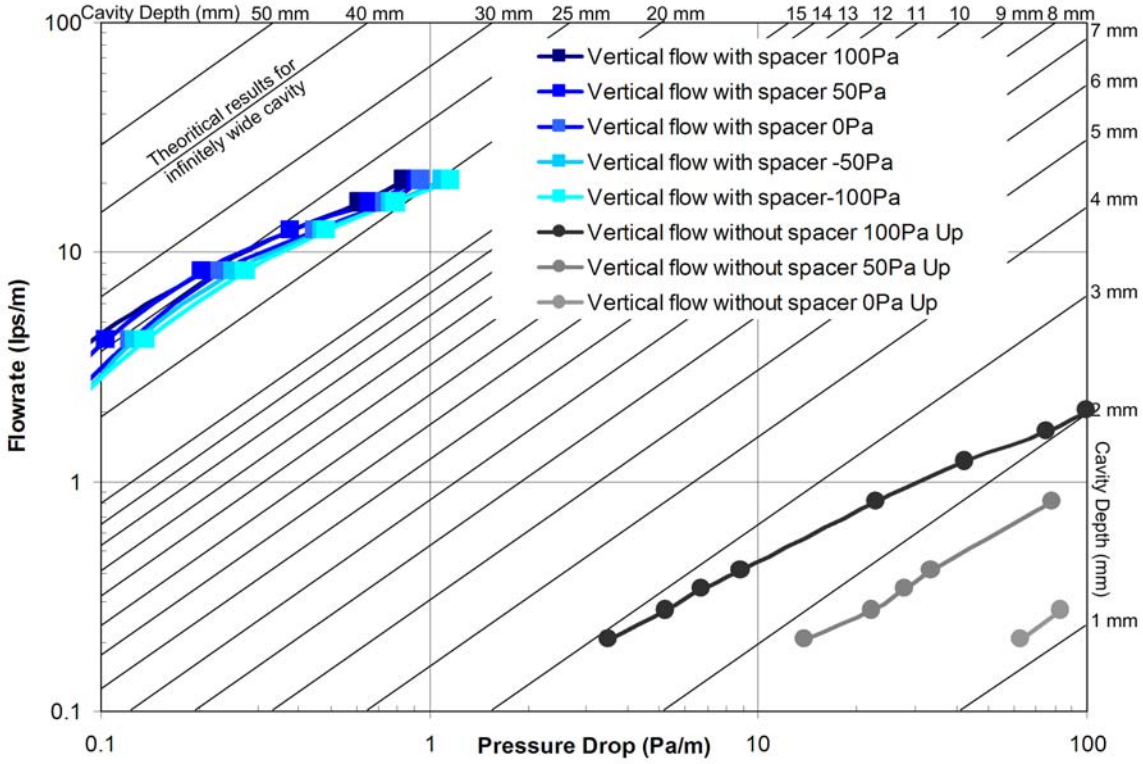

Figure 6-18: Vertical In-Plane Flow Measured Results and Equivalent Cavity Depths (Varying Cavity Pressures)

Airflow resistance tends to increase with greater applied pressures pushing the siding face against the test bed. The dependence of flow resistance on cavity depth is shown in these results. Applying pressure deflected the siding and changed the cross sectional area of flow path behind the siding. To illustrate this effect the plot has been enhanced with lines showing airflow resistance characteristics for an infinitely wide cavity at various cavity depths.

For vertical flow with furring the equivalent cavity depth is between 20 mm and 26 mm regardless of surface applied pressure. The furring strip adds 19 mm to the actual depth

of cavity. The equivalent depth is expected to be slightly larger than 19 mm since vinyl has a hollow profile and negative pressures across the face of the siding will tend to increase the cavity depth by bending the vinyl.

For vertical flow without furring the equivalent cavity depth ranges from 0 to 3 mm. Without a pressure differential across the siding the narrow gaps at the contact lines between the siding and the application surface cause an equivalent cavity depth overall of 1mm. By applying large suction pressures pulling the siding away from the contact surface raises the equivalent depth to 3 mm.

6.5.3. In-Plane Horizontal Airflow Behind Cladding

Airflow resistance for flow behind the installed siding in the in-plane horizontal flow direction (see Figure 6-3) was investigated. A plot of these results is shown below in Figure 6-19.

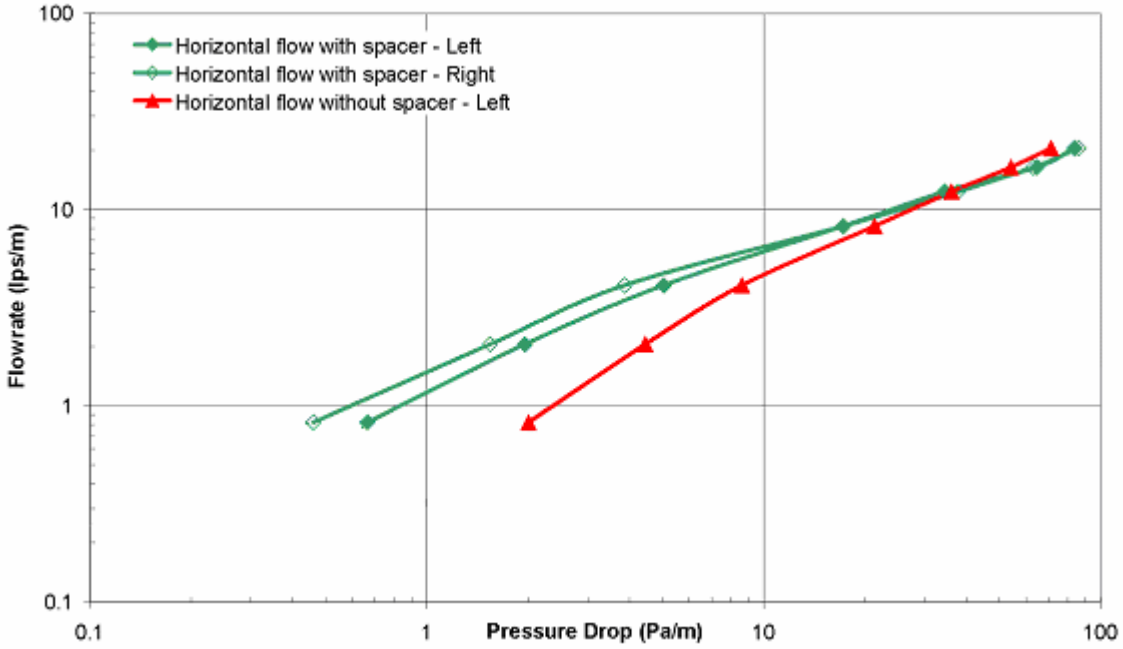

Figure 6-19: Air Flow Resistance of In-Plane Horizontal Flow

The horizontal direction flow displayed less predictable results than the vertical direction results. The effect of the spacers was not as significant as in the vertical direction. This is due the large flow path cross sectional area already provided by the profile of the siding. In fact, at high airflow rates the turbulence cause by the spacer's obstruction to the airflow path caused the inclusion of spacers to increase the pressure drop thereby making airflow more difficult. This effect is illustrated in Figure 6-20 and is yet to be investigated with airflow visualization.

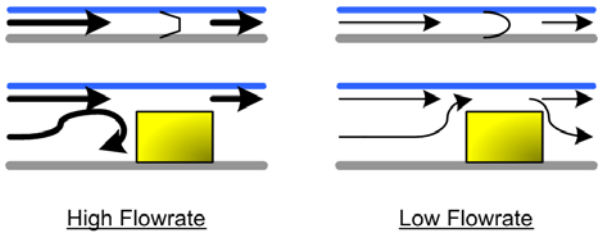

Figure 6-20: Effect of Spacers at High and Low Flowrates

Changing the direction of the flow in the vertical direction had little effect on the airflow characteristics of the vinyl siding as the flow path is similar.

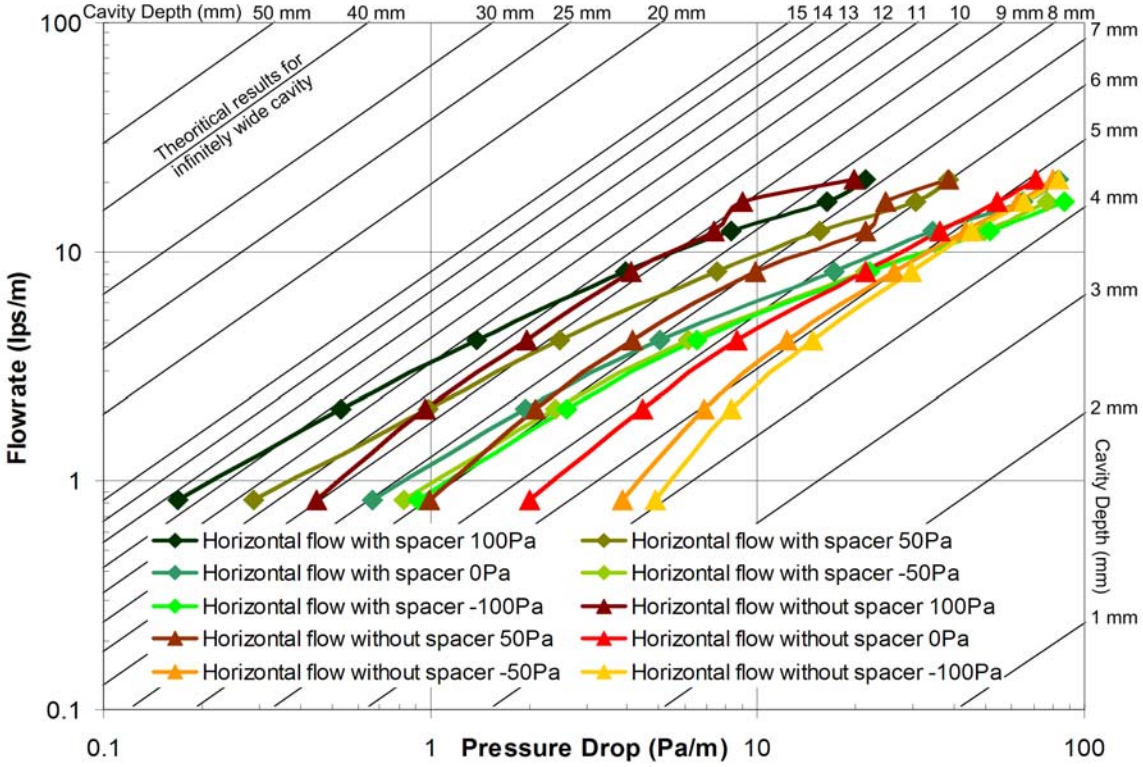

Figure 6-21: Horizontal In-Plane Flow Results and Equivalent Cavity Depth

For horizontal flow without furring the profile of the siding gives an equivalent cavity depth of 5 to 6 mm with a balanced pressure across the siding (i.e. no deflection of the siding). Deflecting the siding by generating a pressure differential across the siding between –100 Pa and 100 Pa resulted in equivalent cavity depths ranging from 10 mm to 4.5 mm respectively.

For horizontal flow with furring the equivalent cavity depth has a greater range between 8 mm and 4.5 mm. The siding installed over the 19 mm spacer had equivalent depth results significantly less than 19 mm. This is expected since the flow has to cross over the spacers as illustrated in Figure 6-20. The greater range in equivalent depths is due to the generation of eddies at greater flowrates impeding the flow.

6.6. Conclusions and Recommendations

6.6.1. Conclusions

A vinyl siding cladding system has been characterized in terms of airflow and resistance for a range of flow paths that are believed to be representative of service conditions. Airflow through the face of vinyl siding can be expected to be in the range of 0.6 to 2.7 lps/m^2 for pressures of 1 to 10 Pa.

Little (likely negligible) airflow will occur along the in-plane vertical flow direction behind contact-applied vinyl siding. The addition of vertical 19 mm strapping behind contact-applied horizontal vinyl siding increases the cavity airflow in the direction of the strapping by at least three orders of magnitude. In-plane horizontal flow could be significant for both contact applied horizontal vinyl siding and vinyl siding over strapping.

Deformation of the vinyl siding due to relatively small pressure differences between the cavity and outside air was found to have a significant effect on airflow resistance for contact-applied vinyl siding.

6.6.2. Recommendations for Future Testing

The flow characteristics of wood siding, brick veneer, steel panel systems, and other claddings of interest should be tested. These claddings and vinyl siding should be tested with the installation of a sheathing membrane to study ballooning affects.

The air permeance testing should be completed for more data points at low driving pressures, and vertical and horizontal airflow resistances behind the siding at lower applied pressure differences (such as 10 Pa) across the face of the siding should be studied. These lower pressures are significant because of their common occurrence during in-service conditions.

The deformation of the vinyl siding had significant effects on airflow resistances. The deformations should be measured and the relevance of this characteristic should be further explored.

The airflow resistance through airflow networks that are created by real wind pressures and buoyancy effects in field should be further explored. Airflow visualization methods should be applied to field exposure conditions to further our understanding. The relationship between the characterizations techniques and real ventilation rates should be determine to guide and make practical use of these measurements.

6.7. References

ASHRAE, *Handbook of Fundamentals* Atlanta, Ga, 2001.

Burnett, E., Reynolds, A. *Final Report - Ontario Wall Drying Study,* University of Waterloo, Building Engineering Group Report for Canada Mortgage and Housing Corporation, Ottawa 1991.

McCuaig, L. *Final Report on the Drying of Walls – Atlantic Canada 1987,* Canadian Mortgage and Housing Corporation, Ottawa 1988.

7. FIELD VENTILATION STUDY

Ventilation airflow behind brick veneers enters through vent openings (A-B), flows through a ventilation cavity (B-C), and then exits through a second vent (C-D) some distance from the first (Figure 7-1).

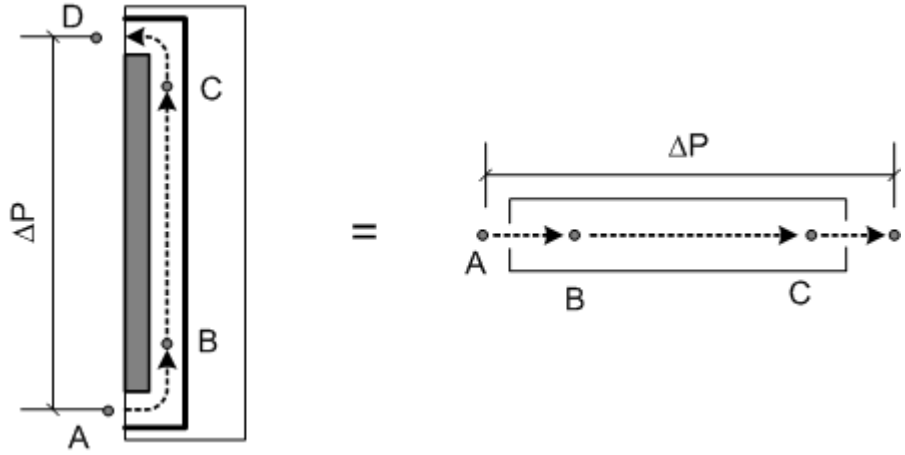

Figure 7-1: Simplified Ventilation System behind Brick Veneer

In North America vents in brick veneer walls typically consist of weep tubes and open head joints (with and without screen or insect control inserts) and either an open top slot or vertical vents at the top of cavities. The top of ventilation cavities behind brick veneers may be defined by the intersection with a window sill, shelf angle, roof overhang, etc. Vents are intentionally included at these interfaces to a encourage ventilation. Open top slots are common in residential buildings as the simplest finishing detail for the roof interface, whereas top vents of open head joints are more common in commercial construction. Figure 7-2 is an illustration of a typical ventilated brick veneer wall (similar to the field tests) with three possible vent openings labeled.

The ventilation cavity is typically between 20 mm (most wood-frame low-rise residential) and 50 mm (some commercial construction). The space is often somewhat blocked with mortar protrusions (or bulging insulation) and mortar droppings at the bottom of the space.

Significant airflows have been measured through ventilation cavities of this size. For example, these results indicate average cavity air velocities of:

- 0.05 to 0.2 m/s for a 40 mm clear cavity with a 30 mm top slot vent and open head joint weep holes every 250 mm at the base (Jung 1985), and
- 0.2 to 0.6 m/s over a range of windspeeds of 0 to 8 m/s for panel cladding systems with open lower and upper slot vents (Schwarz 1973).

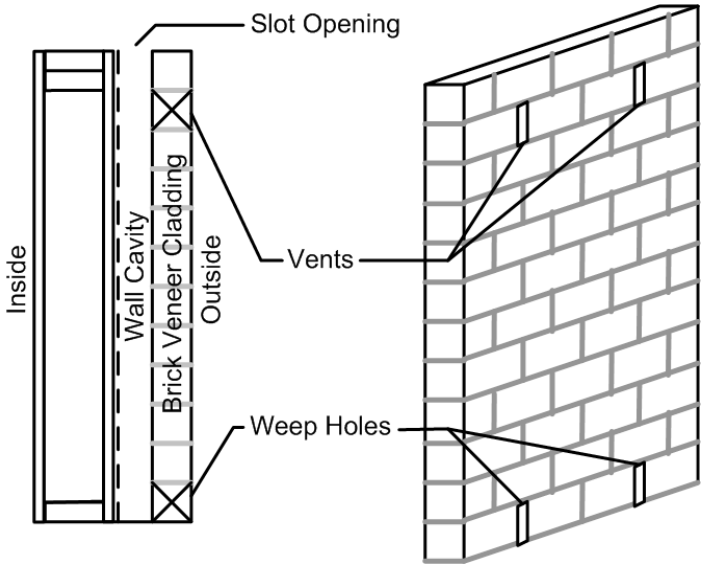

Figure 7-2: Illustration of Field Brick Wall Samples

Ventilation of brick cladding may significantly affect hygrothermal performance (Straube 1998, Popp et al. 1980, Kuenzel and Meyer 1983). Understanding the rate and nature of the airflow behind brick veneers is necessary to predict the impact of ventilation on hygrothermal performance.

The cavity airflow rate may be predicted from fluid mechanics principles of steady-flow system behaviour and driving pressure data (as in Chapters 3 and 4). However, the impact of complex dynamic wind effects, multiple vent points, and complex flow paths are neglected in such a simplified approach. This reports details the measurements of steady state airflow characteristics of field test walls and cavity airspeeds under natural exposure conditions.

7.1. Objective

The field ventilation study had two main objectives:

1. To measure the relationship between the ventilation airflow rate and system pressure drop for field test walls, and
2. To measure the magnitude of naturally induced ventilation and determine the relationship of ventilation flow to exposure conditions.

7.2. Scope

The work included the measurement of steady-state airflow resistance of three brick veneer walls exposed to field conditions. Brick veneer claddings with vents as opposed to slots were selected for this study as the less ventilated case of the two assembly options.

This chapter includes a review of previous related lab studies. The experimental approach, setup, and measurements of systems leakage are included in Section 7.4. Results and discussion of steady-state airflow characterization experiments with forced airflow and correlations between airflow rates and point velocity measurements are

included in Sections 7.5.1 and 7.5.2. Naturally-induced ventilation airflows driven by wind and buoyancy forces are presented in Section 7.5.3. This data is compared to predictions employing methods presented earlier in this thesis. Conclusions regarding the extent of ventilation behind ventilated brickwork and recommendations for further studies are included in Section 7.6 to close the chapter.

7.3. Experimental Program

7.3.1. Test Specimens

Walls were constructed as part of the accompanying field wall drying study (see Chapter 8 and Appendix B for wall details and labeling code). Three walls with brick veneer and two walls with vinyl siding were constructed. The walls clad with vinyl siding have an uneven geometric profile, and the multiple flow path systems (as described in the Chapter 6) of the siding are much more complex than for the brick veneer samples. Point airspeed measurements behind vinyl siding would be very difficult to interpret and were therefore not included in this study.

The basic wall configuration was a 1.22 m wide by 2.44 m high brick veneer wall. The wall design details are described in further detail in Appendix B. The ventilation cavity was either a 20 mm or 50 mm relatively clean space ventilated through two pairs of top and bottom open head joints (approximately 10 mm by 80 mm). These vents were clear and open and did not include any screens (commonly applied to keep pests out of wall cavities). One wall was further monitored for wind and buoyancy induced ventilation. These airflow resistance characteristics and ventilation rate measurements are compared to predictions.

7.3.2. Methodology

The airflow system in the ventilated brick veneer test walls is illustrated in Figure 7-3.

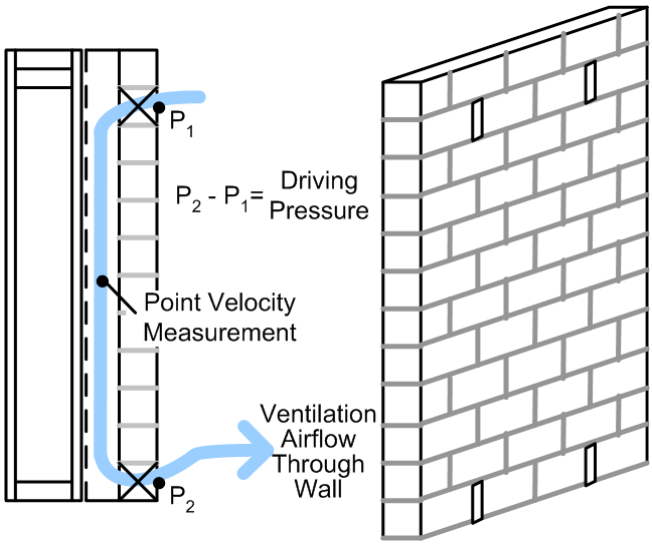

Figure 7-3: Airflow through Ventilated Brick Veneer

The ventilation airflow versus driving pressure relationship was determined for each sample by drawing a steady, measured rate of air from the bottom vents with the top vents left open. The driving pressure was measured as the difference between the suction pressure and the outdoor ambient pressure.

The relationship between driving pressure and ventilation airflow developed can be applied to field driving pressure data to predict flows. Airspeed was measured at several points within the ventilation cavity to confirm this flow versus pressure relationship when exposed to dynamic natural driving forces. It was hoped that the airspeed measurements could be used to confirm airflow rates by applying the continuity equation ($Q = V / A$). To determine if this approach was valid, the relationship between the point airspeed measurements and airflow was determined using the same setup as the airflow and driving pressure experiments.

Ventilation airflows due to natural driving forces were estimated from measured point airspeeds within the ventilation cavity and measured conditions affecting wind and buoyancy driving pressures. Driving pressures for buoyancy effects were determined from ventilation cavity and outdoor condition data. Driving pressures for wind effects were both measured and determined from standard weather station measurement of wind speed and direction measurement. Measurements of driving pressures and point airspeeds were both used to investigate the extent of ventilation airflows. Ventilation airflow due to natural driving forces was also confirmed with smoke pencil testing.

7.3.3. Equipment and Instrumentation

A manifold was attached to each wall to create a negative pressure (relative to outdoors) over the face of the lower wall including the bottom two vent holes. This setup is illustrated in Figure 7-4.

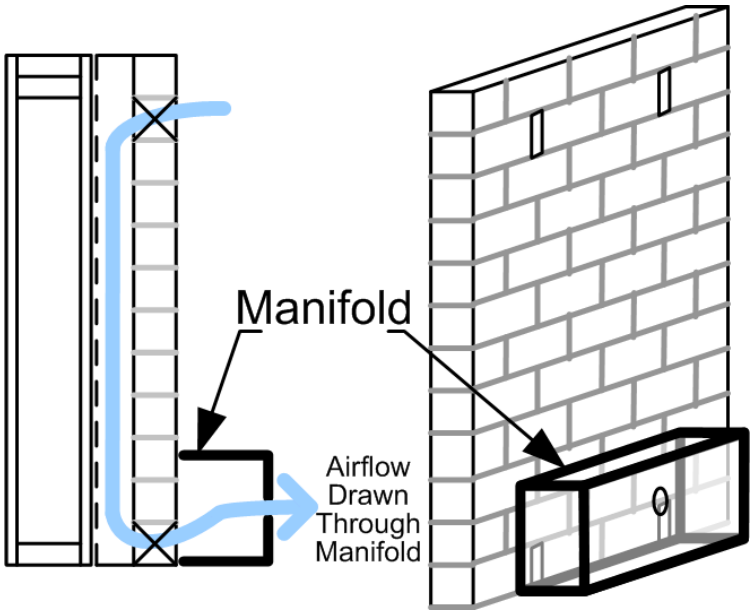

Figure 7-4: Forced Air Flow Path through Ventilation Cavity

Flow rates in forced flow experiments were measured using rotameters (0-1.5 lps with +/- 0.04 lps accuracy and 0-10 lps +/- 0.1 lps). A Modus 0-100 Pa pressure transducer with +/- 0.5 Pa accuracy was employed for the forced flow measurements. The data was logged by hand for both these instruments. All other data was recorded on a data acquisition system. The setup of the manifold and rotameters is shown in Figure 7-5.

Figure 7-5: Photograph of Setup for Induced Flow Measurements

Cambridge Accusense AVS-1000 anemometers were selected to measure point air velocities. These sensors have a range of 0 to 0.500 m/s with an accuracy of +/- 0.025 m/s and a resolution of 0.002 m/s. The sensors were securely installed in the ventilation air space of the brick wall specimens from the indoors. They were positioned to measure vertical airspeed at mid height within the ventilation cavity at the centre of the cavity width, 100 mm from the edge of the cavity, and 230 mm from the edge of the cavity.

Air pressure was measured at various points on the surface of the walls to allow for the study of imposed wind pressures. Pressure was transmitted to transducers by 3.5 m long flexible plastic tubing (3 mm internal diameter, 6 mm external diameter). The pressure was averaged between left and right vents by connecting the pressure taps at a tee. An Ashcroft pressure transducer with a range of +/- 12.5 Pa with +/- 0.07 Pa accuracy was employed. The transducer was calibrated using a precision Betts manometer (of 0.01 mm water column or 0.1 Pa accuracy). The air temperature within the wall cavity was measured using a Fenwal 10 kΩ thermistor with +/-0.2^{o}C accuracy and the relative humidity was measured with a Honeywell HIH-3610 RH sensor with +/- 2% relative humidity accuracy. Outdoor conditions were acquired from a weather station.

The setup of the data acquisition system (DAS) and sensors is shown in Figure 7-6. An illustration of all of the measurement points is included in Figure 7-7.

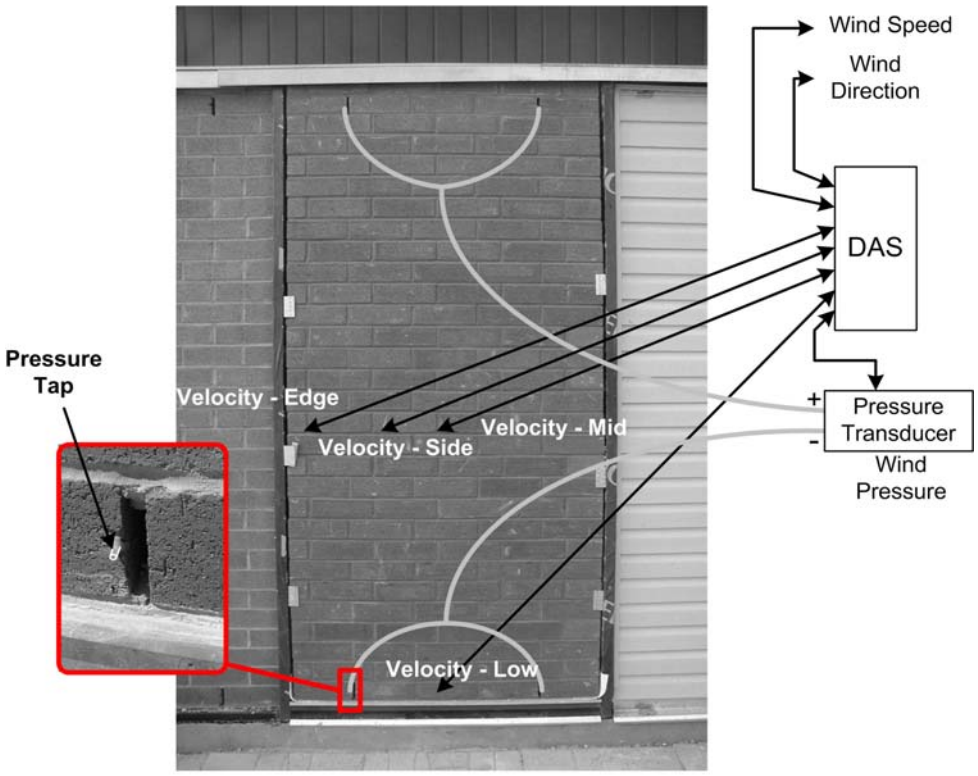

Figure 7-6: Experimental Setup for Natural Flow Measurements

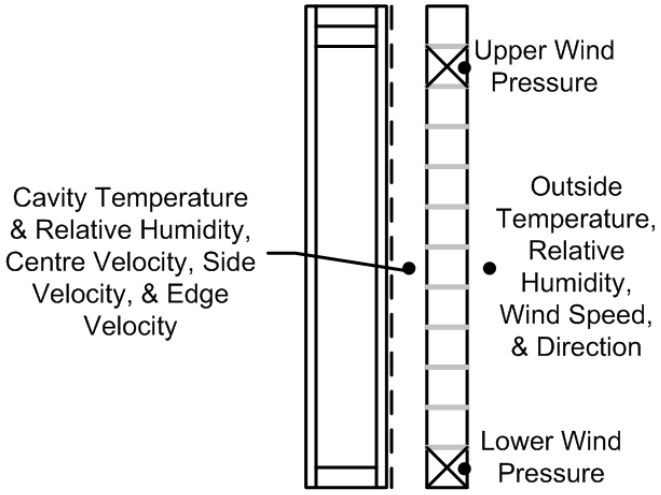

Figure 7-7: Measurement Points

7.3.4. Test Wall and Manifold Air Leakage

Since the manifold was not guarded (see Newman and Whiteside's (1984) guarded manifold), it was assumed that some air would leak from the interface between the manifold and the brickwork and through the brickwork within the manifold area. It was necessary to quantify the leakage through both the seal between the manifold and the brickwork and through the brickwork itself.

The total air leakage of these two alternative flow paths was measured by blocking the bottom vents and then drawing air through the manifold.

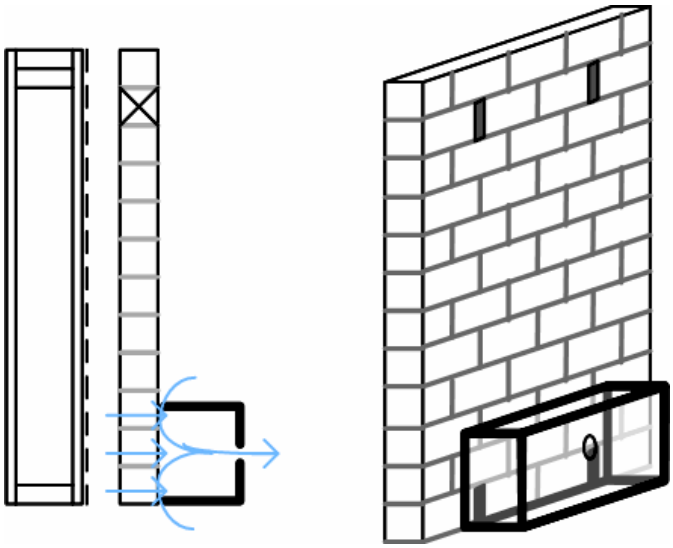

Figure 7-8: Manifold Leakage and Brickwork Air Permeance Testing Setup

The results for the manifold leakage and brickwork air permeance measurements (often termed system leakage in air leakage tests) are shown in Figure 7-9. The results are also compared to measured air permeances of a wide range of brickwork from Newman and Whiteside (1984).

Based on the total system flow reported later in this report, (approximately 10 lps at 50 Pa) it can be concluded that the air leakage through the manifold and brickwork, estimated to be less than 0.2 lps at this pressure, represents only 2% of the total flow. When compared to the results of Newman and Whiteside, it can be seen that the air permeance of the brickwork is a small fraction of the total system leakage.

Most of the remaining air follows the intended path through the top vents, down the ventilation cavity, and out the bottom vents through the apparatus. The portion of the air that does not follow this intended path is termed “air leakage” in this report and is illustrated in Figure 7-10.

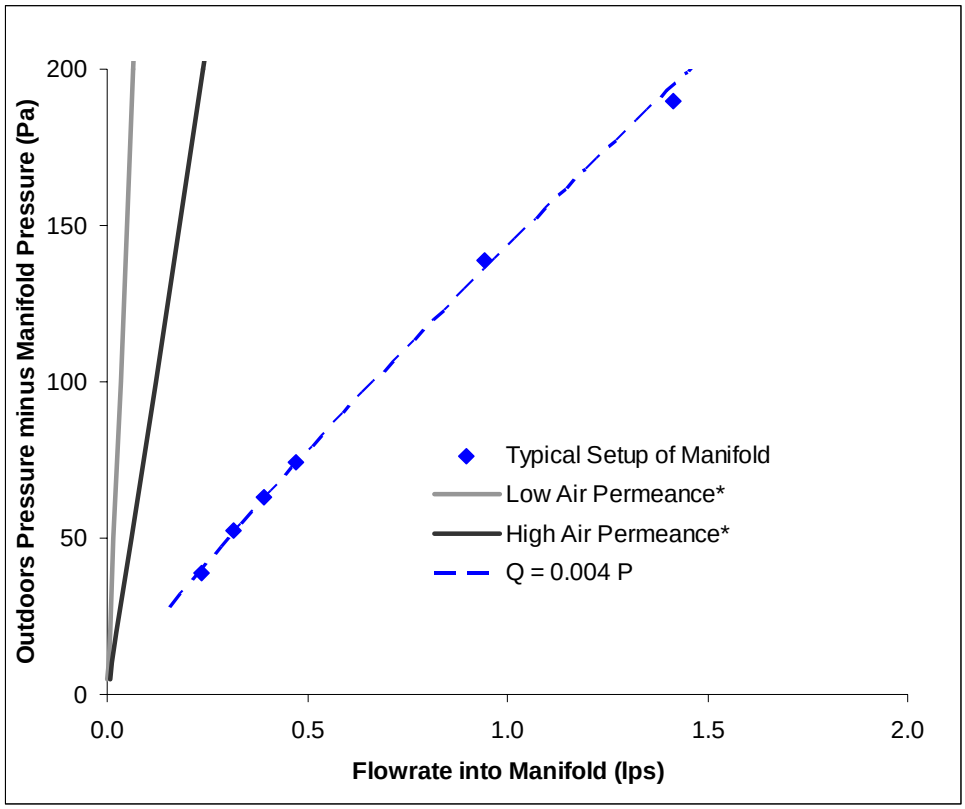

Figure 7-9: Manifold Leakage
*** Newman and Whiteside (1984)**

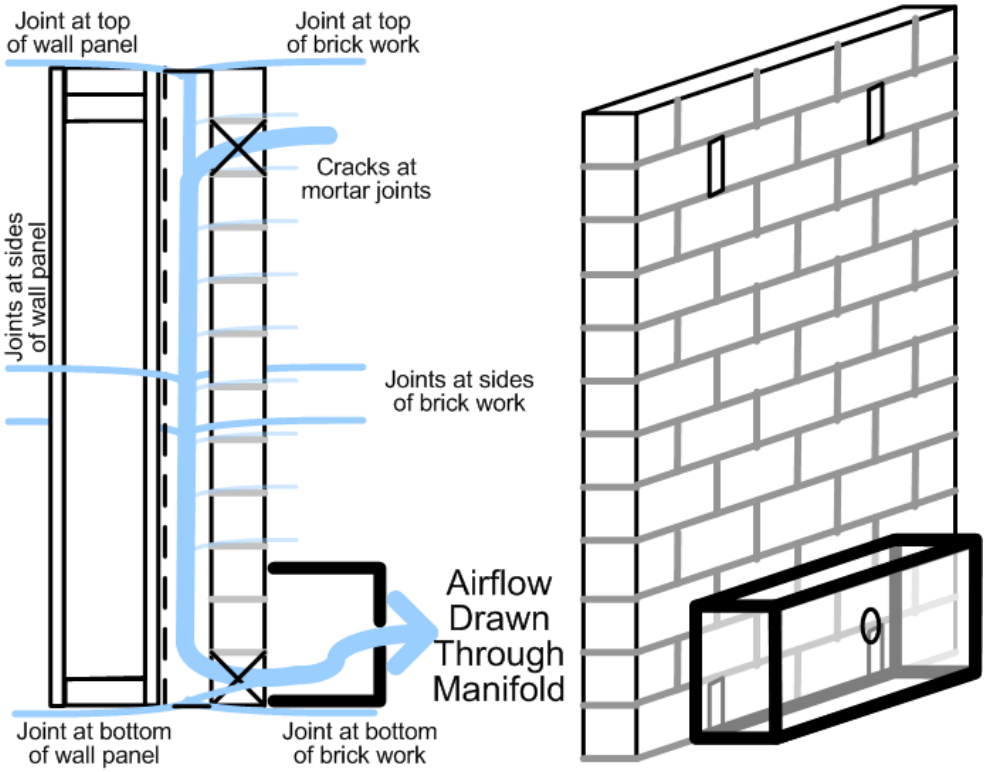

Figure 7-10: Actual Air Flow Forced Through the Wall Cavity

The three field brick veneer walls were tested for air leakage before the ventilation flow. This air leakage was determined by blocking the top vents and drawing a measured rate of air from the bottom vents. This experimental setup is illustrated in Figure 7-11.

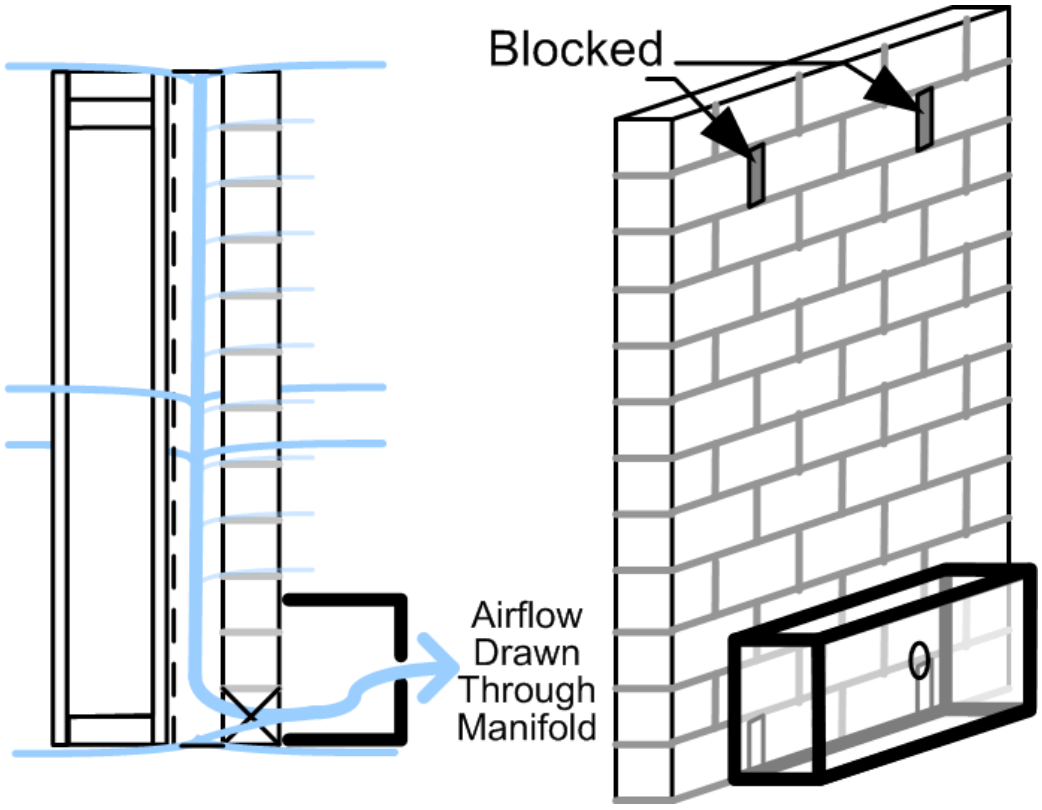

Figure 7-11: Setup for Measurement of Unintentional Air Leakage

The pressure difference between the wall cavity and the outdoors was recorded as the air leakage driving pressure. A relationship between this pressure and airflow rate was determined. This air leakage is critical, as its source may affect both the condition of the air being exchanged in the ventilation cavity (indoor vs. outdoor air) and the portion of the cavity exposed to the ventilation air. The exposure of the cavity to the ventilation air depends on the path of airflow through the cavity (i.e. if the majority of air short-circuits the ventilation cavity, little of the wall may be affected by exposure to the ventilation air). The results of the measurements of unintentional cavity air leakage at varying cavity pressures are provided in Figure 7-12. The labeling is:

B20VT	Brick veneer, 20 mm air space, and top and bottom vents
B20NT	Same as B20VT except the wall is non-ventilated
B20VF	Same as B20VT but with a felt sheathing membrane

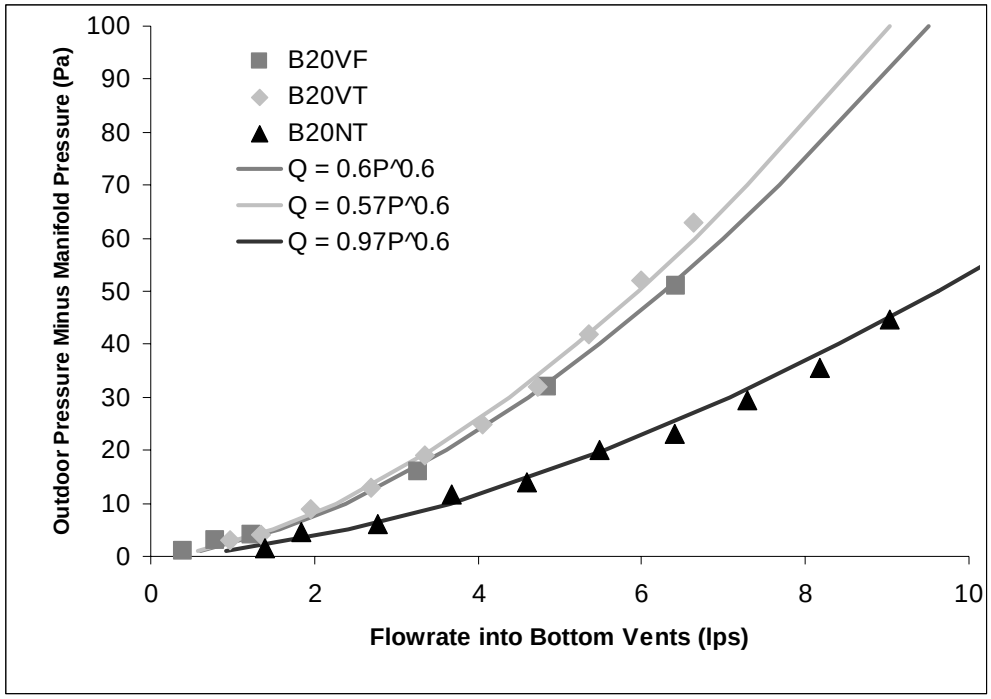

Figure 7-12: Measured Test Wall Air Leakage

It can be seen that the B20NT wall has the greatest air leakage, with about 50% more air leakage than the B20VT and B20VF walls for a given pressure. This difference may play a role in the wall performance, i.e. the non-ventilated wall may in fact have a significant amount of airflow behind the veneer through unintentional openings. Based on the ventilation flows reported later the air leakage through unintentional flow paths therefore comprises about half of the total measured flow in the vented B20NT wall, and about ¼ of the total flow in the B20VF and B20VT walls.

7.4. Results and Discussion

7.4.1. Forced Flow – Pressure versus Flow Characterization

Ventilation airflow resistance data was measured for the B20VT test wall and the B20VT(2) wall. Both walls were brick veneer over a relatively clean 20 mm airspace. The measurement of the B20VT wall was repeated three times (labeled (1), (2), and (3)), to investigate the repeatability of the test.

A series of full-scale laboratory airflow measurements were carried out at PSU. One of the specimens tested incorporated an artificial brick veneer profile over a smooth cavity, and one was an idealized smooth sided ventilation cavity. The PSU results are labeled as:

PSU-B(20)W2 Brick profile, 20 mm air space, and top and bottom vents

PSU-B(20)W2(M) Brick profile, mortar dams, 20 mm air space, and top and bottom vents

PSU-P(20)W2 Smooth profile, 20 mm air space, and top and bottom vents

The results from the field test specimens and PSU are summarized in Figure 7-13.

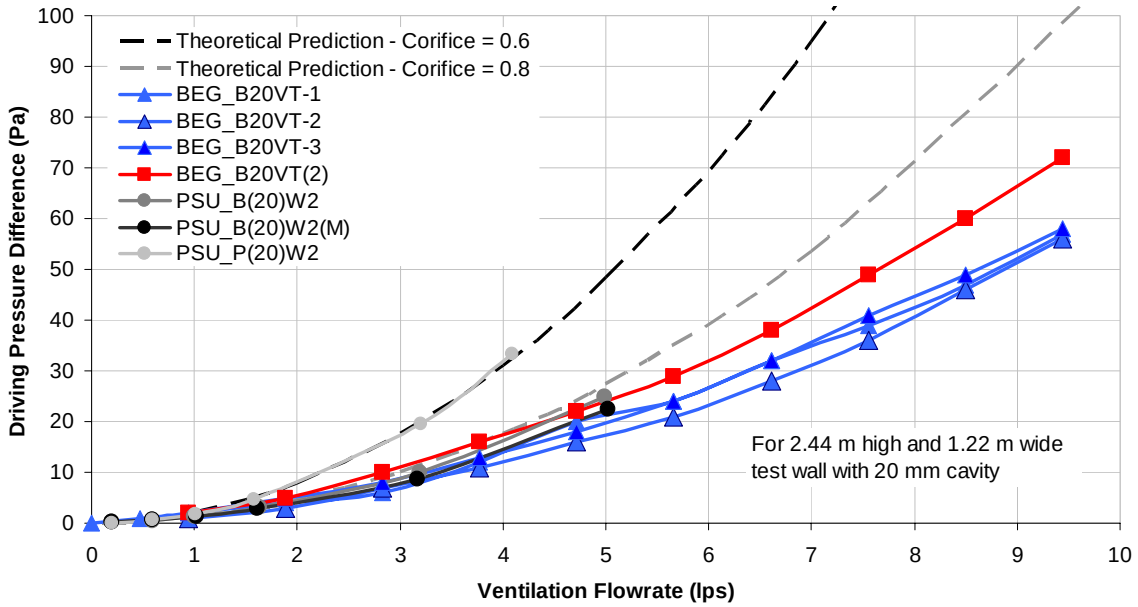

Figure 7-13: Measured Airflow Resistance for Brick over 20 mm Cavity

It can be seen that the results measured in the field test walls were quite similar to the results for PSU's artificial brick profiles. The brick specimens also exhibit less resistance to flow than predicted. The flow resistance of the smooth Plexiglas walled assembly was also greater than the rough brick veneer specimens. Although we have not identified why this is so, it can be postulated that the irregular surfaces reduces the impact of viscosity on friction at low flows.

The use of a vent discharge coefficient of 0.8 (instead of the more theoretically sound 0.6) and Equation 3-42 provides a reasonable fit to the data below 10 Pa (a reasonable upper bound for typical driving pressures). The resulting equation (the results of which are plotted in Figure 7-13) is:

$$\Delta P_{Total} = \left(\frac{Q}{0.8 \cdot h_{v1} \cdot w_{v1}} \right)^2 + \frac{32 k_f \cdot Q \cdot \mu \cdot L}{4 d^3 \cdot w_c} \qquad (7\text{-}1)$$

where

h_v is vent height and $h_{v1} = h_{v2} = 0.08$ m,

w_v is the vent width and $w_{v1} = w_{v2} = 0.015$ m,

k_f is a correction factor for the friction factor and $k_f = 1.5$,

μ is the dynamic viscosity and $\mu = 0.0000172$ N s/m^2,

L is the cavity length and L = 2.4 m,

d is the cavity diameter and d = 0.02 m,

w_c is the cavity width and $w_c = 1.22$m,

and Q is airflow rate in m^3/s.

Equation 3.1 is only valid for laminar flow. Figure 7-14 shows the range of airflow rates used in the induced flow experiments and initial natural ventilation airspeed measurements. This plot was generated using the maximum airspeeds measured during both natural and induced flow experiments. In most cases the range of likely airflow rates in the cavities is well below the laminar-turbulent transition.

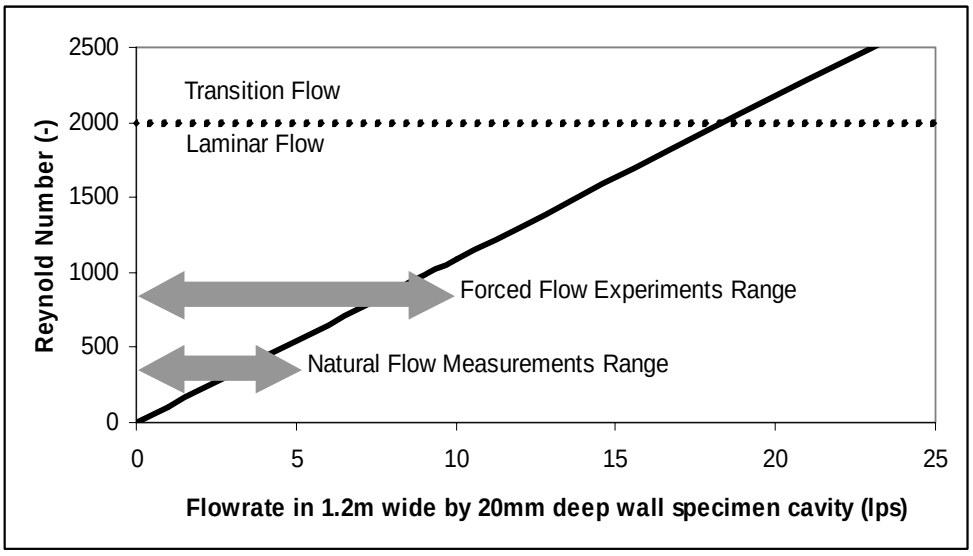

Figure 7-14: Flow Regimes for Likely Airflow Rates

7.4.2. Forced Flow – Airspeed versus Airflow Correlation

Forced flow measurements were undertaken to determine the pressure drop across the ventilation circuit with an externally applied pressure and to develop a correlation between point air airspeed measurements and a steady, mechanically induced ventilation airflow rate. These values were compared to predicted values. Natural ventilation airflow rates were estimated from the point airspeed sensor data by determining the correlation between airspeed measurements and airflow rate when flow was induced with fans.

The use of point airspeed measurements has been considered in other studies. Several difficulties with single point air airspeed measurements have been pointed out by Saelens (2002):

- The airspeed across the cavity may not be even.
- There is no guarantee that the velocity vector is perpendicular to the sensor.
- The use of an array of airspeed sensors may significantly disturb flow.

The validity of using point airspeed measurements in ventilation air cavities was also investigated in laboratory studies at PSU. Other work performed at PSU studied velocity gradients within laboratory models of typical flow systems as shown in Figure 7-15.

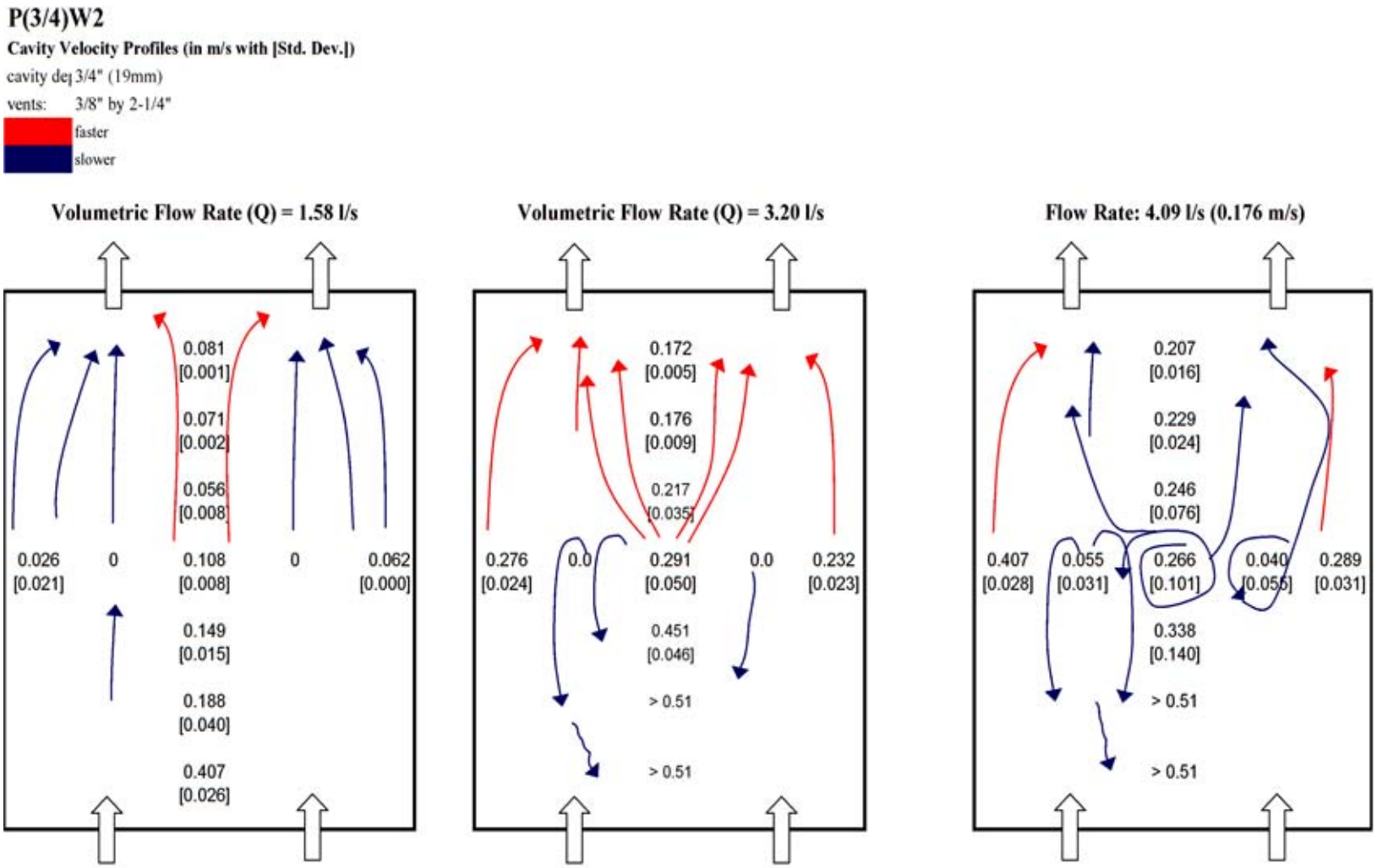

Figure 7-15: PSU Point Velocity Measurements and Smoke Pencil Observations

The researchers at PSU conducted a series of flow visualization and airspeed measurement experiments relevant to this study. They employed a 1.22 m wide by 2.44 m high Plexiglass lined chamber. Some of the test chambers have the same nominal dimensions as the brick veneer wall specimens investigated in this field study. They found that the flow paths, even under steady-state conditions, are complex, and both stagnant zones and recirculation zones were observed.

A summary of PSU's airspeed versus forced flow results is included in Table 7-1. These measurement results will be used for comparison later in this report.

Table 7-1: Cavity Mid Height Airspeed Measurements and Predictions

Flowrate (lps)	*Vcalc (m/s)	Vedge_L (m/s)	Vside_L (m/s)	Vmid (m/s)	Vside_R (m/s)	Vedge_R (m/s)	Vave_L (m/s)	Vave_R (m/s)
Flat plexiglass								
1.58	0.069	0.026	0.000	0.108	0.000	0.062	0.045	0.057
3.20	0.140	0.276	0.000	0.291	0.000	0.232	0.189	0.174
4.09	0.179	0.407	0.055	0.266	0.040	0.289	0.243	0.198
Simulated brick without mortar protrusions								
1.63	0.071	0.009		0.037			0.023	0.037
3.19	0.140	0.192	0.009	0.176	0.061	0.166	0.126	0.134
4.99	0.219	0.327	0.017	0.403	0.115	0.313	0.249	0.277
Simulated brick with mortar protrusions								
1.61	0.071	0.047	0.052	0.060	0.016	0.032	0.053	0.036
3.17	0.139	0.161	0.162	0.153	0.162	0.170	0.159	0.162
5.02	0.220	0.246	0.243	0.243	0.270	0.270	0.244	0.261
*	Vcalc is determined as flowrate over cross sectional area of flowpath							
**	Vave_L is average of Vedge_L, Vside_L, and Vmid							
***	Vave_R is average of Vedge_R, Vside_R, and Vmid							

Averaging multiple measurement points reveals a correlation between flow rate and measurement. These values are plotted in Figure 7-16.

Figure 7-17 shows a plot of point airspeed measurements (5 minute averages of measurements at 10 second intervals) and the average airspeed calculated using Equation 7-2. The position of the BEG airspeed sensors is included in Figure 7-6. The correlation derived for the measured point data and the average calculated airspeed (labeled BEG correlation) is:

$$BEG\_correlation = 2.3 \cdot \left(\frac{BEG\_V\_mid + BEG\_V\_edge + BEG\_V\_side}{3} \right) \quad (7\text{-}2)$$

A correlation between point airspeed measurements within the cavity and the average airspeed (determined from the measured airflow rate) was found at high airflow rates. In the PSU measurements the majority of air flowed along the edges of the cavity with a smaller portion of the flow traveling up the centre. Similar results are seen in the field test results.

Hence, it can be concluded that the point airspeed measurements cannot be directly related by use of the continuity equation (Q=V/A) because of complexities in the flow behaviour. However, an empirical correlation that relates the average of three airspeed

measurements with airflow was developed for the specimen tested under steady-state conditions. It appears that the sensors used cannot measure airspeeds below about 0.1 m/s. It is suspected that at such low velocities the majority of the air flows close the sheathing and may not be passing across the sensors.

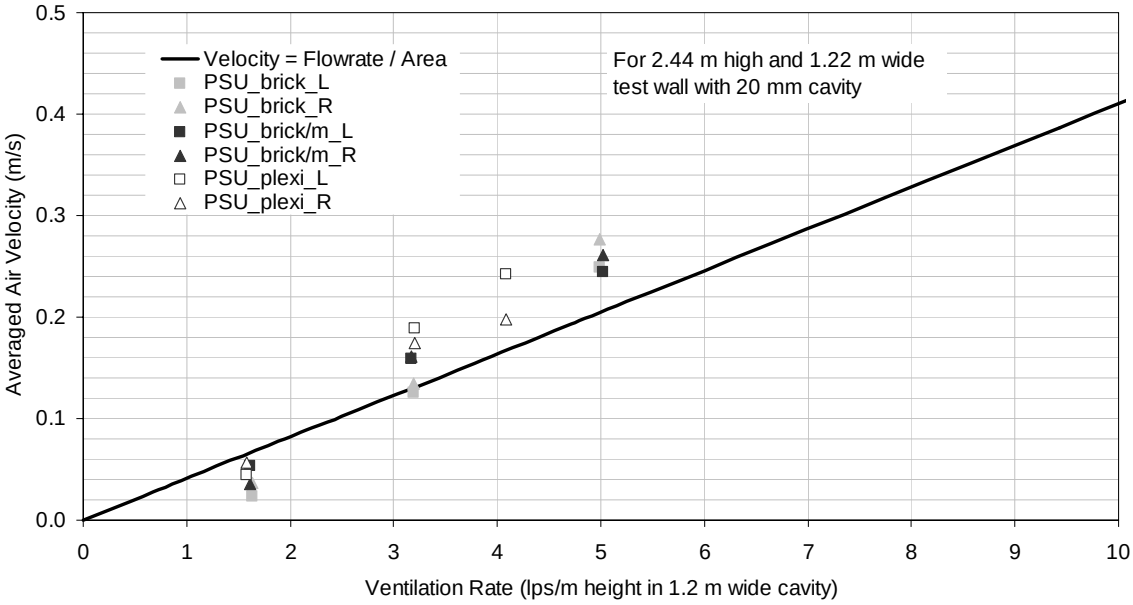

Figure 7-16: PSU Measurements of Point Airspeeds

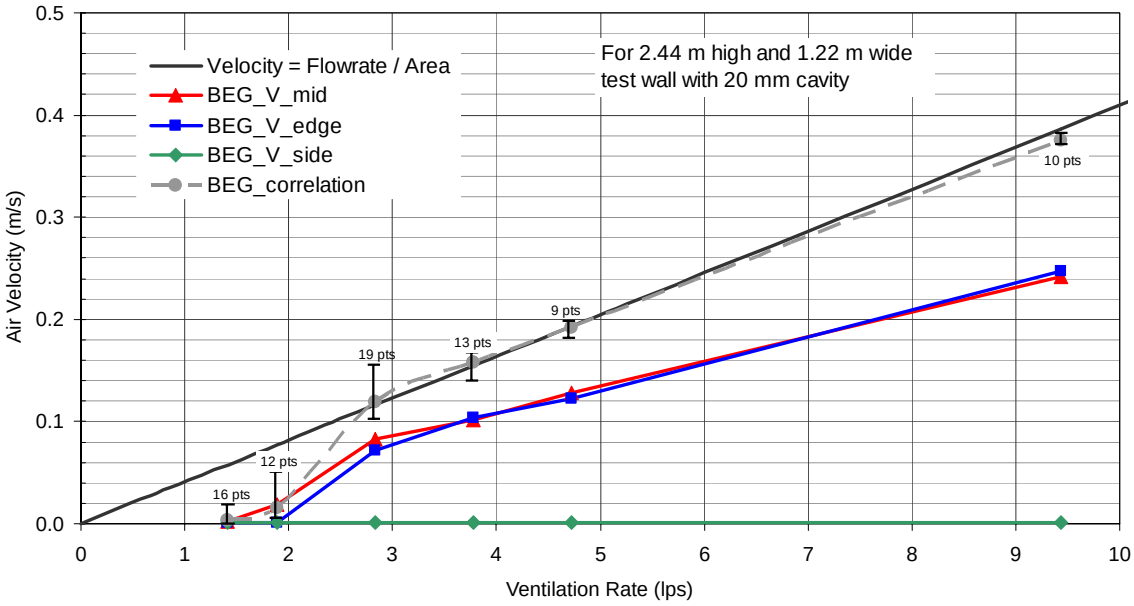

Figure 7-17: Ventilation Airspace Airspeed Measurements
(Bars indicate the range of a number of measurements.**)**

7.4.3. Natural Ventilation Flow Measurements

Measurements were also taken to determine the ventilation airflow due to natural wind and buoyancy effects. The ventilation airflow was determined by using point airspeed

measurements and the steady-state correlation developed in the previous section. Averaging a large number of samples helped remove noise from the measurements, and the 5-minute averaging period chosen allowed enough data points to investigate the distribution over hourly periods.

Wind driven ventilation airflows have in the past been predicted by applying hourly averaged surface pressures and steady state fluid mechanics correlations to ventilation airflow networks (Chapter 4 and Straube and Burnett 1995). This method can easily be applied to hourly wind speed and direction data employing spatial pressure coefficient data for the building, although the accuracy of this approach has not been quantified.

Pressure coefficients have been previously measured by Straube and Burnett (1995) for the BEGHUT test facility with similar vent arrangements and reduced in the form:

$$\Delta P_W = 0.5(c_{p,1} - c_{p,2})\rho \cdot V^2 \tag{7-2}$$

For easterly wind (windward):

$$c_{p,1} - c_{p,2} = -0.1 \tag{7-3}$$

For westerly wind (leeward):

$$c_{p,1} - c_{p,2} = 0.05 \tag{7-4}$$

The wind-driven ventilations acting on the face of a wall can thus be predicted by applying the equations above to measured weather station wind speed and direction data. Predicting surface pressures using this method is common. The accuracy of this approach can be judged from the comparison of measured and predicted ventilation pressures shown in Figure 7-18 and Figure 7-19.

The other significant ventilation driving pressure is buoyancy. Buoyancy forces can be predicted using Bernoulli's equation (as described in Chapter 3):

$$\Delta P_B = \left[\left(\frac{P_{a,exterior}}{R_a T_{exterior}} + \frac{P_{v,exterior}}{R_v T_{exterior}} \right) - \left(\frac{P_{a,cavity}}{R_a T_{cavity}} + \frac{P_{v,cavity}}{R_v T_{cavity}} \right) \right] gh \tag{7-5}$$

where

$$P_T = P_a + P_v \approx 101325 \text{ Pa} \tag{7-6}$$

The buoyancy pressures were determined from measured cavity and outdoor temperature and vapour pressure conditions. The vapour pressure is derived from temperature and relative humidity measurements.

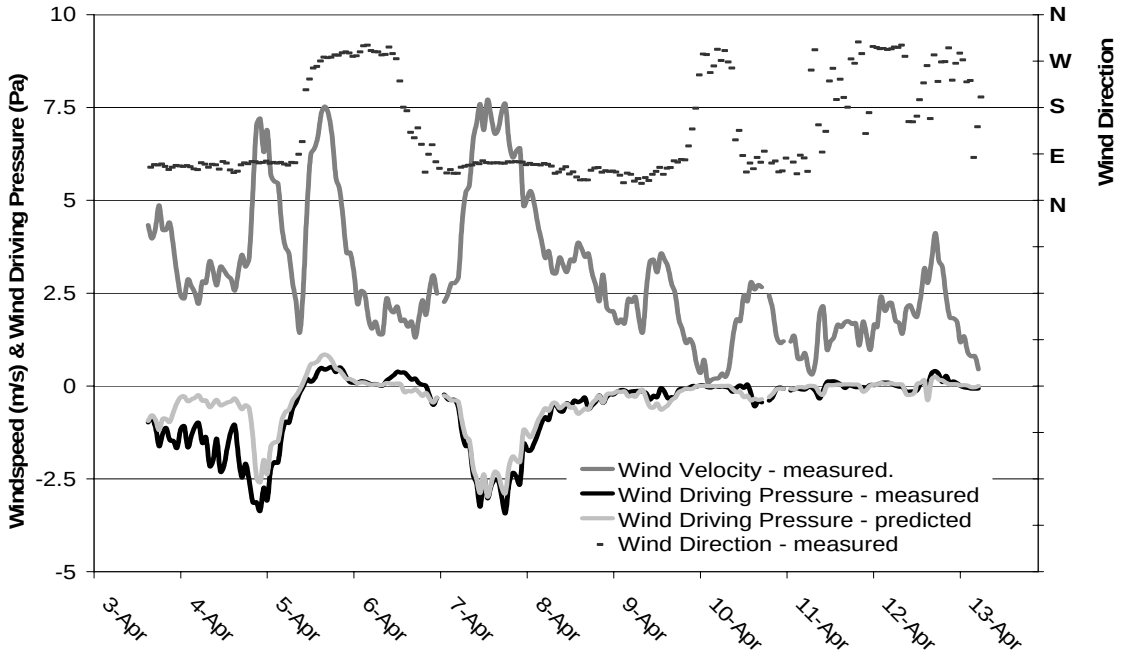

Figure 7-18: Measured and Predicted Wind Induced Driving Pressures
(April 3-13, 2003)

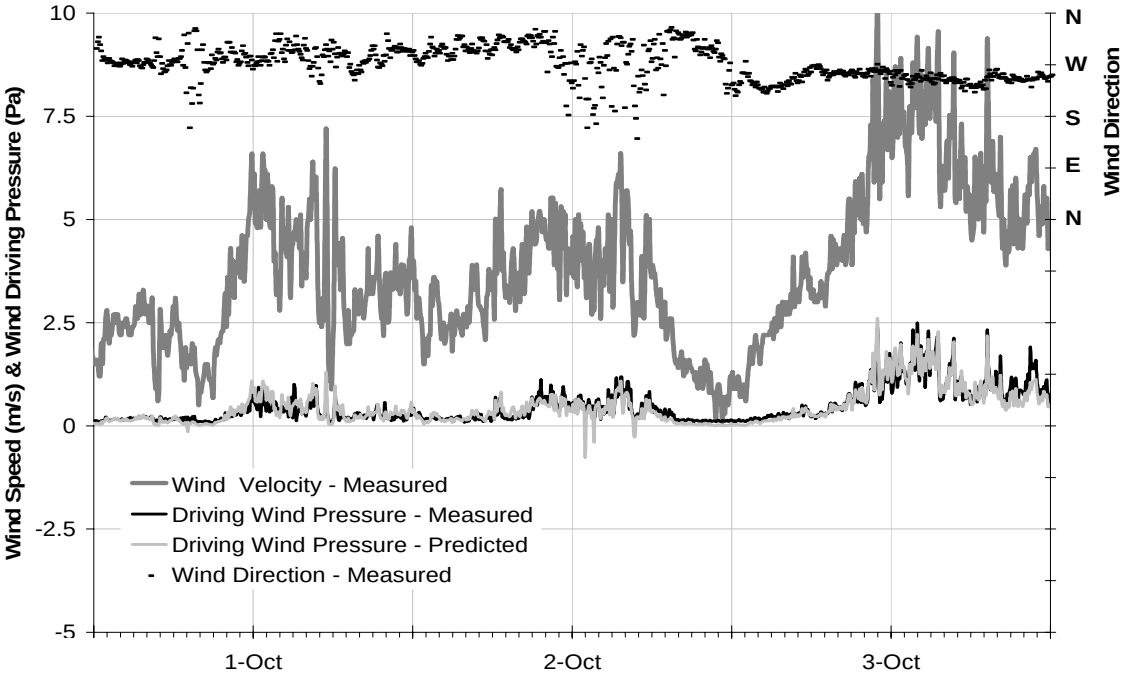

Figure 7-19: Predicted and Measured Wind Induced Driving Pressures
(Oct. 1-3, 2003)

For a number of practical reasons, buoyancy pressures could not be measured directly in the field test walls to confirm the prediction method. However, buoyancy is a well established and easy to predict force. A plot of calculated buoyancy pressures and wind pressures over a study period is given in Figure 7-20.

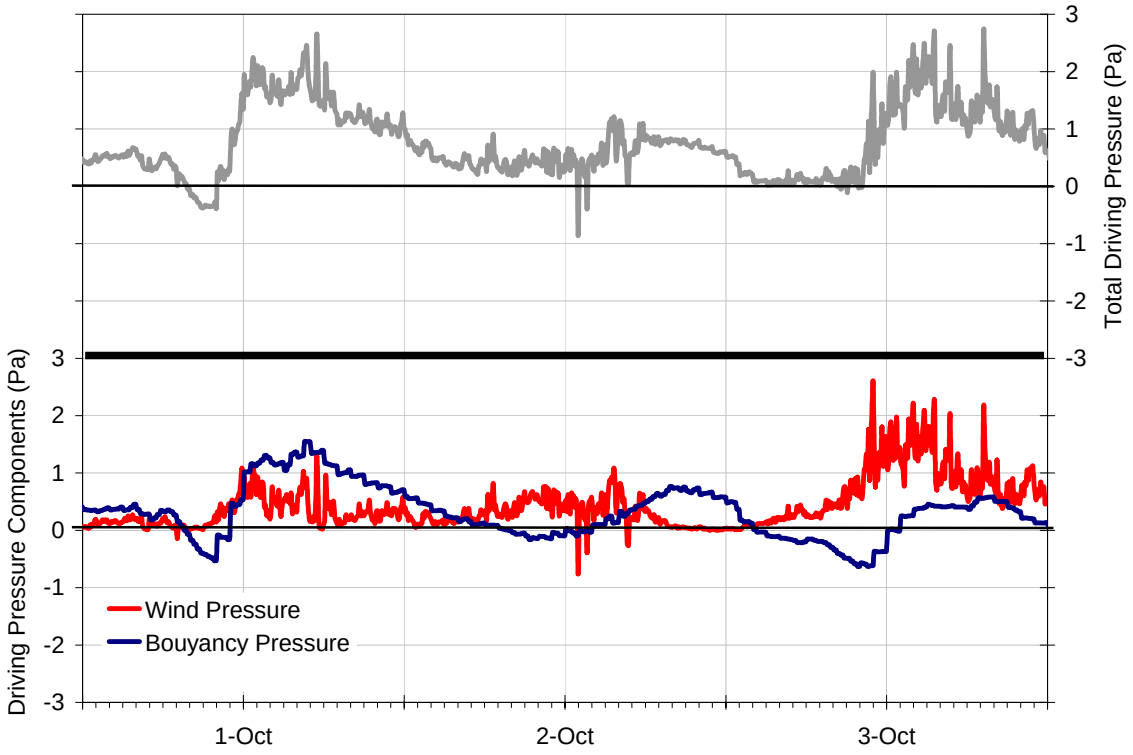

Figure 7-20: Calculated Buoyancy and Wind Pressure (Oct. 1-3, 2003)

Buoyancy and wind pressure can either act together or work against each other. They are also of similar magnitudes for the period shown in Figure 7-20.

The total driving pressure predicted above can be applied to the airflow versus pressure correlation given by Equation 7-1. It can also be compared to the averaged point airspeed measurements in the cavity. Measured point airspeeds are given in Figure 7-21 for the same period as that for the data plotted in Figure 7-20.

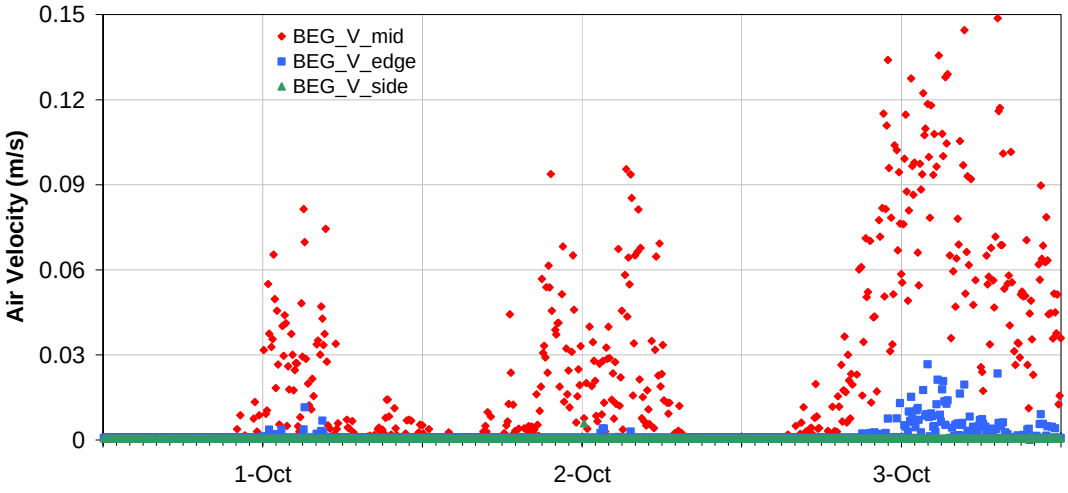

Figure 7-21: Measured Point Airspeed Due to Natural Flows

A comparison of predicted (using both buoyancy and wind pressures) and measured airspeeds is given in Figure 7-22.

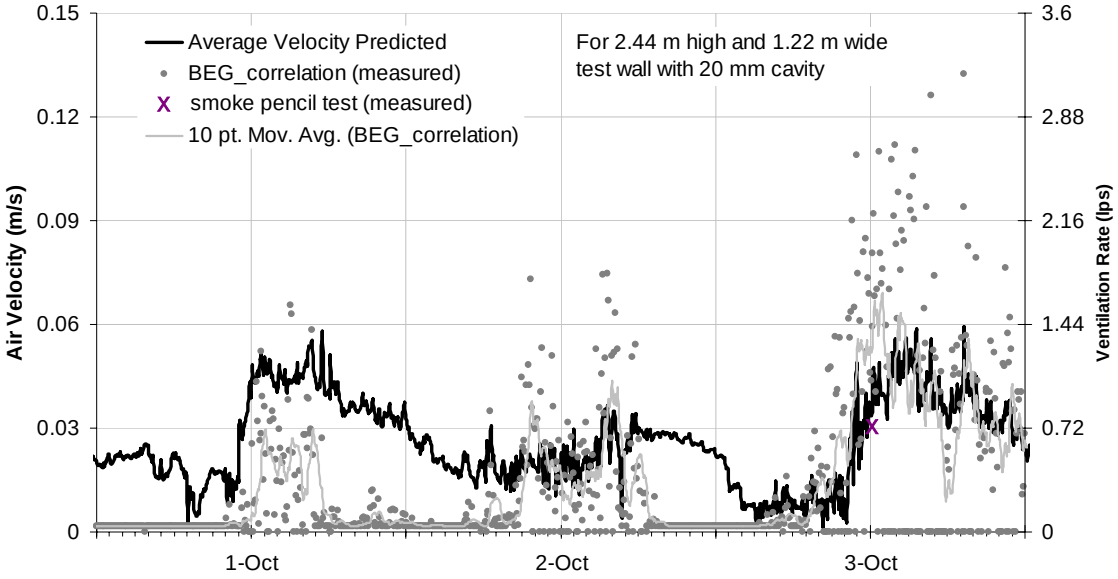

Figure 7-22: Average Air Airspeed and Airflow Rate (Oct. 3-5, 2003)

The predicted and measured airflow rates correlate during periods with high flowrates. The lack of correlation on the afternoons of the 1st and 2nd may be due to limitations in instrumentation or it may be caused by the complex nature of the dynamically varying low flows. The ventilation rates determined from measured velocities are in the range of 0 to 1.5 lps over the test period.

A simple confirmation of flow under sunny conditions (4 pm on October 3, 2003) was undertaken using a smoke pencil. Smoke was readily drawn into the bottom vents (this was also observed on other sunny days). Smoke was released into the bottom vents and the time required for it to exit the top vents was recorded (78 seconds). Since the distance between the top and bottom vents is 2.4 m, the airspeed of the smoke plume front was 0.03 m/s. This airspeed is similar to that measured and predicted and correlates to a ventilation rate of 0.3 lps per meter width (22 ACH).

It is expected that the predicted ventilation rates are closer to the actual ventilation rates than those derived from point airspeed measurements. However, significant velocities of up 0.15 m/s have been measured in the ventilation cavities, and these higher speeds are likely more accurately measured.

7.5. Conclusions and Recommendations

7.5.1. Conclusions

Testing revealed that the brick veneer test walls with 20 mm ventilation cavities had similar airflow resistance as wall specimens tested in the laboratory at PSU. An equation

was developed to predict airflow as a function of driving pressure for the tested wall specimens. The results were also close to theoretical predictions.

Using the flow resistance correlations developed and the driving pressures measured, the in-service natural ventilation rates were predicted to be in the order of 0 to 1.5 lps for a 1.22 m wide and 2.4 m high, 20 mm deep cavity with two open head joints vents at both the top and bottom. This equates to 0 to 90 ACH or 0 to 0.50 lps/m^2 of cladding.

The predicted and measured airflow rates correlate during periods with high flowrates when exposed to naturally occurring dynamic flows. A single ventilation rate was also confirmed with flow visualization techniques.

7.5.2. Recommendations for Further Work

The nature and quantity of air flowing through ventilated enclosure systems other than brick and veneer should also be studied.

Studies of brickwork should be extended to wider sections of brickwork to reduce edge effects. The effect of mortar damming and varying horizontal width (multiple slots) of the ventilation cavity should also be studied.

Comprehensive flow visualization should be performed to study the actual flow paths within ventilation cavities. Using clear Plexi-glass for the back of a ventilation cavity with a real cladding, smoke visualization should be used to allow observation of the flow paths under natural exposure conditions. More advanced visualization techniques incorporating particle image velocimetry should also be considered as a means of generating more complete and quantitative maps of airflow velocities of ventilation cavities. For example, digital video and pattern analysis and particle tracking could be employed together with helium filled neutral buoyancy bubbles. These tests should first be conducted with forced steady flow and then with natural flows. Tracer gas measurements, likely of the constant concentration type to avoid adsorption-desorption problems, should also be considered in future research work.

7.6. References

Jung, E. "Dauerstandverhalten von Verblendziegelmauerwerk unter Witterunsbeansphruchung und Auswirkungen von Kerndämm-Maßnahmen", *Baustoffindustrie*, No. 6, November, 1985, pp. 185-188.

Künzel, H., Mayer, E., "Untersuchung über die notwendige Hinterlüftung an Außenwandbekeidung aus großformatigen Bauteilen", *Schriftenreihe Bundesminister für Raumordnung*, Bauwesen, und Städtebau, 3/1983.

Künzel, H., Mayer, E., *Wärme- und Regenschutz bei zweischaligem Sichtmauerwerk mit Kerndämmung*. BMFT-Forschungbericht T84-191.

Newman A. J., Whiteside D. "Water and Air Penetration Through Masonary Walls – A Device for the Measurement of Air Leakage In-Situ", *Br. Ceram. Trans. J*. 1984, Vol. 83, pp. 190-195.

Popp, W., Mayer, E., Künzel, H., "Untersuchungen über die Belüftung des Luftraumes hinter vorgesetzten Fassadenbekleidung aus kleinformatigen Elementen", Fraunhofer Institut für Bauphysik, *Forschungsbericht B Ho 22/80*, April, 1980.

Saelens, D., *Energy Performance Assessment of Multiple-Skin Facades*. PhD dissertation, Leuven: KU Leuven, Laboratory of Building Physics, 2002.

Schwarz, B., "Witterungsbeansphruchung von Hochhausfassaden", HLH Bd. 24 1973, Nr. 12, pp. 376-384.

Straube, J., and Burnett, E., *Vents, Ventilation, and Pressure Moderation*. Building Engineering Group Report for Canada Mortgage and Housing Corp, Ottawa 1995.

8. FIELD MONITORING OF WALL DRYING EXPERIMENTS

Several full-scale wall assemblies were exposed to field conditions and monitored at the Building Engineering Group natural exposure and test facility (BEGHUT) at the University of Waterloo. These experiments were unique in that the walls were wetted and the subsequent drying of the assemblies was monitored. The results provide hygrothermal data from ventilated wall systems.

8.1. Objective

The objective of this work was to generate field measurements of wall conditions with different claddings, ventilation strategies, and sheathing membranes when exposed to field weather conditions. These measurements were to be used to improve our understanding of the hygrothermal behaviour of ventilated wall assemblies.

8.2. Scope

This report outlines the drying experiments as part of the field measurement experimental program. A description of the test facility, the experimental specimens, and instrumentation are included. The chapter summarizes the measured conditions during the drying experiments. These results are discussed to generate observations of wall specimen performance as a function of ventilation arrangement, cladding type, sheathing membrane type, and weather conditions.

The work includes the design and testing of the wall specimen, conducting the experiments and monitoring, wall disassembly and inspection, preparation of data in a consistent manner amenable to wider dissemination, and initial analysis of the results. An advanced hygrothermal computer model developed at Oak Ridge National Labs (ORNL) is to be benchmarked with the data. It is anticipated that this activity will draw more insights from the data.

The scope was limited to the study of brick veneer or vinyl siding over wood framed wall assemblies because these are the most common residential wall systems in North America. Sheathing membranes of spun bonded polyolefin or #15 asphalt impregnated felt paper were included. All other characteristics of the wall assemblies were similar.

8.3. Approach

The methodology used in the field testing builds upon previous studies. For example, Straube (1998) successfully investigated the hygrothermal performance of many different wall assembly designs using test walls of a similar scale at the same test facility used in this study. Hansen, Nicolajsen, and Stang (2002) also performed a field study investigating the effects of ventilating cavities on timber wall assemblies. However, none of these studies included the impact of accidental wetting. Reynolds (1992) and Hazleden (2001) investigated the drying of walls initially wetted in the field (at the BEGHUT) and in a climate chamber respectively.

Reflecting the current state of knowledge in this field, it was decided to subject the test walls to controlled wetting events during field exposure and to then monitor the drying and redistribution of the introduced moisture. The experiments investigated drying of wood-framed walls that have had the sheathing wetted by rain penetration and/or

exfiltration condensation. The drying mechanisms of ventilation and diffusion through the sheathing membrane were the focus. Part of the work reported here included the development of a methodology (the Intra Wall Wetting system) to inject water into vulnerable portions of the wall assemblies in a controlled manner. This method is described in Appendix A.
The wetting method developed also has the benefit of providing a large enough moisture load (a spike in moisture content readings) at a known location to generate measured data with good reliability and high resolution under a wide range of weather conditions. All of these characterisitics are useful for the validation of computational models.

8.4. Experimental Program

The design and instrumentation of the five test wall panels and their installation in a natural exposure and test facility (BEGHUT) at the University of Waterloo (UW) are outlined in this section. The test procedure and timelines are also described. The five walls were modified by changing ventilation cavity depth and vent arrangement allowing for three wall setups over the course of the monitoring.
Upon completion of the experiment the walls were disassembled. These inspections confirmed that although some mould growth was observed, the wall assembly and Intra Wall Wetting system were still in good condition at the end of the experiments. It is therefore assumed that the hygrothermal characteristics of the walls did not change over the course of the monitoring. The findings from the disassembly and inspection are further described in Section 8.5.4.

8.4.1. The BEGHUT Test Facility

The Building Engineering Group (BEG) at the UW operates a full-scale natural exposure and test building dubbed the BEGHUT. Wall assemblies can be inserted in the BEGHUT and their performance assessed through monitoring, testing, and observation.
The BEGHUT setup allows for walls of 1.2 m width and 2.4 m height to be installed and removed at any time. This facility is a square building approximately 10.5 m x 10.5 m in plan and 3.0 m high on the inside. The walls are oriented to the four cardinal directions. The roof is peaked to the centre with a slope of 1-in-3. A pipe mast rising from the central peak of the roof supports a weather station at 10 m above grade.
The test hut is sited on relatively flat land and is fully exposed to winds from most directions. The roof overhang is sized to avoid shading of the test walls from the sun under all conditions. The small overhang and the drip-edge in lieu of eaves troughs provide very little direct protection from rainfall.
An air-to-air heat pump heating and air conditioning unit and supplementary humidification units control the monitored indoor climate to 20 ^{o}C and 50% relative humidity. Ceiling-mounted diffusers and circulation fans ensure even distribution of the conditioned air.
A view of the east face of the BEGHUT with the five test walls nearing construction completion is included in Figure 8-1. A plan of the BEGHUT is included in Figure 8-2.

Figure 8-1: Mason Installing a Brick Veneer after Instrumented Panels are installed

8.4.2. Wall Specimens

Five different test walls, three clad with brick veneer and two clad with vinyl siding, were installed facing east and monitored under various weather conditions, including hot summer and cold winter conditions. The walls were extensively instrumented to monitor hygrothermal conditions and air pressure and flow.

The 5 different wall designs were monitored in this program. The assembly details are outlined in Table 8-2. All wall specimens have identical base wall systems consisting of:

Nominal 12.7 mm (½") Homasote sheathing (actually approximately 10 mm)
nominal 2" by 6" Eastern White Pine framing (38 by 140 mm) at 405 mm (16") spacing with fiberglass batt insulation, and
an indoor finish of medium density particle board coated with a vapor barrier plastic coating on both sides (Melamine).

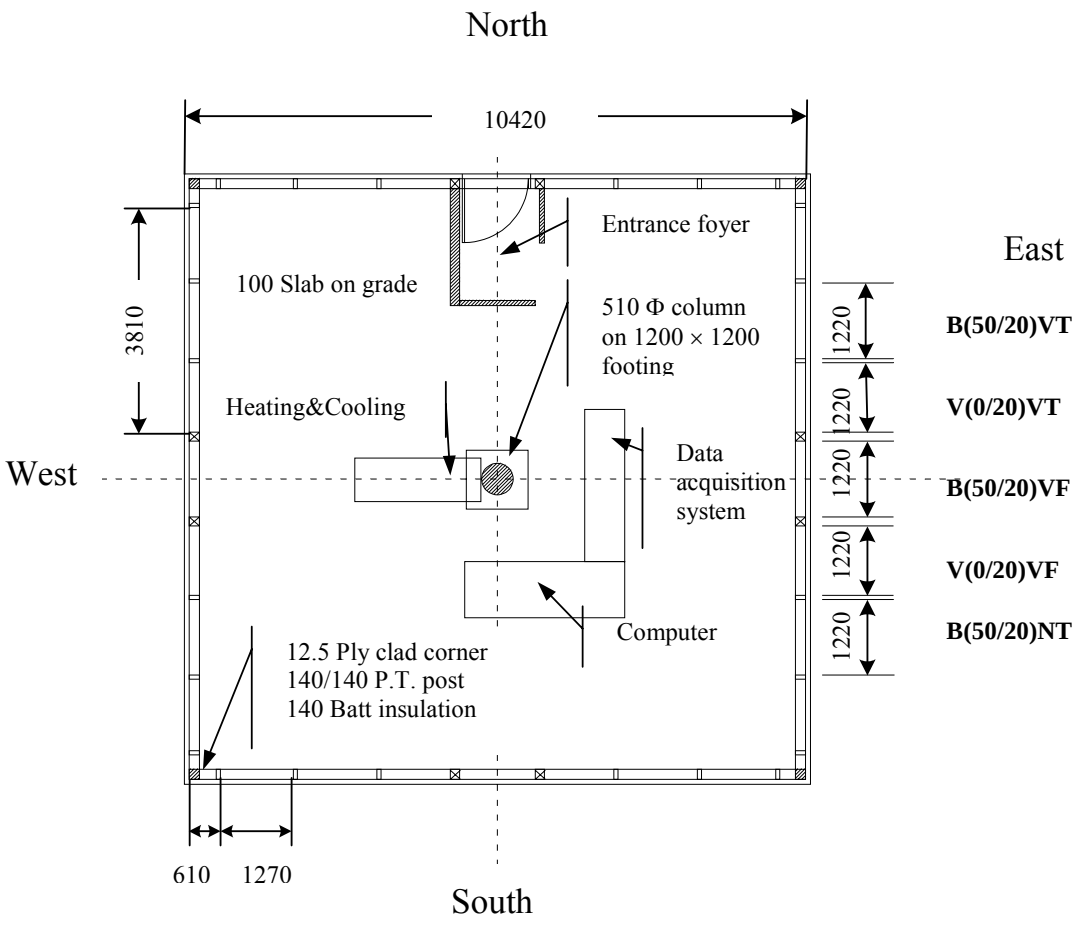

Figure 8-2: Plan of BEGHUT and Location of Test Panels

High moisture (liquid and vapour) diffusivity, hygroscopic, wood-based sheathing with a homogenous consistency was desirable to make the measurement of average sheathing moisture content more accurate, and to limit the influence of the sheathing choice on drying performance. Homasote, made from recycled paper, was chosen. Although it is not commonly used for sheathing of wood frame walls, its unique material properties were desirable.

All test walls also contained an Intra Wall Wetting system that allowed a desired quantity of liquid water to be injected uniformly over the back of the Homasote sheathing. This apparatus, its development, and testing are described in Appendix A.

The test walls used two different sheathing membranes, #15 asphalt impregnated felt (AIF) and spun bonded polyolefin (SBPO).

Two types of cladding, 90 mm brick veneer and horizontally applied vinyl siding. The vinyl siding was similar to that used in the laboratory study described in Chapter 6.

Unique codes were developed to identify each test wall setup. They are summarized in Table 8-1.

Table 8-1: Test Specimen Coding

Cladding	Cavity Depth (mm)	Ventilation Strategy	Sheathing Membrane
B brick	0	V ventilated	F (AIF)
V vinyl	20	N non-ventilated	T (SBPO)
	50		

The vinyl siding was first tested when applied directly on the sheathing membrane (termed contact applied) and after three drying experiments the vinyl was installed over vertical wood strapping in the second wall setup. After a subsequent three drying experiments the joints in the vinyl siding of the wall with #15 asphalt impregnated felt (AIF) were air sealed with sealant leaving only the drainage holes to allow liquid water to exit the cladding. Unfortunately a hole (approximately 6 by 10 mm) was punctured in the siding. The vinyl siding clad wall with spun bonded polyolefin was not altered for the third setup.

The brick veneer was tested with a 50 mm cavity, less blocked with mortar than typical construction. In the second wall setup the cavity depth was reduced to around 20 mm. Weep holes (open head joints) were included in all the brick veneer wall arrangement while upper vents were either left open or sealed. Sealing the upper vents allowed the amount of ventilation in the test brick veneer clad walls to be controlled. All vent openings in the brick veneer were open head joints, approximately 10 mm by 80 mm, with no inserts or insect screens.

Further details including dimensions of the wall assemblies are provided in Appendix B.

Although only 5 wall panels were built, it was possible to monitor two cavity depths for each type of wall panel by an adjustment of the wall during the field study (Wall Setup 1 changed to Wall Setup 2). A third variation involved the alteration of the ventilation arrangement of three of the five walls (Wall Setup 2 changed to Wall Setup 3). Some of the same wall assemblies (V20VT and B20VT) and ventilation arrangements were tested in Wall Setup 2 and Wall Setup 3.

Table 8-2: Wall Specimen Details

Cladding	Cavity Detail	Venting	Sheathing Membrane	Sheathing	Framing	Session
Vinyl Siding (*V*)	Contact Applied (*0*)*mm*	Drained Vented and Ventilated (*V*)	Spun Bonded Polyolefin (*T*)	½" Homasote with IWW wetting installed on inside face	2" x 6" Pine on 16" Centres filled with Fiberglass Batt and including a vapour barrier	1
		Drained Vented and Ventilated (*V*)	#15 Asphalt impregnated Felt (*F*)			1
	Applied on Furring Strips (20)*mm*	Drained Vented and Ventilated (*V*)	Spun Bonded Polyolefin (*T*)			2,3
		Drained Vented and Ventilated (*V*)	#15 Asphalt impregnated Felt (*F*)			2
Brick Veneer (*B*)	Clear 50mm Cavity (*50)mm*	Drained Vented and Ventilated (*V*)	Spun Bonded Polyolefin (*T*)			1
		Drained Vented and Ventilated (*V*)	#15 Asphalt impregnated Felt (*F*)			1
		Drained Vented but not Ventilated (*N*)	Spun Bonded Polyolefin (*T*)			1
	Clear 20mm Cavity (*20)mm*	Drained Vented and Ventilated (*V*)	Spun Bonded Polyolefin (*T*)			2,3
		Drained Vented and Ventilated (*V*)	#15 Asphalt impregnated Felt (*F*)			2
		Drained Vented but not Ventilated (*N*)	Spun Bonded Polyolefin (*T*)			2
		Drained Vented but not Ventilated (*N*)	#15 Asphalt impregnated Felt (*F*)			3

Note: All walls consist of a melamine inside finish, 2x6" pine studs on 16" centers, with R20 fiberglass batts and have flashing with drainage

8.4.3. Wall Instrumentation

All of the test panels were instrumented to measure temperature, relative humidity, and moisture content at points of interest in the test panel assemblies. The typical sensor locations are shown in Figure 8-4 for vinyl siding clad panels and in Figure 8-5 for brick clad panels. The sensors were installed as described in detail by Straube et al (2002).

All of the temperature sensors were Fenwal precision thermistors with a 10000 Ohm resistance at @ 25 degrees Celsius and an accuracy of +/- 0.2 ºC. The thermistors and

soldered connections were coated with an electrically insulating and waterproof liquid plastic. The electrical resistance (R in Ohms) was measured and correlated to temperature (T in ^{o}C) using manufacturers data in the following equation:

$$T = 0.101 \ln R^3 + 4.346 \ln R^2 - 77.18 \ln R + 446.05 \quad (8\text{-}1)$$

Relative humidity was measured with small (4 x 6 x 10 mm) capacitance-based sensors (Honeywell model HIH-3610) with NIST-traceable calibrations and an accuracy of better than 2% RH. Each RH sensor was accompanied by a temperature sensor.

The potential for and incidence of condensation was assessed by combining measured relative humidity and temperature in the batt space with the temperature measurement at the surface of interest.

Moisture-content sensors were installed in the Homasote sheathing and the wood framing. The moisture-content sensor for the wood framing consists of Delmhorst pins driven directly into the wood framing (see Appendix B for details). Brass screws were used in the Homasote sheathing as the Delmhorst pins easily fell out of the Homasote. The screws were covered with a non-conductive paint to within 2 mm of the bottom of the thread. The screws were installed into the sheathing from the inside with the uninsulated portion set midway through the thickness of the Homasote.

Moisture content was measured by passing a 12-volt direct current between the pins or screws. This voltage was applied for about 1 second to allow the readings to stabilize prior to recording the resistance. Moisture content (MC) is determined from the measured resistance (R in Ohms) from the following correlation (Straube et al 2002):

$$\log(MC_{uncorrected}) = 2.99 - 2.113 \cdot \log(\log(R)) \quad (8\text{-}2)$$

The moisture content correction for wood species and temperature (T in ^{o}C) is as follows:

$$MC_{corrected} = \frac{MC_{uncorrected} + 0.567 - 0.026 \cdot T + 0.00005 \cdot T^2}{(0.881 \cdot (1.0056^T) + b)/a} \quad (8\text{-}3)$$

where a and b are species-specific coefficients.

The studs consist of eastern white pine timber (species coefficient a = 0.702 and b = 0.818). The species coefficients for the Homasote sheathing were generated by laboratory testing at PSU (a =1.4 and b =-3.6). The Homasote coefficients were derived at room temperature and it was assumed the temperature correction would be similar to that for wood.

Due to the lower than anticipated liquid diffusivity of the Homasote sheathing, the recorded moisture contents do not necessarily represent the average moisture content immediately following wetting of the Homasote's batt facing surface. Moisture gradients in the sheathing (Figure 8-3) may be present due to:

- non-uniform wetting (the wetting paper may be wetter near the bottom than the top),
- non-uniform liquid diffusivity of the Homasote

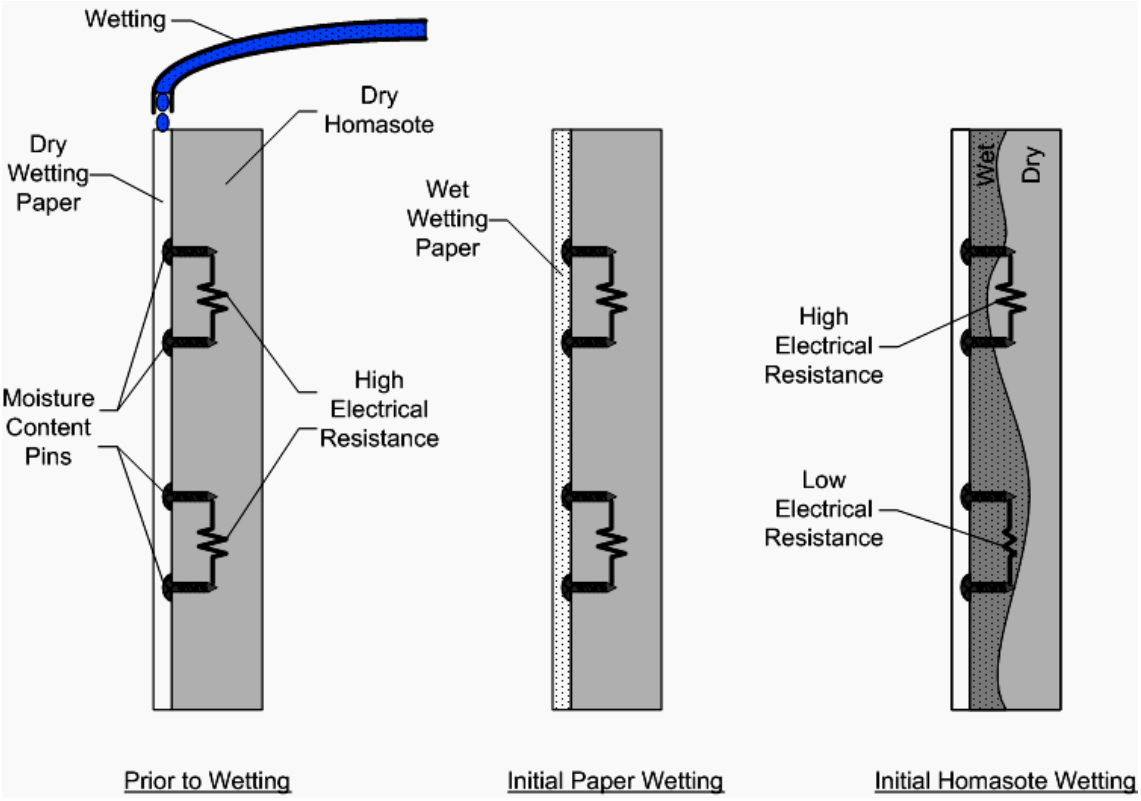

Figure 8-3: Possible Reason for Differential Sheathing Moisture Content Readings

Both of these causes are exacerbated by the low diffusivity of the material. A material with high diffusivity would allow for quick redistribution of moisture and greater uniformity of MC. In the future it is recommended that materials with a higher liquid diffusivity than Homasote be used.

Different MC readings could also be caused by non-uniform installation depth of the screws, short-circuiting between the pins through a wet surface layer, or penetrations through the insulating coating over the screws. The latter two causes are considered unlikely.

The accuracy of the resistance-type meters used in wood is estimated as ±2% within the range of 6 to 25%. A considerable loss in accuracy can be expected outside this range. Above fiber saturation (25 to 30%), the correlations will generally return lower MC values than exist, whereas below 6%, the resistance becomes so high it is difficult to measure properly.

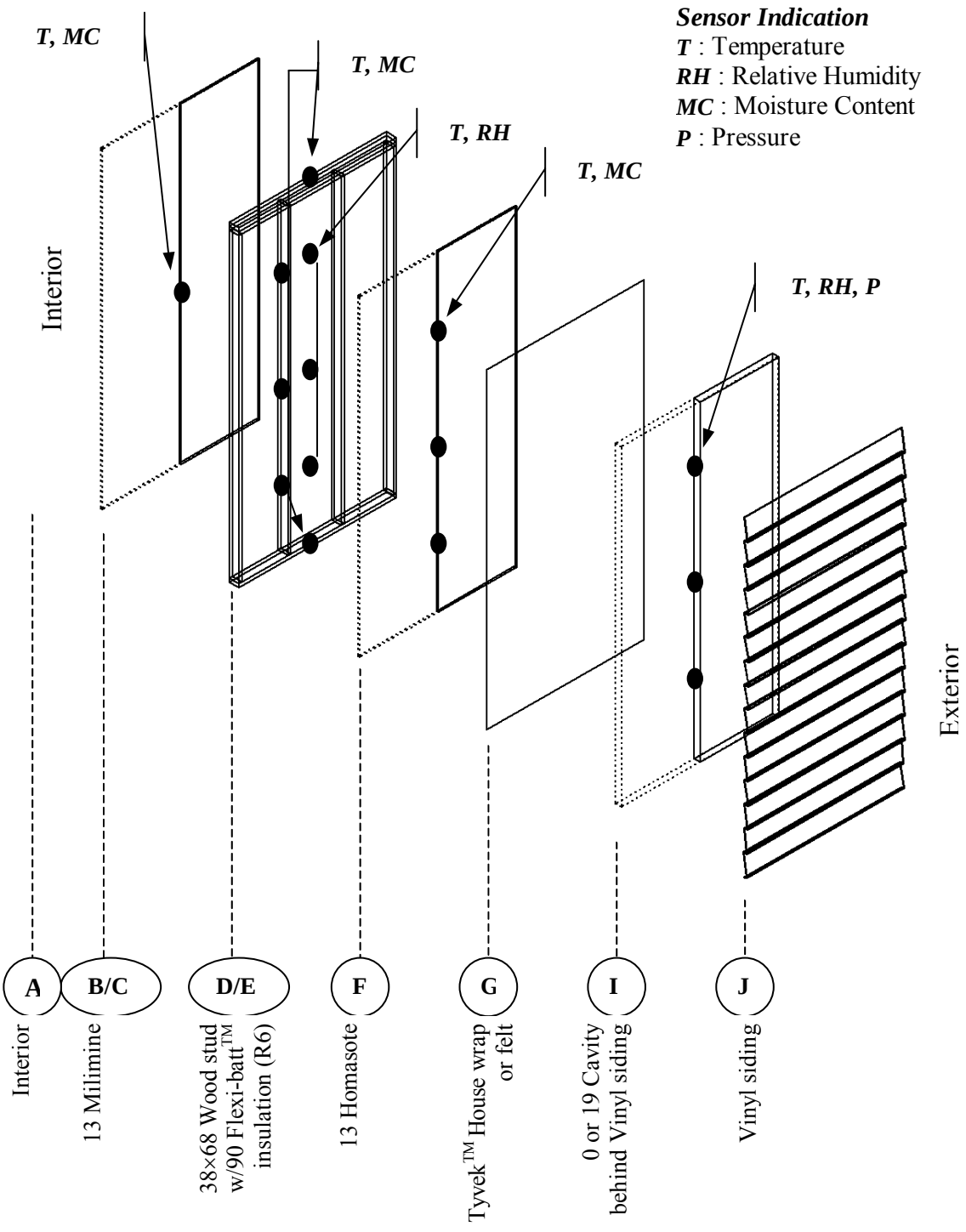

Figure 8-4: Sensor Layout of Vinyl Cladding Test Walls

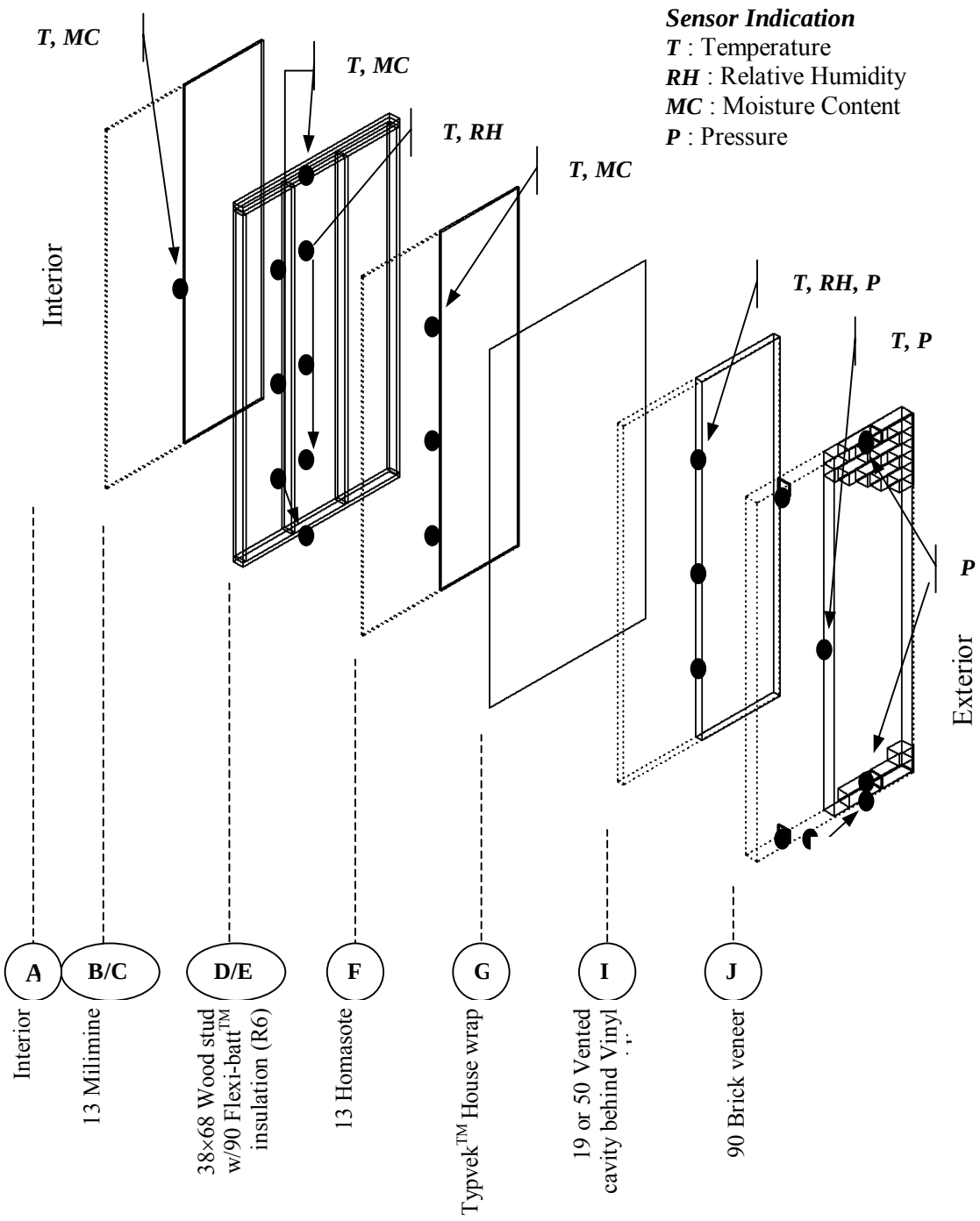

Figure 8-5: Sensor Layout of Brick Veneer Test Walls

8.4.4. Drying Experiment Procedure

Once wall construction and instrumentation was complete the walls were allowed to acclimatize for five months (Sept 2001 to Jan 2001). The sheathings in the wall systems were subsequently wetted a total of nine times and exposed to various weather conditions. Hygrothermal conditions were monitored during the drying periods.

Each wetting event comprised several injections of water. Each injection involved a 30 g charge of distilled water being injected into each of the 15 tubes that lead into the IWW of each test wall. This process required 10 minutes to complete per wall and added a total of 450 g of water to the wetting paper covering the batt facing side of the Homasote sheathing. After a period of at least 4 hours the process was repeated, adding another 450g per wall. In most cases 4 injections (1800 g) were used to define a wetting event. All injections for a particular wetting event were completed within a 24 hour period.

8.4.5. Drying Experiment Schedule

The timelines for the drying experiments are shown in the Gant chart in Figure 8-6. The first drying experiment was begun in the late winter (Feb 11, 2002). The second drying experiment was initiated in early spring (May 2, 2002). The third drying experiment was begun midway through the hot summer of 2002 (July 26, 2002). The timing of the air space depth adjustment (Sept 3, 2002) was chosen to allow a late hot summer experiment to be run with the new cavity widths in 2002. Upon completion of the adjustment the fourth drying experiment was run for the next set of wall test setups starting Sept 4, 2002. The fifth drying experiment was run during cooler fall conditions (Oct 20, 2002). The sixth drying experiment was run during the long cold winter conditions in 2003 (Jan 2, 2003). Data collection for the second wall setup ended in late spring May 22, 2003 with ventilation arrangement adjustments and the walls were wet for the seventh drying experiment. The eighth drying experiment was begun July 16, 2003 during the hot summer. The final drying experiment was started the cool fall Oct 21, 2003. The monitoring ended on January 9, 2004 with the disassembly and inspection of the walls.

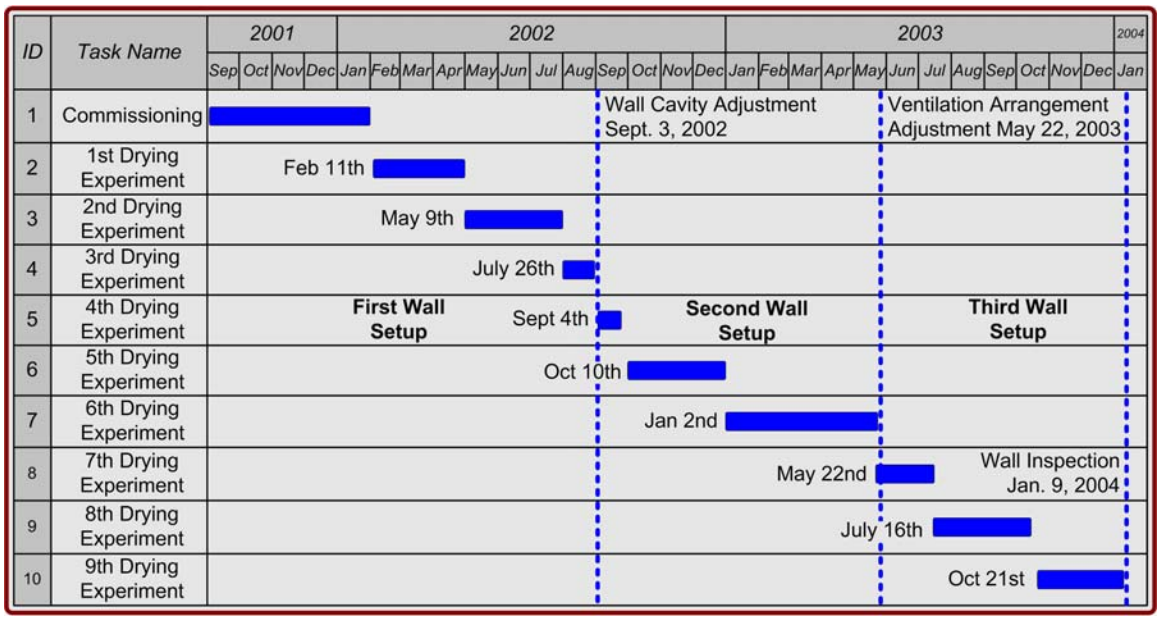

Figure 8-6: Drying Experiment Timelines

8.5. Results and Observations

8.5.1. First Wall Setup – February 2002 to September 2002

The first drying experiment began with the addition of 1350 ml of water (i.e., a 12% increase in Homasote sheathing moisture content) added to each wall over a 24 hour period on February 11, 2002. The second drying experiment began with the addition of 1800 ml of water (a 15% increase in Homasote sheathing moisture content) to each wall over a 24 hour period on May 9, 2002. The third drying experiment began with the addition of 1800 ml of water to each wall over a 24 hour period on July 26, 2002.

Plots of moisture content data and batt space condensation conditions (for water condensing on the surface of the melamine vapour barrier) are shown in Figure 8-8. Weather conditions over the monitoring period are shown in Figure 8-7.

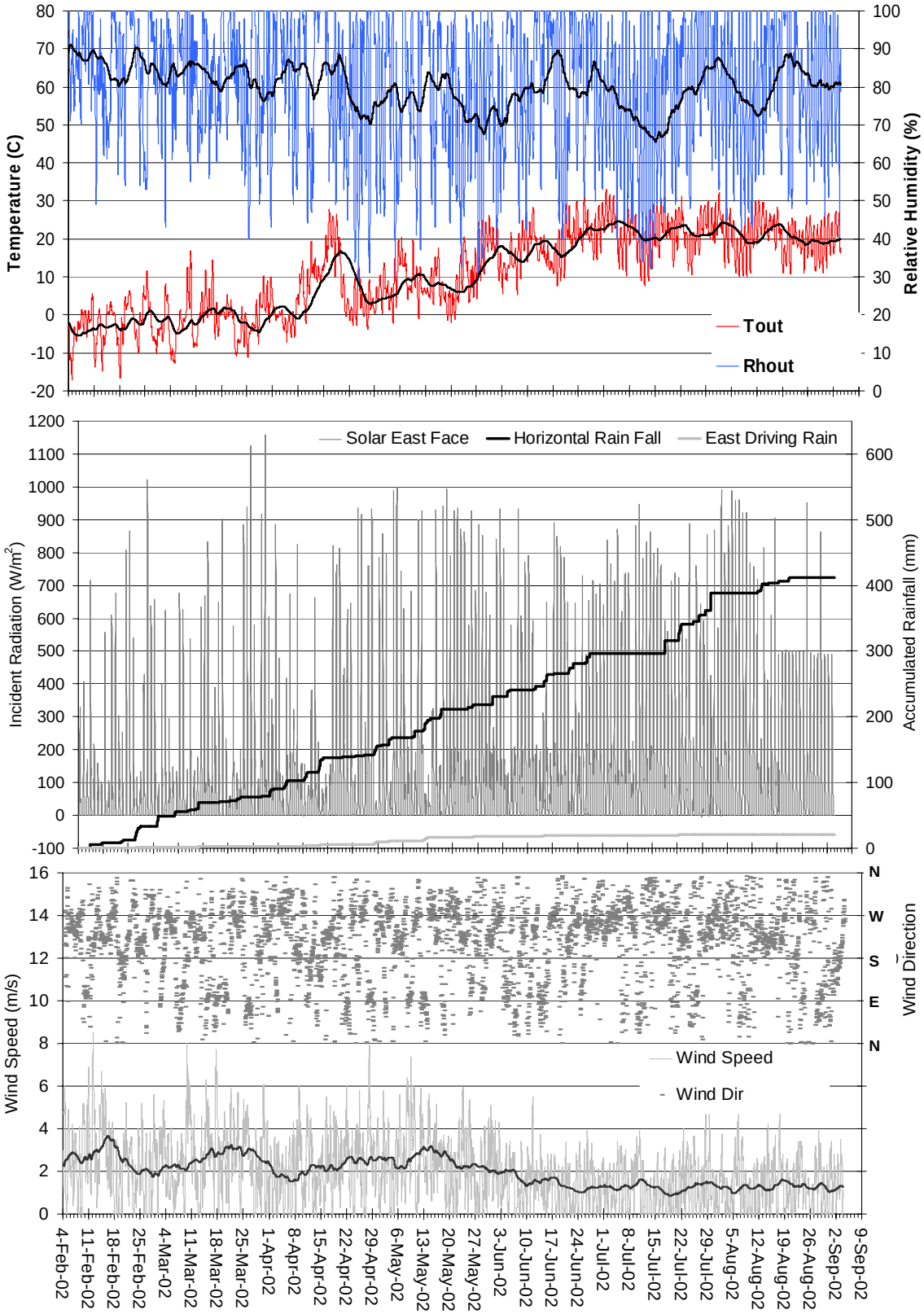

Figure 8-7: First Setup Weather Conditions

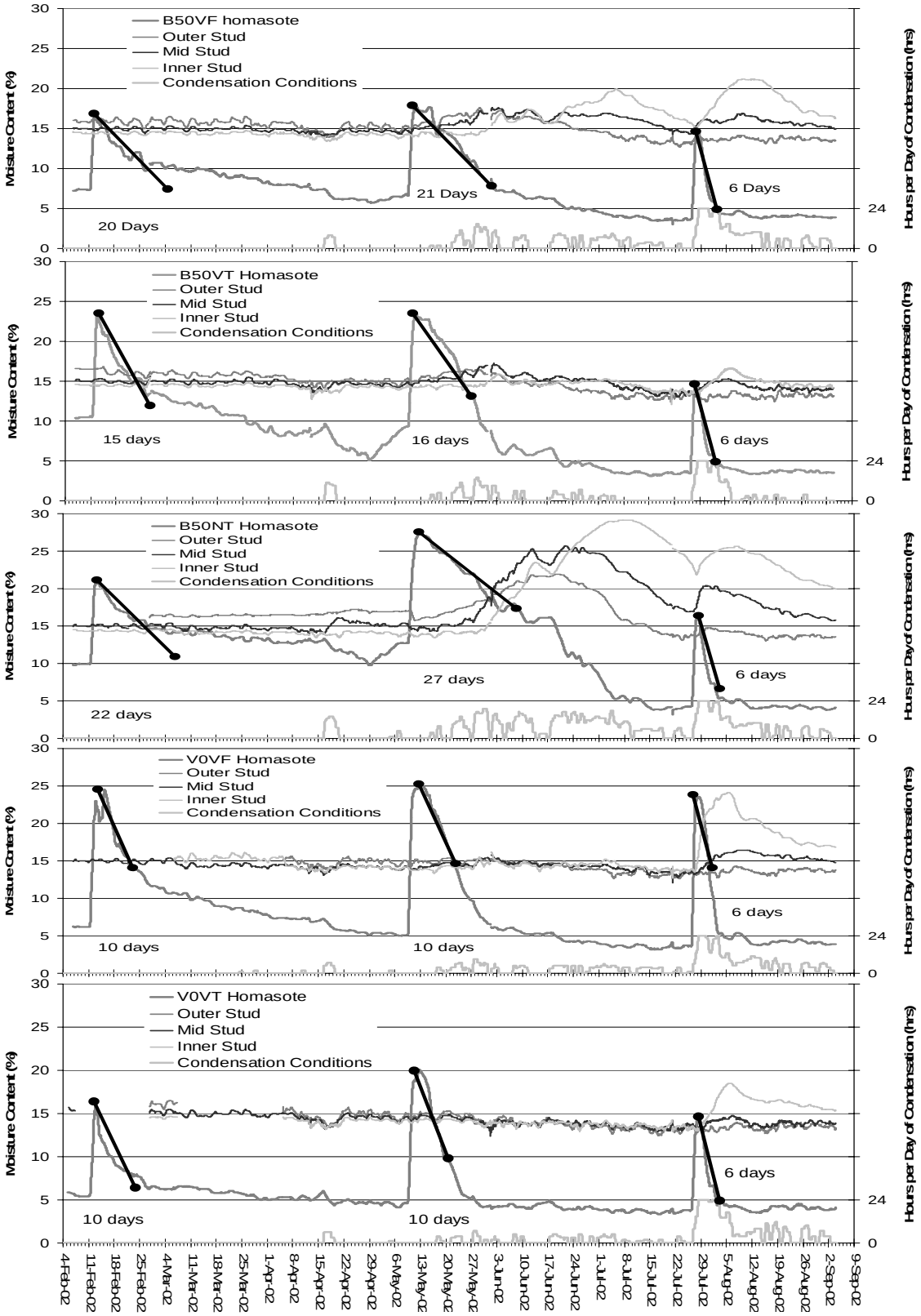

Figure 8-8: First Setup Moisture Content Measurements

The bulk of the Homasote drying occurred during a short period following the wetting. The approximate times required for the Homasote moisture content to drop ten percentage points were determined for each wall and are compared in Table 8-3.

Table 8-3: First Wall Setup – Homasote Sheathing Drying Times

Wall	Time for 10% moisture content drop in Homasote		
	1st Drying Experiment Late Cool Winter	2nd Drying Experiment Cool Spring	3rd Drying Experiment Hot Summer
B50VF	20 days	21 days	6 days
B50NT	22 days	27 days	6 days
B50VT	15 days	16 days	6 days
V0VF	10 days	10 days	6 days
V0VT	6 days	9 days	6 days

High moisture content conditions were recorded at the inner stud MC sensor (10 mm from the Melamine in the middle of the stud). The moisture content conditions at this sensor are summarized in Table 8-4.

Table 8-4: First Wall Setup – Days of Inner Stud Moisture Content

Wall	<=20%	> 20%	> 25%
B50VF	192	13	0
B50NT	110	95	38
B50VT	205	0	0
V0VF	188	17	0
V0VT	205	0	0

During the hot summer conditions the Homasote sheathing dried quickly in all walls. The sheathing in the vinyl siding clad walls (V0VT and V0VF) dried significantly faster than the brick veneer clad walls (B50VT, B50VF, and B50NT) during cold and cool outdoor conditions. For the brick veneer clad walls with a SBPO sheathing membrane, the ventilated wall (B50VT) dried faster than the non-ventilated wall (B50NT).

The non-ventilated brick veneer clad wall (B50NT) had steady very high inner stud moisture contents throughout the summer. The walls with AIF sheathing membranes (B50VF and V0VF) had high stud moisture contents for two week periods following the summer wetting.

Table 8-5: First Setup Condensation Condition Occurrence

Experiment	B50VF		B50VT		B50NT		V0VF		V0VT	
	(hrs)	(%)	(hrs)	(%)	(hrs)	(%)	(hrs)	(%)	(hrs)	(%)
First Feb 11/02 -	21	1%	30	1%	52	2%	24	1%	16	1%
Second May 9/02 -	569	22%	351	13%	897	34%	481	18%	412	16%
Third July 26/02 -	29	13%	4	2%	24	11%	34	16%	31	14%

The occurrence of condensation in the batt space was also investigated. Condensation occurrence was defined as any hour in which the dewpoint temperature of the batt space rose above the temperature of the outward facing surface of the melamine (which acts as a low permeance vapour barrier). Condensation within all of the walls was likely for a significant portion of all hours during the second (late spring) and third (summer) experiments (Figure 8-8 and Table 8-3). The non-ventilated brick veneer clad wall (B50NT) had significantly more hours of condensation than the other test walls throughout the months of May, June, and July. The walls with AIF sheathing membranes had slightly more hours of condensation conditions during the summer than the similar wall assemblies with SPBO sheathing membranes.

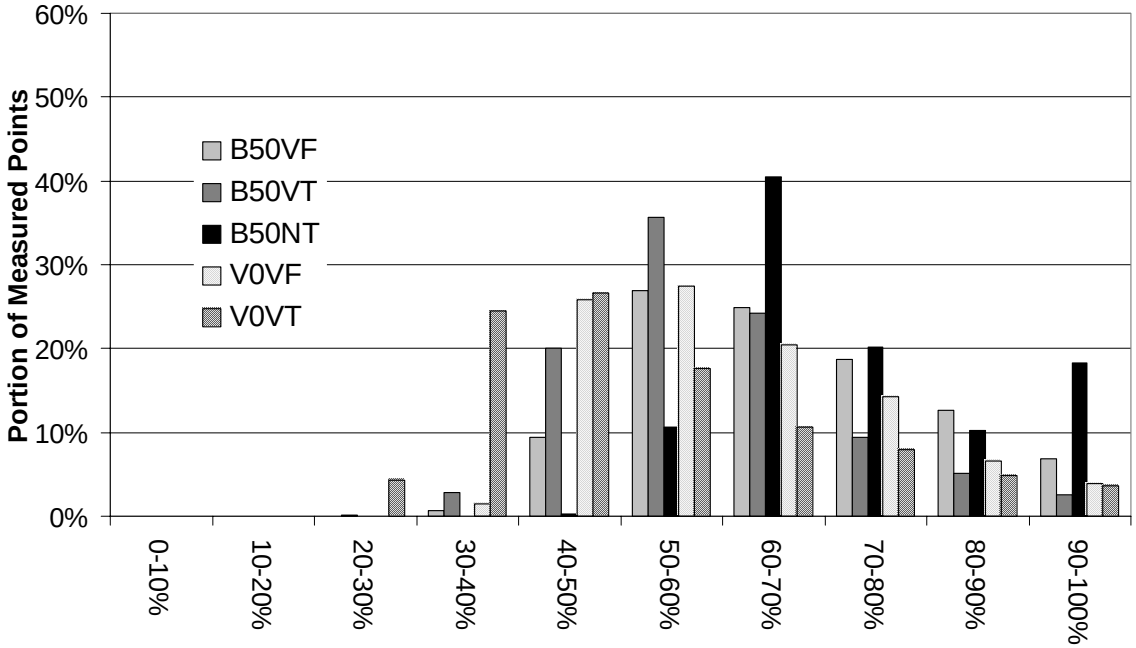

Figure 8-9: First Wall Setup Batt Space Relative Humidity Histogram

Histograms of the distribution of hourly relative humidity measurements are given in Figure 8-9 for the batt space and in Figure 8-10 for the ventilation cavity space. All walls had more than than 90% of batt space relative humidity measurements below 90% RH except the non-ventilated brick clad wall with 18% of measured values above 90% RH.

The vinyl siding walls had similar but lower batt space relative humidity measurements than the brick veneer clad walls.

The ventilation cavity relative humidity measurements had a significantly larger number of relative humidity measurements above 90% RH. The vinyl siding clad wall with SBPO (V0VT) had less high humidity conditions (7%) than the vinyl clad wall with AIF (V0VF) at 19%. The brick veneer clad walls had much higher ventilation space relative humidity than the vinyl clad walls, with 39% and 43% of measured values above 90% RH for the ventilated walls (B50VT and B50VF, respectively). The non-ventilated brick veneer wall (B50NT) exhibited the highest ventilation space RH values with more than half of all readings (53%) above 90% RH.

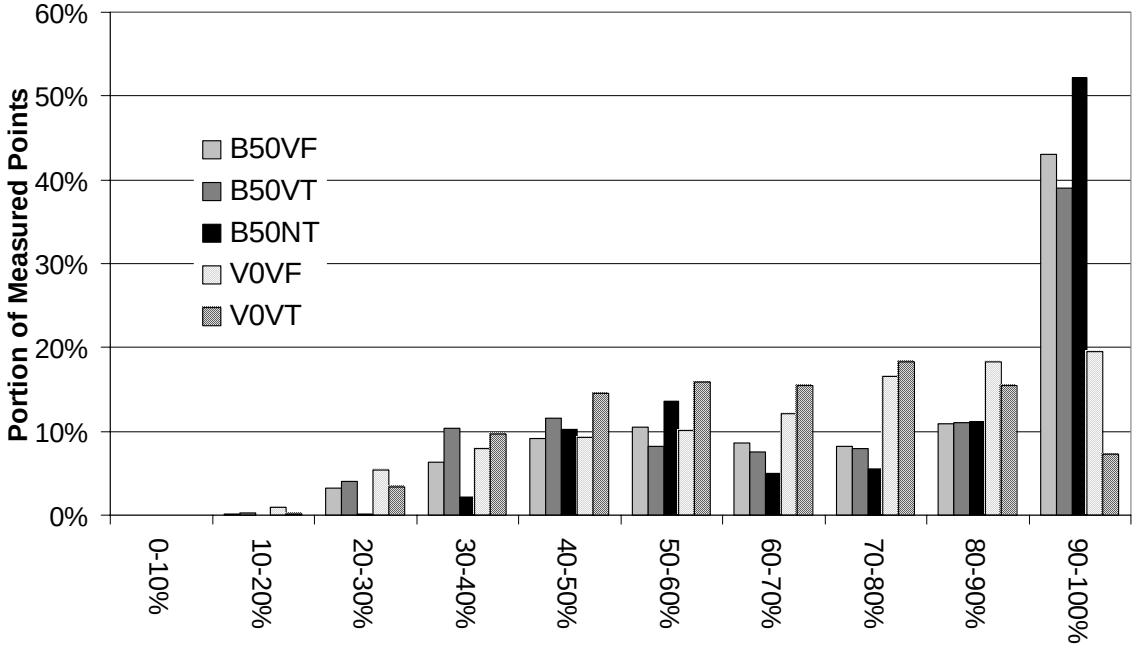

Figure 8-10: First Wall Setup Ventilation Cavity Relative Humidity Histogram

8.5.2. Second Wall Setup – September 2002 to May 2003

On September 3, 2002 the wall cavity depths behind the brickwork were adjusted from 50 mm to 20 mm and 20 mm vertical strapping was applied at 400 mm centers behind the vinyl siding.

The fourth drying experiment began with the addition of 1800 ml (a 15% increase in Homasote sheathing moisture content) of water to each wall over a 24 hr period on September 4, 2002. The fifth drying experiment began with the addition of 1800 ml of water to each wall over a 24 hr period on October 11, 2002. The sixth drying experiment began with the addition of 1800 ml of water to each wall over a 3 day period (delayed because of a frozen wetting line) on January 2, 2003.

Plots of moisture content data and batt space condensation conditions (for water condensing on the surface of the melamine vapour barrier) are included in Figure 8-12. Weather conditions over the monitoring period are included in Figure 8-11.

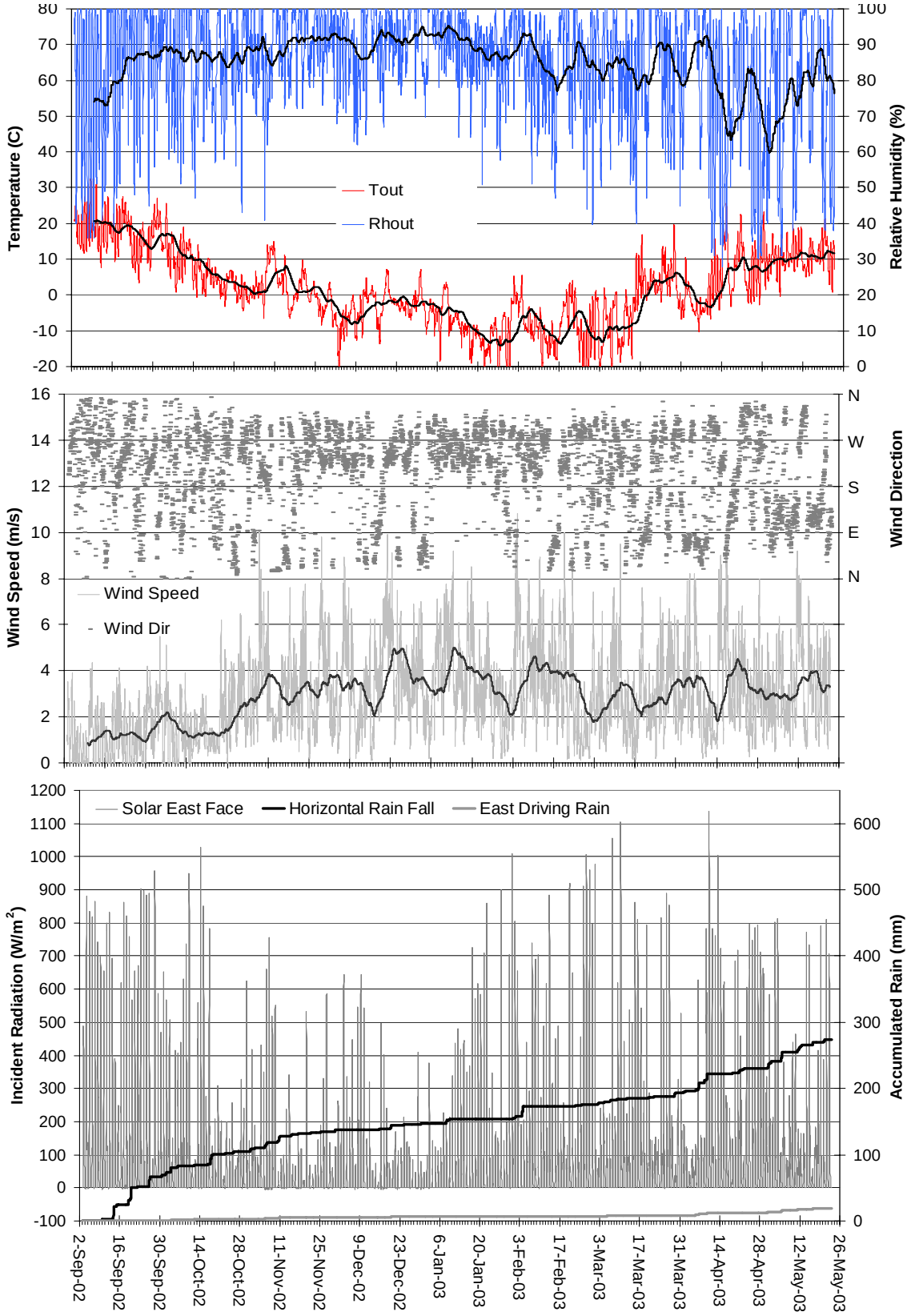

Figure 8-11: Second Wall Setup Weather

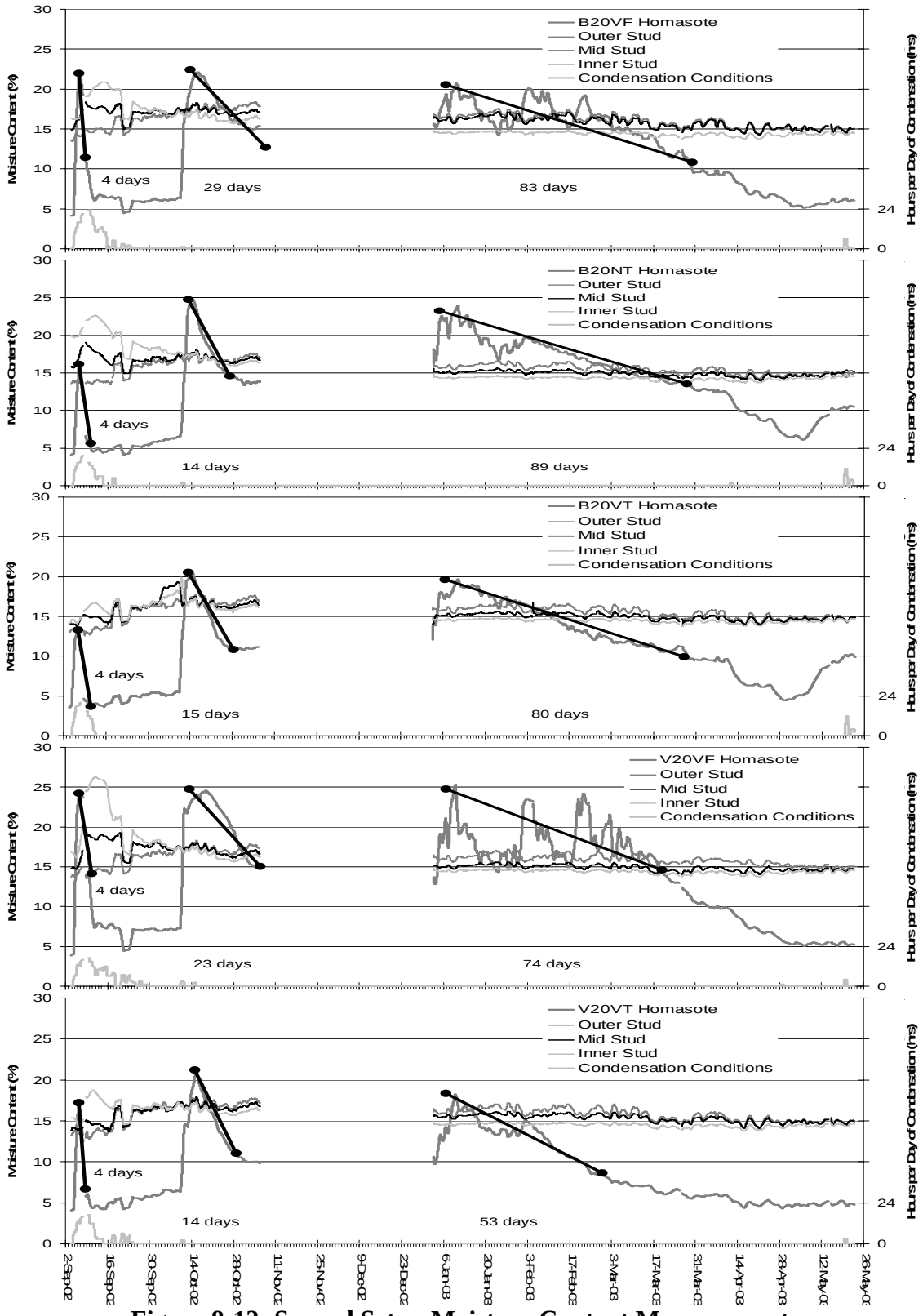

Figure 8-12: Second Setup Moisture Content Measurements

The bulk of the Homasote drying occurred during a short period following the wetting. The approximate times required for the Homasote moisture content to drop ten percentage points were determined for each wall and are compared in Table 8-6. During cold winter conditions, the sheathing moisture content dropped slowly.

Table 8-6: Second Wall Setup – Homasote Sheathing Drying Times

Wall	Time for 10% moisture content drop in Homasote		
	4th Drying Experiment Hot Summer	5th Drying Experiment Early Cool Fall	6th Drying Experiment Cold Winter
B20VF	4 days	29 days	83 days
B20NT	4 days	14 days	89 days
B20VT	4 days	15 days	80 days
V20VF	4 days	23 days	74 days
V20VT	4 days	14 days	53 days

High moisture content conditions were recorded at the inner stud MC sensor (10 mm from the Melamine in the middle of the stud). The moisture content conditions at this sensor are summarized in Table 8-7.

Table 8-7: Second Wall Setup – Days of Inner Stud Moisture Content

Wall	<=20%	> 20%	> 25%
B20VF	255	7	0
B20NT	248	14	0
B20VT	262	0	0
V20VF	249	13	5
V20VT	262	0	0

The Homasote sheathing dried very quickly in the hot summer conditions in all of the test walls. The sheathing in the vinyl siding walls dried at similar rates as the brick veneer clad walls in the cool fall and dried faster in the cold winter conditions. The sheathing in the vinyl siding clad wall with SPBO dried faster than with AIF during the cool fall and cold summer conditions. The sheathing in the ventilated brick veneer clad wall with SPBO dried slightly faster than with AIF during the cool fall and at a similar rate in the cold winter. The sheathing in the ventilated brick veneer clad wall dried at a similar rate as in the non-ventilated test wall under cold winter conditions.

The non-ventilated brick veneer clad wall (B20NT) exhibited a two week period of high (>20%) inner stud moisture contents following the summer wetting. The ventilated wall with similar materials (B20VT) did not experience any high inner stud moisture contents. The ventilated brick veneer clad wall with AIF experienced a week of high inner stud moisture contents following the summer wetting. The vinyl siding clad wall with AIF sheathing membrane (V20VF) had a two week spike in inner stud moisture content following the summer wetting. The vinyl siding clad wall with SBPO did not experience high inner stud moisture contents throughout the period.

Table 8-8: Second Setup Condensation Condition Occurrence

Experiment	B20VF		B20VT		B20NT		V20VF		V20VT	
	(hrs)	(%)	(hrs)	(%)	(hrs)	(%)	(hrs)	(%)	(hrs)	(%)
Fourth Sept 4/02 -	163	17%	88	9%	109	11%	167	17%	106	11%
Fifth Oct 10/02 -	0	0%	0	0%	0	0%	2	0%	0	0%
Sixth Jan 2/03 -	6	0%	19	1%	18	1%	5	0%	3	0%

Condensation conditions occurred in the walls following the September 2002 wetting and in early May 2003. The walls with SBPO sheathing membranes had significantly less hours of condensation occurrence than the AIF walls following the September 2002 wetting. A few hours of condensation occurred in all walls in early May 2003. The walls with brick veneer and a SBPO sheathing membranes exhibited noticeably more hours of condensation.

Histograms of hourly relative humidity measurements are plotted in Figure 8-13 for the batt space and in Figure 8-14 for the ventilation cavity space. The relative humidity in the batt space was over 90% for 5% of all hours. The non-ventilated brick veneer clad wall tended to have the highest batt space relative humidity measurements. The vinyl siding clad walls tended to have lower batt space relative humidity measurements than the brick veneer clad walls.

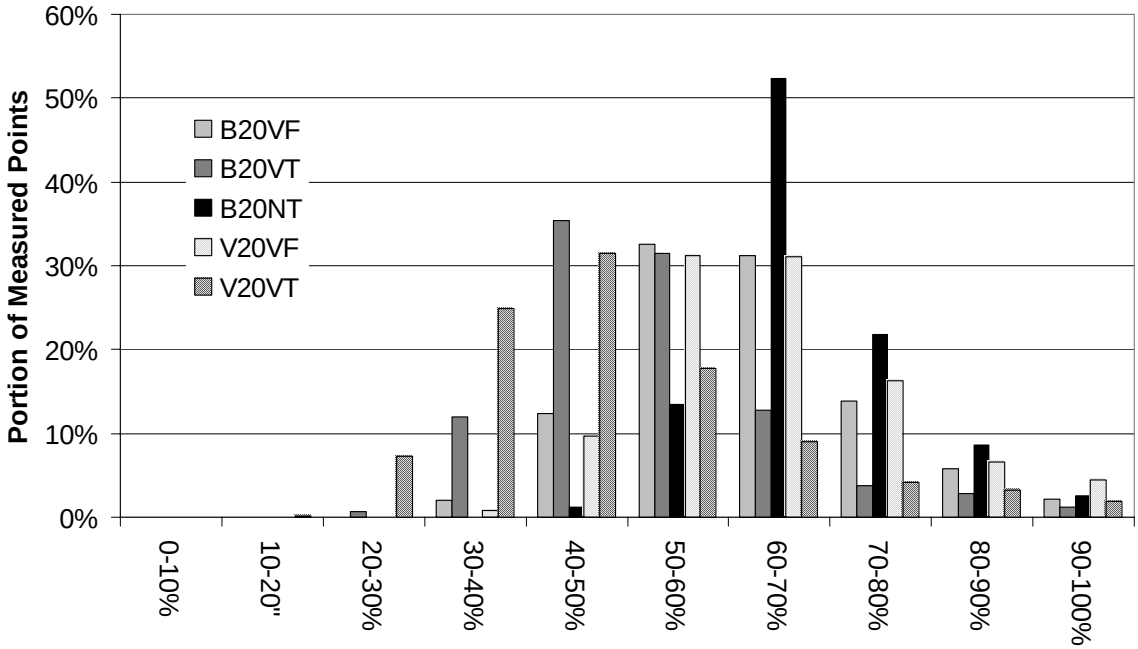

Figure 8-13: Second Wall Setup Batt Space Relative Humidity Histogram

A large number of ventilation cavity relative humidity measurements were 90%RH. The vinyl siding clad wall with SBPO (V20VT) had fewer hours of high humidity conditions

(18%) than the V20VF (vinyl clad wall with AIF) wall (33%). The brick veneer clad walls had much higher relative humidity with 41% and 45% of measured values above 90%RH for the ventilated walls (B20VT and B20VF, respectively) and 62% for the non-ventilated wall (B20NT).

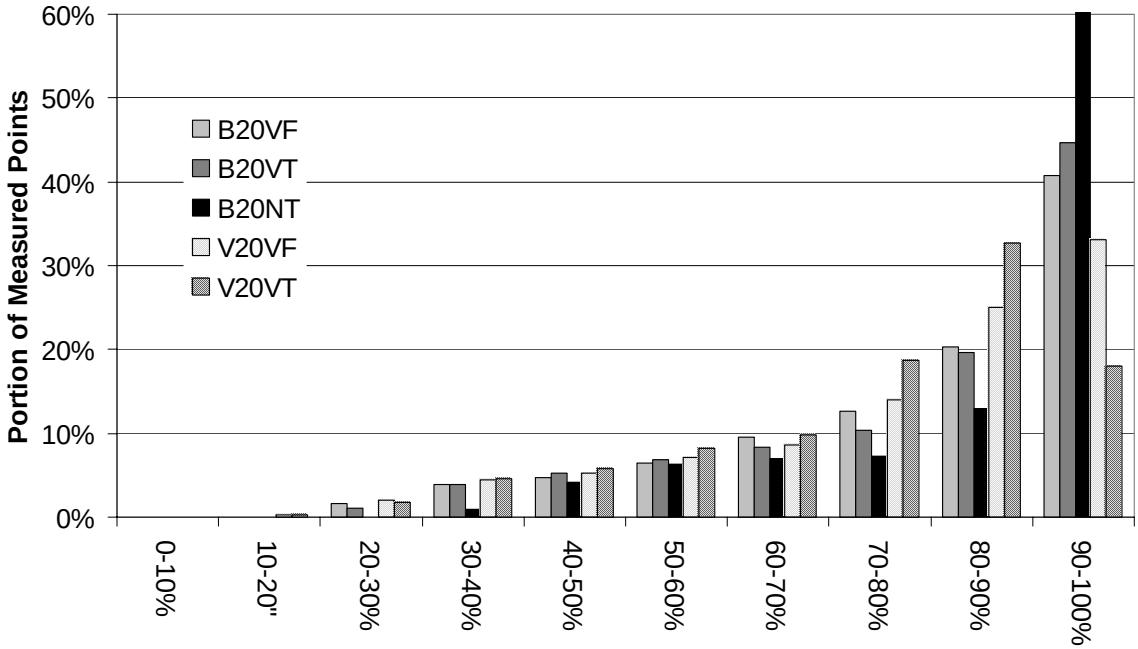

Figure 8-14: Second Wall Setup Ventilation Cavity Relative Humidity Histogram

8.5.3. Third Wall Setup – May 2003 to January 2004

Data collection for the second wall setup ended May 22, 2003. The ventilation arrangement of three of the walls were changed as follows:

- The top vents of the B20VF wall were sealed (the wall was then labeled B20NF).
- The top vents of the B20NT wall were opened (the wall was then labeled B20VT(2)).
- The joints of the V20VF were sealed with caulking (the wall was then labeled V20NF).

The seventh drying experiment was started the same day with 1800 ml (15% increase in Homasote sheathing moisture content) of water injected into each wall over a 24 hr period. The eighth drying experiment was begun July 16, 2003 with a similar wetting volume and procedure. The final drying experiment was started Oct 21, 2003 with a similar wetting volume and procedure and ran through cool fall conditions. The monitoring ended on January 9, 2004 with the disassembly and inspection of the walls.

Plots of moisture content data and batt space condensation conditions (for water condensing on the surface of the melamine vapour barrier) are included in Figure 8-16. Weather conditions over the monitoring period are included in Figure 8-15.

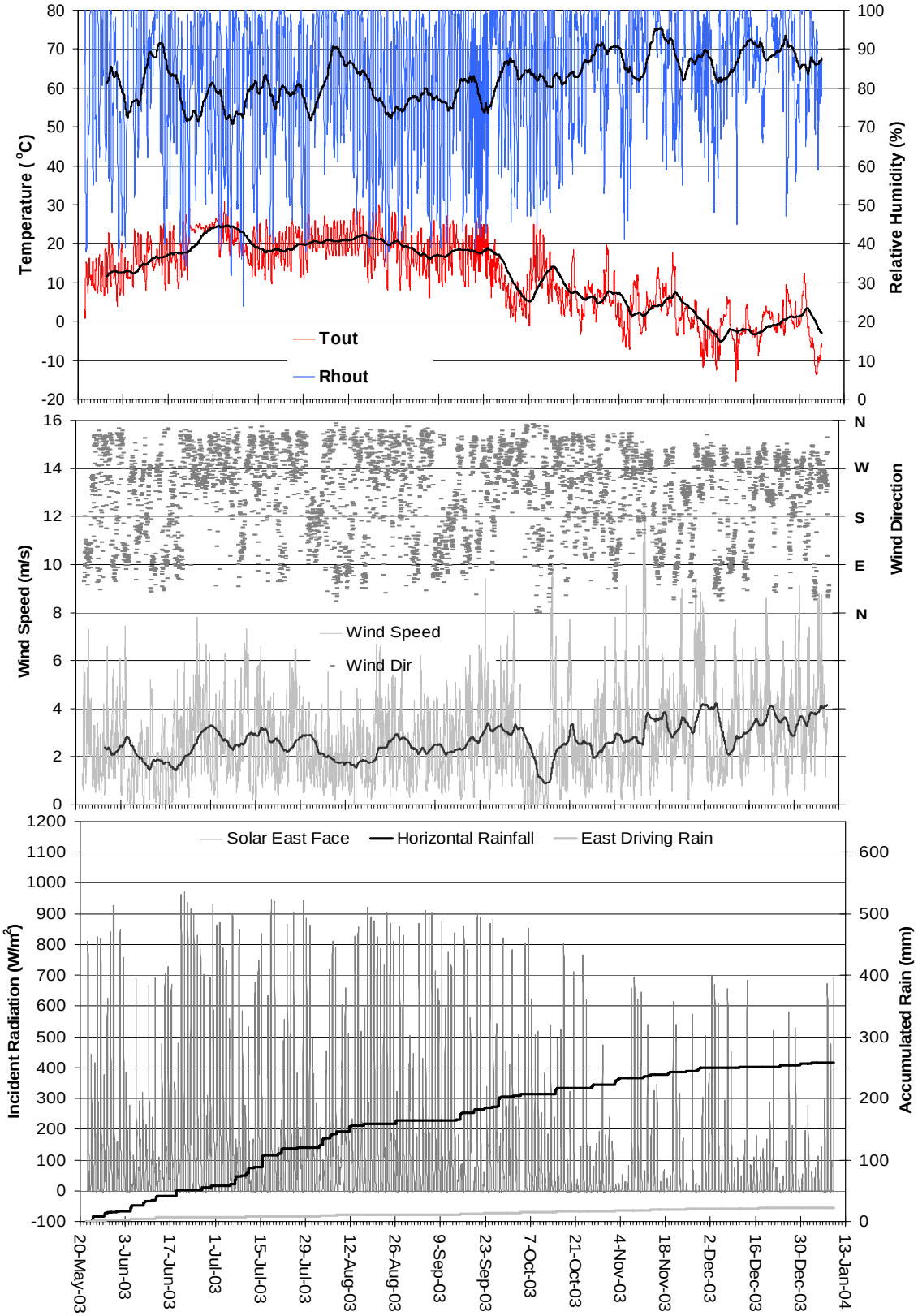

Figure 8-15: Third Wall Setup Weather

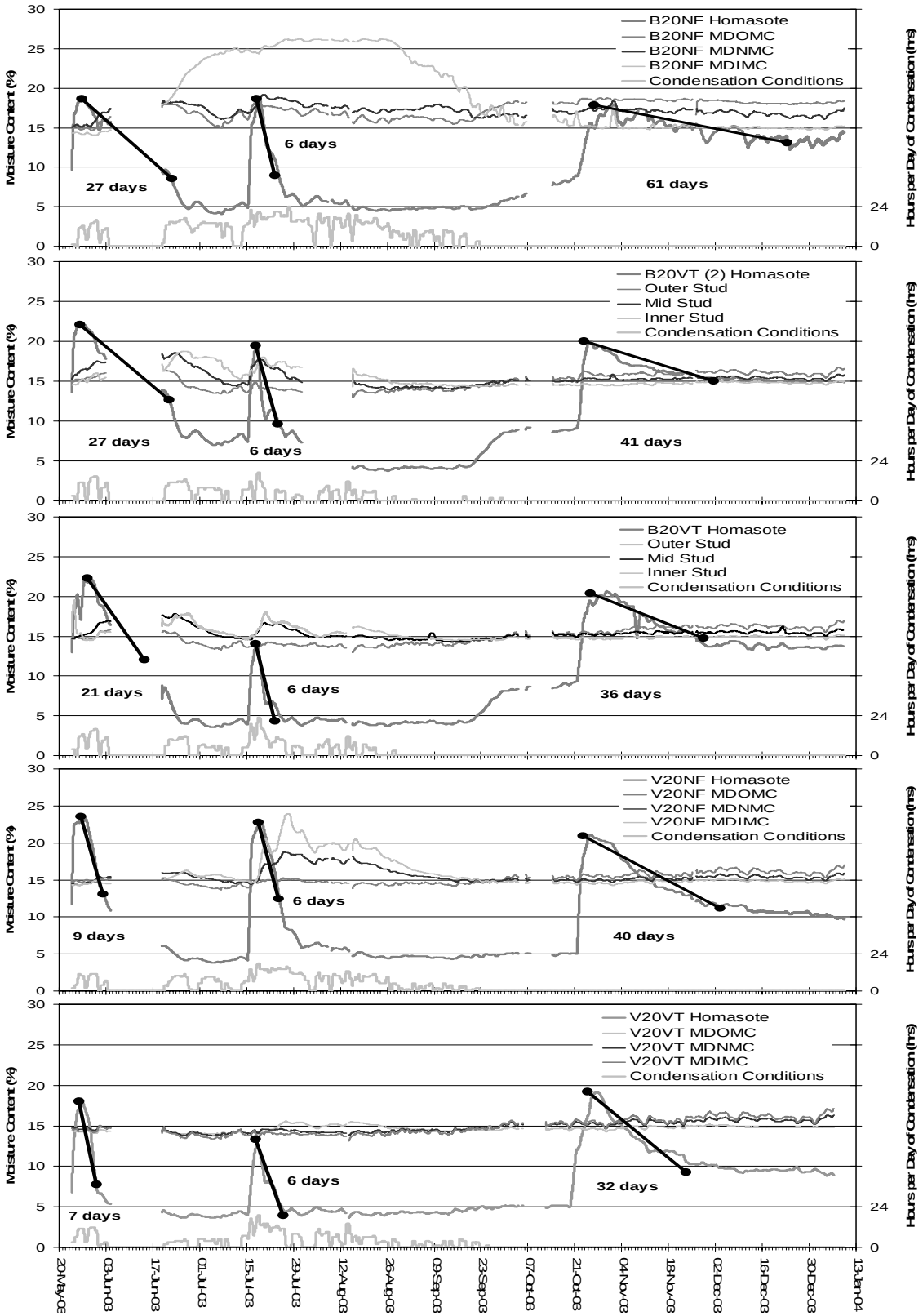

Figure 8-16: Third Setup Homasote Sheathing Moisture Content

The bulk of the Homasote drying occurred a short period after the wetting during the first two drying experiments of the third wall setup. The approximate times required for the Homasote moisture content to drop ten percentage points were determined for each wall and are compared in Table 8-9.

Table 8-9: Third Wall Setup – Drying Times

Wall	Time for 10% moisture content drop in Homasote		
	7th Drying Experiment Cool Late Spring	8th Drying Experiment Hot Summer	9th Drying Experiment Cool Fall
B20NF	27	6	61
B20VT(2)	27	6	41
B20VT	21	6	38
V20NF	9	6	40
V20VT	7	6	32

High moisture content conditions were recorded at the inner stud MC sensor (10 mm from the Melamine in the middle of the stud). The moisture content conditions at this sensor are summarized in Table 8-10.

Table 8-10: Third Wall Setup – Days of Inner Stud Moisture Content

Wall	<= 20%	> 20%	> 25%
B20NF	146	86	41
B20VT	232	0	0
B20VT	232	0	0
V20NF	218	14	0
V20VT	232	0	0

The Homasote sheathing in the test walls dried very quickly following the summer wetting. The test walls with vinyl siding dried significantly faster than the brick veneer clad walls in the early summer conditions but at similar rates in the cool fall. During the early summer conditions the non-ventilated brick veneer clad wall (B20NF) and newly ventilated wall (B20VT(2)) dried at similar rates but both were slower than the ventilated brick veneer clad wall (B20VT). During the fall conditions the non-ventilated brick veneer clad wall (B20NF) dried significantly slower than all other test walls. The vinyl clad wall (V20NF) dried quickly. This was not anticipated as the natural ventilation was limited by sealing the joints, and the siding is completely vapour impermeable. However, the vinyl siding was accidentally punctured in this wall (by vandals). This may have provided some unintended ventilation (especially since the cladding was installed over a 20 mm space).

High inner stud moisture content was measured in the non-ventilated brick veneer clad wall (B20NF) throughout the months of July, August, and September 2003. High inner stud moisture content was also measured in the the vinyl siding clad test wall with AIF

sheathing membrane during a two week period following the mid-summer wetting. All other test wall stud moisture content measurements remained below 20% throughout the period.

Table 8-11: Third Setup Condensation Condition Occurrence

Experiment	B20NF		B20VT (2)		B20VT		V20NF		V20VT	
	(hrs)	(%)	(hrs)	(%)	(hrs)	(%)	(hrs)	(%)	(hrs)	(%)
Seventh	399	30%	230	18%	257	20%	216	17%	159	12%
Eighth	766	33%	224	10%	157	8%	444	19%	316	14%
Ninth	0	0%	0	0%	0	0%	0	0%	0	0%

Condensation conditions occurred within the non-ventilated brick veneer clad wall with AIF (B20NF) for about a third of the total time during the entire summer. The two brick veneer clad walls with SBPO (B20VT) had a similar number of hours of condensation occurrences. Both exhibited significantly fewer condensation hours than the B20NF wall. The vinyl siding clad wall with AIF had more condensation conditions than with SBPO.

Histograms are given for the hourly measurement points of relative humidity in the batt space in Figure 8-17 and in the ventilation cavity space in Figure 8-18. All of the walls had less than 10% of relative humidity measurements in the batt below 90%RH except the non-ventilated brick clad wall with 19% of measured values above 90%RH. The vinyl siding walls tended to have lower batt space relative humidity measurements than the brick veneer clad walls.

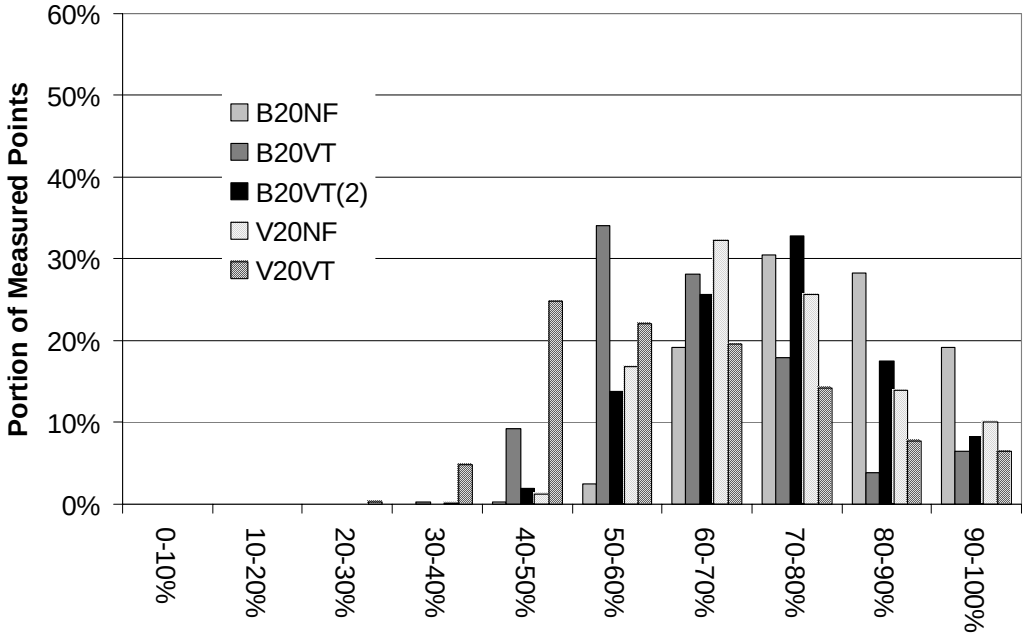

Figure 8-17: Third Wall Setup Batt Space Relative Humidity Histogram

The ventilation cavity relative humidity measurements had a significantly larger number of relative humidity measurements above 90%RH than the batt space measurements in all walls. The fully ventilated (V20VT) vinyl siding clad wall had fewer high humidity conditions (16% of hours) than the vinyl clad wall with reduced ventilation (V20NF) (35% of hours). During about 50% of the hours the ventilation cavity of the two ventilated brick veneer clad walls had relative humidities above 90%RH. The ventilation cavity in the unventilated brick wall experienced high relative humidity for a slightly greater portion of the time (55%).

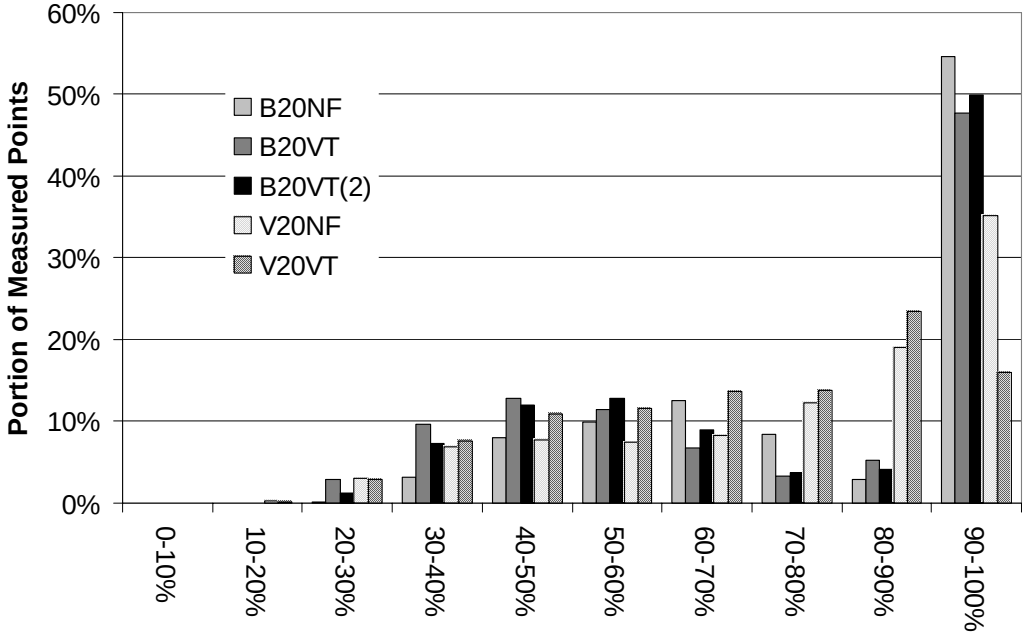

Figure 8-18: Third Wall Setup Ventilation Cavity Relative Humidity Histogram

The moisture content of the Homasote showed an increase in the last week of September in all of the brick walls, but especially the brick walls with SBPO. This rise correlated with driving rain on the east face and a significant drop in outdoor temperature.

8.6. Discussion

Results from these field experiments pertaining directly to the effect of ventilation on wall performance are discussed in this section. The influence of sheathing membrane, weather, and cladding type will also be discussed as they impact ventilation drying or are significant to overall wall performance.

8.6.1. Influence of Ventilation – Brick Veneer

The non-ventilated brick veneer clad test walls exhibited a slower sheathing drying time, more hours of batt space condensation, and maintained higher stud moisture contents than ventilated wall assemblies of similar construction. During the disassembly of the wall systems the non-ventilated walls (B20/50NT and B20NF) showed significant mold growth colonies. This helps verify the measured high moisture conditions within the batt

space. Condensation on the view window (as shown in Figure 8-19) was also more frequently observed in the non-ventilated walls. All of these observations strongly suggest that ventilation behind brick veneer assists drying and reduces warm weather inward vapor drives.

Figure 8-19: Condensation Observed on View Window

A summary of predicted cavity ventilation rates for the ventilated brick clad test walls is shown in Figure 8-20, Figure 8-21, and Figure 8-22. Buoyancy driving pressures were determined from measured cavity and outdoor temperature and relative humidity. Wind driven pressures were determined from wind speed and direction measurements. The airflow rate was determined by applying these combined pressures to the airflow resistance characteristics documented in Chapter 7.

The ventilation flowrate for all ventilated brick veneer walls is predicted to have been greater than 0.1 lps/m^2 (about 0.24 lps per meter width for a 2.4 m high wall) for more than 80% of the time. With a ventilation flowrate of 0.1 lps/m^2 the ventilated brickwork can be calculated to have an equivalent permeance of greater than 1000 ng/Pa·s·m^2 (from Chapter 5) for at least 80% of the time. Typical brick veneers have a permeance of 45 to 200 ng/Pa·s·m^2. The relatively high equivalent permeance of the ventilated walls allowed faster sheathing drying rates. It is also expected that the quantity of moisture driven inward from the brickwork into the batt space is reduced by ventilating the cavity. It can be noted that higher wind speeds led to slightly more predicted ventilation during winter periods, which is characteristic of Waterloo's climate.

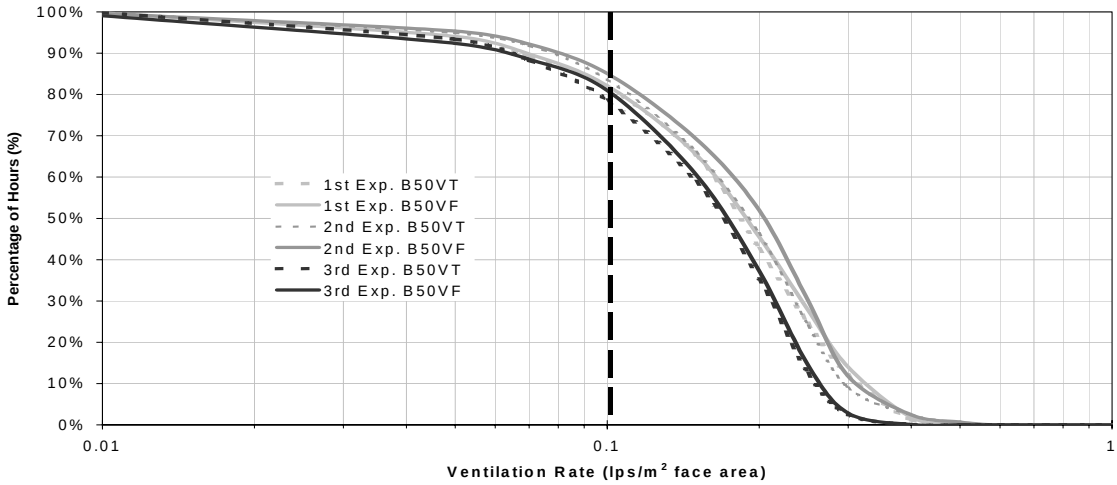

Figure 8-20: Percentage of Hours above Ventilation Rates – 1st Wall Setup

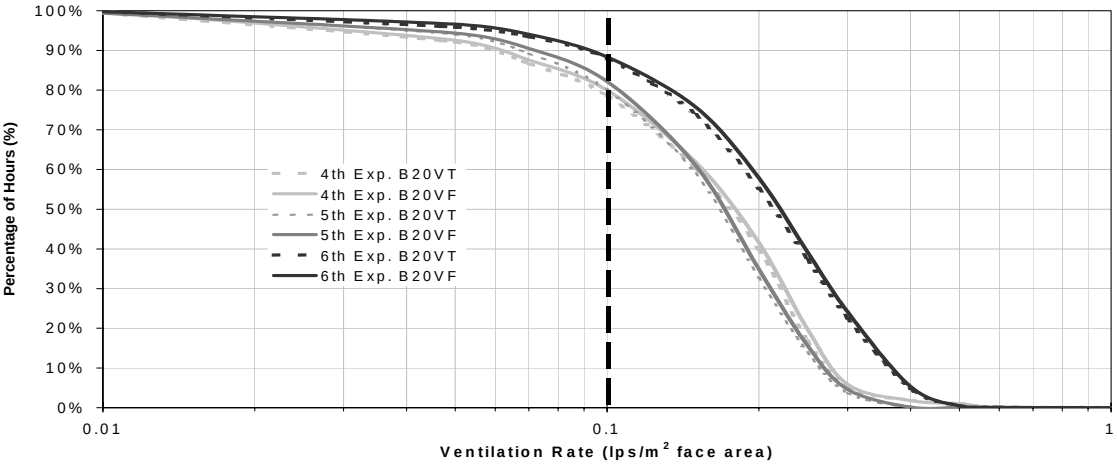

Figure 8-21: Percentage of Hours Above Ventilation Rates – 2nd Wall Setup

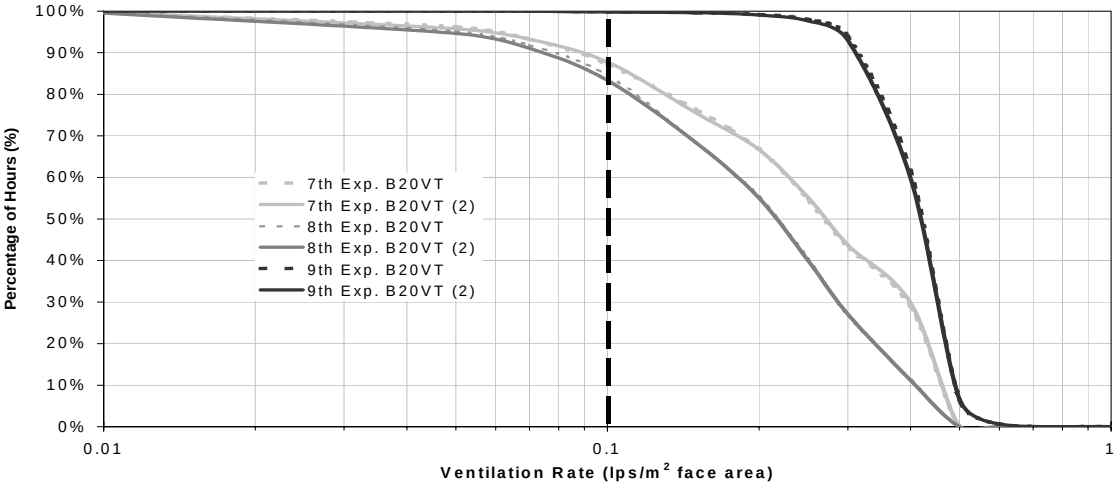

Figure 8-22: Percentage of Hours above Ventilation Rates – 3rd Wall Setup

Ventilation effects may have played a small but still important role in the non-ventilated brick veneer clad wall. Significant airflows may exist between the bottom weep-hole vents driven by wind induced pressures. More work is necessary to determine an equivalent vapour permeance but based on the slower observed drying rates it is likely well below the equivalent permeance of the ventilated walls.

The different cavity widths (50 mm in the first setup, 20 mm in the second) did not have a large impact on the drying rates of the sheathing or the wall assemblies. A direct comparison was difficult since the weather conditions between the first set up and the second setup were different. The airflow testing reported in Chapter 7 did not show large difference in flow since the vents comprise the majority of the resistance. Hence, large differences in performance would not be expected.

8.6.2. Influence of Ventilation – Vinyl Siding

The Homasote sheathing behind the vinyl siding dried faster than the sheathing behind the brick veneer clad walls during winter and spring conditions but had similar drying rates during fall. It dried very quickly in both types of walls under summer conditions.

The number of hours of condensation on the vapour barrier, the batt space relative humidities, and high levels of inner stud moisture contents experienced were similar for both the *ventilated* brick clad walls and the two vinyl clad walls. However, there were behavioural differences, which may help explain the differences in Homasote sheathing drying rates and wall panel drying.

The fact that the vinyl clad walls dried readily is evidence that ventilation plays an important role in these test walls. Recall that the vinyl siding clad test wall systems consisted of an assembly enclosed by vapour impermeable materials on all sides. The only open surface area (e.g., joints and cracks) through which vapour can diffuse is through the vinyl siding. This area is limited. The only practical route for moisture to leave the assembly is through ventilation behind and through the cladding. Therefore it can be concluded that the moisture must leave through the cladding by ventilation.

The peak ventilation cavity air temperatures in the vinyl clad walls were higher than those in the brick clad walls, although the duration of the peak was much less. (Note that the cladding surface temperatures were similar). The higher vinyl air cavity temperatures resulted in large short-term inward vapor drives from the wet Homasote, and subsequent occurrence of condensation in the batt space. Thus, immediately following wetting the inward vapor drive and condensation were observed and measured to be more severe. Therefore, much of the fast Homasote drying was in fact redistribution of moisture to the inner layers of the wall system rather than removal of moisture from the wall system. However, the same high temperatures also likely contributed to outward drying, which should have helped drying of the whole wall panel.

There were in fact some indications that the vinyl clad panels were somewhat drier than the ventilated brick panels. For example, although the ventilation cavity humidity levels fluctuated much more behind vinyl than behind the brick, they were lower on average. The inward drive phenomenon was much less evident in cold weather (compare the

number of hours of condensation and inner stud moisture content) but the Homasote still dried more quickly in the vinyl clad walls than the ventilated brick veneer panels. This also supports the conclusion that the vinyl clad walls dried more quickly than the brick walls. The very fast sheathing drying rates may simply be overstating the drying rate of the whole panel.

There are three reasons in addition to redistribution that may explain why the Homasote sheathing dried more quickly in the vinyl siding clad wall specimens than in the brick veneer clad walls:

1. The vinyl siding may allow more ventilation to occur. The airflow resistance characteristics of the vinyl siding (explored in Chapter 6) are not easily comparable to the brick assembly characteristics (discussed in Chapter 7) but they do suggest that the siding will be well ventilated in service.
2. Brick is a hygroscopic material that can store a significant amount of moisture from rain and moist outdoor air. Hence, even though the sheathing may be releasing moisture readily into the ventilation cavity, the wetting caused by moisture driven inward from the brickwork may reduce the net drying rate.
3. Since vinyl siding has a lower thermal mass than brick, it reaches higher ventilation cavity air temperatures when exposed to the sun. These high air temperatures increase the rate of desorption of moisture from the Homasote. It might also be noted that high temperatures have a non-linear influence on the saturation vapour pressure of air – that is, the saturation vapour pressure increases more rapidly than temperature. Hence, high temperatures will result in very fast drying. The impact of the third effect may however be reduced by the longer period of time that the ventilation cavity air temperature remains elevated behind the brick veneer due to its thermal storage.

The use of strapping behind vinyl siding did not have an obvious impact on the drying rates of the sheathing or the wall assemblies. Neither the Homasote sheathing drying rate, batt space RH, condensation occurrence nor cavity RH values behaved in fundamentally different ways between the two setups. A direct comparison was difficult since the weather conditions between the first set up (contact applied) and the second setup (strapping) were different. Nevertheless, large differences should have been detected, especially relative to the companion brick walls in each setup.

8.6.3. Influence of Sheathing Membrane

Differences between the drying rates of walls with AIF and SBPO were consistently observed. The Homasote sheathing in the walls with SBPO tended to dry more quickly than the walls with AIF.

The walls with AIF experienced more solar-driven inward vapor drives from the Homasote sheathing than the SBPO walls. Significantly higher levels of inner stud moisture content were measured after the summer wetting events and a greater number of hours of condensation conditions throughout the summer than similar walls with SBPO.

The measured ventilation cavity air conditions show that the membranes are operating at over 90% relative humidity for large (20 to 55%) portions of the time (see Figure 8-10, Figure 8-14, and Figure 8-18). It is suspected that a large portion of the outward drying occurs when the ventilation cavities are heated by the sun. During these periods of the day the relative humidity of the air in the cavity tends to drop as the temperature rises (see Appendix C). Hence, a large portion of the drying may occur during hours when the cavity is at lower relative humidities. Available data on the permeance of the sheathing membranes is plotted in Figure 8-23. The different curves for AIF are for three different manufacturers. SBPO and AIF have similar (and high) permeances at relative humidities (over 90%), but even at 80%RH the AIF permeances are an order of magnitude lower. Thus, during peak drying hours, the permeance of the AIF sheathing membrane is significantly lower than the SBPO. This explains the slower sheathing drying rates and the greater inward vapor drives in the AIF walls. The moisture storage capacity of the AIF may dampen the response of the AIF RH relative to the cavity air RH.

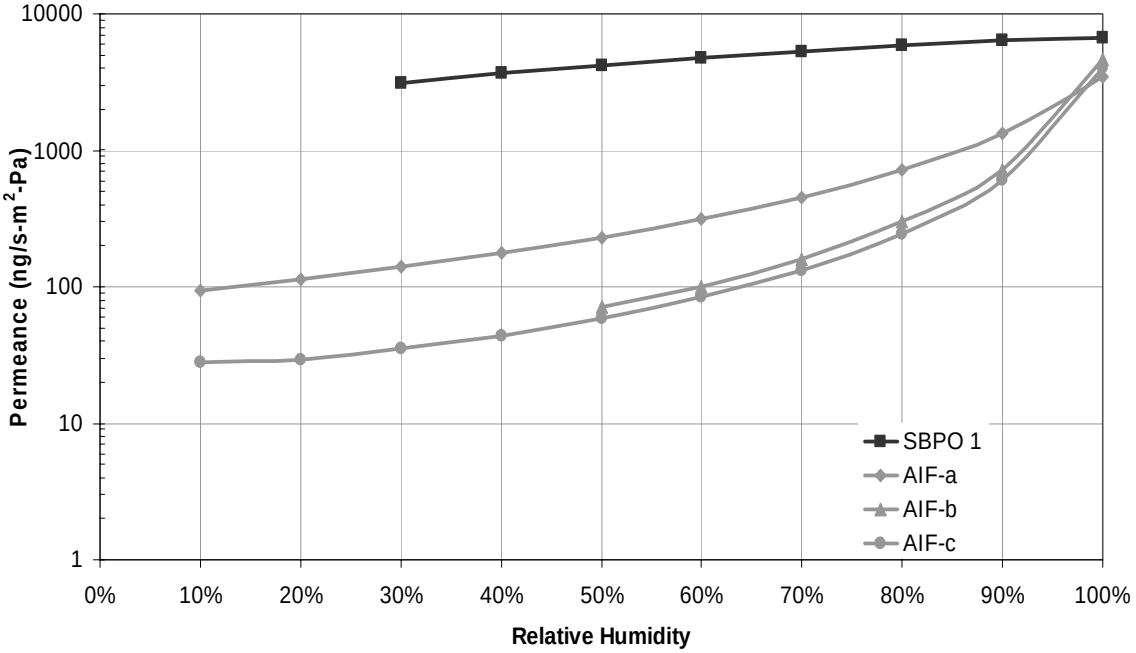

Figure 8-23: Vapour Permeance of SBPO and AIF (Treschel 2001, Kumaran et al. 2002)

A potentially negative impact of the use of high vapour permeance sheathing membranes is the increased inward driven moisture from *cladding* that stores moisture and is wetted (e.g., brick veneers). This phenomenon is suspected to have caused the spring moisture uptake in the brick veneer clad walls with SBPO. In this case the material moisture levels are still well below deterioration thresholds, however, the influence of this phenomenon should be investigated for other climates and situations.

The difference in moisture storage between the two types of sheathing membrane may also significantly affect hygrothermal behaviour at low temperatures. The AIF can

absorb and store liquid water. It is suspected that the AIF was saturated with frozen water (frost) during the initiation of the first drying experiment and to a greater extent during the sixth drying experiment. As ice has a very low vapor permeance, the frosting may have caused the observed delay in drying. This behaviour of AIF membranes should be studied in more detail. It can be noted that the same behaviour has been observed in yet-to-be-published climate chamber research at PSU.

8.7. Conclusions and Recommendations

8.7.1. Summary and Conclusions

The test wall assemblies dried most of the water added within 4 days to 3 months depending on weather conditions and the assembly design. Walls dried much more slowly in colder weather. During the hot summer weather the sheathing dried very quickly and in some cases a significant amount of moisture was redistributed inward resulting in condensation on the melamine vapour barrier and absorption into the wood studs. Over about 3 years, each of the walls dried almost 16 kg of water that was introduced to the batt facing side of the sheathing. Most of the walls ended the study in good condition with few signs of damage.

Ventilation of the brick veneer clad test walls was effective in both increasing sheathing drying rates and avoiding condensation and excessive stud moisture contents caused by inward vapour drives. The brick clad walls with vent openings at the bottom only (non-ventilated) dried more slowly, experienced moisture conditions in the batt space close to or above damage thresholds, and suffered from more severe inward vapor drive wetting. Physical inspection upon disassembly confirmed that the non-ventilated walls performed more poorly than the ventilated walls.

No large difference in hygrothermal performance was found between the 20 mm and 50 mm ventilation cavity wall setups for the brick veneer test walls, likely because there was no significant difference in ventilation flow.

The vinyl clad walls behaved as though they were very well ventilated. The Homasote sheathing dried more quickly in the walls clad with vinyl siding than the walls clad with brick during winter and spring conditions. The vinyl and ventilated brick walls had similar drying rates and batt space conditons during summer and fall conditions. In general, vinyl clad walls were somewhat drier than similar brick clad walls, because of higher solar-induced temperatures and lack of cladding moisture storage.

No fundamental difference in behaviour was found between walls with vinyl siding cladding on strapping or contact applied.

Walls incorporating SBPO sheathing membranes dried slightly faster than those with AIF membranes. More significant to long term performance was that the test walls with SBPO maintained significantly drier conditions within the batt space and framing, and experienced less severe inward vapor drive wetting.

8.7.2. Recommendations for Further Work

Transient hygrothermal modelling should be performed to further investigate this data. The contribution of a range of sheathing membrane properties, ventilation strategies, and climates should be further assessed using a model benchmarked with the data generated in these field experiments.

Other walls assemblies should be studied in a manner similar to this study. Test wall candidates should include, but not be limited to, the following;

- Similar vinyl siding installation with ventilation restricted (i.e. seal the joints in the siding). This will allow further assessment of the effect of ventilation by controlling the possible sources of ventilation.
- Different siding products with some, but limited, ventilation (such as wood siding or fiber cement that has been painted in-situ).
- Walls without vapour barriers inside of the batt space. These walls would improve our understanding of inward vapour flow and inward drying.
- Walls with different insulation sheathing inside the ventilation cavity. These systems are very typical in Ontario and the drying of moisture in the batt space would be significantly affected by the relatively low permeance of the insulation.
- Brick veneer walls with both bottom and top holes sealed (e.g. no intentional ventilation). This type of specimen could act as a baseline "no ventilation" specimen with rain absorptive cladding.

The wetting apparatus developed for this study was quite successful. However, improvements and changes should be investigated. It would be useful both to distribute water more uniformly through the sheathing material (to improve the accuracy of the moisture content readings) and to more realistically simulate accidental wetting scenarios (i.e., greater concentrations at one spot).

It would be very useful to investigate gravimetric measures of moisture content in wall systems to provide more accurate and reliable measurements of moisture movements.

Further laboratory material testing should be undertaken on the effects of frozen wet AIF. This would aid the understanding of the results from this study.

8.8. References

Hansen, M., Nicolajsen, A., Stang, B., "On the influence of ventilation on moisture content in timber framed walls", *Building Physics 2002 – 6th Nordic Symposium,* Trondheim Norway 2002.

Hazleden, D., Morris, P., "The Influence of Design on Drying of Wood-Framed Walls Under Controlled Conditions", *Proc of Thermal Performance of Building Envelopes VIII* Florida, 2001.

Kumaran, K., "Hygrothermal Properties of Building Material", *Moisture Analysis and Condensation Control in Building Envelopes,* Ed. H Trechsel, Amercian Society for Testing and Materials, Philadelphia 2001, pg. 64.

Kumaran, K., Lackey, J., Normandin, N., van Reenen, D., Tariku, F., *Summary Report from Task 3 of MEWS Project at the Institute for Research in Construction Hygrothermal Properties of Several Building Materials,* IRC RR-110 2002.

Ojanen, Tuomo "Improving the Drying Efficiency of Timber Frame Walls in Cold Climates by Using Exterior Insulation Wood Siding", *Thermal Performance of the Exterior Envelopes of Buildings VII*, Clearwater Florida, 1998.

Salonvaara, M., Ojanen T., Kokko, E., Karagiozis, A., "Drying Capabilities of Wood Frame Walls with Wood Siding", *Thermal Performance of the Exterior Envelopes of Buildings VII*, Clearwater Florida, 1998.

Straube, J., Burnett., E., "Drainage, Ventilation Drying, and Enclosure Performance", *Thermal Performance of the Exterior Envelopes of Buildings VII*, Clearwater Florida, 1998.

Straube, J., *Moisture Control and Enclosure Wall Systems.* PhD Dissertation University of Waterloo 1998.

Straube, J., Onesko, D., Schumacher, C., "Methodology and Design of Field Experiments for Monitoring the Hygrothermal Performance of Wood Frame Enclosures", *Journal of Thermal Envelope and Building Science*, Vol 26, No 2, October 2002.

9. CONCLUSIONS

This thesis has explored the contribution of inter layer air space ventilation to heat and moisture flow through and within building enclosures. Ventilation is commonly encouraged in the design of a variety of building enclosure assembly types because of the perception that ventilation will reduce moisture problems. Ventilation is often unintentional because of holes and inter-layer gaps that are inherent in assemblies.

Fluid mechanics theory has been reviewed and applied to airflow systems in ventilated enclosures. This theory can be applied to systems as diverse as double-facades and contact applied vinyl siding. However, it can be concluded that because of complex geometries and flow conditions, experimental (or CFD) results are required to accurately predict airflow through most systems.

The three mechanisms that drive ventilation are buoyancy (thermal and moisture), wind pressure differences, and mechanical equipment. A formulation to predict natural buoyancy pressures due to both temperature and air moisture content was derived from the ideal gas laws. This showed that moisture buoyancy can be significant, especially under conditions during which ventilation drying is possible. Wind pressures are more difficult to predict because of the stochastic nature of the wind. Results from the literature were used to develop a means of predicting wind pressures. These three driving pressures can be combined algebraically.

A review of heat and moisture flow through multilayer layer assembly was completed. A simple method of determining the maximum and minimum impact of ventilation at was presented and a practical example of its application was also provided. The equivalent vapour permeance and equivalent thermal resistance of different claddings were plotted as a function of ventilation flow rate and cladding vapour and thermal conductance. From these plots several conclusions were drawn:

- The equivalent vapour permeance of relatively impermeable cladding (e.g, M< 50 ng/Pa s m^2 for claddings such as steel and thick EIFS) can be significantly increased by very low rates of ventilation (Q<0.1 lps/m^2).
- The equivalent vapour permeance of claddings with mid-range vapour permeance values (50<M<1000 ng/Pa s m^2, brick, wood siding, etc.) will not be significantly increased by ventilation unless higher rates of ventilation occur (Q>0.1 lps/m^2).
- The equivalent permeance of claddings with high vapour permeances (M> 1000 ng/Pa s m^2) are not increased by even high rates of ventilation (Q>1 lps/m^2).
- The equivalent thermal resistance of typical cladding systems is significantly reduced at ventilation rates between 0.05 to 2 lps/m^2. The greater the thermal resistance, the less flow required to impact the thermal resistance. For practical insulated cladding systems (such as EIFS), flows of 0.1 lps/m^2 can be tolerated.

Experimental work was conducted to characterize flow behind cladding in the lab, to measure ventilation flow in the field, and to measure the impact of ventilation flow on drying in full-scale natural exposure testing.

The airflow through and behind two of the most common residential cladding systems (brick veneer and vinyl siding) was investigated to provide experimental data to improve our approximations of ventilation flow rates. A methodology for assessing the complicated airflow resistance characteristics of sidings was developed and applied to a sample product. It was found that vinyl siding allows a significant amount of airflow through its face at low pressure differentials, and that there is little resistance to airflow along the profile, or along strapped cavities. A high airflow resistance was measured behind contact applied siding perpendicular to the profile. It is proposed that other siding products tested with the same methodology be compared to this sample product in the future to assess the likely extent of ventilation in field exposure.

The airflow versus pressure relationship for airflow through and behind a brick veneer was quantified. Theoretical predictions under-estimated the measured flow rate for given steady driving air pressures. The inclusion of top vents in brick veneer clad walls with clear airspaces significantly increased the ventilation of the brick veneer wall assemblies. From field testing of cavity point airspeeds, driving pressure calculated from measurements, and smoke pencil testing ventilation rates of 0 to 0.5 lps/m^2 are expected within such systems when exposed to field conditions. Most of the time (90%) ventilation flow is above about 0.1 lps/m^2. Such ventilation rates would provide an equivalent permeance of more than 1000 ng/s·m^2·Pa for ventilated brick veneers. This equivalent vapor permeance is in the range found in the previous EDRA wall drying climate study.

Significant drying and inward moisture redistribution were measured in the five full-scale test walls. Walls dried quickly in hot summer conditions but significant inward driven moisture flow occurred in some cases. In cool and cold weather the walls dried more slowly and much less moisture moved inward.

Increased cladding ventilation significantly increased drying rates (by increasing the effective permeance of the cladding) and reduced internal wall assembly moisture levels. Ventilation also reduced the impact of solar driven inward moisture drives.

The use of spun bonded polyolefin sheathing membrane in lieu of #15 asphalt impregnated felt improved the hygrothermal performance in the test walls. It was concluded that the difference is due to the higher vapour permeance of the spun bonded polyolefin. This conclusion may not be relevant for wall assemblies with lower permeance sheathings (e.g., foam plastic or OSB).

Walls clad with vinyl siding dried faster than those clad with brick veneer. Hence, it was concluded that vinyl siding is a well ventilated cladding system and that hygrothermal storage capacity of brickwork may act to reduce wall drying rates.

APPENDIX A: DEVELOPMENT AND DESIGN OF INTRA WALL WETTING MECHANISM

Purpose and Criteria for Mechanism

The Intra Wall Wetting mechanism (IWW) was designed to allow the application of a known amount of water to a desired location within a wall system. Monitoring the drying of wall system after such simulated wetting events was considered a practical assessment of drying strategies.

The IWW was designed to fulfill the following criteria:

- Adds a controlled amount of water to the wall system,
- Distributes water uniformly over entire surface of a layer within the wall,
- Allows the water to be added repeatedly,
- Adds a sufficient amount of water, and
- Does not impede mass or energy flows through the wall system and has negligible mass.

Design

The design consists of injection tubes that carry water to highly absorbent wetting paper. In the case of the UW and PSU applications, Homasote board sheathing was used as the substrate to be wetted. A drawing of the system with stud framing (as used at UW) is included in Figure A-1. A drawing of the system modified for an idealized wall without framing (as used by PSU) is included in Figure A-3.

Injection tubes allowed water to be sent into the wall spray across the top of each wetting paper covered section. The injection tubes were clear Tygon plastic tubing. The tubes were tied in a knot at the end inside the wall, had three 1/16" holes punctured along a 16" length from the end of the tube. The tube was stapled along top of the various wetting paper sections, and then ran up to the top plate of the test wall through access channels, and finally exiting the wall system. The access channels were then sealed with silicone and were effectively filled by the tubing to avoid air infiltration. The Tygon tubes were selected for their flexibility, small size, and the fact that they do not kink easily.

The wetting system utilizes 15 double sheets of a thick, highly adsorptive paper that is reinforced with a plastic mesh. Wetting paper spread the water over the inside of the fibreboard sheathing to allow it to soak. The wetting paper was WYPALL® X60 TERI® Reinforced Wipers from Kimberley-Clark. The paper was laid out over the area of the sheathing, folded once over the injection tubes and then stapled down to the sheathing. The wetting paper does not contact the wood studs or plates and thereby ensures that the water did not wick directly into the wood. For the studies carried out for ASHRAE RP 1091, 335 mm by 440 mm wetting sheet were used and a dedicated injection tubes supplied each sheet. This required 15 injection tubes. One side of the wetting paper was stapled to the Homasote sheathing and a 4 mm inside diameter plastic (Tygon) injection tube was attached with cable staples near the top of each sheet of wetting paper. The

injection tubes were then sandwiched between the two side of the wetting paper by folding over the excess paper and stapling it to the Homasote. The insulation contained in the batt space pressed the paper into firm contact with the fibreboard sheathing.

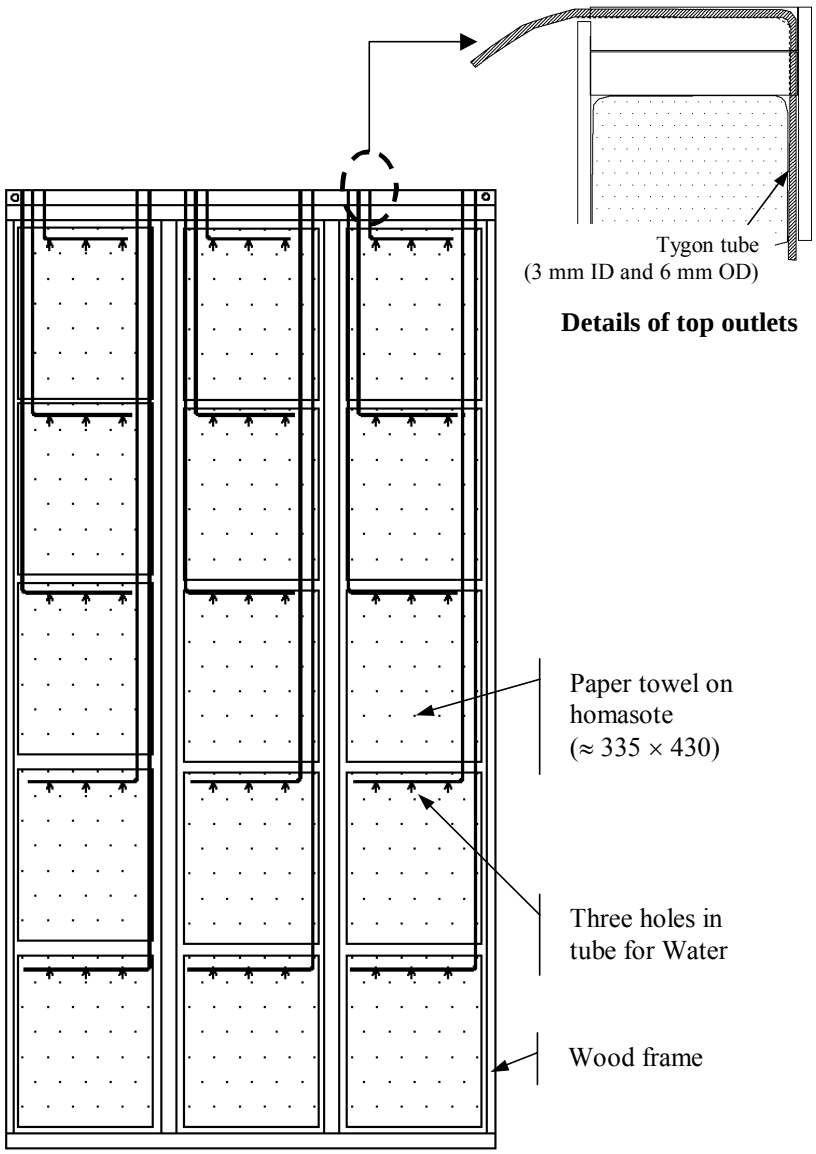

Figure A-1: InterWall Wetting Mechanism with Stud Framing

The water soaking the inside surface of the fiberboard sheathing is wicked into the material. Since the water is evenly distributed by the wetting paper, the addition of water could be modeled in computer simulations as a thin layer of water set in contact with the inside of the sheathing. Homasote 440 board was used for the sheathing in the ASHRAE RP 1091 project because of its high liquid transport and high vapour permeance. The high liquid transport was necessary for the wetting mechanism because the water had to wick into the material without running down the applied surface. The high liquid

transport also helped redistribute unevenly applied moisture. The high vapour permeance was important to minimize any influence on normal wall behavior.

Figure A-2 shows an installed IWW on a 4' by 8' wall specimen with 2x6 wood framing. The specimen has instrumentation installed and is ready to be filled with batt insulation contained by the inside finish (in this case melamine board).

The design was further modified for use at PSU. One change is the use of textured spun bonded polyolefin sheathing membrane. The membrane is stapled to the Homasote sheathing over the wetting paper with the texture running horizontally. When the batt insulation presses the wrap against the wetting system, it is believed that the grooves further inhibit drainage of injected water. In the ASHRAE 1091 testing performed at PSU some of the test panels for the ventilation drying tests did not include studs. This is shown in the assembly drawing in Figure A-3. The difficulty of pressing the wetting paper against the Homasote was solved with a second modification employing a plastic drainage mesh in place of fiberglass insulation. The plastic mesh is available in ¼" thick sheets and is easy to place evenly over the wetting paper. The plastic mesh still required a sturdy backing to compress it against the wetting paper.

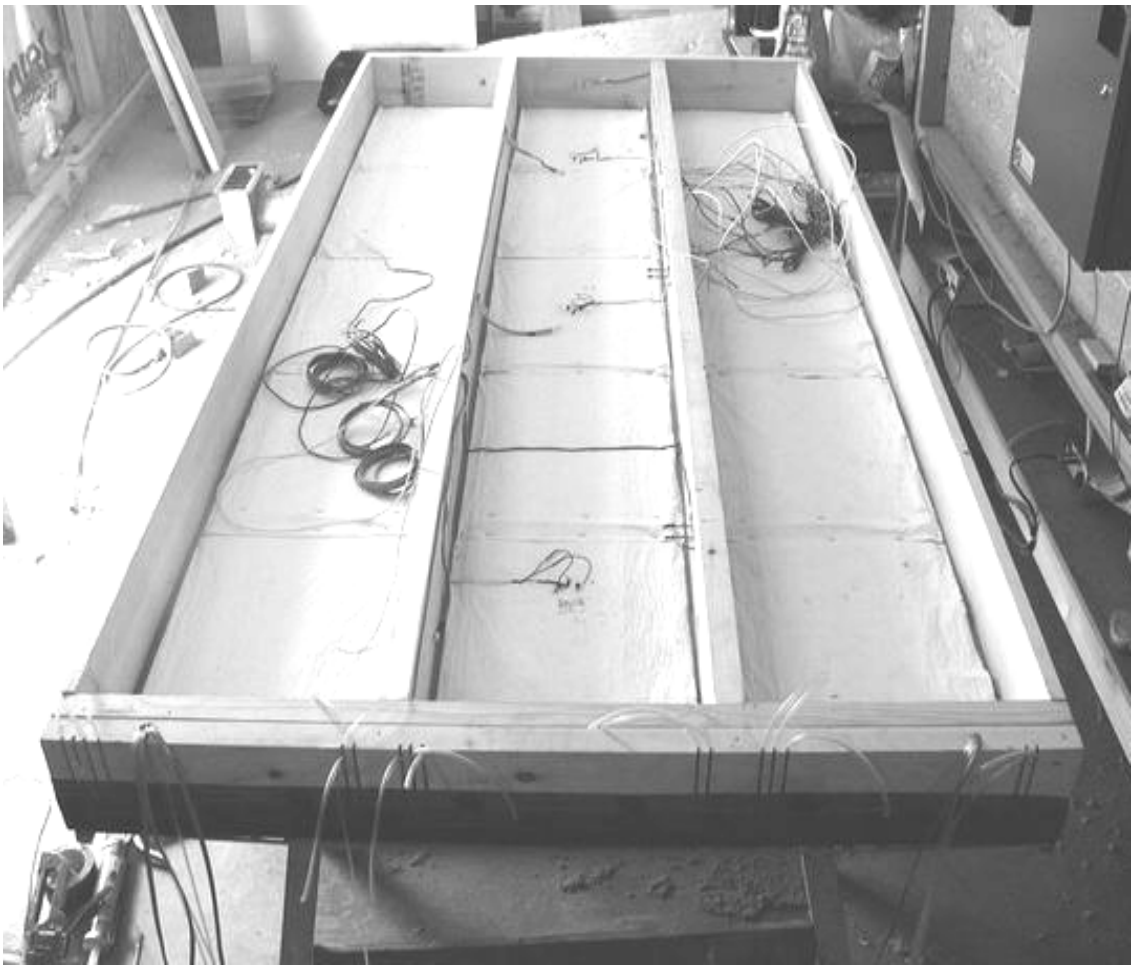

Figure A-2: Installation of IWW on a 4' by 8' wall specimen with 2x6 wood framing

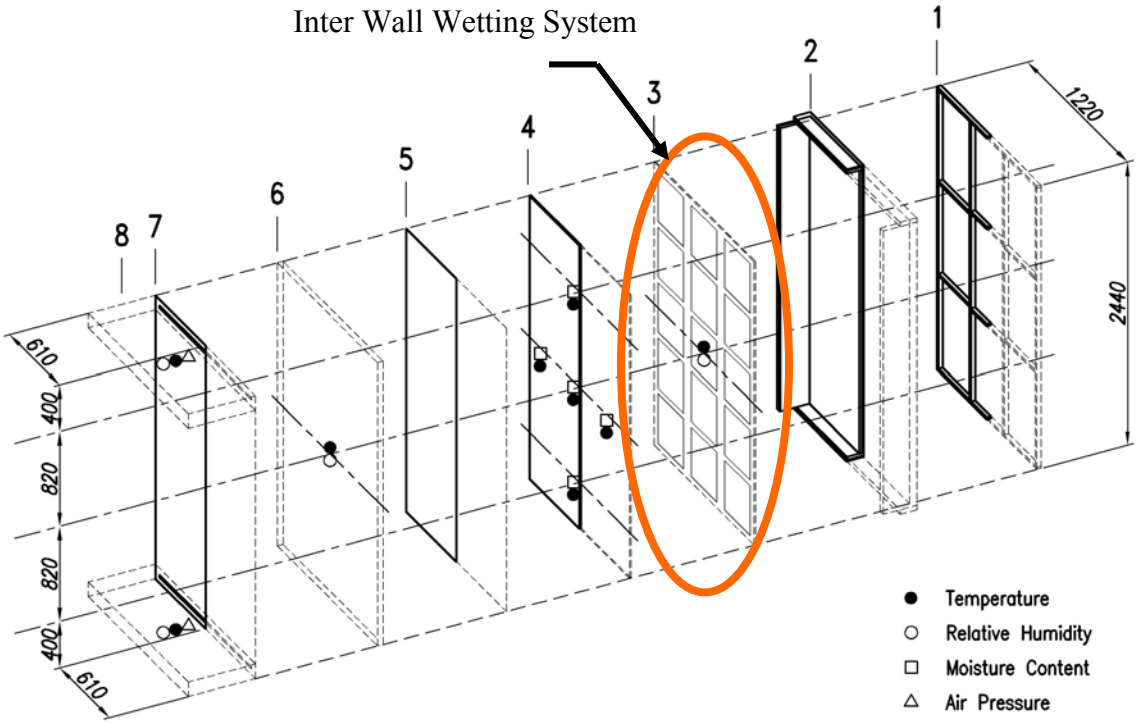

Figure A-3: PSU Wall Specimen with IWW

The arrangement of the wetting paper on the Homasote sheathing for the PSU wall panels is shown Figure A-3. Moisture content screws and thermistors installations can also be seen. This photograph shown in Figure A-4 was taken after the wetting system had been used four times, i.e., when the test panel was opened to confirm the durability of the wetting paper. No deterioration was evident. A similar observation that the wetting paper does not deteriorate was observed after 3 years of installation in the field test walls at the BEGHUT.

Figure A-4: Wetting Paper after 4 Tests

Procedure

Water is introduced by injecting a "dose" of 30 ml of water and then +30 ml of air quickly into each injection tube. Using this approach, the water is evenly distributed between the outlet holes and cleared from the injection tube of water. When 30 ml of water is added to each of the 15 sheets of wetting paper through the injection tubes, the total does for the panel is 450 ml or 450 grams.

Figure A-5 shows a researcher injecting 30g of distilled water into one of the 15 tubes in one of the wall specimens. It was determined from laboratory trials that the distilled water should be injected as quickly as possible for the best balance of water leaving the exit pinholes in the wall. Also highlighted is 60 ml of air at the top of the syringe. This air is included to effectively purge the supply lines of water. The remaining drops of water left in the lines is insignificant relative to the total water added but have been found to freeze and hence plug the lines. It is recommended that the injection trials be repeated for other test setups to determine injection rates appropriate for specific circumstances different than those described here.

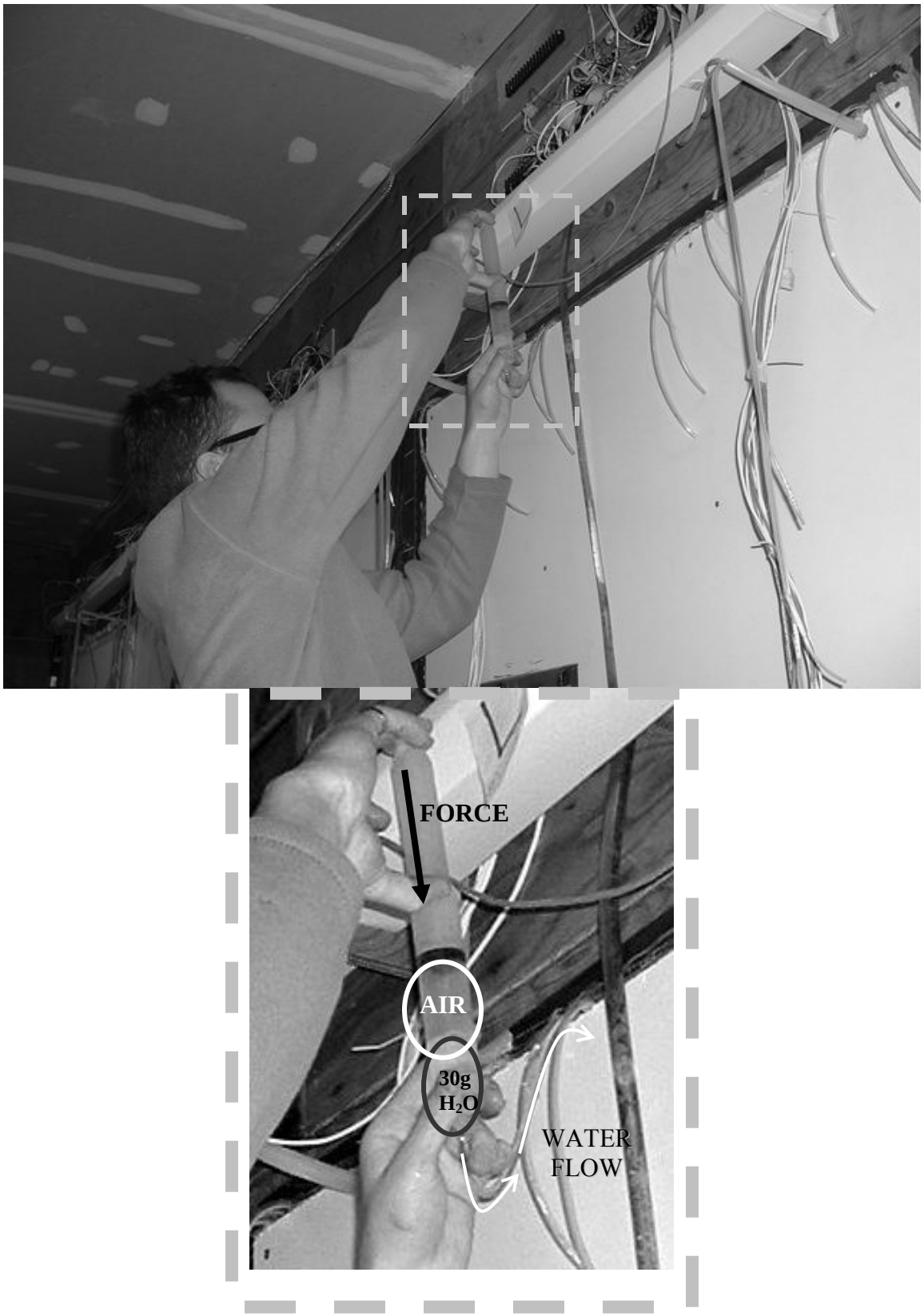

Figure A-5: Injection of Water into InterWall Wetting Mechanism

Testing - Water Injection Rates

Testing was performed at UW to determine the quantities of water that could be added at certain regular time increments without causing leaking or drainage beyond the intended wetting area. Each wetting area is defined by a single piece of wetting paper with a dedicated injection tube. In the case of the specimen above, this ensures even distribution between the 15 sections.

An experiment was completed to determine possible amounts of water and application rates without failure (leakage from a segment to a lower segment). A wetting system was applied and temporarily covered with batt insulation contained with cardboard. Eight sequences were tried repeatedly for 23 trials to find adequate sequences and investigate the wetting procedure techniques. A successful test was declared when an injection of water was found to be balanced across the sheets. The resulting acceptable application sequences are included in Table A-1. These sequences have been tested twice or more without failure.

Figure A-6: Lab Testing of InterWall Wetting Mechanism

Figure A-6 shows the general arrangement of the wetting paper between the framing as installed in the field test panels at the University of Waterloo. In this experiment, two of the lower sheets of wetting paper have been removed to show the uniformity of the wetting on the back of the Homasote sheathing.

Table A-1: IWW Test Wetting Schedules

Water Injections	Frequency	# Injections	Total Water	Total Time Required
30 g	2 hour	3	90 g	5 hour
35 g	4 hour	3	105 g	8 hour
45 g	4 hour	2	90 g	4 hour

Verification of Injection Rate

A second experiment was conducted to verify the wetting schedule. A mock up was constructed and wetted with blue and red dyes at alternate wetting sections. Sides A & B had 30 ml added to each sheet (except the bottom sheet of side A which was plugged) at 3 hour intervals and Side C had 40 ml added at 3 hours intervals. The mockup was left for 24 hours and then disassembled. No leakage occurred in sides A and B while leakage did occur in side C as determined by the purple traced on the sheet and the dye left on the bottom plate. These results are shown in right part of the sketch in Figure A-8. Hence, it was concluded that the 40g wettings were too large and that a 30 g wetting at 3 hr interval was acceptable to avoid the possibility of drainage.

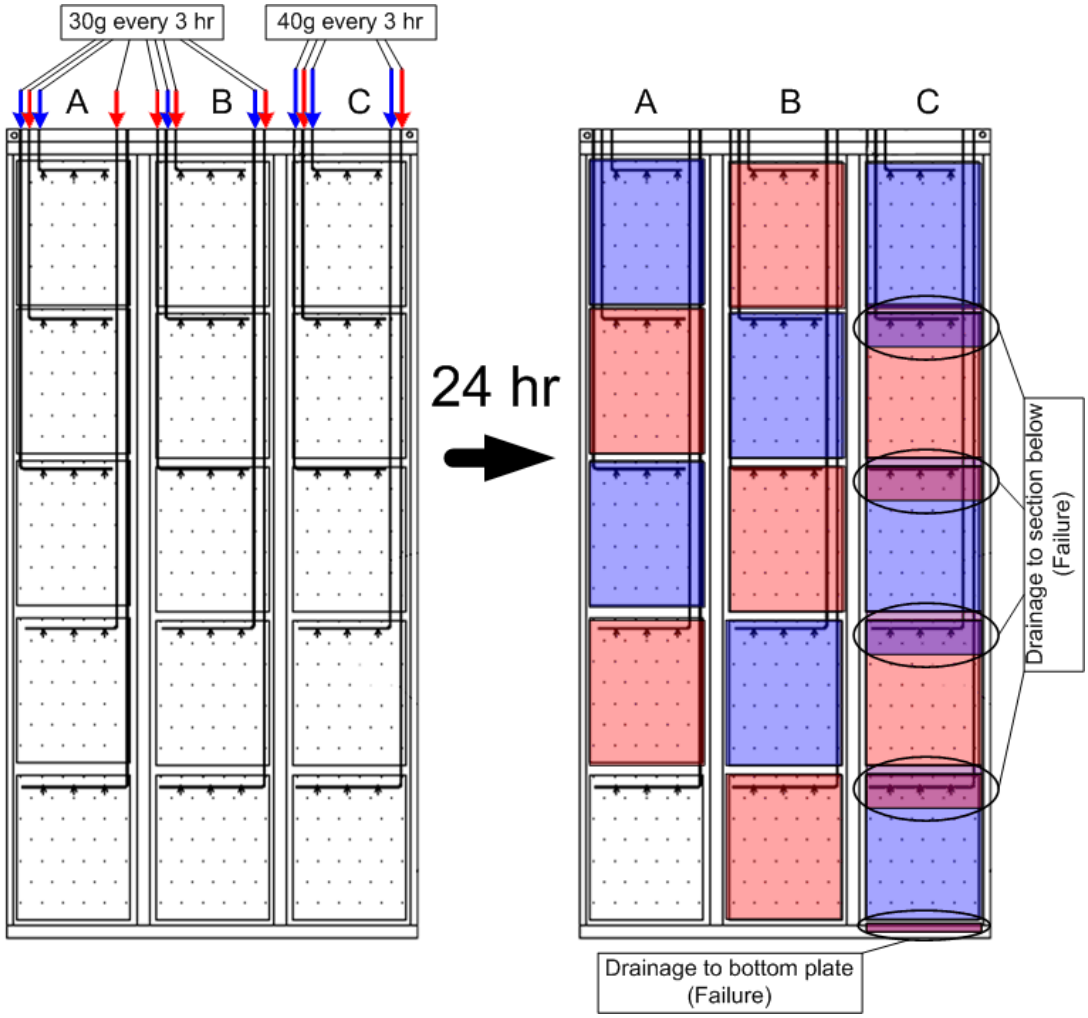

Figure A-8: Verification of Wetting Schedule

Homasote Redistribution Testing

Initially it was assumed that the water absorbed into the Homasote would redistribute evenly throughout the material over a relatively short period of time (e.g., 1 to 2 days). Higher than predicted moisture content readings in the field monitoring lead to a deeper investigation of liquid diffusion in the Homasote.

A sample sheet of Homasote was instrumented with moisture content pins spread out from a central wetting area as show in Figure A-9. A 60g dose of distilled water was added in one injection to the wetting paper. The container was then sealed to minimize drying to the lab air. The moisture content of Homasote under the wetted paper increased to a level predicted assuming little liquid transport outwards (or downwards in this case). Other moisture pins outside the wetted paper showed no reaction to the wetting. This implies that distribution of liquid water through the thickness occurs quickly, but does not occur laterally.

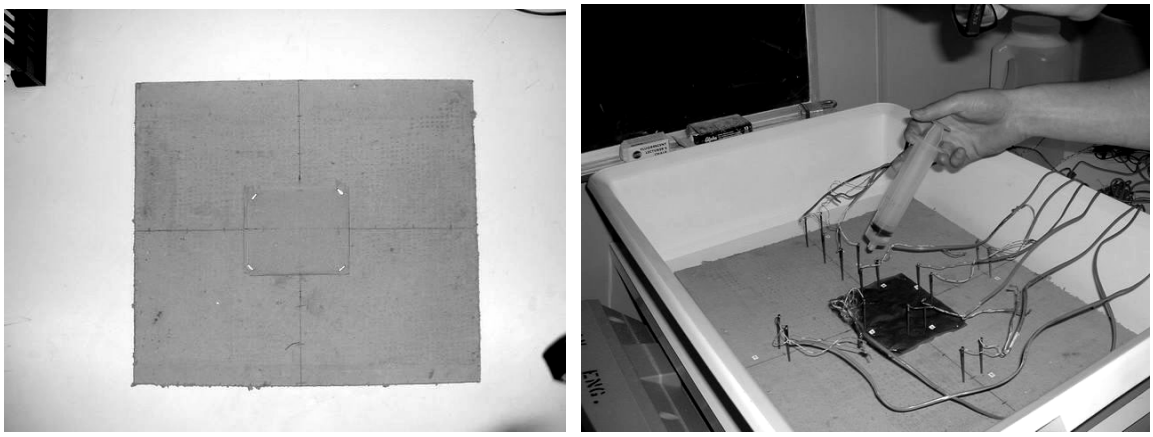

Figure A-9: Sample Sheet (on left) with wetting paper, instrumented, and 60 g distilled water added.

The experiment was run for three day. The time stepped visual results are shown in Figure A-10. The water did not redistribute quickly across the Homasote. Therefore, it is suspected that the applied moisture may not have redistributed beyond where the paper towel was applied. Because the paper is not covering the Homasote at the studs a significant area of the Homasote will not be wetting. This should be adjusted for in analysis.

Closure

An Intra Wall Wetting system was successfully developed. It is advised that other users of such a system should consider the important points addressed in this appendix.

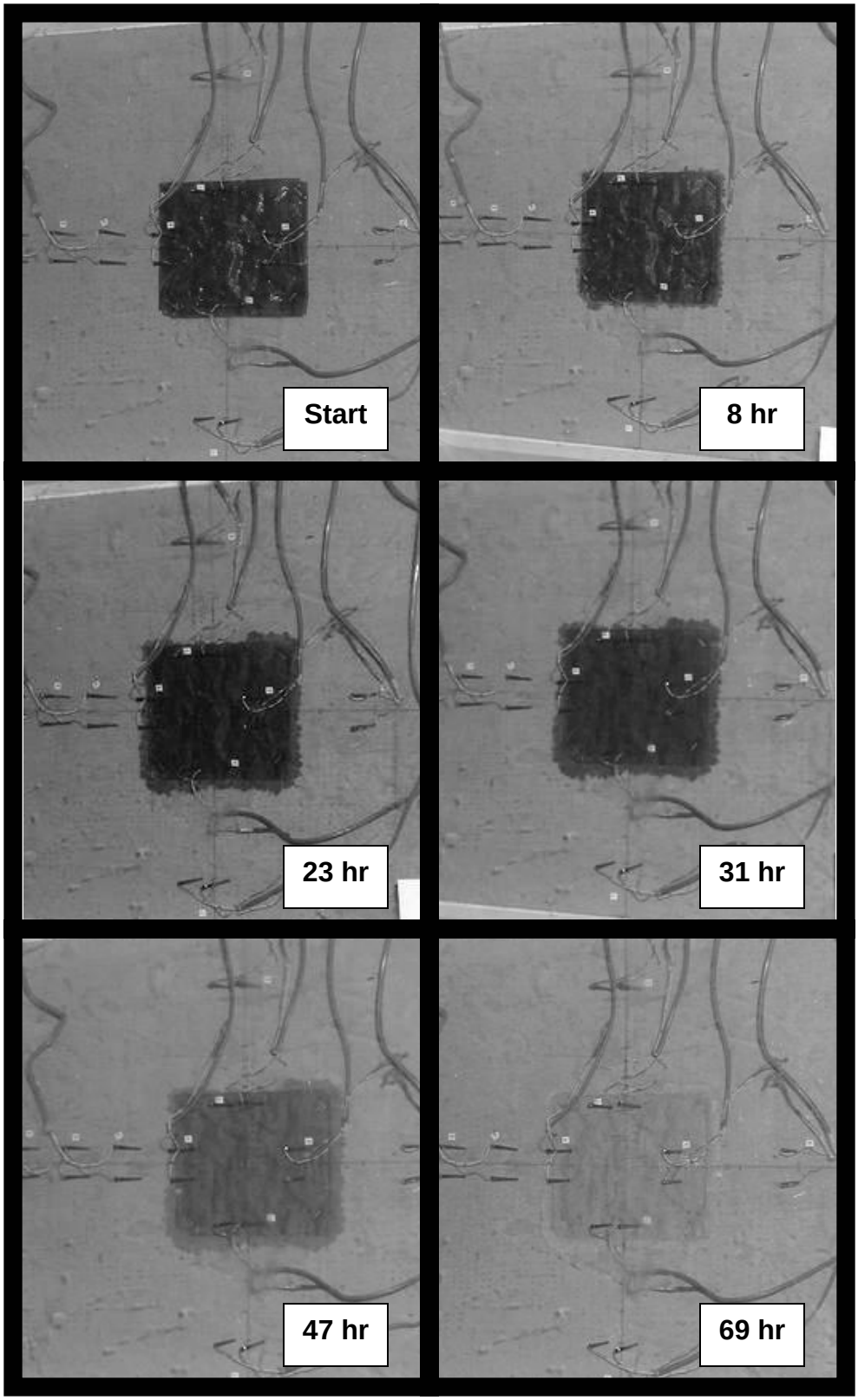

Figure A-10: Water Absorption and distribution with time

APPENDIX B: CONSTRUCTION DRAWING

B1: Location of Meteorological Sensors and Test Walls on the BEGHUT

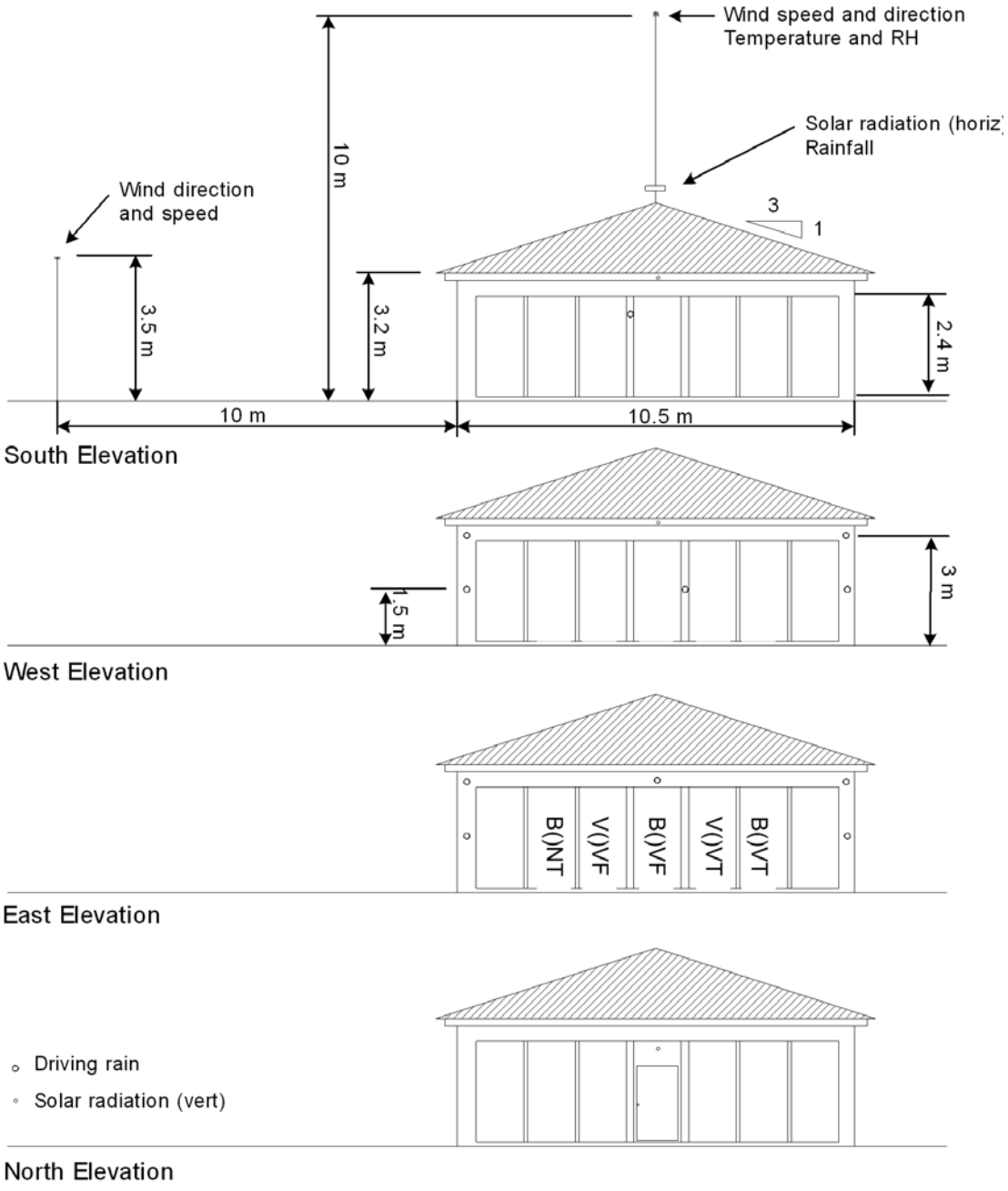

B2: Horizontal Section Through Vinyl Siding Clad Test Walls

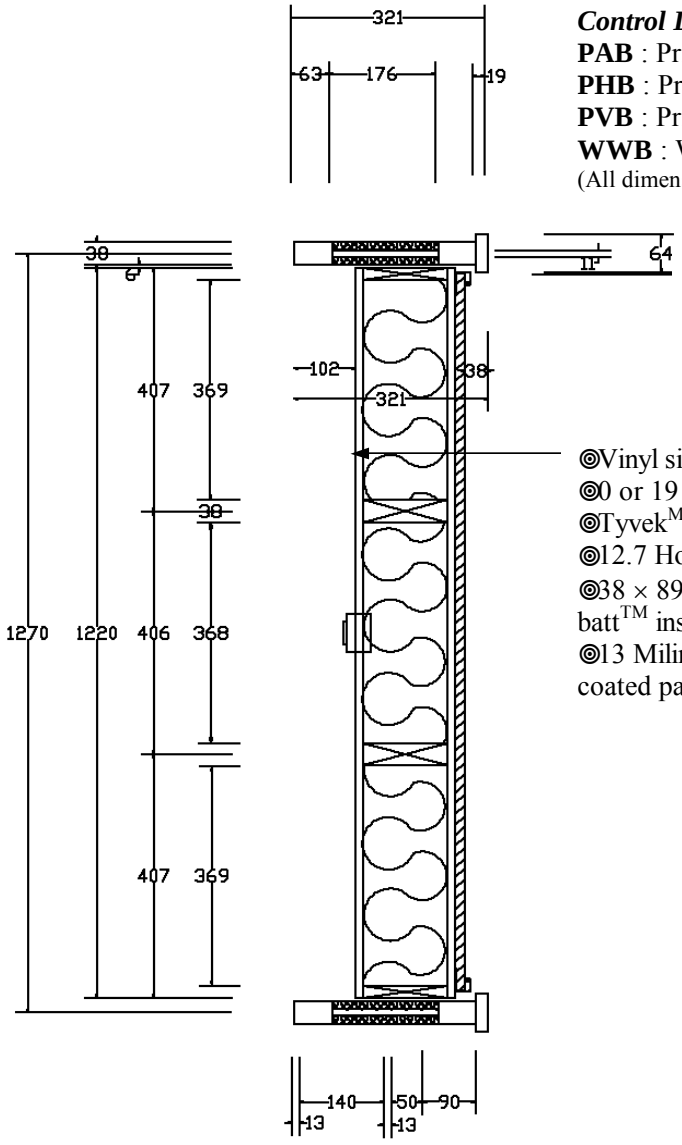

Control Layers
PAB : Primary Air Barrier
PHB : Primary Heat Barrier
PVB : Primary Vapour Barrier
WWB : Weather and Wind Barrier
(All dimensions in mm unless noted otherwise)

◎Vinyl siding - **WWB**
◎0 or 19 Cavity
◎Tyvek^{M} housewarp or felt - **PAB**
◎12.7 Homasote
◎38 × 89 Wood stud frame filled with Flexi-batt^{TM} insulation (R 13) - **PHB**
◎13 Milimine (vapour impermeable plastic-coated particle board) - **PVB**

Wood Frame Wall Section with Vinyl Siding

B3: Vertical Section Through Vinyl Siding Clad Test Walls

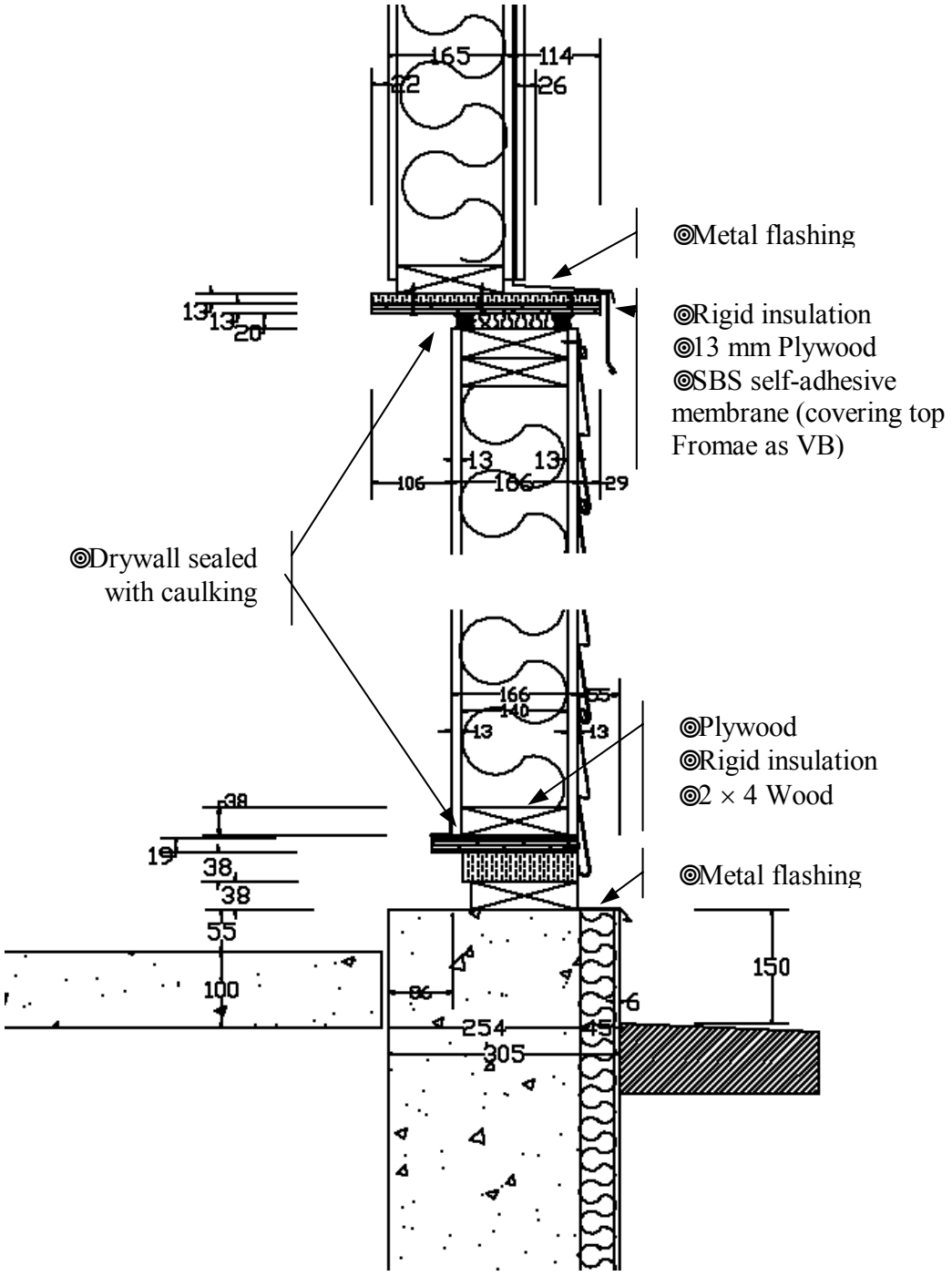

B4: Horizontal Section of Brick Veneer Clad Test Walls

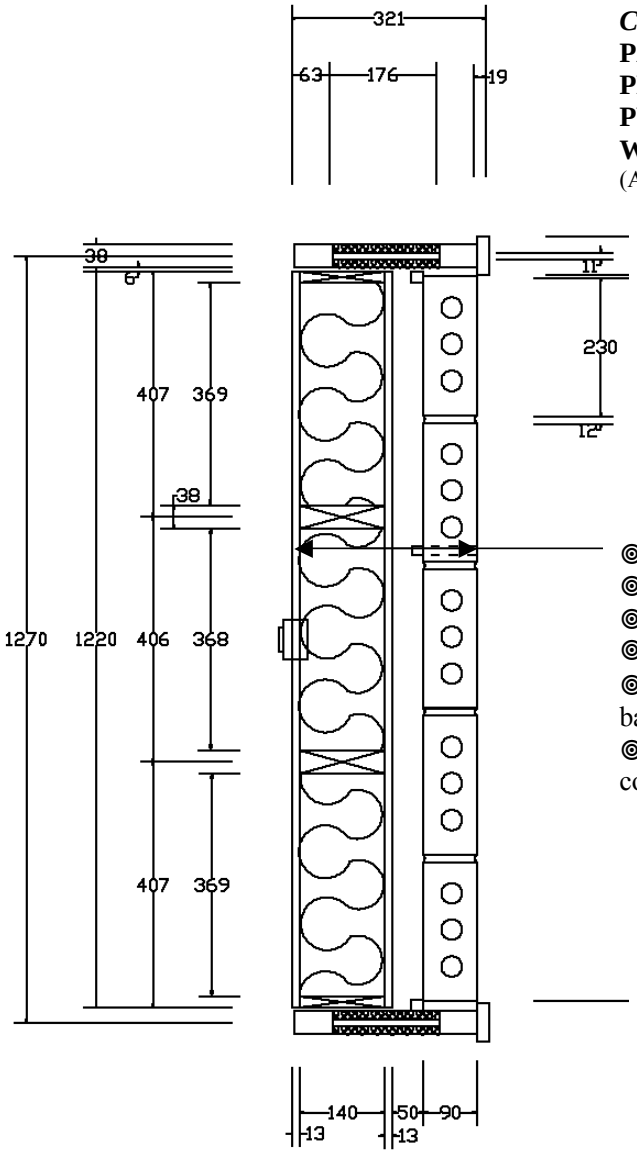

Control Layers
PAB : Primary Air Barrier
PHB : Primary Heat Barrier
PVB : Primary Vapour Barrier
WWB : Weather and Wind Barrier
(All dimensions in mm unless noted otherwise)

◎90 Brick veneer - **WWB**
◎13 or 50 Cavity
◎Tyvek™ Housewarp or felt - **PAB**
◎13 Homasote
◎38 × 89 Wood stud frame filled with Flexi-batt™ insulation (R 13) - **PHB**
◎13 Melamine (vapour impermeable plastic-coated particle board) - **PVB**

Wood Frame Wall Section with Vinyl Siding

B5: Vertical Section of Brick Veneer Clad Test Walls

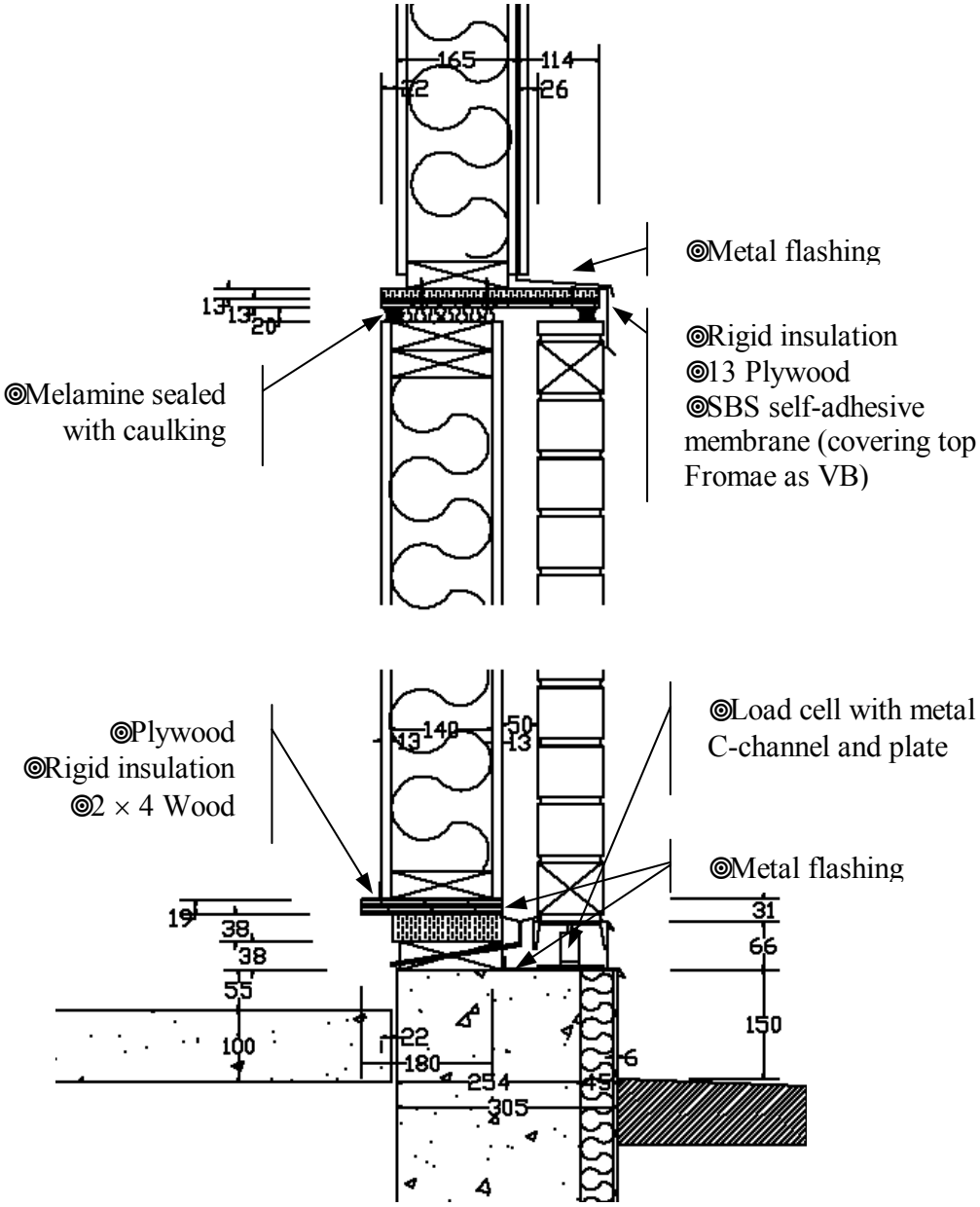

B6: Wire Distribution of Instruments in Test Walls

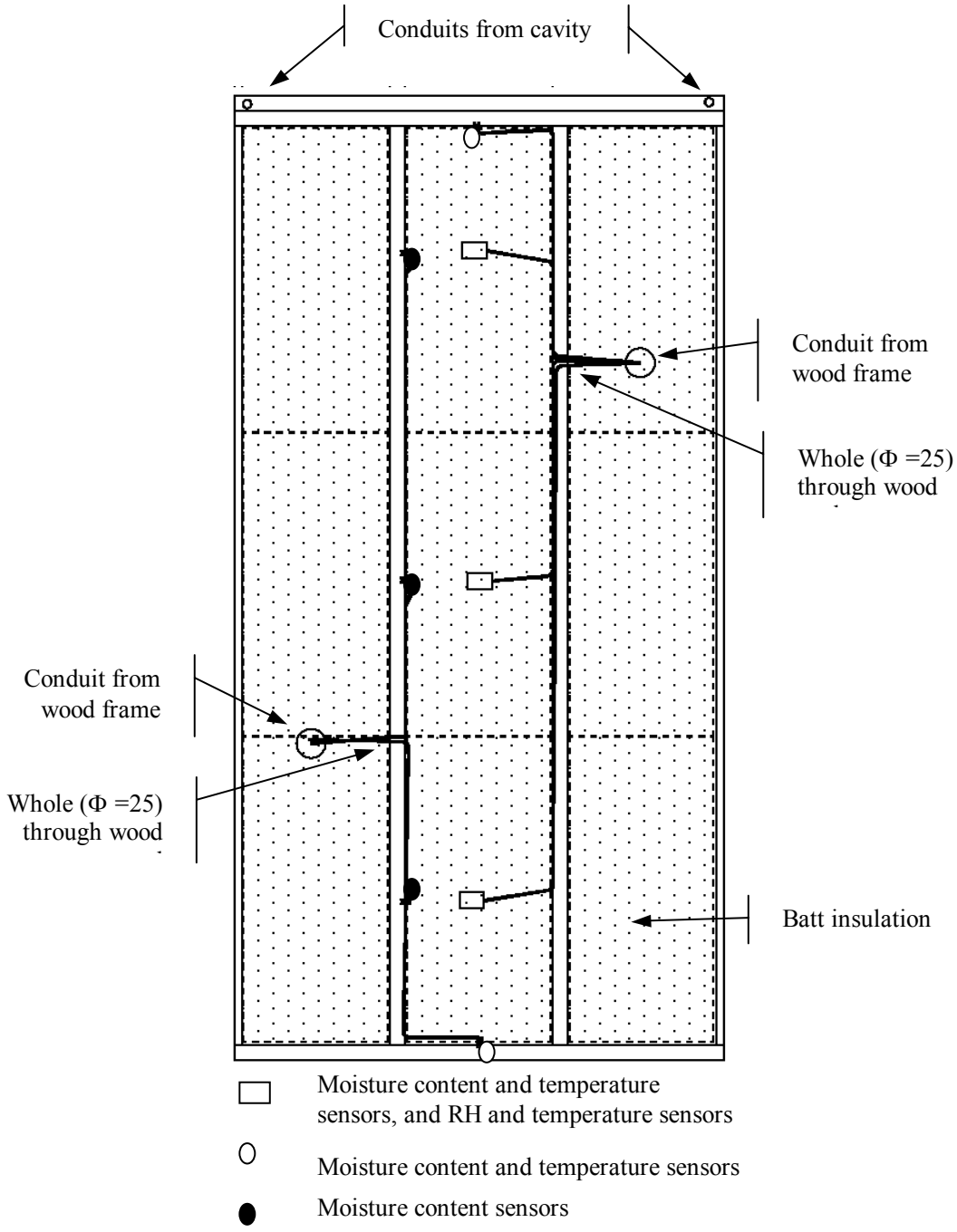

B7: Wood Moisture Content Pin Positions

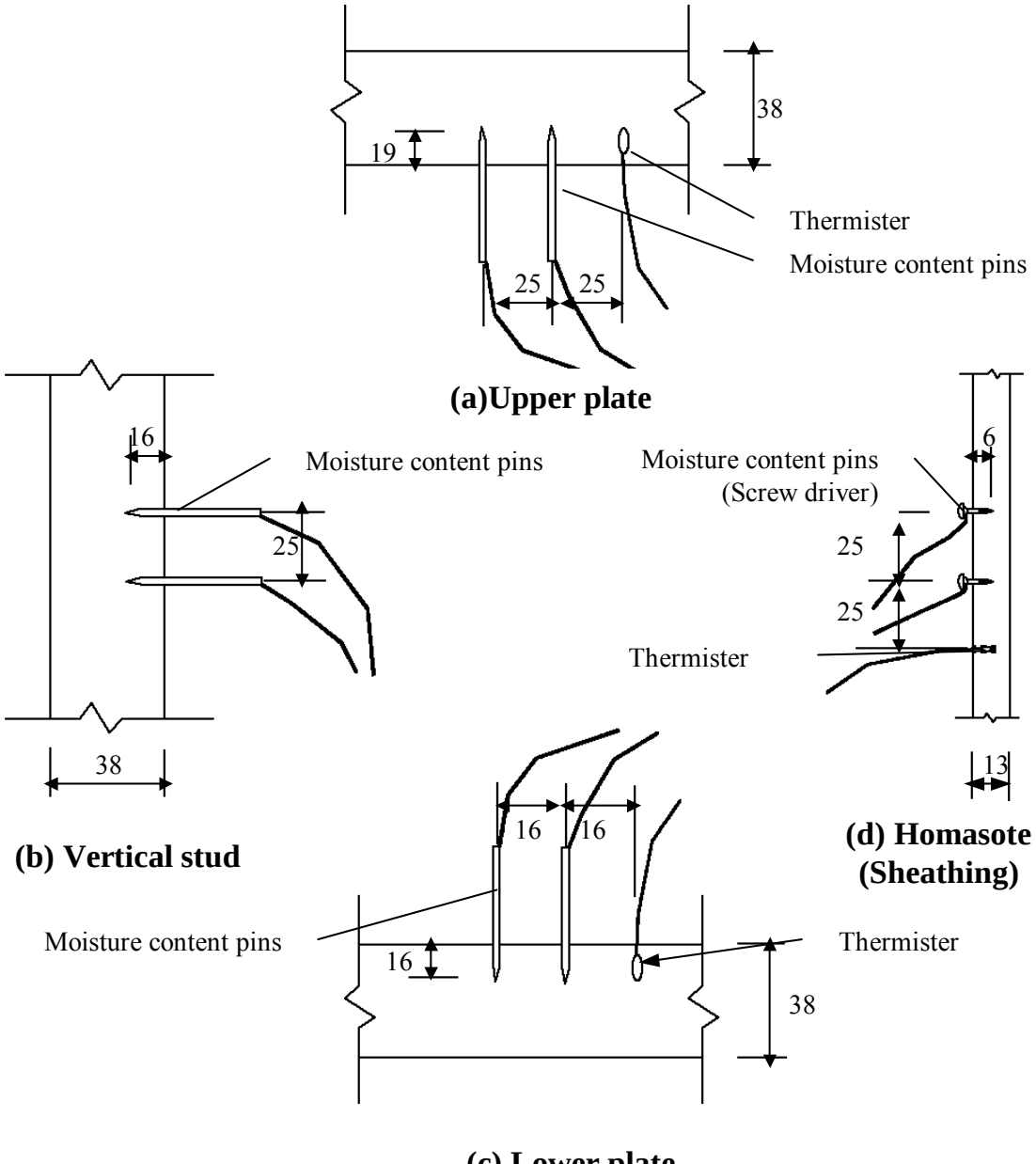

APPENDIX C: SELECTED HOURLY DATA PLOTS

C1-1.1: Solar and Rain

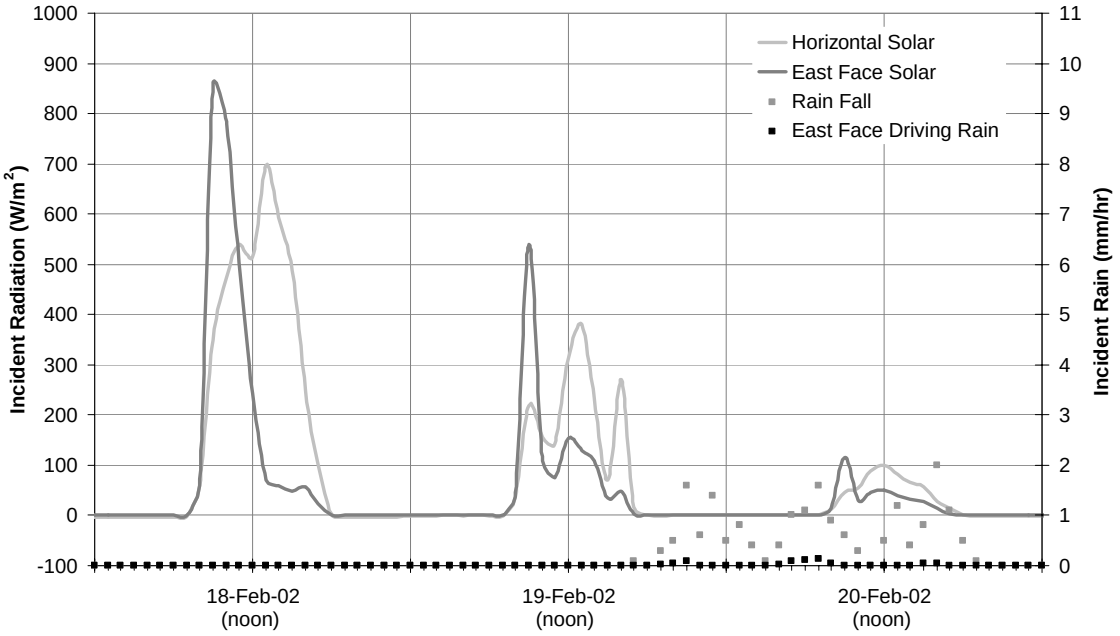

C1-1.2: Wind Speed and Direction

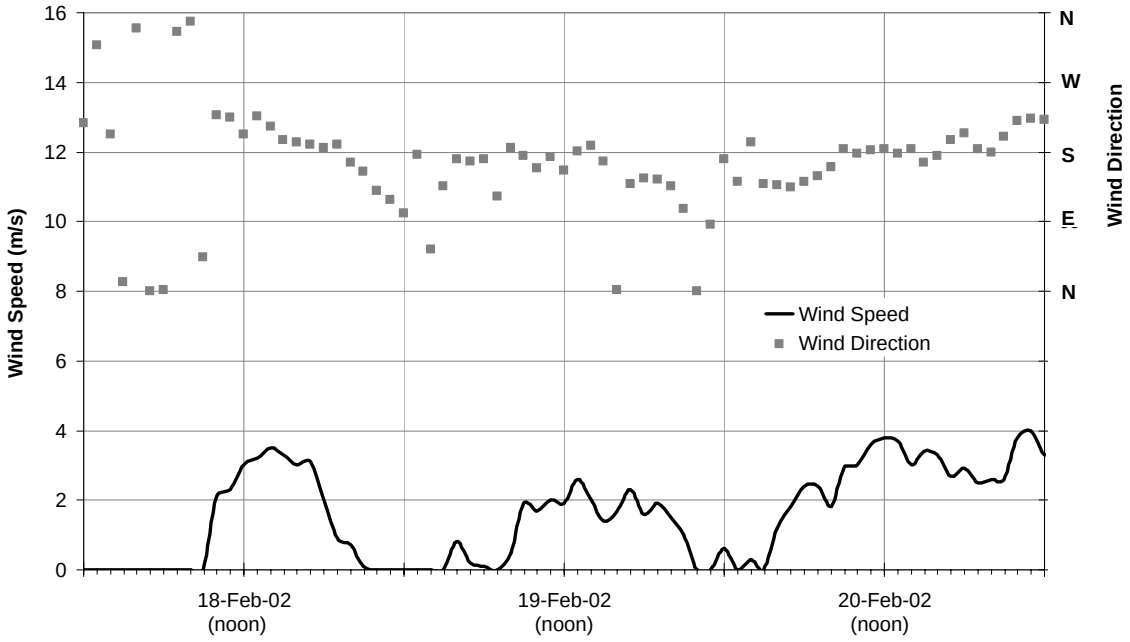

C1-1.3: Cladding Temperatures

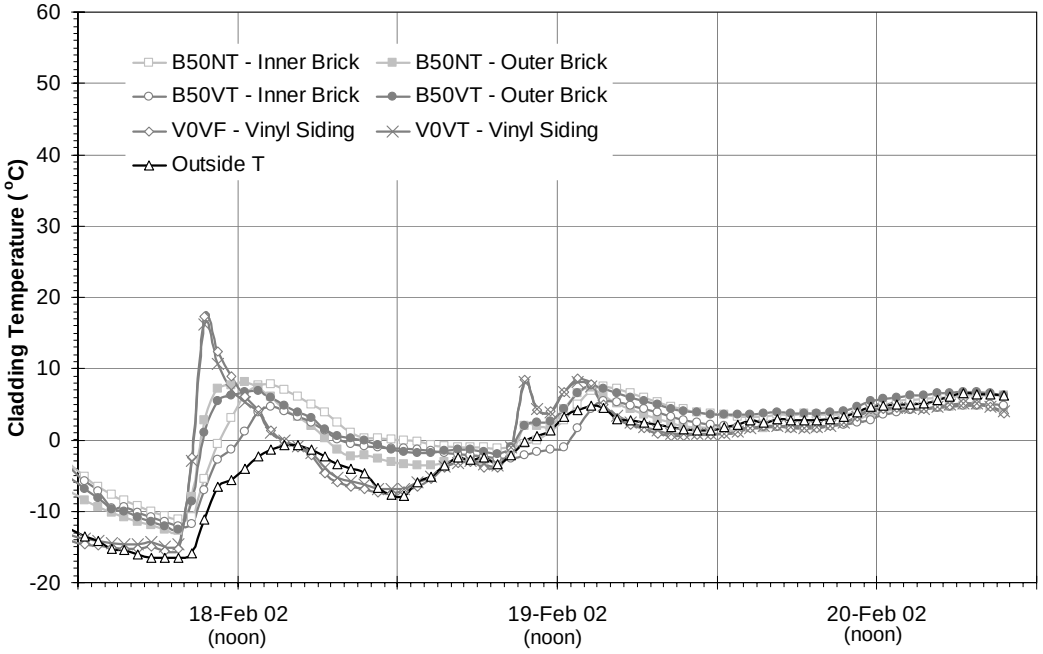

C1-1.4: B20VF Cavity Conditions

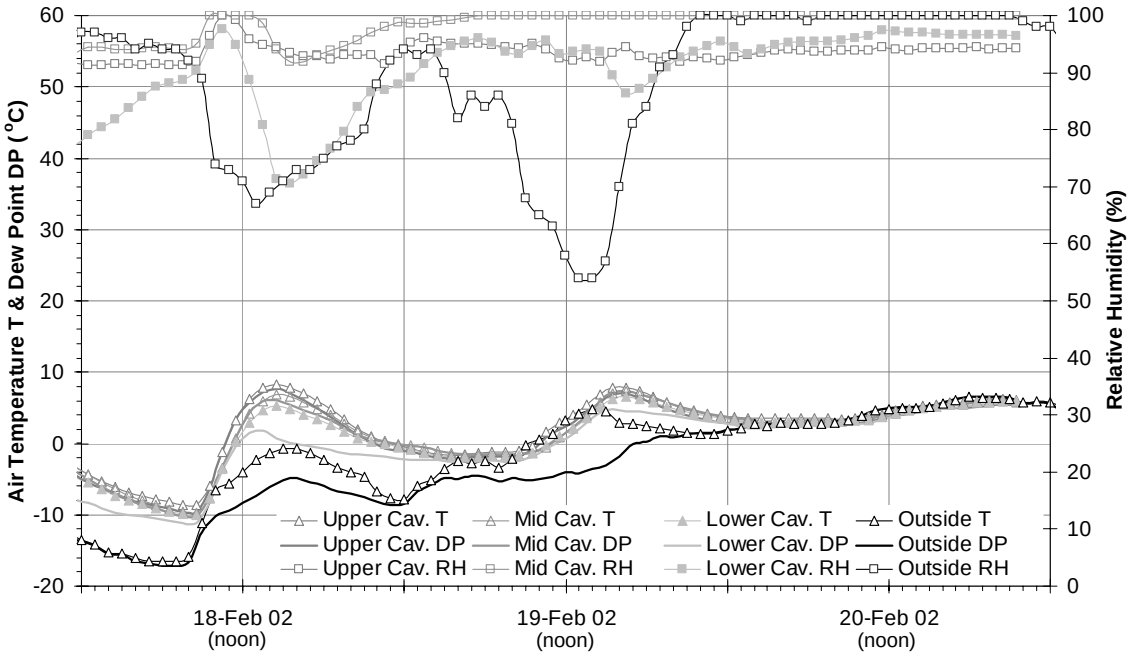

C1-1.5: B20NT Cavity Conditions

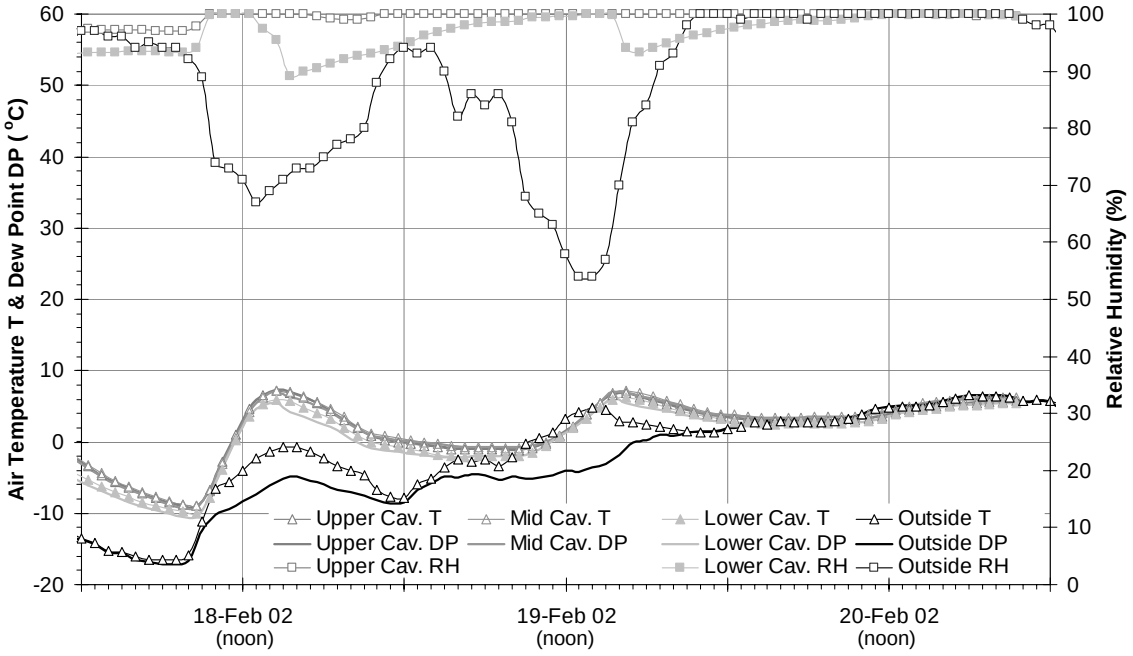

C1-1.6: B20VT Cavity Conditions

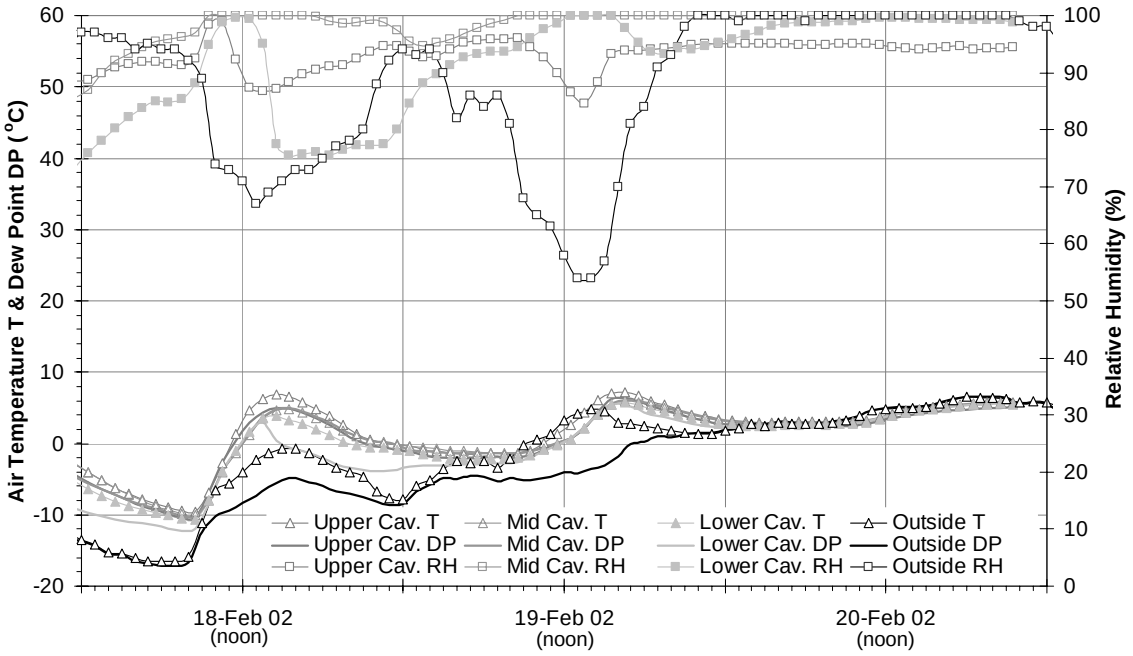

C1-1.7: V0VF Cavity Conditions

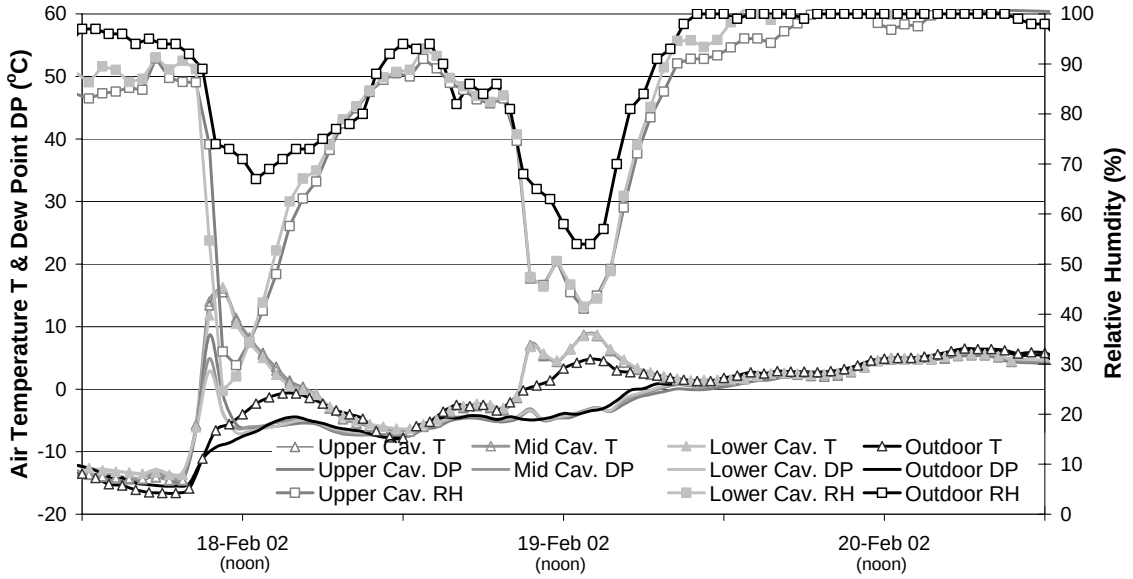

C1-1.8: V0VT Cavity Conditions

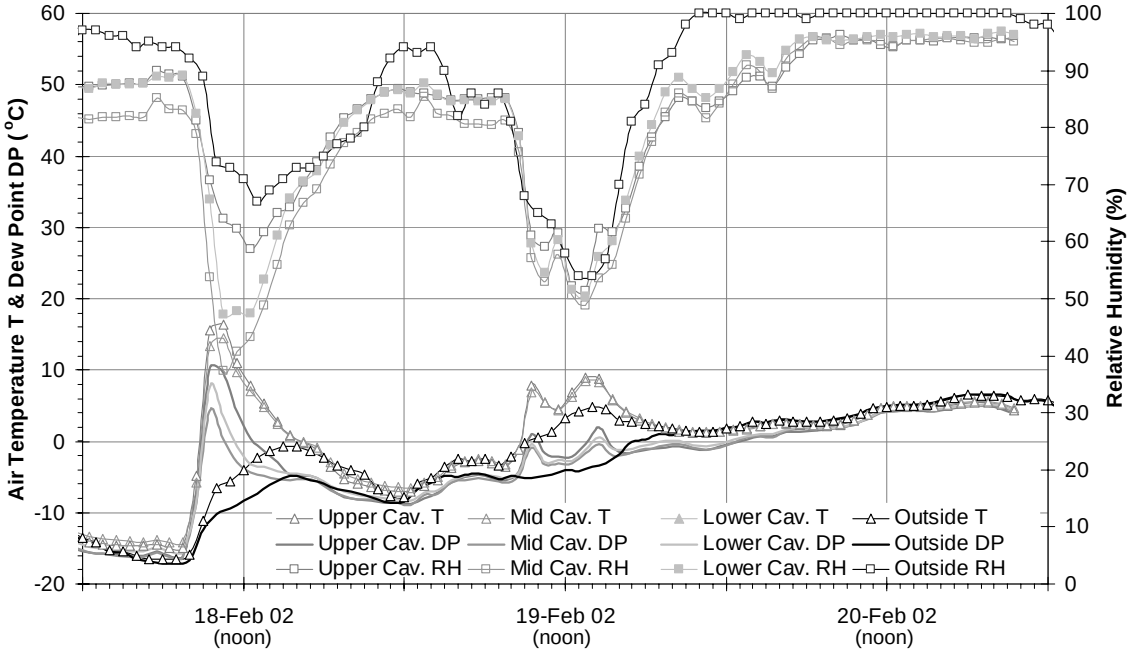

C1-1.9: B50VF Batt Space Condition

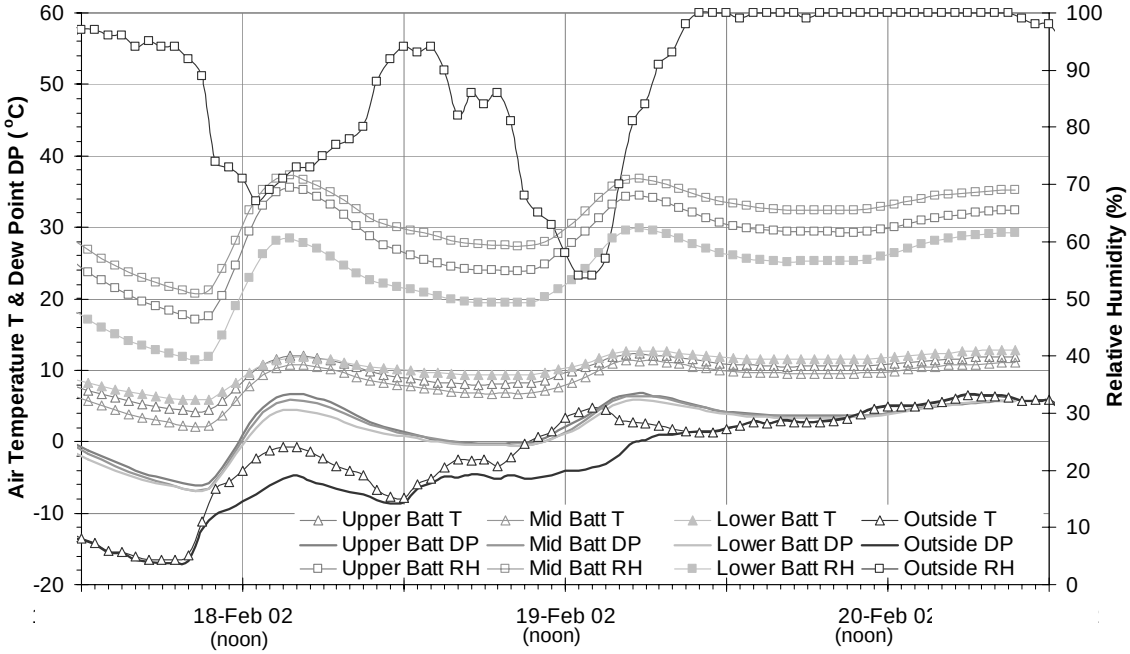

C1-1.10: B50NT Batt Space Conditions

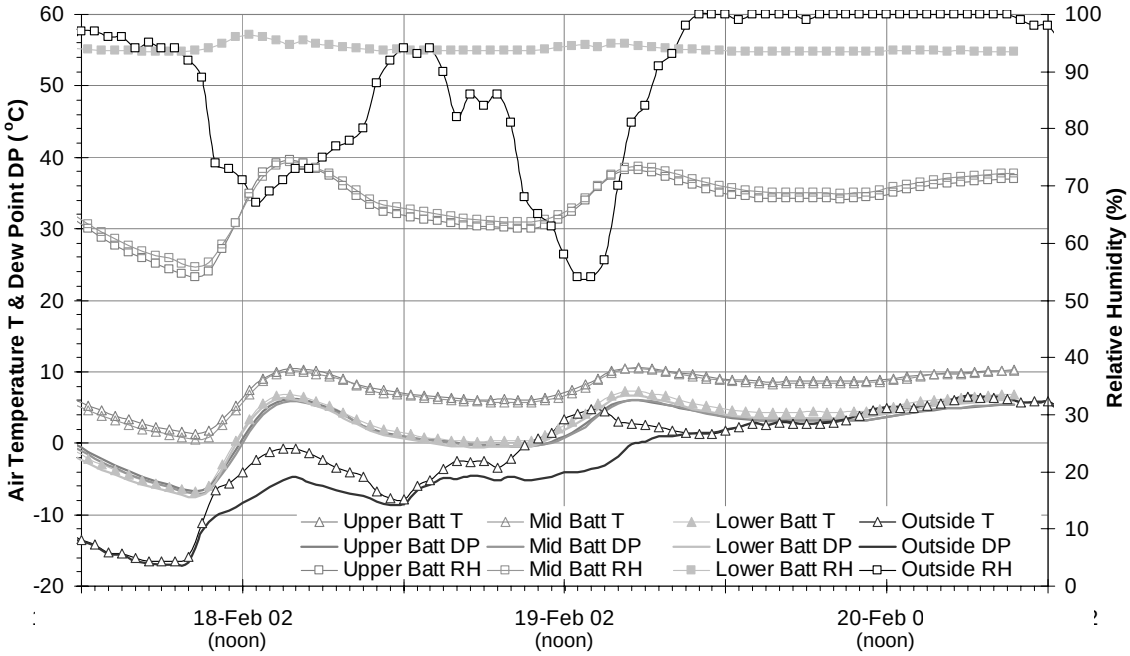

C1-1.11: B50VT Batt Space Conditions

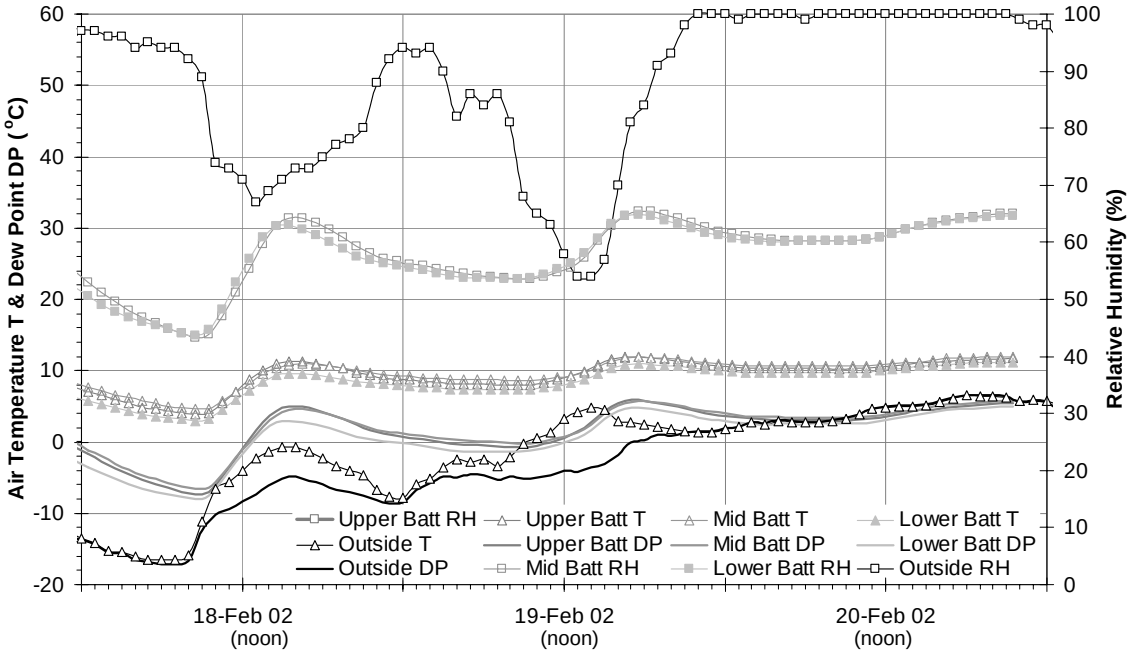

C1-1.12: V0VF Batt Space Conditions

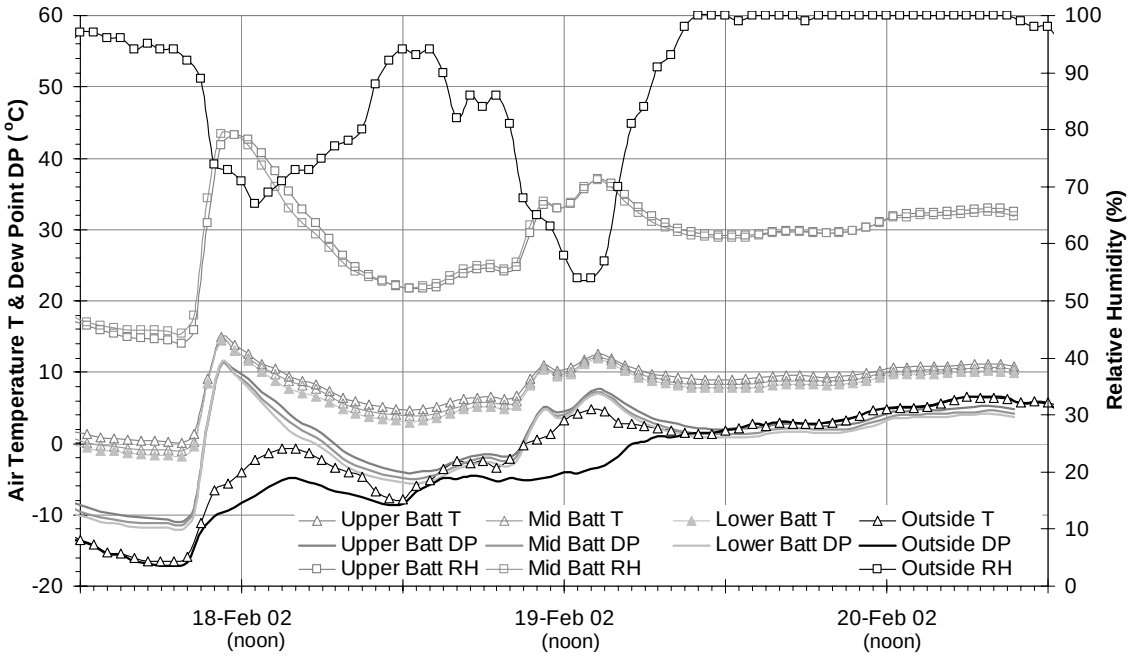

C1-1.13: V0VT Batt Space Conditions

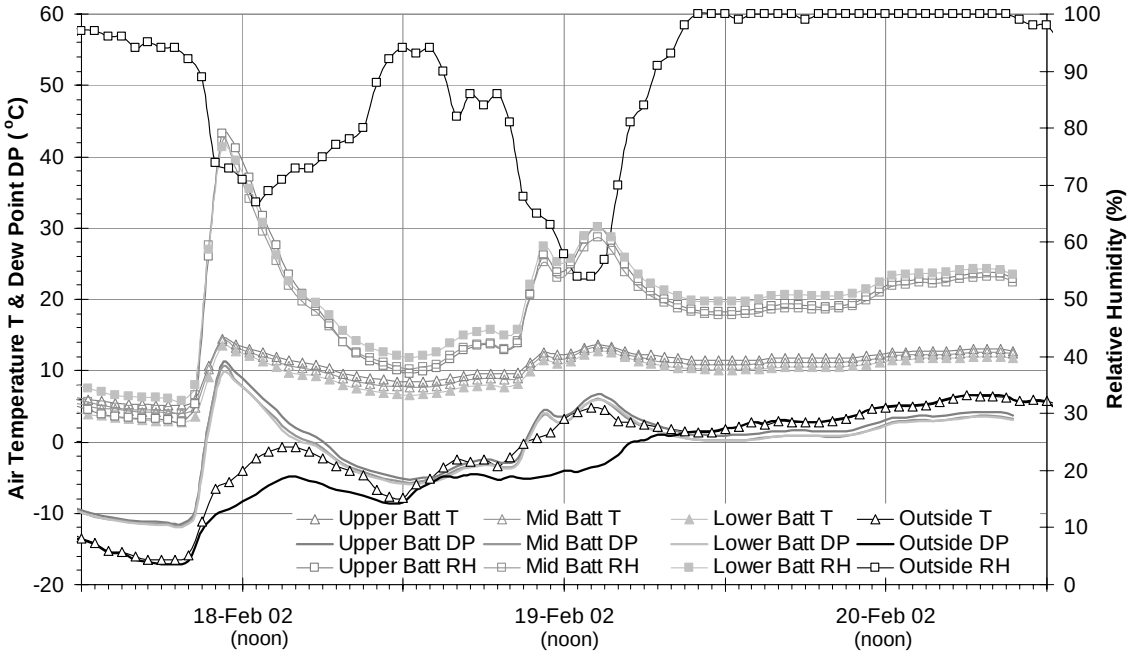

C1-2.1: Solar and Rain

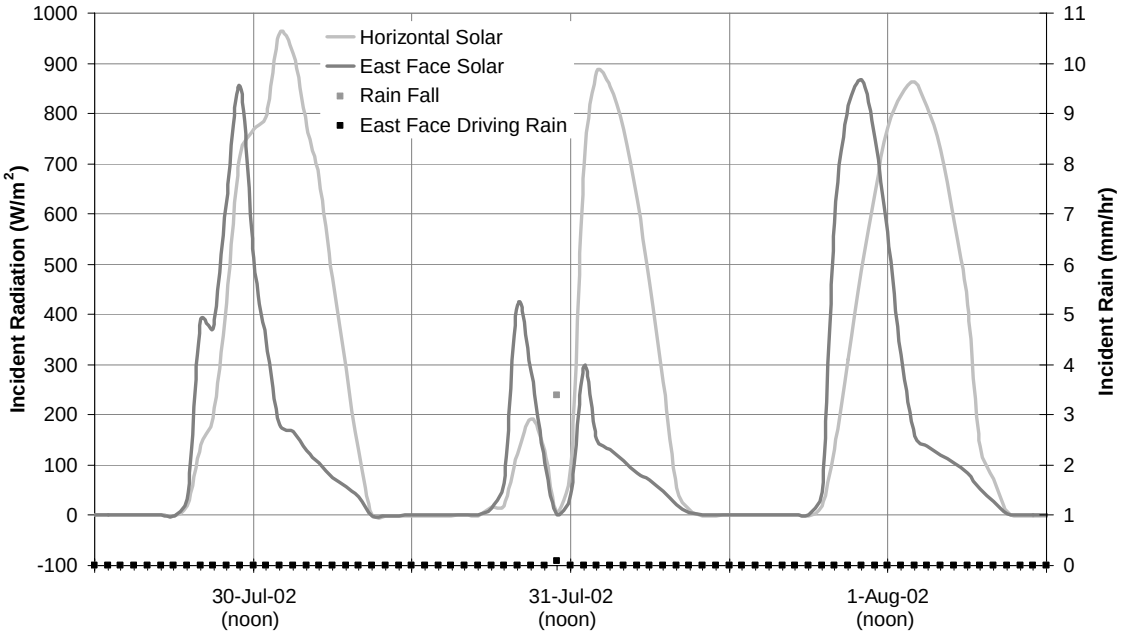

C1-2.2: Wind Speed and Direction

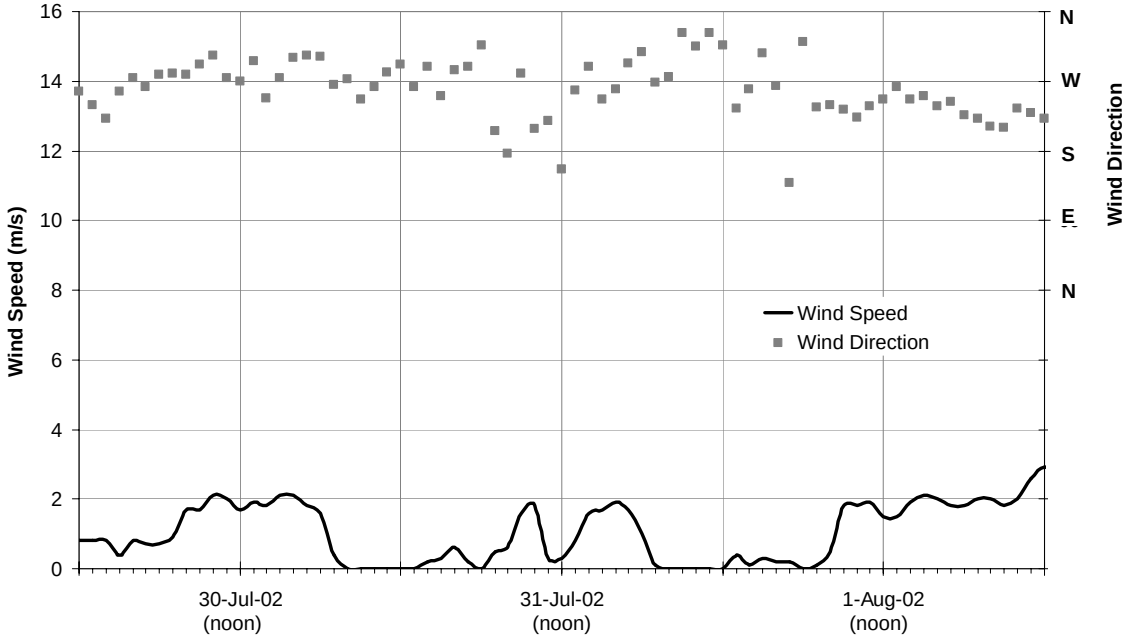

C1-2.3: Cladding Temperatures

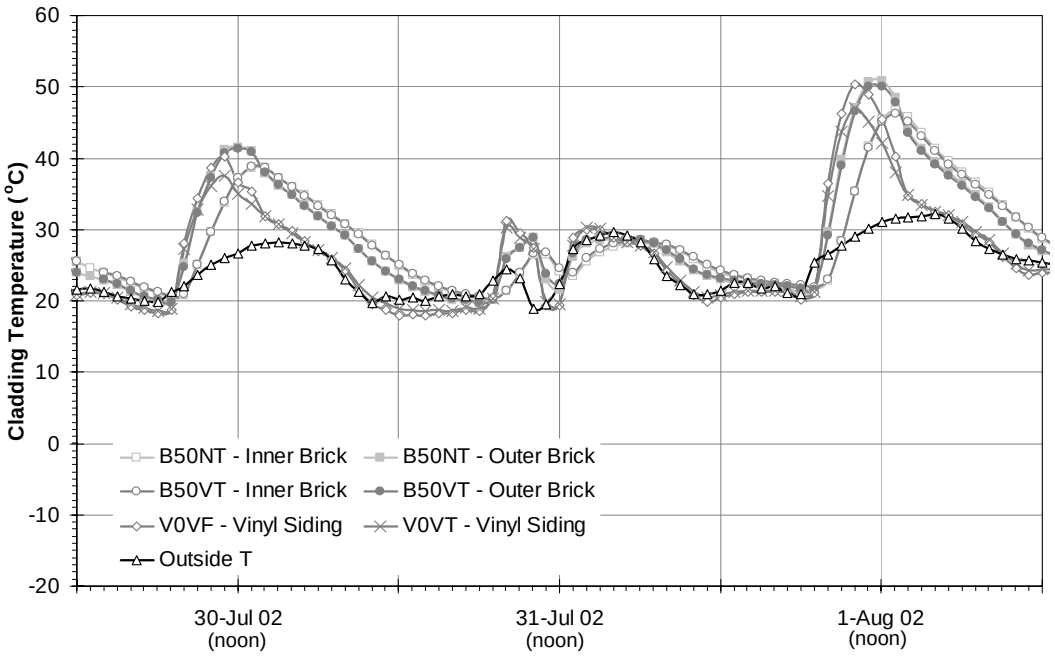

C1-2.4: B50VF Ventilation Cavity Conditions

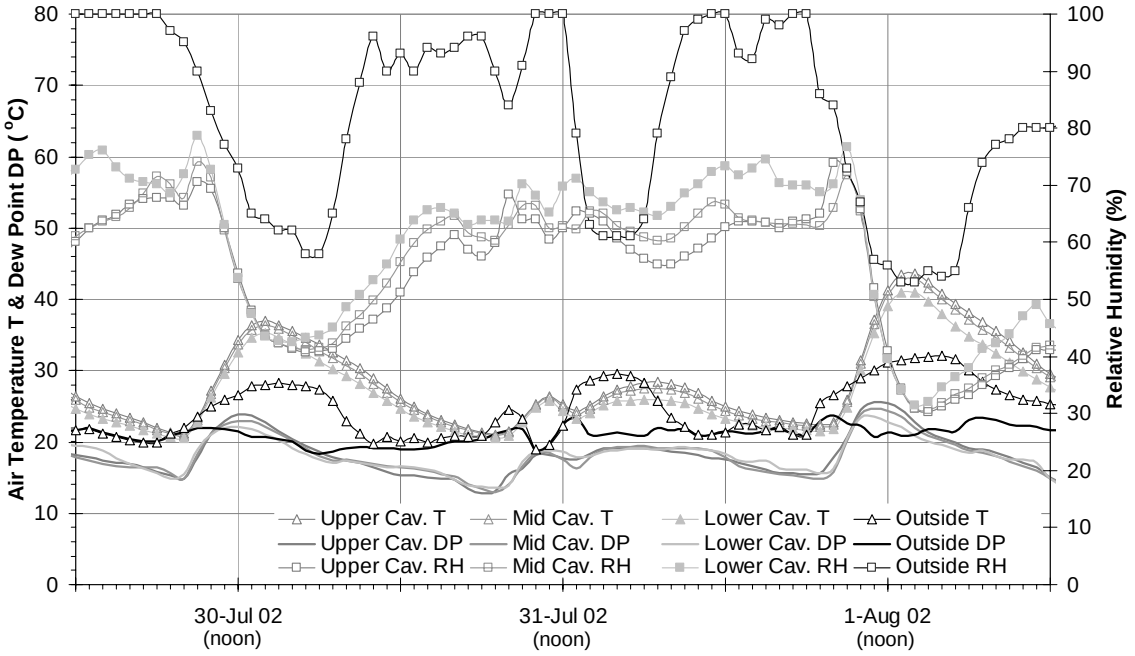

C1-2.5: B50NT Ventilation Cavity Conditions

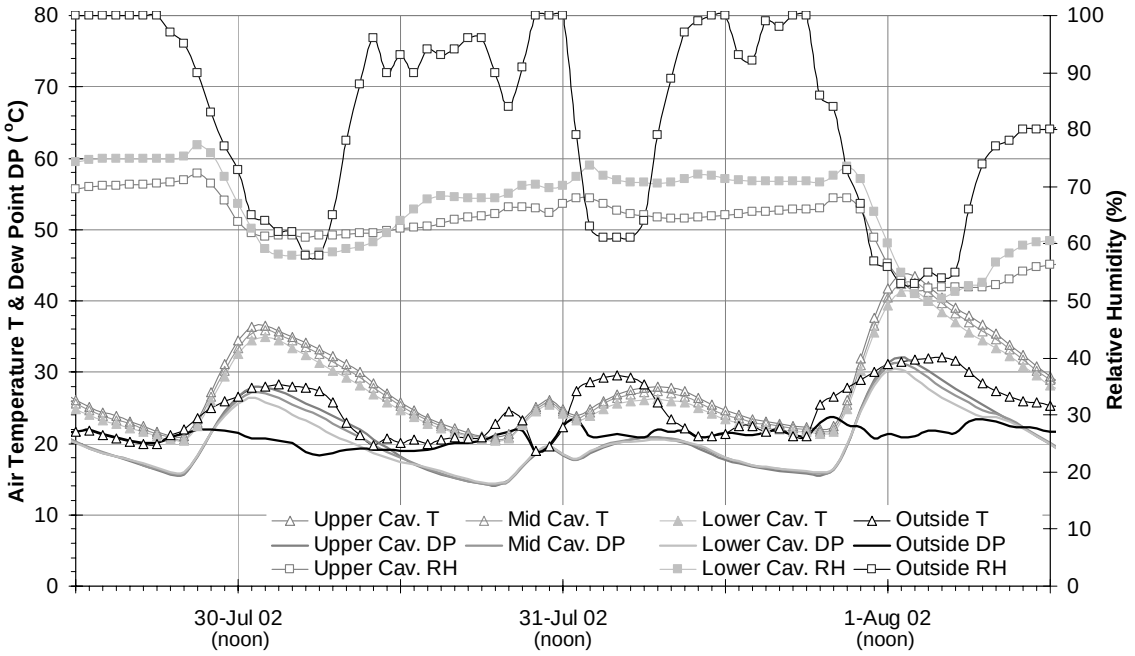

C1-2.6: B50NT Ventilation Cavity Conditions

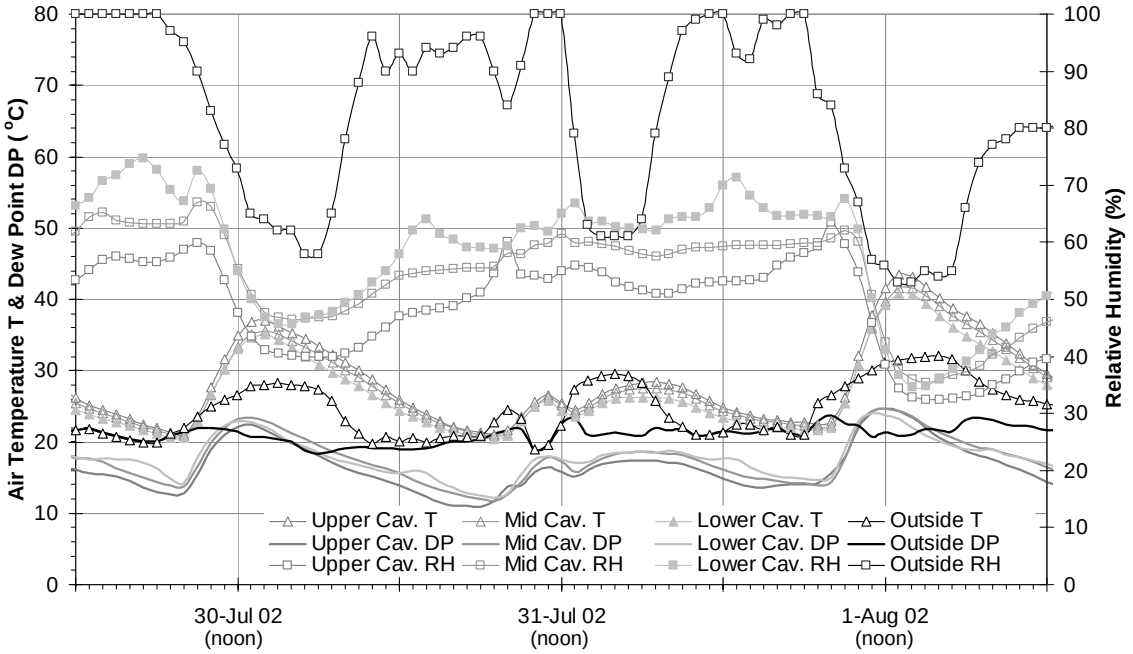

C1-2.7: V0VF Ventilation Cavity Conditions

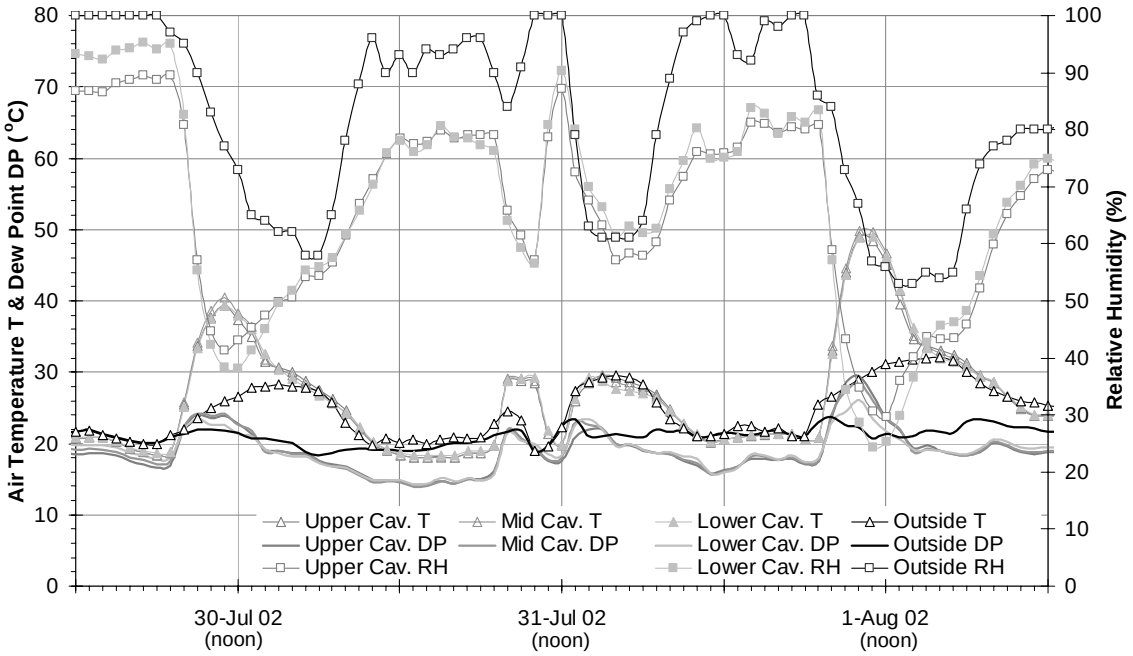

C1-2.8: V0VT Ventilation Cavity Conditions

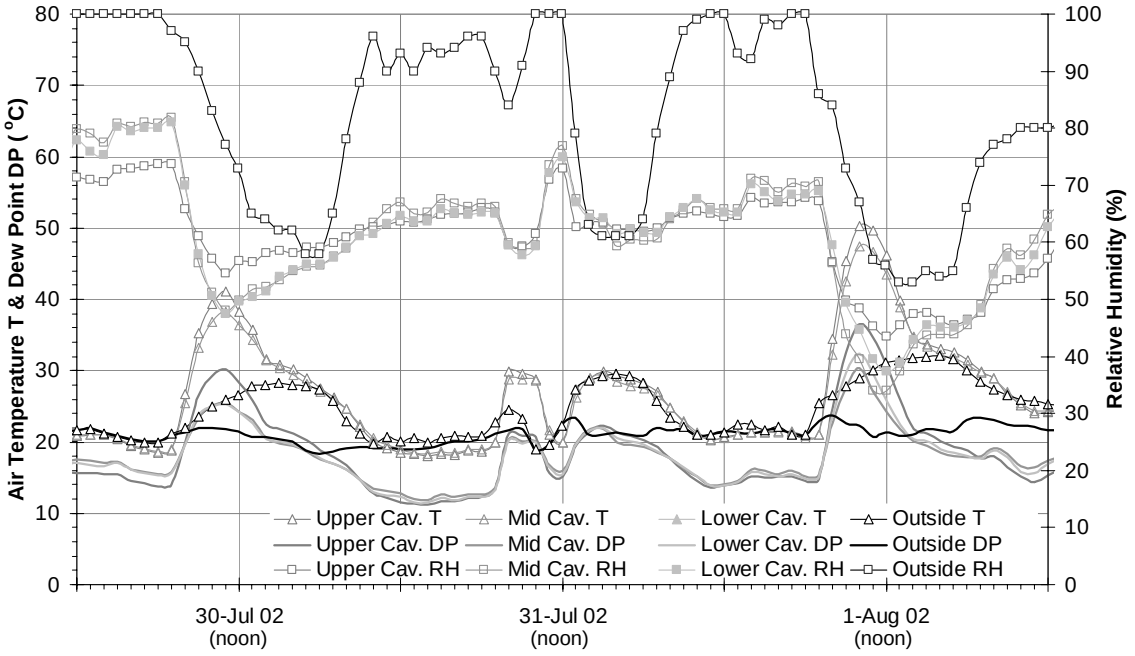

C1-2.9: B50VF Batt Space Conditions

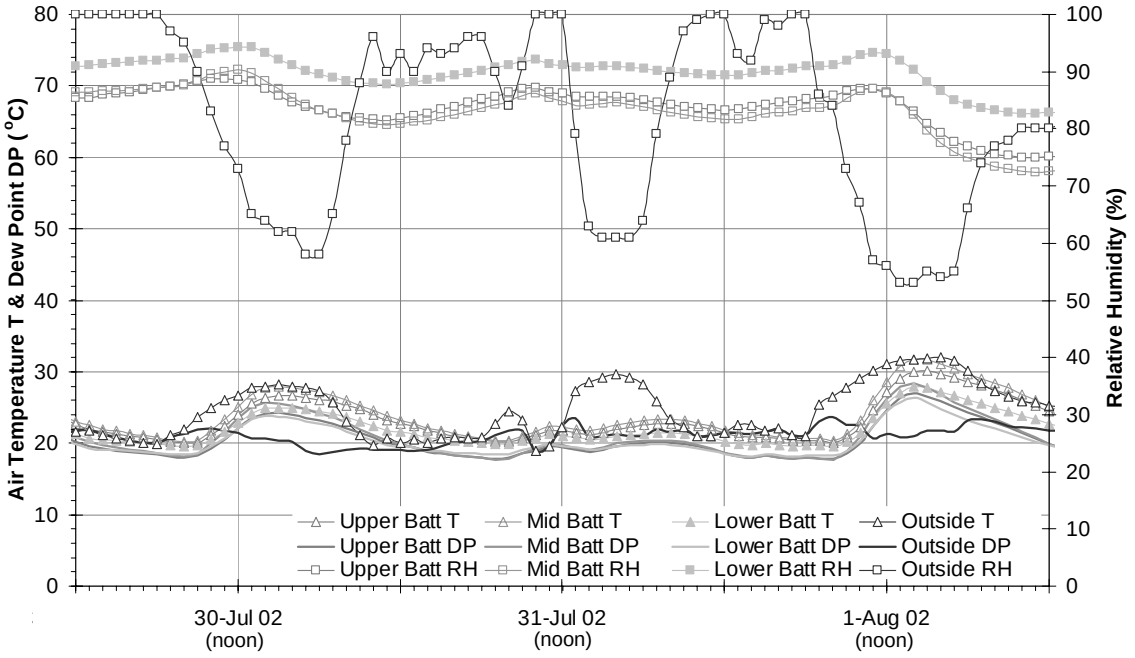

C1-2.10: B50NT Batt Space Conditions

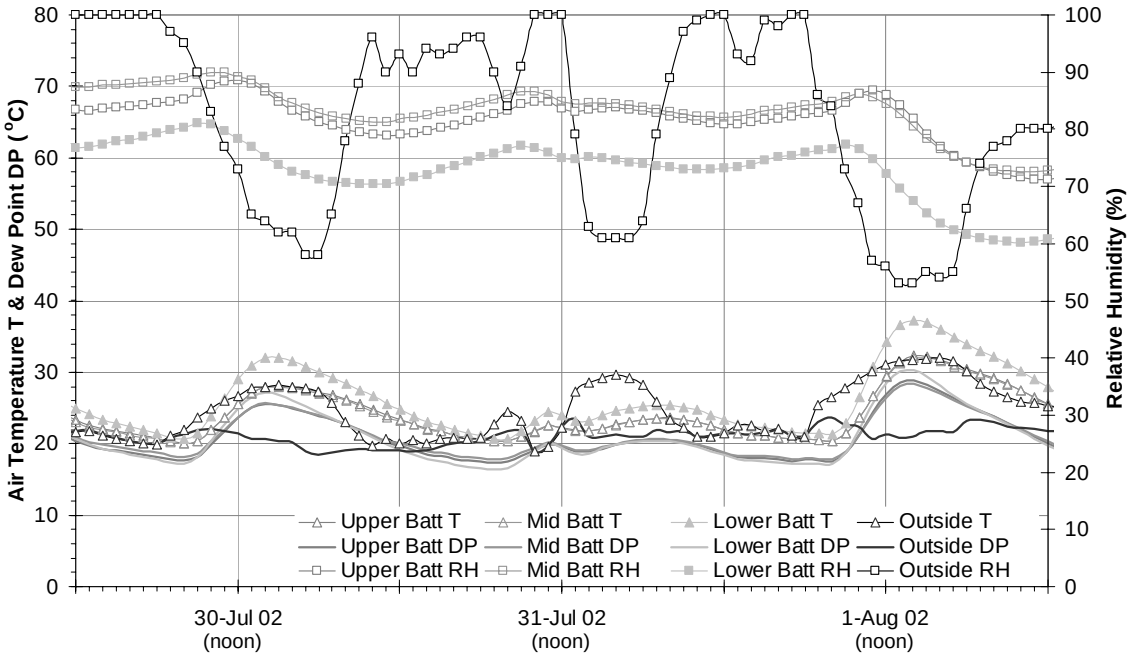

C1-2.11: B50VT Batt Space Conditions

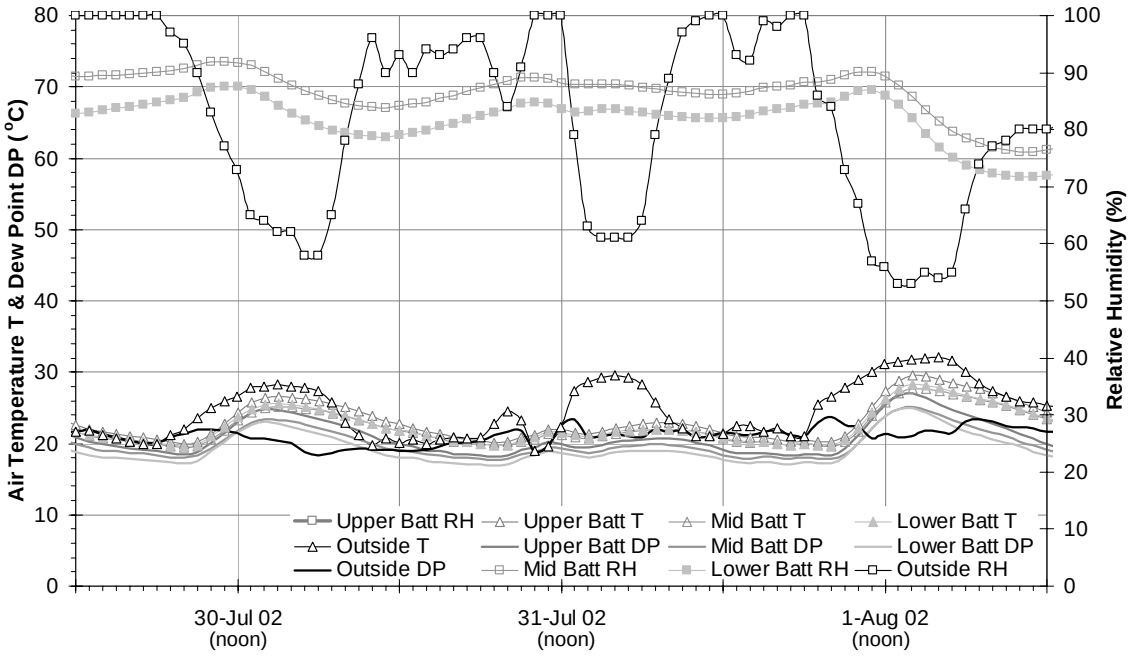

C1-2.12: V0VF Batt Space Conditions

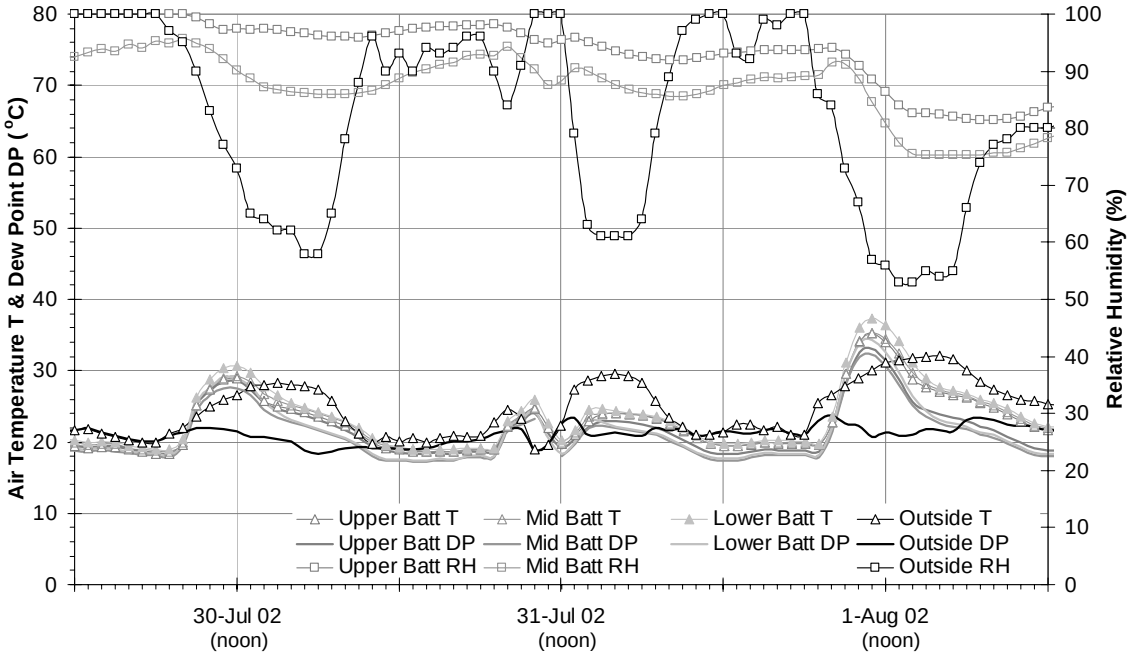

C1-2.13: V0VT Batt Space Conditions

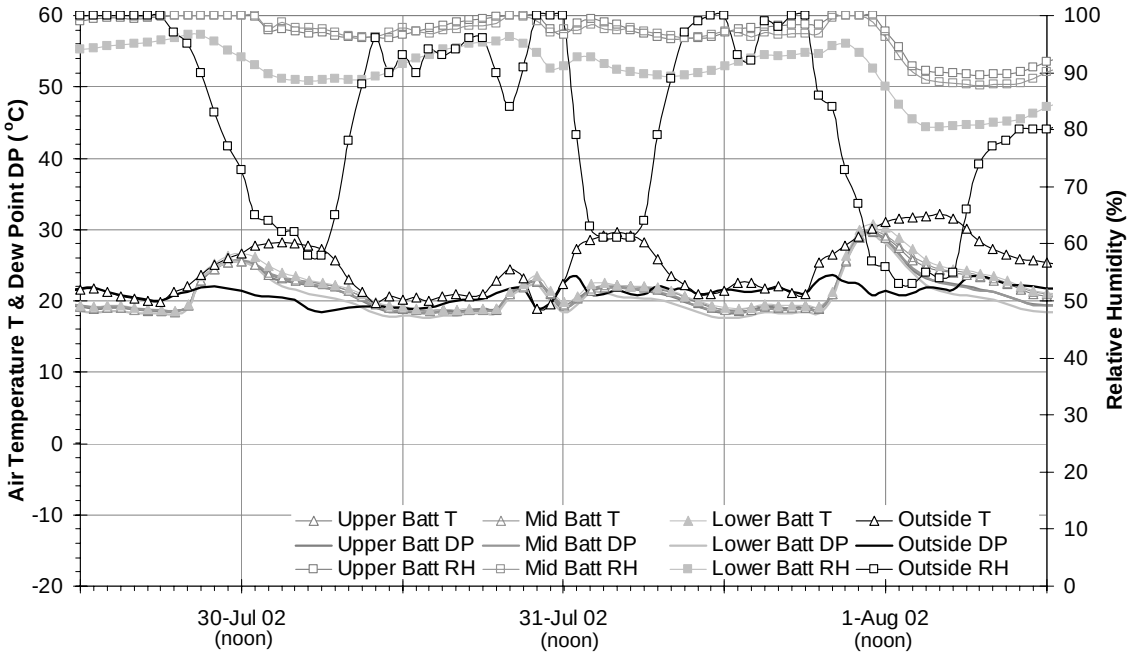

BIBLIOGRAPHY

Allen, E., *How Buildings Work,* 2nd Ed. Oxford Press 1980.

ASHRAE, *Handbook of Fundamentals* Atlanta, Ga, 2001.

Burnett, E., Reynolds, A. *Final Report - Ontario Wall Drying Study,* University of Waterloo, Building Engineering Group Report for Canada Mortgage and Housing Corporation, Ottawa 1991.

CMHC Best Practise Guide Wood-Frame Envelopes in the Coastal Climate of British Columbia, Canadian Mortgage and Housing Corporation, Ottawa 1999.

Dangleish, W., Schiever, W., "Wind Pressures on Buildings", *Canadian Building Digest* 34.

Handegord G., Hutcheon, N. Building *Science for a Cold Climate,* Canadian Institute for Research in Construction, Ottawa 1995.

Hansen, M., Nicolajsen, A., Stang, B., "On the influence of ventilation on moisture content in timber framed walls", *Building Physics 2002 – 6th Nordic Symposium,* Trondheim Norway 2002.

Hazleden, D., Morris, P., "The Influence of Design on Drying of Wood-Frame Walls Under Controlled Conditions" *Thermal Performance of Building Envelopes VIII 2002* Clearwater Florida 2002.

Holman, J., *Experimental Methods For Engineers* 6th Ed. McGraw-Hill 1994.

Idelchik *Handbook of Hydraulic Resistance* Hemisphere Publishing 1993..

Incropera, F., DeWitt, D., *Fundamentals of Mass and Heat Transfer* 4th Ed. Wiley 1996.

Jung, E. "Dauerstandverhalten von Verblendziegelmauerwerk unter Witterunsbeansphruchung und Auswirkungen von Kerndämm-Maßnahmen", *Baustoffindustrie*, No. 6, November, 1985.

Kumaran, K., "Hygrothermal Properties of Building Material", *Moisture Analysis and Condensation Control in Building Envelopes,* Ed. H Trechsel, Amercian Society for Testing and Materials, Philadelphia 2001.

Kumaran, K., Lackey, J., Normandin, N., van Reenen, D., Tariku, F., *Summary Report from Task 3 of MEWS Project at the Institute for Research in Construction Hygrothermal Properties of Several Building Materials,* IRC RR-110 2002.

Künzel, H., Mayer, E., "Untersuchung über die notwendige Hinterlüftung an Außenwandbekeidung aus großformatigen Bauteilen", *Schriftenreihe Bundesminister für Raumordnung*, Bauwesen, und Städtebau, 3/1983.

Künzel, H., Mayer, E., *Wärme- und Regenschutz bei zweischaligem Sichtmauerwerk mit Kerndämmung*. BMFT-Forschungbericht T84-191.

Lawton, B., Brown, W., and Lang, A., "Stucco Clad Wall Drying Experiment" *Thermal Performance of Building Envelopes VIII 2002* Clearwater Florida 2002.

Loomans, M., *The Measurement and Simulation of Indoor Airflow,* Techniche Universiteit Eindhoven 1998.

McCuaig, L. *Final Report on the Drying of Walls – Atlantic Canada 1987,* Canadian Mortgage and Housing Corporation, Ottawa 1988.

Merrian Webster Dictionary – www.m-w.com, 2003.

Munson, Young, Okiishi *Fundamentals of Fluid Mechanics,* 3rd edition Wiley, 1998.

Newman A. J., Whiteside D. "Water and Air Penetration Through Masonary Walls – A Device for the Measurement of Air Leakage In-Situ*", Br. Ceram. Trans. J*. 1984, Vol. 83.

Oesterle, E., Lieb, R., Lutz, M., Heusler, W. *Double-Skin Facades.* Prestel, Munich, 2001.

Ojanen, Tuomo "Improving the Drying Efficiency of Timber Frame Walls in Cold Climates by Using Exterior Insulation Wood Siding", *Thermal Performance of the Exterior Envelopes of Buildings VII*, Clearwater Florida, 1998.

Oliver, P., *Dwellings,* Phaidon Press Inc. NewYork 2003.

Popp, W., Mayer, E., Künzel, H., "Untersuchungen über die Belüftung des Luftraumes hinter vorgesetzten Fassadenbekleidung aus kleinformatigen Elementen", Fraunhofer Institut für Bauphysik, *Forschungsbericht B Ho 22/80*, April, 1980.

Potter, I. "Effects of fluctuating wind pressure on natural ventilation rates" *ASHRAE Transactions* 1979, Vol. 85(2).

Pressnail K., Timusk J., Kan L., Dong B., Kan V., University of Toronto "In Search of a Wall for All Season: Controlling Sun Driven Moisture", *9th Canadian Conference on Building Science and Technology,* Vancouver 2003.

Saelens, D., *Energy Performance Assessment of Multiple-Skin Facades*. PhD dissertation, Leuven: KU Leuven, Laboratory of Building Physics, 2002.

Salonvaara, M., Ojanen T., Kokko, E., Karagiozis, A., "Drying Capabilities of Wood Frame Walls with Wood Siding", *Thermal Performance of the Exterior Envelopes of Buildings VII*, Clearwater Florida, 1998.

Schwarz, B., "Witterungsbeansphruchung von Hochhausfassaden", HLH Bd. 24 1973, Nr. 12.

Straube J., Burnett E., *Building Science for Building Enclosures*, in progress, 2004.

Straube, J. Joeng, J. "Analytical Means of Assessing the Influence of Ventilation on Crawlspace Performance" *9th Canadian Conference on Building Science and Technology* Vancouver Canada 2003.

Straube, J., and Burnett, E., *Vents, Ventilation, and Pressure Moderation*. Building Engineering Group Report for Canada Mortgage and Housing Corp, Ottawa 1995.

Straube, J., Burnett., E., "Drainage, Ventilation Drying, and Enclosure Performance", *Thermal Performance of the Exterior Envelopes of Buildings VII*, Clearwater Florida, 1998.

Straube, J., *Moisture Control and Enclosure Wall Systems* PhD dissertation, University of Waterloo 1998.

Straube, J., Onesko, D., Schumacher, C., "Methodology and Design of Field Experiments for Monitoring the Hygrothermal Performance of Wood Frame Enclosures", *Journal of Thermal Envelope and Building Science*, Vol 26, No 2, October 2002.

Streeter, V., Wylie, B., *Fluid Mechanics,* McGraw-Hill 1985.

White, F., *Viscous Fluid Flow,* McGraw-Hill 1991.

www.jameshardie.com July 2003.